IDENTIFICATION OF AN APPROPRIATE DATA ASSIMILATION APPROACH IN SEISMIC HISTORY MATCHING AND ITS EFFECT ON PREDICTION UNCERTAINTY

Nureddin R. Edris

Submitted for the degree of **Doctor of Philosophy**

Heriot-Watt University
Institute of Petroleum Engineering
Edinburgh – Scotland, UK
April, 2009

ACADEMIC REGISTRY
Research Thesis Submission

Name*:*	**NUREDDIN R. EDRIS**		
School/PGI:	**INSTITUTE OF PETROLEUM ENGINEERING**		
Version: *(i.e. First, Resubmission, Final)*	**Final**	Degree Sought (Award **and** Subject area)	**Ph.D**

Declaration

In accordance with the appropriate regulations I hereby submit my thesis and I declare that:

1) the thesis embodies the results of my own work and has been composed by myself
2) where appropriate, I have made acknowledgement of the work of others and have made reference to work carried out in collaboration with other persons
3) the thesis is the correct version of the thesis for submission and is the same version as any electronic versions submitted*.
4) my thesis for the award referred to, deposited in the Heriot-Watt University Library, should be made available for loan or photocopying and be available via the Institutional Repository, subject to such conditions as the Librarian may require
5) I understand that as a student of the University I am required to abide by the Regulations of the University and to conform to its discipline.

* *Please note that it is the responsibility of the candidate to ensure that the correct version of the thesis is submitted.*

Signature of Candidate*:*		Date:	

Submission

Submitted By *(name in capitals):*	**NUREDDIN R. EDRIS**
Signature of Individual Submitting:	
Date Submitted:	

For Completion in Academic Registry

Received in the Academic Registry by *(name in capitals):*			
Method of Submission *(Handed in to Academic Registry; posted through internal/external mail):*			
*E-thesis Submitted (**mandatory for final theses from January 2009**)*			
Signature:		Date:	

Abstract

Reservoir management may be improved if the present state of the field is known and if changes can be predicted. The former requires information about current fluid sweep and pressure change, while the latter requires accurate reservoir description and a predictive tool such as a simulation model. With this information, important decisions can then be made, including facility maintenance and well optimisation. We apply an automated history matching method which updates a parameter such as permeability, barrier transmissibilities and NTG (Net:Gross) by matching 4D seismic predictions from the simulations to observed data. Firstly, we look at the choice of starting model in the history matching process by testing our parameterisation and updating scheme to see whether it can convert a realisation into a better representation resembling reality. We set up some synthetic test cases to validate the history matching and parameterisation scheme. We find that, if we use a pilot point separation that is equivalent to the range of the variogram used in a generation of permeability distributions, we can obtain a good representation of the model. Secondly, we investigate the impact of successively updating barriers by adding new data to our observed dataset and comparing this to a single history match where all data is used. We demonstrate the method by applying it to the UKCS Schiehallion reservoir. We update an upscaled version of the operator's model for increased speed. We consider a number of parameters to be uncertain, including barrier transmissibilities. Our results show a good match to the observed seismic and dynamic well data with significant improvement to the base case. The best result occurs when early data is used in short simulations first as we learn about optimum parameter values. Later data may be added for fine tuning or to explore new parameters. We investigate the value of seismic data in reducing forecasting uncertainty. The aim here is to look at the reduced uncertainty that we obtain in Schiehallion when we add 4D seismic to the history matching procedure. We look at the change to parameters and then take some of the best models and predict the behaviour of an in-fill well. We quantify the accuracy of history match predictions and the impact of time-lapse seismic data.

Dedication

This thesis is dedicated to my parents, my wife and my lovely daughter Mais

Acknowledgements

In The Name of Allah, The Most Gracious, The Most Merciful

I would like to express my endless gratitude to my parents, who always supported me and made many sacrifices in order to provide me with advantages they never had.

Very special thanks to my beloved wife, Omaima, for her support and encouragement at every step that our small family has taken since we have been together.

Special thanks to Mr. Mukthar Idris, Dr. Bashir Elashahab, Dr. Mustafa Idris and my friend Osama Abukraza for their endless support.

I also would like to express my heartfelt thanks to my supervisor, Dr. Karl D. Stephen, for his invaluable directions and encouragement. His enthusiasm toward new and practical research encouraged me in my studies at Heriot-Watt. His contribution extended to the improvement of my presentation skills as well as thousands of small corrections in my writing.

I also wish to thank the examiners, Dr. Eric Mackay from the Institute of Petroleum Engineering of Heriot Watt University and Dr. Marcus Marsh from BP, for the time they invested in the reading and evaluation of this thesis.

I would also like to thank the other members of the SHM Group, ETLP Group and my colleagues at the Institute of Petroleum Engineering for their support for my work and my life in Edinburgh. Thanks to those friends, my studies have been enjoyable ever since I arrived at Heriot-Watt. I appreciate the kind help from all the staff and students in this department. The financial support from Akakus Oil Operations is highly appreciated.

I would also like to thank the Schiehallion field partners (BP, Shell, Amerada Hess, Statoilhydro, Murphy Oil and OMV) for providing the data and permission to publish the results, and Malcolm Sambridge deserves thanks for use of the Neighbourhood Algorithm.

Publications

Part of this work is presented in the following publications:

- Edris, N., and Stephen, K. D. (2008). *History matching with time-lapse seismic: will any starting model do?* Presented at the SPE Europec/EAGE Annual Conference and Exhibition held in Rome, Italy, 9–12 June 2008.
- Edris, N., Stephen, K. D., Shams, A., and MacBeth, C. (2008). *Updating Barrier transmissibilies in Simulations by Successively Adding Data to an Automated Seismic History Matching Processes: A Case Study.* SPE113557. Presented at the SPE Europec/EAGE Annual Conference and Exhibition held in Rome, Italy, 9–12 June 2008.
- K.D. Stephen & N. Edriz . *Assessing the Value of Time-lapse Seismic in History Matching and Forecasts of the Schiehallion*, SPE Europec/EAGE Annual Conference and Exhibition, Amsterdam 7–14 June 2009.

Contents

List of Figures

List of Tables

Nomenclature

A	Raw attribute at time *t*, observed or predicted, prior to normalisation
a	Normalised attribute at time *t*, observed or predicted
C_i	Covariance matrix of the i^{th} variable
E_κ	Excess compliance of the bulk modulus, m/Lt^2, Pa
E_μ	Excess compliance of the shear modulus, m/Lt^2, Pa
I	Impedance, m/L^2t, kg $m^{-2}s^{-1}$
I_{ij}	Impedance on the seismic grid, m/L^2t, kg $m^{-2}s^{-1}$
I_{IJ}	Impedance on the simulation grid, m/L^2t, kg $m^{-2}s^{-1}$
I_{ij}^{interp}	Interpolated impedance, m/L^2t, kg $m^{-2}s^{-1}$
Ji	Misfit of the i^{th} variable
w	weighting factor when downscaling impedances
k	Permeability, L^2, mD
M	P-wave modulus, , m/Lt^2, Pa
M^{cell}	P-wave modulus for a cell, m/Lt^2, Pa
M	P-wave modulus of lithofacies within a cell, m/Lt^2, Pa
N	Number of bins (observed data) in the sector
n_r	Number of best models resampled by the NA
n_s	Number of models per iteration
NA	Neighbourhood algorithm
NTG	Net:Gross
P	Pressure, , m/Lt^2, Pa
P_{eff}	Effective (overburden – pore) pressure, m/Lt^2, Pa
P_κ	Stress sensitivity of the bulk modulus, m/Lt^2, Pa
r	Position vector of a cell centre, L, m
RMS	Root Mean Square
S_g	gas saturation
S_o	oil saturation
S_w	water saturation
α	$(1-\kappa^r_{dry}/\kappa_{gr})$

β	Interpolation weighting coefficient, 1/L, m^{-1}
γ_A^o	Areal mean of seismic attribute, A, calculated for the pre-production survey
m	Model error for the ith variable
W_P	Production weighting factor
φ	Porosity
κ	Bulk modulus, m/Lt^2, Pa
κ_f	Fluid bulk modulus, m/Lt^2, Pa
κ_g	Gas bulk modulus, m/Lt^2, Pa
κ_{gr}	Grain bulk modulus, , m/Lt^2, Pa
κ_{inf}	Bulk modulus at STP, m/Lt^2, Pa
κ_o	Oil bulk modulus, m/Lt^2, Pa
κ_{dry}	Dry bulk modulus, m/Lt^2, Pa
κ_{sat}	Saturated bulk modulus, m/Lt^2, Pa
κ_w	Water bulk modulus, m/Lt^2, Pa
μ	Shear modulus, m/Lt^2, Pa
ρ	Density, m/L^3, kg m^3
x^{obs}	Observed variable
x^{mod}	Predicted variable
σ_A^o	Areal standard deviation of the attribute, A, calculated for the preproduction survey.
ψ	mother wavelet
τ	real number and defines the shift
x	variable, observed or predicted
Q	Production rate
O	Observed data
PDF	Probability Density Function
PPD	Posterior Probability Distribution
SCAL	Special core analysis

Subscripts

cell	Cell average
d	Data

dry	Dry rock
eff	Effective pressure, overburden – pore
f	Fluid modulus
g	Gas
gr	Grain
i	ith variable
Inf	At infinite effective pressure
m	Model
o	Oil
r	Sample number for number of best models in NA
s	Sample number per iteration of NA
sat	Saturated rock
w	Water
x	x direction
y	y direction
z	z direction
t	time
error	Error component
mod	Model (predicted)
obs	Observed

CHAPTER ONE

Introduction

This chapter provides an introductory description of Seismic History Matching and how time-lapse seismic analyses may be incorporated into the reservoir characterisation technique. This type of information may be used to guide geological and simulation model building, vastly improving confidence in forecasting. Applying this approach manually, however, is quite labour intensive. In an integrated team, a geologist, a geophysicist and a reservoir engineer may all be used while simulations are run to predict the observed data as the model is modified iteratively. The chapter ends by discussing the main challenges and contribution of this thesis.

1.1 Improving history matching using time-lapse seismic data: an introduction

Knowledge derived from reservoir modelling provides both qualitative and quantitative information. With this information, important decisions affecting facility maintenance and well optimisation can then be made.

One of the most critical problems in reservoir prediction is the process of generating the field properties as starting points for modelling. It is difficult to obtain accurate realisations of the reservoir model, owing to the limitation of the available information, thus leading to poor history matching. The main idea in classical history matching is to change the properties of the reservoir model in an iterative loop until there is a reasonable match between the observed and the predicted reservoir dynamic properties (production rates,

water cut, wellbore pressure, etc.) (Mattax and Dalton, 1990). In classical history matching, modifications to the reservoir parameters are conducted manually and rely on the information that the geoscientists provide, such as the engineering data, geological understanding of the reservoir and perhaps subjective experience throughout the entire matching process.

Time-lapse (4D) seismic technology has been introduced to monitor the reservoir during production at different times, since changes in the reservoir (pressure and saturation) can be detected via changes in compressibility. The number of 4D seismic acquisition surveys has increased in the last twenty years, and the interpretation of this type of data is currently moving towards quantifying non-produced hydrocarbons within the reservoir. 4D seismic analysis is a conventional tool for reservoir characterisation, monitoring and management. From Figure 1.1 (Foster *et al.*, 2008), it can be seen that, during 2001, there were 75 active time-lapse seismic projects worldwide in which BP was involved. This is illustrative of the industry in general. These cost approximately US$50 million to US$100 million (Lumley, 2004). Most time-lapse seismic surveys have been carried out in the North Sea (Figure 1.2), but the technique is expanding to other regions of the world. Figure 1.3 shows the geographical distribution of the main 4D projects undertaken over the last five years.

Another important issue is that geological modelling is performed on a small scale, similar to the seismic grid in an areal resolution. We require fast simulation methods, however, and must upscale to reduce the number of cells. With this there are potential problems: inaccurate upscaling, numerical dispersion and failure to capture the effect of small-scale heterogeneity lead to simulation model errors. The errors in saturations and pressures from the coarse grid affect the predicted seismic differences. The error varies depending on the location relative to the wells, and may bias the misfit calculation. We are currently investigating error models to reduce the bias. On the other hand, 3D seismic imaging and interpretation is a technique that can be used to create images of the geological variations between wells. These images can help to complete a picture of the subsurface that should

enhance the ability of the reservoir description team to select future well locations and/or completions successfully.

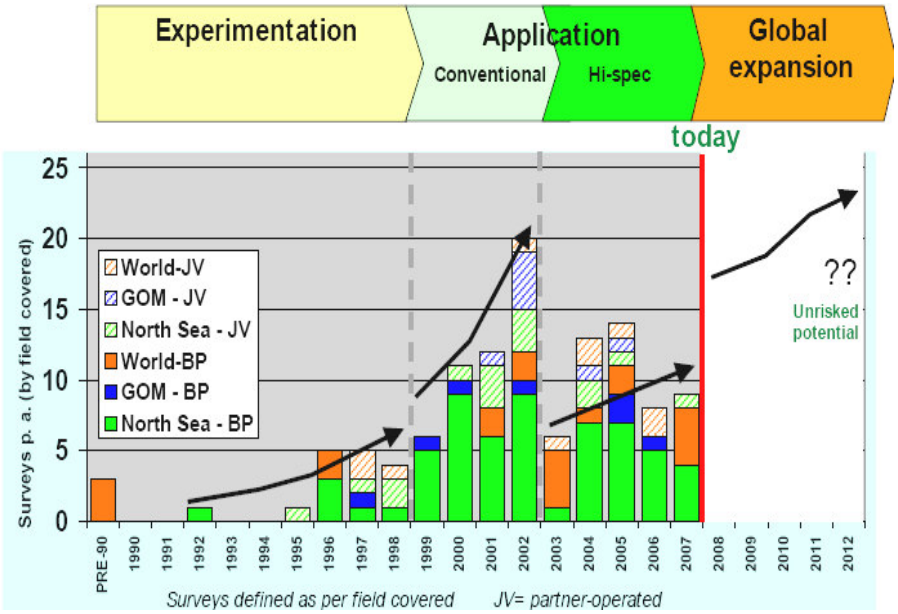

Figure 1.1: *Growth of 4D seismic acquisition in the North Sea related to BP (Foster et al., 2008).*

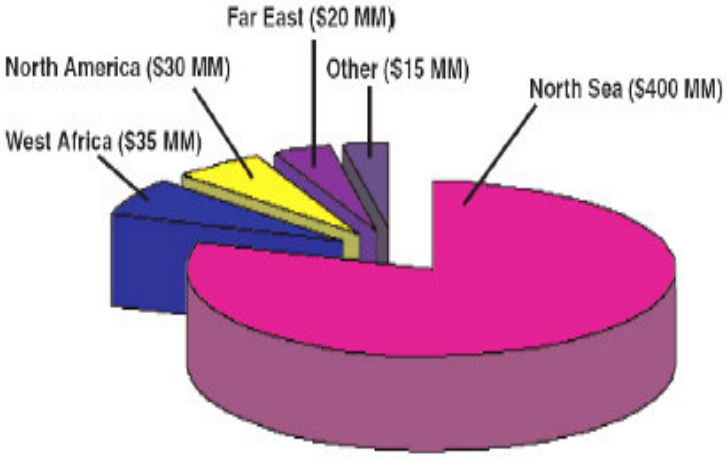

Figure 1.2: *Cumulative expenditure in the worldwide on time-lapse seismic services by contractor and service companies for 2000–2003 (after Lumley, 2004).*

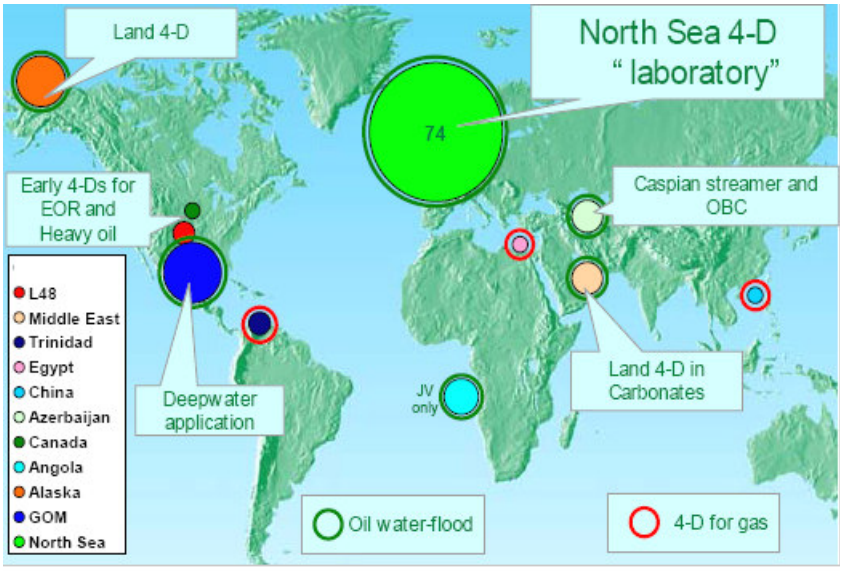

Figure 1.3: *4D seismic global historical activity (Foster et al., 2008).*

1.2 Integration of reservoir engineering and seismic data

Real-time reservoir management (also known as Closed-loop Reservoir Management), consists of life-cycle optimisation based on uncertain reservoir models as they are updated using production measurements, 4D seismic and other data. Essential elements of closed-loop reservoir management are model-based optimisation (automatic history matching) and, in particular, their integrated application in a reservoir-management workflow which leads to a decrease in the uncertainty of the reservoir model.

Automatic history matching is proposed with the intention of improving manual work while honouring the information consistency. With an automated procedure it is feasible to construct multiple models and analyse the associated uncertainty rather than work with one deterministic model. The purpose of history matching is to minimize the discrepancies between observed data and simulated results. Typically, such discrepancy minimization is expressed by an objective function.

In such workflows for reservoir characterisation, the integration of several disciplines, including geology, geophysics and reservoir engineering among many others, is fundamental for success. In a number of fields, time-lapse seismic analysis has the potential to provide the missing areal information, but lacks precise details of the pressure and saturation states. To extract maximum learning from the 4D seismic data, we should integrate seismic data with other properties such as petrophysical data and reservoir simulation.

This integration of 4D seismic data with reservoir simulation can be wholly qualitative, i.e. a visual interpretation of the 4D signal to understand changes in saturation and pressure, or more quantitative by the derivation of a seismic synthetic volume (Sønneland *et al*., 1996; Anderson *et al*., 1997; He *et al*., 1998). The spectrum of approaches is summarised in Figure 1.4 (O'Donovan *et al*., 2000).

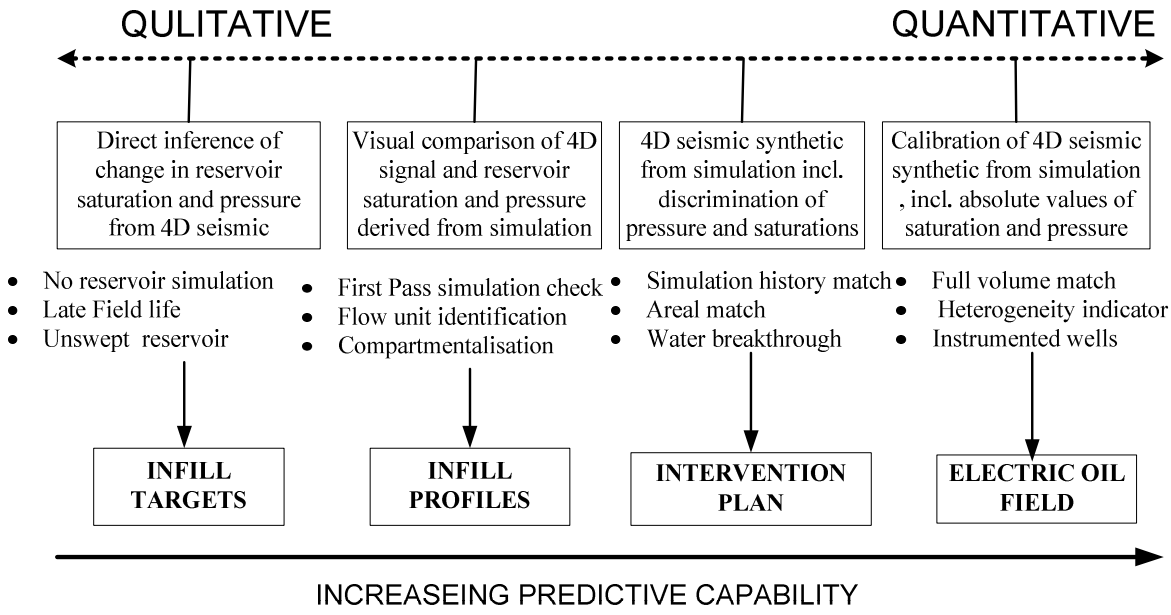

Figure 1.4: *Integration of 4D seismic data with reservoir simulation. The more quantitative the approach, the greater the degree of predictive capability that can be derived from the 4D data taken from (O'Donovan et al., 2000).*

Qualitative no simulation: Direct inference of change in reservoir saturation and pressure from 4D data. This approach can be used separately from reservoir simulations and is most appropriate for classifying upswept reservoir and infill targets (Figure 1.5).

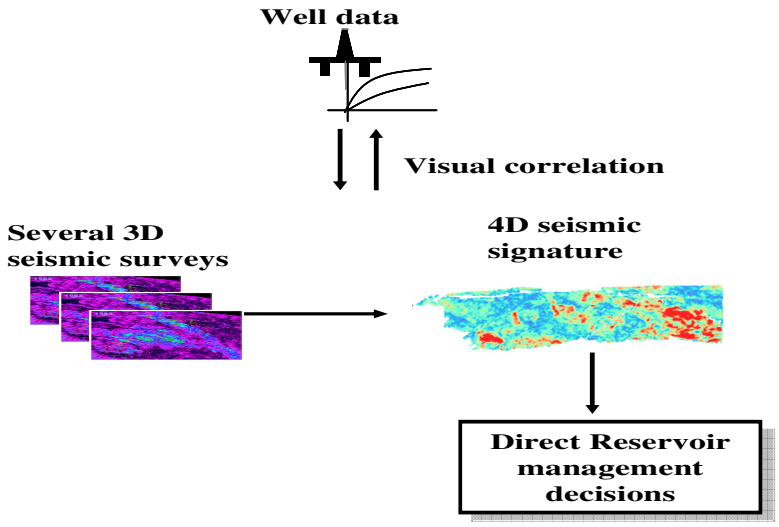

Figure 1.5: *Conventional 4D seismic interpretation.*

Staples (2006) presents an example of qualitative comparison of the Gannet-C field, in which the 4D results indicate the extension of the 4D signal to the south of the originally prognosed field boundary (Figure 1.6).

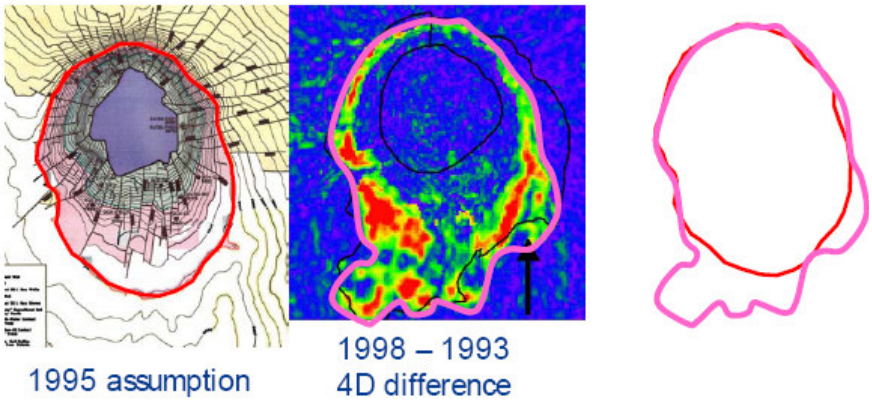

Figure 1.6: *Oil–water contact assumptions compared before and after 4D seismic analysis (Staples, 2006).*

Qualitative comparison to simulation: A direct inference of change in reservoir saturation and pressure from 4D data. Conventional 4D seismic interpretations have aided the mapping of reservoir compartmentalisation (Figure 1.7). This approach can be used independently from reservoir simulation and is most appropriate for identifying bypassed oil for infill drilling. In addition, it tracks the lateral movement of injected gas and water fronts, identifies fluid contact movement and provides insight into pressure maintenance.

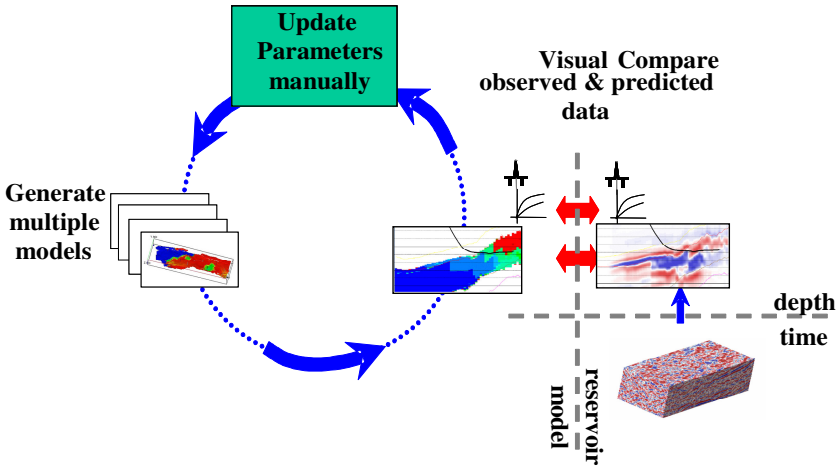

Figure 1.7: *Workflow for model screening or updating. Comparison of the measured seismic change against predictions from multiple simulation models.*

An example of the qualitative comparison of simulations to 4D seismic results indicate no change in areas expected to be in-flowing; it is likely that these areas are isolated reservoir compartments (Figure 1.8). This identifies areas where oil that may have been booked as recoverable, but will be left behind with the current well pattern, resulting in a shortening plateau of production and lower ultimate recovery. By locating the compartment, 4D surveys quantify the lost reserves and allow the placement of a well for access.

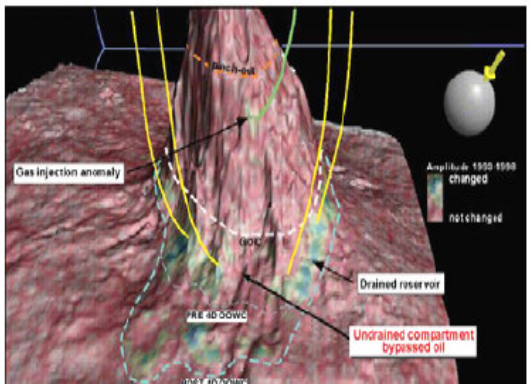

Figure 1.8: *Illuminated top reservoir depth map in Gannet-C. Amplitude extracted from the difference volume is superimposed. (after Koster et al., 2000).*

Semi-quantitative comparison: 4D seismic synthetic derived from reservoir simulation (Figure 1.9). In some sense, the measured seismic change against predictions from multiple simulation models allows simulation history matching, aerial/volume match, along with targets, profiles and accurate prediction of water breakthrough by identification of flood fronts. The simulator results can be taken through forward rock physics modelling to acoustic impedance or amplitude, and can be screened against the time-lapse seismic results.

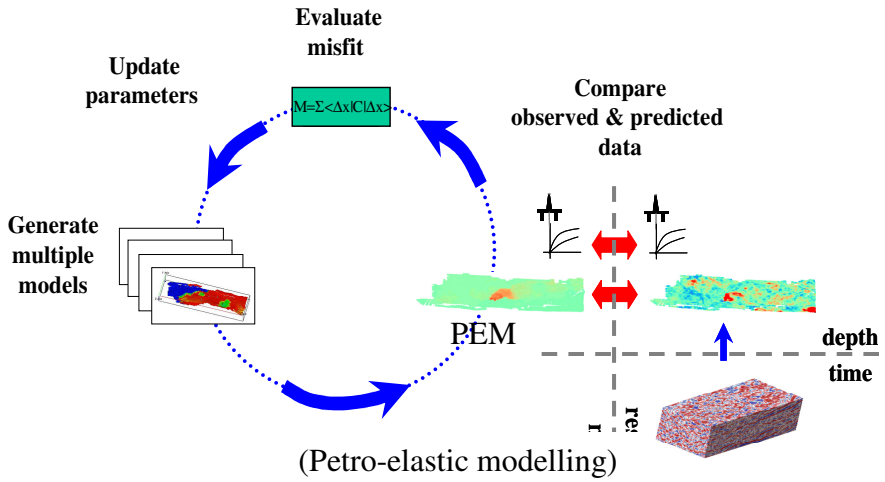

Figure 1.9: *Workflow for model screening and updating. Comparison of the measured seismic change against predictions from multiple simulation models.*

The Lena Field in the Gulf of Mexico (Johnston *et al.*, 1999) provides an example in which a comparison between the time-lapse differences using production data was performed, along with flow simulations and forward seismic models (Figure 1.10). Interpretation of the time-lapse seismic difference indicates a region of gas invasion. Areas undrained by the injected gas are recognised from 4D seismic data, which increases the opportunities for infill drilling.

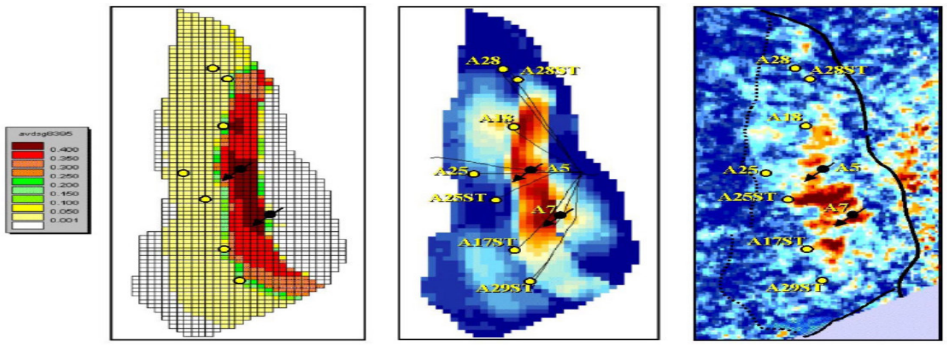

Figure 1.10: *Comparison of gas saturation change (left), modelled seismic difference (centre) and real seismic difference (right) (after Johnston et al., 1999).*

The Schiehallion Field is another example of the use of 4D seismic analysis (Hatchell *et al.*, 2002). Figure 1.11 shows maps of the difference between the pre- and post-production amplitude maps. From these, more information about pressure compartments and connectivity was obtained and used to update the reservoir model to aid in locating the infill wells.

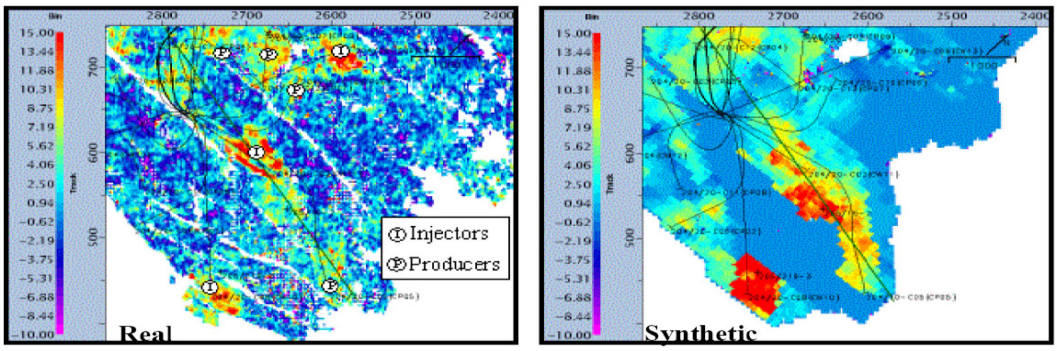

Figure 1.11: *Schiehallion Field example shows time-lapse amplitude differences for real (left) and synthetic (right) seismic data (after Hatchell et al., 2002).*

The case of the Draugen Field was presented by Koster *et al.* (2000). The reservoir model had predicted that water movement would occur along the flanks of the field (Figure 1.12). These models display significantly different forecast production profiles for the field. Therefore, knowledge of the true communication path would allow optimisation of the production plan. In addition, a northern fault is clearly shown to be sealing during the production time. The reservoir model that was closest to the 4D result was selected for reservoir management purposes.

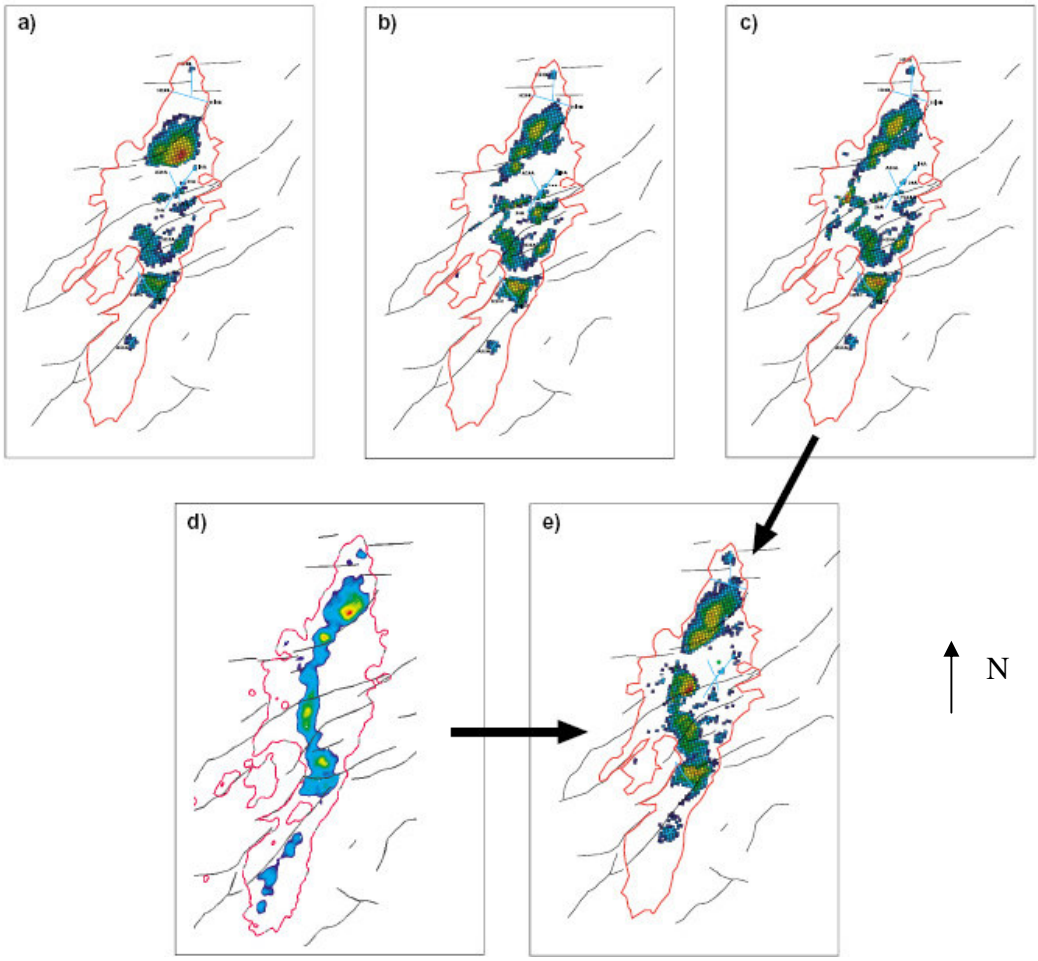

Figure 1.12: *The time-lapse interpretation and the updated simulation model. Faults (black) and the extent of the OOWC (red) are indicated. Three models are built for the field, using different communication paths between the aquifer and the reservoir: (a) communication in the north; (b) communication through faults; (c) communication in the west; (d) actual observation from time-lapse seismic; (e) final model matched to seismic and production history (after Koster et al., 2000).*

Fully quantitative: Calibration of 4D seismic synthetic from simulation, including absolute values of saturation and pressure; full volume match and integration with instrumented wells; targets, profiles of water breakthrough and heterogeneity indicators (Figure 1.13). This is a possible direction for the future use of 4D in conjunction with developments in well technology. The main part of quantitative integration of time-lapse seismic data into reservoir management is to use it to improve reservoir simulation models, to make them more representative of the truth, which leads to a good reservoir performance prediction.

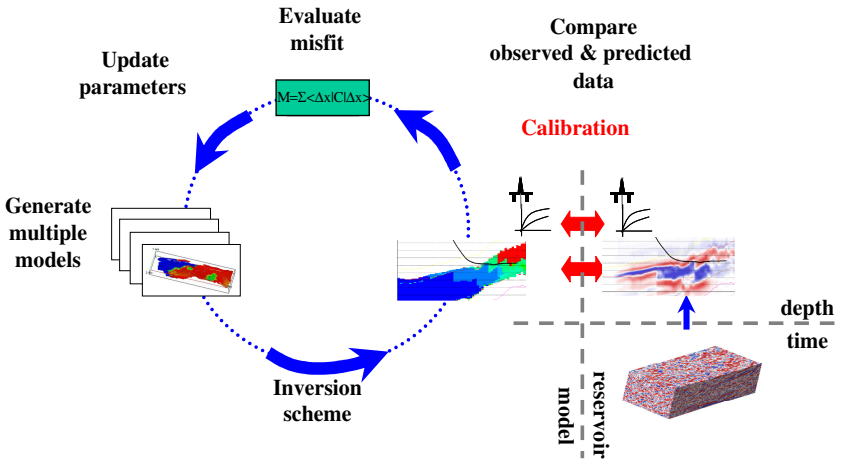

Figure 1.13: *Quantitative 4D seismic interpretation: pressure and saturation are estimated from time-lapse seismic data and compared with simulation models.*

The process of seismic history matching attempts to overlap the benefits of both types of information in order to improve estimates of reservoir model parameters. In this context, history matching and time-lapse seismic analysis are among the most important tools that the geoscientist can utilise, as outlined in Figure 1.14. The type of time-lapse seismic data used for property estimation has varied among researchers, as listed in Table 2.1.

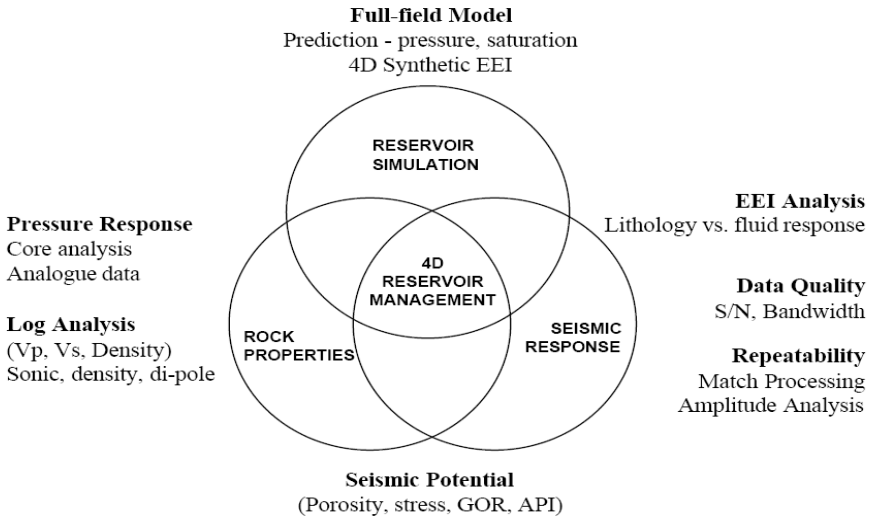

Figure 1.14: *Components of an integrated study for 4D seismic interpretation. (O'Donovan et al., 2000).*

1.3 Benefits of including seismic information in the history matching process

In general, field economics can be improved by speeding up production, growing or enlarging plateau production rates, reducing the rate of decline after plateau, or extending field life to delay abandonment. The plateau production rate is often limited by external restrictions and is thus not changeable if the well is poorly placed: the well may immediately encounter high water saturation, or it may water out rapidly, for example.

One of the advantages of 4D information is the cost savings from an unnecessary well, by assessing the state of the reservoir at a designed well location. When 4D seismic data results indicate no reservoir change in areas expected to be in production, it is likely that these areas are isolated reservoir compartments (Figure 1.15). In some cases we cannot see the 4D seismic signal change because the opposite effects for the pressure and saturation may cancel each other. Alternatively, wells can be located away from advancing fluid fronts and/or protected from fronts by natural flow barriers within the field. By doing this, it may be possible to extend plateau production or decrease the decline rate after plateau.

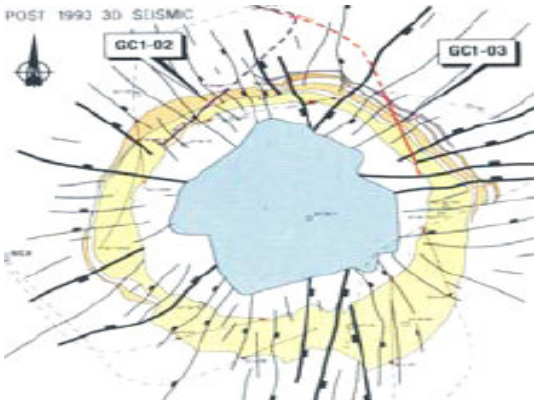

Figure 1.15: *Horizontal depth slices through Gannet-C (based on interpretation of seismic data). Two additional producers were then drilled successfully between complex fault zones (Koster, 2000).*

Reducing uncertainty in reservoir models

Reservoir models always contain a degree of uncertainty, but 4D seismic data results can reduce some of that uncertainty. As a spatial measure of fluid movement, 4D provides unique information that can be used to constrain the generation and selection of reservoir flow properties. With less uncertainty, there is less risk in many reservoir development and production decisions, which could result in the acceptance rather than the rejection of an economically viable project.

1.4 Applications

The main purpose of a reservoir model is to predict the future behaviour of the reservoir and analyse the effect of reservoir management decisions. Forecasts are based on the reservoir model that best fits the observed static and dynamic data. An important issue is the quantification of the forecast uncertainty.

This processof integrating 4D seismic and reservoir engineering data is affected by scale and process dependent model errors. Flow simulations are often created such that computer resources are optimised and some level of accuracy is sacrificed. To speed up simulations,

some form of upscaling is required to capture two-phase flow properties such as relative permeability but also to represent geological heterogeneity. The upscaling may be over-simplified or ignored.

Seismic History Matching (SHM) is a modification of the petroleum engineering practice of a production history match. In SHM, a group of static parameters of the reservoir model, such as porosity, permeability and fault transmissibility, is (automatically) updated in an iteration loop until it reaches a minimum misfit value. The objective function measures the differences between observations (this is represented as a combination of production and seismic observables) and predictions, which are obtained through reservoir forecasting and seismic modelling based upon pressure and saturation. A number of publications on SHM can be found in the literature (Huang *et al*., 1998; Lumley and Behrens, 1998; Arenas *et al*., 2001; Mantica *et al*., 2001, 2002; Cominelli *et al*., 2002; Waggoner *et al*., 2002; Gosselin *et al*., 2003; Stephen *et al*., 2004, 2005 and 2006), which are described in more detail later. Parameterisation, the definition of the objective function, the choice of optimisation algorithm, and the stopping criterion are the most important factors in SHM, and incorporate reservoir engineering skills with geophysics.

The main targets of SHM techniques are to:

a) make use of 4D seismic data to add additional constraints to the modelling workflow, leading to an improved reservoir characterisation.

b) evaluate the model predictions and determine uncertainties via statistical parameters obtained after inversion (i.e. standard deviation, mean, etc).

c) make the reservoir more understandable in the case of fluid flow patterns throughout the life of the reservoir.

The main strengths of SHM are:

a) It is supported by two main types of data (production and seismic).

b) The use of a Bayesian approach for inversion provides uncertainty estimation.

c) It helps to improve the location of wells for field development.

d) It allows better identification of fluid flow patterns and barriers.

On the other hand, there are some weaknesses in this approach, such as:

a) Inversion may be too costly in terms of time.

b) Since inversion is non-unique, special care must be taken with final estimates.

c) The requirement of an appropriate timing for time-lapse seismic surveys.

1.5 Main issues and challenges of the thesis

Subsequent chapters aim to address the issues and challenges in the following ways:

- Improving the workflow for seismic history matching, which is needed in order to obtain a well-developed strategy for reservoir parameter inversion.
- Exploring the effectiveness of the workflow, to compare the residual geological parameter error against the model error, and also to measure the upscaling error using the 4D seismic data as truth.
- Investigating the parameterisation scheme (the pilot point method) and how the residual error compares to scale-dependent errors.
- Designing an optimum filter for production-data noise estimation. The wavelet transform is used to measure data error.
- Identifying an appropriate history matching scheme that makes the most of the seismic data and updates the model parameters effectively.
- Investigating the value of seismic analysis in reducing forecasting uncertainty.

1.6 Content of the thesis

Chapter 2: A brief description of the principles of time-lapse seismic analysis as well as history matching is given. The main challenges of integrating these two disciplines are outlined, followed by a discussion of how they lead to a better reservoir model. A variety of literature published on seismic history matching are reviewed. The range of issues for

the application of SHM are summarised, and a sequential description of its evolution given.

Chapter 3: A full description of the seismic history matching approach used in this thesis is provided. Issues such as the Bayesian approach, the quasi-stochastic optimisation algorithm used, the different components of the objective function and the domain of comparison are discussed.

Chapter 4: The aim of this chapter is to answer two questions: can we use the pilot point method to update permeabilities, and how does the residual error compare to scale-dependent errors? A description is given of how some synthetic test cases were set up to validate the history matching and parameterisation schemes. Scale-dependent model error is discussed, along with a determination of whether it is indeed possible to convert the initial model to match the observed data.

Chapter 5: This chapter describes the Schiehallion field, which is used for applications to the SHM approach, including geological settings, reservoir and management characterisation, time-lapse seismic acquisition and model construction.

Chapter 6: This chapter provides an overview of the selected area from the Schiehallion field (Segment-4) for seismic history matching application. The 4D response in the reservoir is described, and a description of the data analyses of the history data (production and seismic) is presented.

Chapter 7: In this chapter, an optimisation of the use of historical data, particularly time-lapse seismic data during history matching, is sought. How the choice of model parameters is guided is shown: a multi-dimensional inversion technique is used, based on calculated misfits between observed and predicted data. The method is then demonstrated by applying it to the UKCS Schiehallion reservoir, using six years of production data and six seismic surveys. An upscaled version of the operator's model is updated.

Chapter 8: A study is presented in this chapter that follows up on previous work investigating the value of seismic analysis in reducing forecasting uncertainty. The aim here is to look at the reduced uncertainty obtained in the Schiehallion field when 4D seismic data is added to the history matching procedure. Changes to parameters are looked at, and some of the best models are then used to predict the behaviour of an infill well. The accuracy of history match predictions and the impact of time-lapse seismic data for an infill well placement is quantified. This is then compared to an earlier study, in which there was no historical data with which to validate forecasting.

Chapter 9: In this chapter, NTG is predicted using two baselines: 1993 seismic and 1996 seismic data. Before history matching to dynamic data, the model is first modified to match the observed baseline RMS (root mean square) amplitudes of the migrated stack quantitatively. In addition, different combinations of the parameter space are looked at, such as: permeability and "Net:Gross" and its effect on the uncertainty of the model's predictability. The results show a good match to the observed seismic and dynamic well data with significant improvement to the base case.

Chapter 10: Finally, the thesis ends with a summary, conclusion and recommendations for further work.

CHAPTER TWO

Automated Seismic History Matching: An Overview

The purpose of this chapter is to give a brief description of the principles of time-lapse seismic analysis as well as history matching, and to outline the main challenges of integrating these two disciplines in order to produce a better reservoir model. A variety of literature in the area of seismic history matching is reviewed, summarising the various issues for its application. Also provided is a sequential description of the evolution of the technique. Finally, the concept of history matching and the basic formula and development process of automatic history matching is reviewed.

2.1 Overview of seismic history matching

Seismic history matching (SHM) is an automatic procedure for matching both production and 4D seismic data. By combining the excellent areal resolution of the seismic data with the sparser data from wells, which include production rates and pressure measurements, it is anticipated that the parameters of the reservoir model can be more accurately estimated. Additionally, the procedure has many possible benefits in the reduction of uncertainty for forward predictions from reservoir simulation and hence better economic forecasts. A number of such SHM schemes have been developed, such as in the studies presented by Huang *et al.* (1997) integrating time-lapse seismic and production data in an automatic scheme. Huang *et al.*'s case study used two volumes of 'off-the-shelf' data from the Gulf of Mexico, with a time difference of five years. The objective function was defined as a linear combination between the production and the 4D seismic objective functions. The inversion was run in two independent stages: in the first stage, a global parameter (relative

permeability for water as a function of saturation, since the laboratory data consisted only of the end of this curve) was determined, while in the second stage a local parameter (grid block porosity) was obtained to capture the reservoir heterogeneities.

The type of time-lapse seismic data used for property estimation has varied among researchers, as shown in Table 2.1. Huang *et al.* (1997) used amplitude difference or other seismic attributes differences, while Arenas *et al*. (2001) used velocity difference. Gosselin *et al*. (2003) assumed that pressure and saturation changes were available. Landa and Horne (1997) also assumed that saturation changes could be obtained directly from time-lapse surveys. Whereas a number of geophysicists (Tura and Lumley, 1999; Landrø, 2001; Meadows, 2001) obtained changes in saturation and pressure directly from time-lapse seismic data (including offset data).

Favergik *et al.* (2001) used SHM in the North Sea Tordis field, where two seismic surveys were available. A general agreement was obtained between the modelled change in oil saturation and that suggested by the 4D seismic data observations. The seismic dataset was used in this case to modify fault transmissibility multipliers in some areas where local discrepancies were observed.

Mantica *et al.* (2001) and Mantica *et al.* (2002) presented another automatic history matching for production and seismic data. This combines global and local inversion algorithms. In their approach, the inverse problem was tackled by approximating the solution in a two-stage process: a stochastic algorithm was used in order to sample the parameter space, avoiding the entrapment of local minima, and then a gradient method was used to refine the searched parameter space.

Waggoner *et al.* (2002) and Cominelli *et al.* (2002) used 4D seismic information to constrain the automatic history matching for a gas condensate reservoir, applying a global inversion technique. It was shown that the predictability of the best model obtained using the SHM technique was improved to identify new fluid barriers through a new reservoir

porosity model. Time-lapse seismic analysis with a considerable amount of production data was handled for the inversion, showing a minor improvement in the final history-matched reservoir model. They used acoustic impedance difference derived from time-lapse seismic data (Waggoner *et al.* (2002).

An interesting study was conducted by Arenas *et al.* (2001) using the pilot point method. As a result of using this method, the parameter space is reduced considerably, and the inversion approach is faster.

In 2003, the software package SIMOPT-ECLIPSE HUTS (History Matching Using Time-lapse Seismic) became available commercially. This software was the result of a two-year joint industry project which focused on the quantitative use of 4D seismic data in the history matching process. The results of the implementation of this technique were shown, and it was tested in various cases (Aanonsen *et al.*, 2002; Gosselin *et al.*, 2003; Aanonsen *et al.*, 2003). Bogan *et al.* (2003) used multiple time-lapse seismic attributes, including velocity, impedance and amplitude, in a GOM (Gulf of Mexico) field to estimate fluid flow barriers, facies parameters and variogram structures.

Gosselin *et al.* (2003) tested automatic history matching with both production data and time-lapse seismic data, using a gradient-based inversion method. Kretz *et al.* (2004) used the gradual deformation method.

Pannett *et al.* (2004) matched synthetic amplitude data generated using software based on some rock physics parameters. Mezghani *et al.* (2004) used acoustic impedance in history matching together with production data. The finite perturbation method was used to compute the required derivatives. Dong and Oliver (2005) matched both seismic impedance change data and production data in a medium-scale problem. The adjoint method was used to compute the gradient, and the LBFGS (Limited memory Broyden–Fletcher–Goldfarb–Shanno) method for search direction calculations.

Mezghani *et al*. (2004) presented a joint inversion scheme for estimating petrophysical properties by integrating both production and the history matching of production data; 4D seismic-related data leads to a better prediction of petrophysical reservoir properties and production forecast. Stephen *et al.* (2004), with a 4D seismic attribute and a stochastic Neighbourhood Algorithm (NA) (Sambridge, 1999a) in a multi-dimensional inversion technique, have used normalised impedance.

In 1994, Evensen (1994) introduced the ensemble Kalman filter (EnKF) as a modification of the traditional Kalman filter which could be applied to non-linear systems. It outputs a set of estimated models suitable for uncertainty analysis. Skjervheim *et al.* (2005) outlined how the ensemble Kalman filter method could be used to update a combined reservoir simulation/seismic model using the combination of production data and inverted 4D seismic data.

So far we have illustrated chronologically the evolution of the technique in the industry. possibly a more interesting perspective can be obtained by comparing the achievement, methodology and some results of the different studies published to date in order to have a better understanding of the progress, difficulties and expertise gained from using the technique.

In previous studies, the grid of comparison between observed and predicted changes on impedances are either on the reservoir simulation scale (after upscaling, see Waggoner et al., 2002; Aanonsen et al., 2002) or in the geological scale (previous to upscaling, see Mezghani et al., 2004). However, there is a need to find alternatives to these approaches, since for instance, the correlation lag for the data errors may be shorter than the size of the simulator grid cell. The optimisation procedure has been approached in the past using local and global methods, but there is no uncertainty analysis on the estimates. By introducing bayesian techniques in this thesis, there is quantification on the possible range of predictions after the inversion of any parameter. In all the previous work the domain of comparison is either the fluid saturation domain (i.e. Favergik et al., 2001; Mantica et al., 2001) or the impedance domain (i.e. Aanonsen et al., 2003). In case that the observed seismic is coloured inversion stack, even though the changes in amplitude reflect the

changes in impedances, there is a normalisation step previous to comparison. This allows the possibility of incorporating seismic reflectivity information into the seismic history matching workflow, without the implementation of seismic inversion.

Paper (Author, year)	Field or area	Type of fluid	Seismic attribute of comparison	Inversion Type
Huang (1998)	Gulf of Mexico	Oil	Reflectivity	Global and local
Favergik (2001)	North Sea	N/A*	Fluid saturation	Gradient and simulated annealing
Mantica (2001)	PUNQ-S3	Oil	Fluid saturation	Global and local
Waggoner (2002)	Gulf of Mexico	Gas condensate	Impedance	Global
Arenas (2001)	Synthetic	N/A*	P-wave	Levenberg–Marquardt
Kretz (2002b)	PUNQ-S3	Oil	Fluid saturation	Gradual deformation
Aanonsen (2002)	North Sea	Oil	Impedance	Gradient
Gosselin (2003)	Adriatic Sea	Dry gas	Impedance	Gradient
Stephen (2004) and (2006)	UKCS	Light oil	Normalised pseudo-impedance	Neighbourhood algorithm
Skjervheim *et al.* (2007)	North Sea	Oil	Impedance	Ensemble Kalman filter (EnKF)

* Not mentioned

Table 2.1: *Summary of publications related to seismic history matching.*

2.2 4D seismic analysis as a new reservoir monitoring tool

Time-lapse seismic analysis consists of multiple seismic surveys, which can be 2D, 3D, VSP (Vertical Seismic Profiles) and cross well seismic, acquired at various times for the same reservoir. Generally, the first survey is called the baseline survey, and subsequent surveys are monitor surveys. Seismic data is sensitive to both static properties (such as lithology and porosity) as well as dynamic fluid flow related parameters (for example permeability and porosity) via pressure and saturation changes. By comparing seismic data obtained from surveys at different times, it is possible to infer the dynamic changes arising from pressure and saturation redistributions because of production.

2.2.1 The definition of 4D seismic

4D seismic is the difference between two (or more) 3D surveys taken at different calendar times over the same reservoir. The baseline survey is usually carried out before production starts in the field, and the monitor is obtained after several years of production. By first processing each survey using standard approaches for 3D seismic, then taking the difference between the monitor and the baseline (Figure 2.1), very useful information can be obtained from 4D seismic for the reservoir engineer regarding how the reservoir has been affected by production.

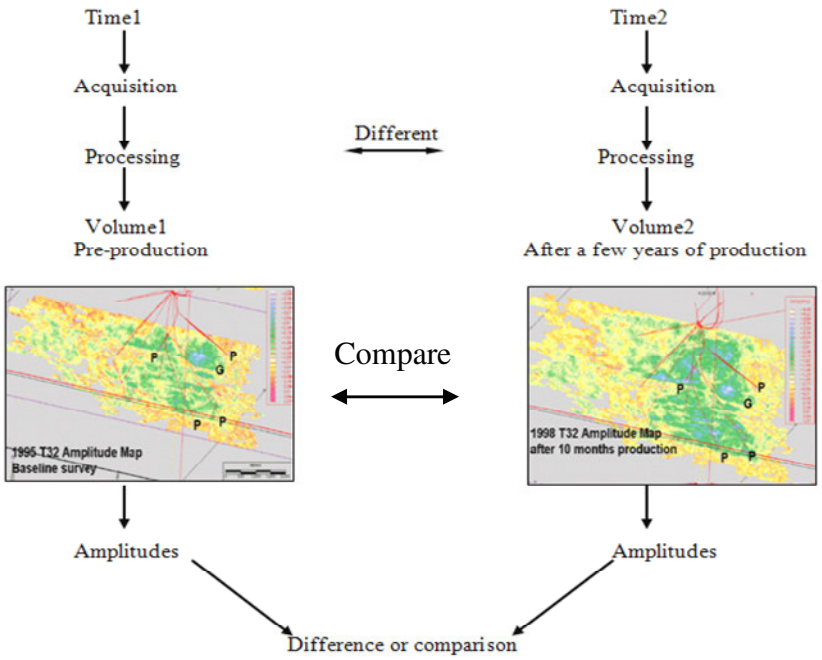

Figure 2.1: *Processing stages for 4D seismic. Amplitude maps of the T32 reservoir in Foinaven for the baseline (left) shoes the pre-production survey and after 10 months of production (right). (after O'Donovan et al., 2000).*

It is imperative for the industry and for consumers that this remaining oil is produced as reliably and efficiently as possible. If we do not know what is occurring in our reservoirs, we cannot hope to produce them optimally. 4D examples from the North Sea Gullfaks field (Figure 2.2) can be used to explain the simple physical principles of the 4D seismic. If we compare the baseline survey with the monitor survey, this obviously clarifies the effect of production specifically. Changes in both pressure and fluid saturation are expected during the field life. The fluid substitution that occurs during the production of hydrocarbon reservoirs changes the compressibility of the pore fluids, thus changing the bulk velocity. In water flooding, the injected water increases the overall compressibility of the rock and its contents, raising the velocity (Figure 2.3). In water injection, for instance, the substitution of oil for water increases the P-wave velocity, but increases pore pressure. The magnitude of these changes is controlled by the physical properties of the rock frame and

the fluids. Figure 2.4 illustrates the net effect of pore pressure and fluid saturation changes on acoustic impedance (AI), which is a function of density and P-wave velocity and therefore has a combined response to pressure and saturation change. The time-lapse seismic response in general is a combination of these two effects (e.g. pressure and fluid saturation changes).

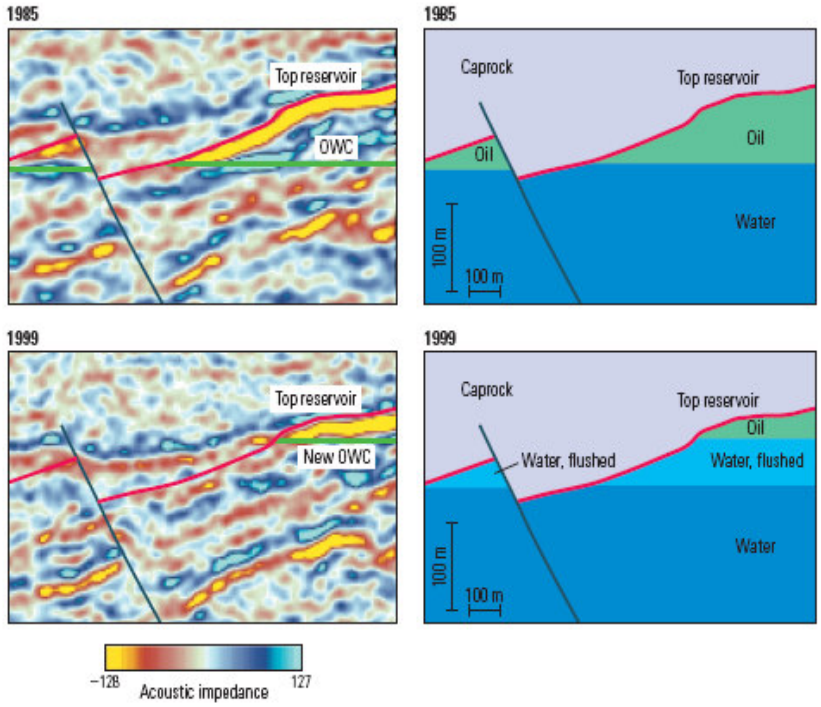

Figure 2.2: *The changes in seismic reflection amplitude between two surveys (1985 and 1999) due to production. The difference in the signal strength of the top of the reservoir is related to a decrease in oil saturation and the original oil-column height. The strong seismic response from oil–water contact (OWC) in 1985 has also been dimmed by oil production. In the left panels, red and yellow represent a reduction in acoustic impedance, while the blues correspond to an increase (Traine et al., 2002).*

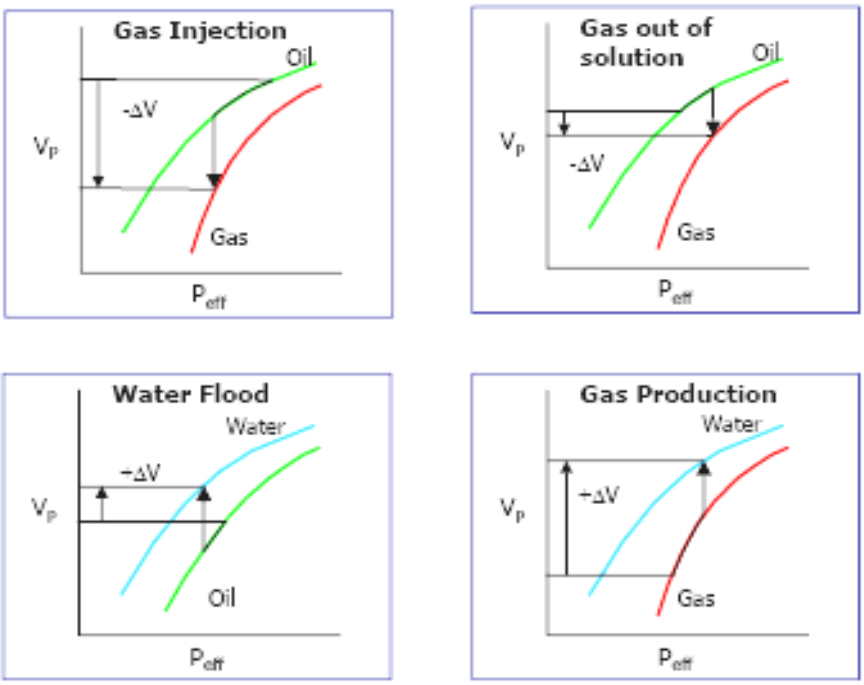

Figure 2.3: *Effects of production processes on P-wave velocity (after Waggoner, 2000).*

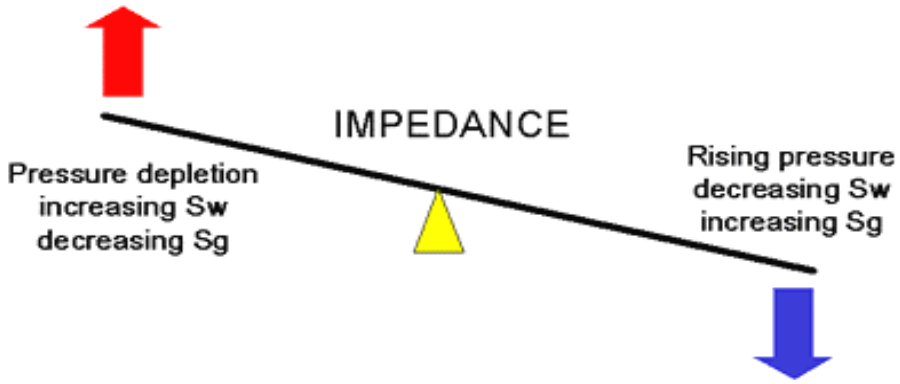

Figure 2.4: *Change in acoustic impedance (AI) in response to production and injection (after Marsh, 2004).*

With time-lapse 3D seismic, information regarding changes in the reservoir is provided by the difference between surveys, and these differences are related to reservoir changes as long as the seismic measurements are repeatable. By using an acquisition set-up similar to the previous seismic survey(s), the reservoir is similarly sampled.

2.2.2 Feasibility study

Feasibility studies are designed to examine various reservoir properties, such as fluid saturation contrast and dry bulk modulus and it is important for several purposes. Firstly, they indicate whether a time-lapse seismic survey is likely to succeed given the reservoir parameters, the base survey quality and acquisition repeatability. Secondly, indicate the optimum timing for a repeat survey. Finally, they form an important part of expectation management, indicating to the asset team which production features are likely to be observed and which are not. Lumley *et al.* (1994, 1997) gave an excellent discussion about which types of reservoirs tend to be good candidates for time-lapse seismic projects which will have the features listed in tables 2.2, 2.3 and 2.4.

Property	*Property type*	*Optimum cases*
Reservoir	Depth	Shallow
	Overburden pressure	Low
	Pore pressure	High
	Net pressure	Low
	Temperature	High
	Unit thickness	High
Rock	Dry bulk modulus	Low
	Dry density	Low
	Porosity	High

***Table 2.2**: Ideal parameters of reservoir and rocks in time-lapse seismic analysis: Part I (Lumley et al., 1997).*

Property	*Property type*	*Optimum cases*
Oil	Solution GOR (gas oil ratio)	High
	Gravity	High
	Density	Low
	Bulk modulus	Low
Water	Salinity	High
	Density	High
	Bulk modulus	High
Gas	Density	Low
	Bulk modulus	Low
Time-lapse fluids	Fluid saturation change	High
	Fluid saturation contrast	High

***Table 2.3**: Optimum parameters for reservoir fluids in time-lapse seismic analysis: Part II (Lumley et al., 1997).*

Seismic properties	*Optimum cases*
Dominant frequency	High
Average resolution	Low
Image quality	High
Fluid contact visibility	High
Predicted travel time changes (samples)	High
Predicted impedance change	High

***Table 2.4**: Ideal parameters for time-lapse seismic qualities: Part III (Lumley et al., 1997).*

2.2.3 Repeatability study

Repeatability does not mean that data from multiple seismic surveys should be as similar as possible everywhere; the most important purpose of time-lapse seismic is to highlight the changes due to production. Repeatability is a problem caused by variations in acquisition noise or because the environment has changed over time, e.g. when new production facilities are installed. Seismic (re-)processing thus plays a key role in equalising the responses over the static parts. To test how repeatable the time-lapse seismic data will be in a possible survey area, i.e. how strong the non-repeatable noise is, a zero-time repeatability study (Porter-Hirsche and Hirsche, 1998) is sometimes employed. 4D difference noise' can express itself either as coherent or incoherent noise. For example, if surface statics vary between surveys and are not accurately removed, seismic events will not cancel out properly, leaving residual coherent energy in the 4D difference section. A similar effect might be observed with the incomplete cancellation of groundroll, or variations in marine multiples due to tides. Incoherent events are caused, for example, by acquisition changes such as variations in ground coupling, and by environmental noise (which by definition does not repeat). If the monitor survey is too different from the base survey the 4D difference noise may overwhelm the production-induced signal. It is therefore important that the level of 4D difference noise can be assessed and compared to the expected 4D signal before investing in a repeat survey

. If the magnitude of expected seismic changes due to production does not go above the threshold noise, the prospect of a successful time-lapse seismic survey is low.

2.2.4 Cross equalisation

Feasibility and repeatability studies provide well-built assurance for 4D seismic success. A typical situation is that the baseline survey and the monitor survey are taken from two seismic surveys in the same field. It is not uncommon to find acquisition systems differing, with geometrical coordinates not aligning and data processing using different parameters. Since it is not practical to reshoot the surveys, the only feasible way to reduce these artificial distinctions is through reprocessing the data, applying cross equalisation.

According to Ross *et al.* (1996) and Rickett and Lumley (2001), cross equalisation is the process of match-filtering, amplitude scaling and static corrections necessary for time-lapse seismic analysis in order to take out non-production changes from acquisition and processing. Cross equalisation is necessary when a time-lapse seismic project engages inheritance data, but it also aids a well-designed project by fine-tuning some minor inconsistency between surveys (Dong, 2005).

2.2.5 Advantage of using time-lapse seismic data

Time-lapse seismic data may provide the changes in dynamic parameters (saturation and pressure) with time. Fluids (brine, oil and gas) within the reservoir could change dramatically when an enhanced oil recovery process is used. In contrast, for CO_2 or gas injection, these fluids displace the hydrocarbons, increasing the overall compressibility of the rock and lowering the velocity. Gas is a highly compressible fluid, and therefore, if pressure drops below the bubble point, gas will be released from oil-saturated rock, and velocity and density will substantially decrease (see Waite and Rusdinadar, 1997; Waite *et al.*, 1997; Benson and Davis, 1998). The effect of temperature changes in thermal EOR processes has been measured for different values of hydrocarbon saturation (Wang and

Nur, 1988), showing that the laboratory compressional wave velocities in the hydrocarbons decrease with increasing temperature.

2.3 An overview of reservoir simulation

Reservoir models are very important tools in the petroleum industry and are used by engineers to estimate the amount of oil available from a specific reservoir and to maximise oil recovery. Reservoir simulation is routinely employed in the petroleum industry, and the basic theory has been summarised by Aziz and Settari (1979) and Ewing (1983). In order to be represented in the mathematical model, the petroleum reservoir is divided into cells that make up a simulation grid. Traditionally, reservoir models were constructed by reservoir engineers with the input of geologists and geophysicists. The reservoir engineer is responsible for entering the data into the reservoir simulator and for obtaining a match of the production history. Most of the time, this match is achieved by modifying the rock properties in some regions of the reservoir, usually porosity and permeability. Porosity measures the capacity of the rock to store fluids, whereas permeability measures the capacity of the rock to allow the movement of fluids within it. Recent trends in reservoir characterisation aim to generate models automatically that honour the production history and satisfy our prior knowledge of the reservoir without the subjective intervention of the user to achieve the match. To run a reservoir simulation, it is necessary to:

- Define of a geological model of the reservoir including the distribution of the reservoir parameters within that model by a complete integration of all datasets available such as, well wirelog, well flow testing, seismic data interpretation and outcrops analogue models.
- Define the most appropriate gridding for subdivision of the model into blocks, and the estimation of the fluid transmissibilities between these interblocks. If present, the aquifer must be also defined; in terms of geometry, zonation, spatial distribution of blocks properties, initial saturation and pressures.
- Gather and input the fluid and rock (PVT and petrophysical properties) data.

- Choose certain numerical features of the grid, such as the number of cells and time steps.
- Set up the correct field well controls, such as rate and pressure.
- Choose the preferred output to print the flow simulation.
- Prediction of the reservoir behaviour under any future development program that the geoscientist may wish to identify.

Figure 2.5 illustrates this schematically. Four basic oil recovery mechanisms can be identified: fluid expansion, displacement, gravity drainage, and capillary imbibitions when pressure declines and fluid expansion induces flow through the porous rock to the production wells. Displacement occurs because of injected gas or water.

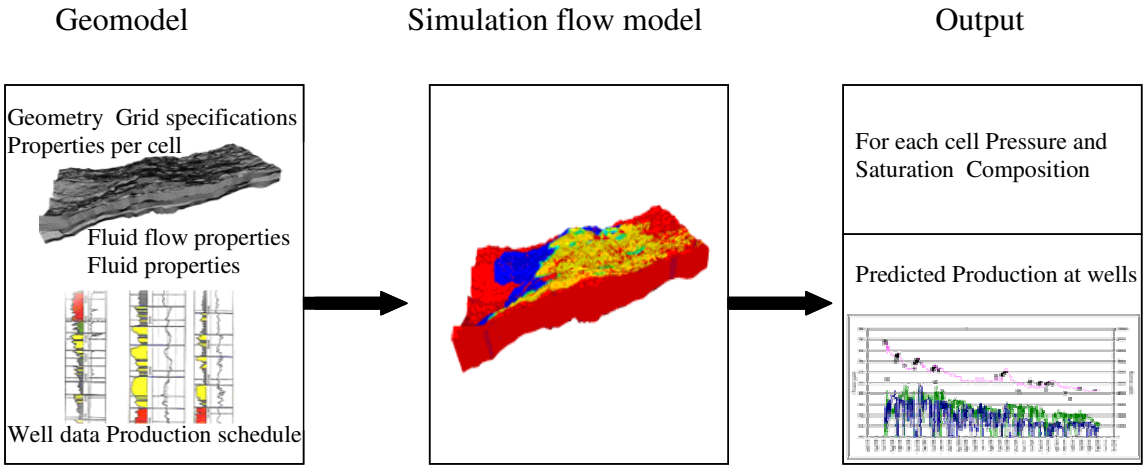

Figure 2.5: *Flow chart of mathematical simulation conditions.*

2.3.1 History matching

The observed historical data, such as well tests, production data measured at the wells, and time-lapse seismic data, has to be used to constraints. The reservoir model is run either manually or in an automated loop. Fluid flow is simulated for the model, and a comparison is made between the simulated production behaviour and the observed behaviour. Reservoir parameters are perturbed until agreement between modelled and observed behaviour is reached. This inversion procedure is called history matching. History

matching in general is an ill-defined problem with non-unique solutions. Given production data from an actual field, it is possible to construct many reservoir models that can differ significantly from each other. Nevertheless, a history match can be achieved, particularly in determining optimal well placements (Guyanguler and Horne, 2001; Yeten *et al.*, 2002a) and optimising well-rate controls (Brouwer *et al.*, 2001; Brouwer *et al.*, 2002; Brouwer *et al.*, 2004; Yeten *et al.*, 2002a; Yeten *et al.*, 2002b; Sarma *et al.*, 2005; Sarma *et al.*, 2006).

2.3.2 Model forecasting

The main aim of this stage is to study future possibilities and select those that maximise recovery. A major problem is uncertainty quantification. It is always challenging to reduce and quantify reservoir prediction uncertainty. The non-uniqueness of history matching makes the forecasting more difficult, and the incompleteness of information forces reservoir engineers to interpret beyond the data. Such interpretations are subject to personal experience and intuition and are associated with a great deal of uncertainty.

2.4 Automated history matching

Automated history matching is becoming standard technology for several reasons. Computers are getting faster, and data storage capacity is becoming much greater and cheaper. With an automated procedure, it is possible to assemble multiple models and analyse uncertainty rather than work with one deterministic model. Constraining the different models to the observed data is work-intensive unless (semi)-automated procedures are introduced.

A mathematical solution to the history-matching problem may be a non-physical model that is significantly different from the input model. The key challenges are how to identify the misfit function between modelled and observed data, how to parameterise the model, how to optimise the inversion parameters and when to stop the iteration procedure. To handle and lock up the models to the large amount of seismic data, computer power is required.

2.4.1 Top–down reservoir modelling

Top–Down Reservoir Modelling (TDRM) is an integrated workflow developed by British Petroleum (BP) to integrate history data into reservoir simulation models that enable a faster and stronger exploration of uncertainty. The Top Down philosophy is *"to start investigations with the simplest possible model and simulator appropriate for the business decision"*. (Williams *et al.,* 2004). TDRM has become BP's standard method for performing history-matching studies with conventional well data.

The TDRM approach aims to fully explore reservoir uncertainty through generating multiple reservoir descriptions that match both well-based and 4D seismic observations. A search is made over a large number of reservoir parameters, an uncertainty space with dozens of dimensions. The parameter values controlling properties in the simulation model are adjusted to match the observed data. These parameters are typically the same ones that might be tuned in a manual history match, such as reservoir pore volumes and/or permeabilities, aquifer strength or fault transmissibilities (Walker *et al*., 2006).

Only a few such parameters can be tuned at one time in a manual history match, owing to the complexity of interactions that take place between these parameters in the reservoir model. A Genetic Algorithm (GA) inversion has been used in the TDRM workflow to assisted history matching in the direction of tuning all chosen parameters together to provide sensible fits to the available well and 4D seismic data. The TDRM approach has been successfully applied to eighteen BP reservoirs, such that risk has been reduced through a better understanding of the uncertainty, and faster works cycle time means that an increase in the estimated net present value of up to 20% has also been achieved (Williams *et al*., 2004).

2.4.2 Parameterisation

In history matching procedures, the most crucial step is the parameterisation. The reservoir simulation model is defined by a large set of parameters, for example, porosity,

permeability and NTG, some of which are specified for each grid block, while others apply to the entire model such as, fault transmissibilities . Perturbing all parameters is not feasible from a computational perspective. The parameter space must be reduced by defining only a few parameters to be perturbed. The selection of these inversion parameters must be limited to those parameters that have a first-order impact on the reservoir. The selection of these parameters is often based on the reservoir engineer's experience. Parameters with a high degree of uncertainty should be selected. For example, the porosity near a well should not be selected, as it is already known to within a few tenths of a percentage. Sensitivity and uncertainty analyses are often a requirement before the inversion parameters are selected in an automated manner. The parameters obtained by inversion in SHM change between studies. Huang *et al.* (1998) undertook this problem, focusing on a first-order global parameter such as water relative permeability for inversion, and later modified a second-order parameter (porosity). In other cases (Arenas *et al.*, 2001) pilot points were used in order to control the areal distribution of horizontal permeabilities. As a result of this method, the parameter space was reduced significantly and the inversion approach was faster. In Waggoner *et al.* (2002), the parameter optimised was porosity distribution throughout the reservoir. Many parameterisation approaches have been proposed in the petroleum engineering literature, and will be explained in more detail in the following sections. See the summary in Table 2.1.

2.4.2.1 Pilot point method

One of the first geostatistical parameterisation techniques was introduced by Marsily *et al.* (1984): it is often referred to as the Pilot Point Method or the Master Location Method. This technique was extended later by RamaRao *et al.* (1995) and Gomez-Hernandez *et al.* (1997) for the calibration of permeability fields to pressure data.

The values of the properties at pilot points are regarded as unknowns, which are progressively adjusted to minimise the objective function. Pilot points were used to control absolute permeability and Net to Gross (NTG) multipliers at the pilot points. The

multipliers are interpolated using Kriging with a defined variogram range in order to obtain a lowest misfit. (Kriging is used to interpolate changes to permeability – see Appendix 1.)

The pilot point method allows a reduced number of parameters while honouring the prior constraints; provided that the pilot point locations are not too close to each other, the values are modified without accounting for possible correlations (Figure 2.6). It is also possible to fix values at some pilot points when hard data is available, such as at wells. The parameter must be conditioned to both the new values at the pilot point and the unchanged values at the wells. Backer *et al.* (2001) used the same synthetic test as Floris *et al.* (2001), who focused their investigation on sampling the history matching of multiple realisations using the pilot point method. A study was also conducted by Arenas *et al.* (2001) using the pilot point method approach.

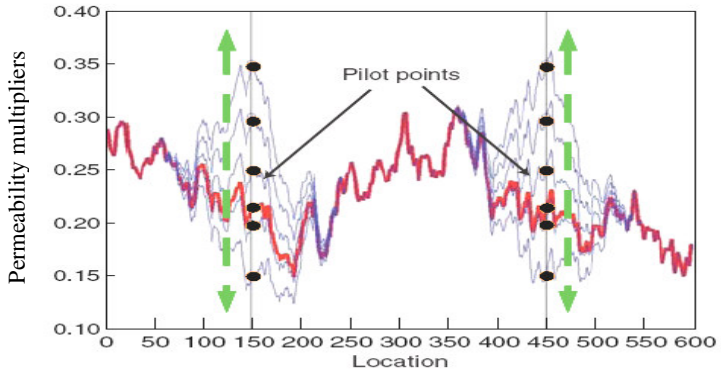

Figure 2.6: *Applying the pilot point method to change the values of points at locations 150 and 450 for a one-dimensional realisation of a normal random function (Le Ravalec-Dupin and Hu, 2007).*

2.4.2.2 Geostatistical methods

Geostatistical methods are widely used to characterise heterogeneity and to generate realisations of spatially variable property fields. A number of interpolation methods (e.g. Kriging) and simulation techniques (e.g. sequential Gaussian simulation and sequential indicator simulation) may be incorporated on the basis of the modules. Internal generation of the heterogeneous property field and its mapping onto the numerical grid make geostatistical parameters accessible to estimation by inverse modelling (Deutsch and

Journel, 1992). This means that geostatistical parameters such as the correlation length can be adjusted automatically to match pressure and concentration data directly. The geostatistically generated property fields can be conditioned according to given values at certain locations, and honour measured values.

Sequential Gaussian Simulation

Stochastic simulation techniques have become popular as a way of generating numerical models that better represent subsurface heterogeneities. Sequential Gaussian Simulation (SGS) comprises an algorithm for simulating a signal attribute using values of only that attribute, then accounting for secondary information (Goovaerts, 1997). The theory behind SGS is based on using each and every one earlier-simulated value and on input data throughout the simulation process. The basic idea is to generate models that mimic the spatial variability expected in the reservoir. In stochastic modelling, this is achieved by generating samples from multi-dimensional random fields whose spatial correlation structure is analogous to that expected in the reservoir. Stochastic simulation is often said to be conditional in that simulated models are constrained with well log information, seismic data and other data types such as production profiles or well test data. After conditioning, multiple realisations can be fed into a fluid-flow simulator to evaluate uncertainty in production forecasts. SGS (Deutsch and Journel, 1992) is a frequently used algorithm. It can be used to generate realisations for one parameter, such as permeability.

2.4.2.3 Structural parameters: faults and barriers

During history matching, the structural and geological input to the reservoir model remains fixed. Given time-lapse seismic data, however, this procedure may differ. The dynamic content of time-lapse seismic data provides additional information on structural, geological and sedimentological characteristics. Barriers are likely to change the efficiency of fluid communication from one part of the reservoir to the next (e.g. Yielding *et al.,* 1999a). Within reservoir simulations, the effect of barriers on fluid flow is modelled using a

quantity called a 'transmissibility multiplier' (see Knai and Knipe 1998; Manzocchi *et al.*, 1999; Yielding *et al.*, 1999b). The properties required to determine transmissibility multipliers, in particular barrier zone thickness and barrier zone permeability, are usually not well understood or defined. Thus, barrier transmissibility multipliers are generally considered a great source of uncertainty for reserve estimation (Lia *et al.*, 1997) and for reservoir management. Most flow barriers compare quite well with the borders of channels or faults observed in 3D seismic analysis. However, there seem to be some additional barriers, probably related to local channel boundaries, that are not identifiable using only 3D seismic data.

2.4.3 Objective function

The objective function is defined to quantify the mismatch between the modelled and observed behaviour. The objective function enables the ranking of various model realisations. Furthermore, in automated history matching, the misfit function is used by the inversion algorithm to determine how to perturb the inversion parameters. During subsequent iterations, the objective is to minimise the misfit function. The objective function can also be used as a stopping criterion by defining a particular range.

Several types of objective functions exist, but the most commonly used is the sum-of-squares objective function. It calculates the sum of the squares of the differences between modelled and observed data.

In early studies in history matching (Jacquard and Jain, 1965; Jahns, 1966; Carter *et al.*, 1974; Chen *et al.*, 1974; Chavent *et al.*, 1975), only dynamic data was included, and the objective function was simply defined by the weighted norm or distance between the observed production data and predicted data. In history matching, this is an underdetermined problem since the amount of data is less than the number of model parameters adjusted. Therefore, regularisation techniques for inverse problems were introduced to obtain the non-uniqueness solution using additional information or

assumptions (Jacquard and Jain, 1965; Gavalas *et al.*, 1976; Jackson, 1979; Tarantola and Valette, 1982).

Time-lapse seismic data is very densely scattered and often available only at a limited number of time steps (Oldenziel *et al.*, 2002). The more information is added to the objective function, the better the history match obtained. Every piece of additional conditioning data reduces the non-uniqueness inherently associated with the inverse problem of history matching. The objective function is not limited to quantifying the differences between dynamic data – it can also be extended to include terms for quantifying differences in several other types of data, such as (1) a priori geological knowledge and (2) the shape, or trend, of a dataset. Most papers to date use the assumption of building a linear combination of the production and the seismic objective function:

$$O_T = w_P * O_P + w_S * O_S \tag{2.1}$$

where O_p represents the production misfit and O_S the seismic misfit. The weights w_P and w_S determine the internal construction of the total production misfit O_T. Aanonsen *et al.* (2002) used the maximum likelihood approximation for the objective function:

$$O_S(\underline{m}) = 0.5 * \left(p(\underline{m}) - d\right)^t C^{-1} \left(p(\underline{m}) - d\right). \tag{2.2}$$

In this postulation, m is the vector equivalent to the parameter space to be estimated, $p(m)$ is the predicted data (production or seismic), and d is the observed data (production or seismic). Here, C is the covariance matrix and represents the error in the data and the modelling.

2.4.4 Inversion algorithm

In the automated history matching procedure, an inversion algorithm is employed to find the smallest misfit. Efficient sampling of the parameter space may provide a solution. There is a wide variety of inversion methods, including global and local inversion methods. We define global and local in the following way. Consider some $f(x)$ where x lies between some maximum and minimum values, where these may be a physical boundary if we consider some sub-regions of x between x_1, x_2, then a local minimum of $f(x)$ may be an n-

dimension parameter space, or it could be three-dimensional geographical space describing the location of the reservoir. A global inversion strategy continuously updates the parameter model according to some range of prior probabilities. The objective function eventually converges to the global minimum (Corana *et al.*, 1987; Sen and Stoffa, 1995).

In local inversion methods, the solution is usually strongly dependent on the initial model; the inversion's cost function is prone to becoming trapped in a local minimum. Local methods are advantageous in that they are computationally fast, but they require accurate constraints as input. Local optimisers, such as a gradient optimiser, are not very well suited to handle varying objective functions and tend to be stuck in local optima. A gradient optimiser is capable of handling a certain amount of noise as long as large steps can be taken to calculate the gradient. Near the solution, the increments to calculate the gradients must be small, and the algorithm is then affected by the noise. A method used by many scientists, owing to its simplicity, is the steepest descent technique (Fletcher, 1987). This is known for its robustness, but its performance deteriorates as the solution is approached. More advanced methods require that the objective of the misfit function is twice differentiable.

The Gauss–Newton method is widely applied and uses an approximation of the second-order derivative (Fletcher, 1987). However, for highly nonlinear problems or if the initial guess is far from the solution, the algorithm may become unstable. The Levenberg–Marquardt method (Levenberg, 1944; Marquardt, 1963) uses a regularisation term to overcome this problem. This method may be regarded as a hybrid between the steepest descent method (away from the solution) and the Gauss–Newton (when the solution is approached). The difficulty lies in updating the Marquardt parameter, which is often based on empirical criteria. The Fletcher–Powell method (Powell, 1971) is also a hybrid between steepest descent and Gauss–Newton. All methods discussed above are local optimisers.

Global optimisers are more likely able to find the global optimum, but in general require a large number of function calls. Only when the number of iterations can be kept low are

these methods regarded as an alternative to local optimisers. The parameter space has to be sampled efficiently. Global inversion algorithms comprise simulated annealing and genetic algorithms. Genetic algorithms solve complex problems by emulating principles of biological evolution: the survival of the fittest (Goldberg, 1989).

A genetic algorithm comprises an initial population of individuals, each member represented by a binary string within computer memory. These strings represent chromosomes and contain the genes describing individual members of the population. A quality of fitness (objective function) is determined for each individual chromosome. The quality of fitness is used to determine the probability that an individual is permitted to reproduce. Breeding occurs by exchanging substrings of genes between parents, creating a new population. Over many generations, the population steadily increases in overall fitness.

Such methods can be classified under two main categories – deterministic and stochastic algorithms – which will be explained in more detail in the following two sections.

2.4.4.1 Deterministic methods

The main goal of history matching is to decrease the deviation between observed data and simulated results (i.e. objective function). Deterministic algorithms use straight inversion approaches and find one local-optimum reservoir model contained by the number of simulation iteration limits. The gradient of the objective function is consequently calculated, and the direction of the inversion search is after that determined.

Adjoint method

Most of deterministic methods need the calculation of sensitivity coefficients. Sensitivity is usually defined as the partial derivatives of the simulator output with respect to the parameters being attuned. The adjoint method needes derivations and solutions of adjoint equations, which generate the sensitivity of each production datum with respect to all the

reservoir model parameters. Such a system of adjoint equations is similar to the system of finite-difference equations in the reservoir simulator.

The adjoint method was applied to a water–oil problem by Wu *et al*. (1999) and to three-dimensional three-phase problems by Makhlouf *et al.* (1993). Rodrigues (2005) used the truncated singular value decomposition and adjoint method for sensitivity matrix calculations. Frequently, the computational time for adjoint equations in each time step is less than the matching time necessary for the forward simulation equations. Nevertheless, if the quantity of observed data is huge, this method is computationally costly and is not practical for real life problems.

Gradual, local and global deformation

Gradual deformation enables a gradual varying of the initial model, without compromising the geological continuity of the reservoir model, in anticipation of a history match is achieved. The gradual deformation method was initially developed for progressively changing Gaussian stochastic reservoirs models while conserving their spatial inconsistency (Hu, 2000a). It was afterwards extended to non-Gaussian reservoir models simulated from a sequential indicator (Hu *et al.*, 1999) and Boolean (Hu, 2000b; Le Ravalec-Dupin and Hu, 2007) algorithms. The gradual deformation method has been proposed as a history matching approach (Roggero and Hu, 1998). Various types of gradual deformation methods have been projected. The method of Hu *et al.* (2000) relies on a perturbation of the random numbers of a sequential simulation algorithm generating the geostatistical realisations. This method is adaptable in the common sense that any type of sequential algorithm can be used. Furthermore, variogram-based methods (e.g. sequential simulation) can be used. However.

Gradual deformation has received wide attention. Caers (2003) combined the gradual deformation method, multiple-point geostatistics and streamline simulation for history matching under a variety of geological scenarios. Liu and Oliver (2004) assessed the

gradual deformation method by comparing the distribution of conditional realisations for a small problem with the standard distribution from a MCMC (Markov chain Monte Carlo) method, with the results showing that gradual deformation produced an acceptable distribution. Hu and Jenni (2005) extended the application from pixel-based models (e.g. Gaussian-related stochastic models) to object-based models (e.g. Boolean models).

2.4.4.2 Stochastic algorithms

The advantages of applying stochastic algorithms are retained mostly by the massive computational time required. However, with an appreciation of the quick development of computer memory and computing speed. Stochastic algorithms have two main direct advantages. Firstly, the stochastic approach generates a number of reservoir models and therefore is more suitable to non-unique history matching problems. It is simple to quantify the uncertainty of performance forecasting by using these models. Uncertainty quantification through stochastic history matching has become a focus of interest at present. Secondly, with different local solutions from all the deterministic algorithms, stochastic algorithms in theory reach the global optimum (Liang *et al.*, 2007). In this section, we review the most representative methods, including genetic algorithms, simulated annealing and ensemble Kalman filter algorithms.

Genetic algorithms

Genetic algorithm (GA) procedures were developed by Holland in the early 1970s at the University of Michigan (Holland, 1975). The GA is a reproduction of biological principles of evolution, or 'survival of the fittest'. This means that the algorithm will continue to search around the best combinations of parameters to further improve the match and reject the inferior ones. GAs have been frequently and successfully used to tackle difficult multi-modal inversion problems (Liang, 2007).

After a number of generations (iterations), an ensemble of improved solutions is obtained. When applied to history matching, GA has been shown to be able to cope with multiple

optima while returning an ensemble of history-matched reservoir models in a single run (Floris *et al.*, 2001). This ensemble represents a mapping of those regions of the parameter space that have a low misfit value. An extra advantage of using GA is that it can be easily parallelised in order to reduce the required computation time. GA was first used in petroleum engineering in the mid 1980s (Goldberg, 1989).

Simulated annealing

Simulated annealing (SA) is a probabilistic algorithm for global optimisation problems. The name originates from annealing in metallurgy, a technique involving the heating and controlled cooling of a material to increase the size of its crystals. The heat causes the atoms to become unstuck from their initial positions and wander randomly through states of higher energy. The slow cooling gives them more chance of finding configurations with lower internal energy than the initial one. SA has been presented in the petroleum industry in many case studies. In particular, Panda and Lake (1993), Ouenes *et al.* (1993) and Portellaand and Prais (1999) have applied the SA technique to reservoir history matching.

Neighbourhood algorithm

The neighbourhood approximation (NA) algorithm is a stochastic sampling algorithm. NA was originally developed for solving a seismic waveform inversion problem in earthquake seismology (Sambridge, 1999a, 1999b), but it has recently been adapted to the problem of generating multiple history matching models in petroleum engineering (Christie *et al*., 2002; Subbey *et al*., 2002). The sampling of parameter space in this method is guided directly by the spatial properties of Voronoi cells. In particular, Christie and co-workers applied it to history matching and uncertainty quantification in some hydrocarbon production forecasts (Subbey *et al.*, 2004; Litvak *et al.*, 2005; Stephen *et al.,* 2006; Nicotra *et al.*, 2005; Christie *et al.*, 2006; Rotondi *et al.*, 2006; Erbas and Christie, 2007). More details can be found in Chapter 3.

Ensemble Kalman filter

The EnKF (Ensemble Kalman filter) is a Monte Carlo-type sequential Bayesian inversion and provides an approximate solution to the combined parameter and statistical estimation problem. The result is an ensemble of solutions approximating the posterior probability density function for the model input parameter (e.g. permeability and porosity), state variables (pressure and saturation) and other input data (e.g. well production history) conditioned to measured, dynamic data. The EnKF is an extension of the traditional Kalman filter (Kalman, 1960), which has been widely applied to the optimal control fields. The formulation used in EnKF reduces the nonlinear minimisation problem in a huge parameter space, involving the minimisation of an objective function with multiple local minima, to the statistical minimisation problem in the ensemble space. The EnKF has recently been utilised with simulation models for oil and gas reservoirs, with the purpose of estimating poorly known parameters and to improve the predictive capability of models. The EnKF, initially proposed by Evensen (1994), sequentially updates multiple models to capture the probability density function in the parameter map, such as the mean and variance of statistical information. The EnKF is a Monte Carlo method that does not require the adjoint equations and is independent of reservoir simulators. It updates an ensemble of reservoir models whenever new observations are available, starting with a given probability density function (PDF) of the state of the modelled system (the prior, often called the forecast in geosciences) (Figure 2.7). The final output is a set of 'history-matched' models, which are well-suited for uncertainty analysis. Reinlie (2006) used the traditional EnKF and conditioned local permeability information around the wellbore. Lorentzen *et al*. (2006) applied the EnKF as an inversion routine for controlling downhole chokes in smart wells with the aim of optimising water flooding. Their simple synthetic reservoir case demonstrated that the EnKF works robustly, and the results are in good agreement with their reference. With a streamline simulator, Park and Choe (2006) studied two issues: the low value of the estimate error covariance after some history matching periods, and the number versus quality of the measurement data.

Haugen *et al.* (2006) presented a successful application of the EnKF to a North Sea field case, using the production data. Similarly, Evensen *et al.* (2007) studied a North Sea case and investigated more parameters, including initial fluid contacts, vertical transmissivity multipliers and fault transmissivity multipliers. They discussed the non-Gaussian parameter distribution and pointed out that the EnKF is theoretically unrealistic if used directly on a multimodal prior, such as a reservoir consisting of channels.

Skjervheim *et al.* (2005) used the EnKF to incorporate 4D seismic data and showed that the EnKF could handle large seismic data and had a positive impact on matching the permeability field, even in a case with extremely noisy measurement data. Dong *et al.* (2006) used the EnKF for reservoir description to history match both production data and time-lapse 4D seismic data.

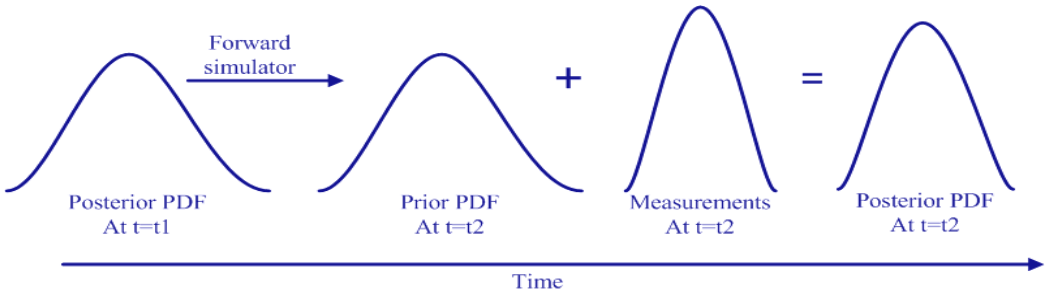

Figure 2.7: *Illustration of the EnKF from the viewpoint of Bayesian thought. Adopted from Liang, 2007.*

2.5 Summary

A comprehensive literature review of history matching, representative methods for deterministic and stochastic categories, and a wide number of applications have been presented in this chapter. A set of time-lapse seismic examples were given from early studies in the North Sea. The types of reservoir properties that are likely to change with calendar time in the life of a reservoir and, as a consequence of this, can generate a 4D

effect were also outlined. In terms of seismic history matching, literature on the topic has been comprehensively reviewed. This review was considered in terms of how different authors tackled the workflow, for example the type of inversion algorithm, components and combination of the objective function and domain of comparison were among the main issues in their seismic history matching approaches. The inversion techniques used in seismic history matching vary between the different works, and today, either global or local inversion algorithms can be used without difficulty. In all cases, it was shown that the incorporation of time-lapse seismic data into the inversion workflow improved the final estimations of the parameters that were inverted.

CHAPTER THREE

Quantitative Integration of Time-Lapse Seismic Data into Automatic History Matching: The Approach Used

This chapter contains a full description of the seismic history matching (SHM) approach applied in this study, where simulations are quantitatively compared to observe seismic and production data and then updated in an objective manner. It discusses the inversion algorithm used, the different components of the objective function and the domain of comparison and parameterisation.

3.1 Seismic history matching approach

A multi-dimensional quasi-global inversion approach was applied to SHM by Stephen *et al*. (2006). The technique fits within the category of inversion processes widely known as seismic history matching. In this technique (Figure 3.1), a group of static parameters of the reservoir model, such as porosity, permeability and fault transmissibility, are automatically updated in an iteration loop until the models produce a minimum misfit value. The objective function measures the differences between observations (this is represented as a combination of production and seismic data) and predictions, which are obtained through reservoir forecasting and seismic modelling. Prior history-matching time-to-depth conversion is used to create maps of observed seismic which can then be compared to predict seismic along with production data. The basic aims of this technique are:

- To improve the reservoir characterisation by adding additional constraints given by the 4D data.
- To quantify the model predictions and uncertainties via statistical parameters obtained after inversion (i.e. standard deviation, mean, etc).
- To understand the fluid-flow directional patterns throughout the life of the reservoir.

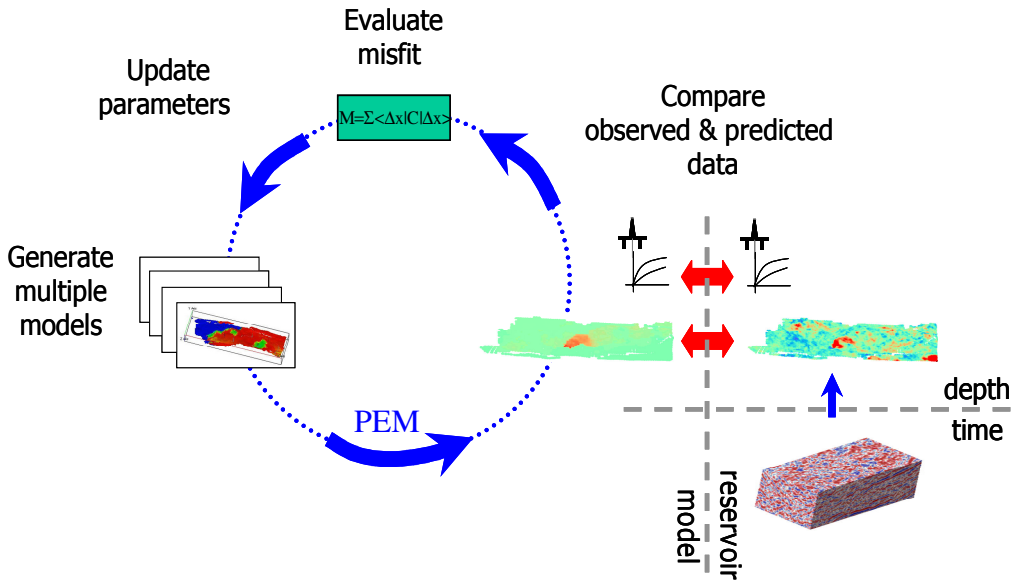

Figure 3.1: *Schematic of the iterative automatic history matching process.*

The workflow proposed (Figure 3.1): can be divided into a number of components:

- **Generation of Multiple Models:** In this study, the Pilot Point method is used with Kriging (e.g. de Marsily, 1984) to reduce the number of unknown permeability values in the model and to enable efficient updating. A number of cells are identified as pilot points and their properties modified independently, while neighbouring cells are updated using Kriging, effectively an interpolation. In this way Net:Gross (NTG), porosity and permeability parameters can be updated. Fault properties may also require modification. Fault locations are very difficult to determine as part of an automated scheme (Staples *et al.*, 2004) and perhaps should be defined during the model-building process. Their flow properties, the transmissibility multipliers, can be included in the seismic history matching process.

- **Seismic to Reservoir Model Comparison:** Impedances are predicted via a petro-elastic transform and converted to a map by vertical upscaling (Backus, 1962), then downscaled areally onto the seismic grid with inverse exponential distance weighting in order to compute the predicted impedances and compare them with the time-lapse seismic observations.
- **Evaluation of the Misfit:** A single misfit objective function is obtained for each model, incorporating a comparison between observed and predicted production and seismic data.
- **Parameter Space Exploration:** The neighbourhood algorithm (NA) is used. This process begins by randomly sampling the parameter space and calculating the misfits using the above three steps (Stephen *et al.*, 2006). Then a number of best models are selected, and their neighbourhoods are identified using Voronoi cells. New models are distributed randomly in the neighbourhoods of the best models, and new misfits are calculated. This process is repeated a number of times until the misfits are reduced to the minimum misfit. The misfit surface may contain many minima, with the NA samples correctly finding the global minimum and those that are local.
- **Uncertainty Analysis:** Using Bayes' theorem, the misfits provide the conditional likelihood of each model for the given data, and these are used to update prior model probabilities. The updated probabilities may be resembled using Markov chain Monte Carlo (MCMC) methods as part of the uncertainty analysis of the unknown parameters, giving a set of probability distributions. These probabilities can also be used as weights to determine the ensemble average and spread of variables such as saturation or pressure in each cell when predicting long-term reservoir behaviour. This is because the parameter space near the most likely models is refined.

3.2 Seismic to reservoir model comparison

Seismic P-wave impedance is defined as the multiplication of body density and P-wave velocity. If a rock is very hard to compress, its impedance will have a high value; if a rock is soft, it will have low impedance value. During production, elastic properties of reservoir rocks will change because pressure and saturation vary from time to time. For example, if a reservoir is under water-flooding conditions, its rocks usually become stiffer because water is generally more difficult to compress than oil. These changes in rock properties can be inferred through changes in seismic impedance data. On the other hand, some fluid flow parameters, such as permeability and porosity, may be indirectly inferred from changes in pressure and saturation distributions. It can be seen that seismic impedance is actually a bridge between permeability and porosity, and pressure and saturation distributions. Based on preliminary investigations by Dong and Oliver (2002), seismic impedance change data is used because it is relatively insensitive to variations in poorly constrained variables such as shaliness.

In this study, a petro-elastic model is used to convert changes in fluid saturations and pressures from the simulations into predicted impedances for each simulation cell. The stress dependency of the rock is captured in an empirical relationship (MacBeth, 2004), and Gassmann's equation (1951) captures the saturation effects. The resulting P-wave modulus is upscaled vertically over the reservoir interval approximately (one-quarter wavelength thick) using Backus averaging (1962) before calculating a map of impedances for the simulation grid. The observed seismic attribute consists of relative impedance, so observed and predicted attributes are normalised to the respective pre-production mean and standard deviation.

3.2.1 Petro-elastic transform

A petro-elastic model is used to convert changes in fluid saturations and pressures from the simulations into predicted impedances for each simulation cell, as shown in Figure 3.2. The stress dependency of the rock is captured in an empirical relationship (MacBeth, 2004):

$$\kappa^r_{dry} = \frac{\kappa^r_{\inf}}{1 + E^r_\kappa \exp\left(-P_{eff} / P^r_\kappa\right)} \tag{3.1}$$

where the superscript r identifies rock type (sand or shale), and the parameters κ_{inf}, E_κ and P_κ are determined from lab measurements or by history matching (Stephen and MacBeth 2006b) and represent the dry bulk modulus at Standard Temperature and Pressure, the excess compliance present in the rock as a result of geological or mechanical processes, and stress sensitivity, respectively. Here, P_{eff} is the difference between the overburden pressure and the pore pressure. It is assumed that the effective stress equals the differential. The shear modulus μ^r has the same form with equivalent parameters.

Shale is assumed to consist of a dry frame only, and the shear modulus is unaffected by saturation for both rock types. Sand is saturated, however, and therefore Gassmann's equation (1951) is used to obtain the saturated bulk modulus for each lithofacies within a cell:

$$\kappa^r_{sat} = \kappa^r_{dry} + \frac{(1-\alpha)^2}{\frac{\phi}{\kappa_f} + \frac{\alpha - \phi}{\kappa_g}} \tag{3.2}$$

where ϕ is the porosity, κ_g is the bulk modulus of the mineral, and $\alpha = (1-\kappa^r_{dry}/\kappa_{gr})$. Here, κ_f is the fluid modulus and is given by the saturation weighted harmonic average of the individual phase bulk moduli:

$$\frac{1}{\kappa_f} = \frac{S_w}{\kappa_w} + \frac{S_o}{\kappa_o} + \frac{S_g}{\kappa_g} \tag{3.3}$$

where S_w, S_o and S_g are the water, oil and gas saturations respectively, and κ_w, κ_o and κ_g are the water, oil and gas moduli respectively, obtained using Batzle and Wang (1992) and lab data for the field. MacBeth and Stephen (2008) discuss the scale dependence of this equation, suggesting an improved representation in cases where statistics of the fine scale properties of the reservoir are known. In this study, however, it is assumed that Eq. 3.3 may be applied and inaccuracies may be captured by model error analysis following Stephen (2007).

The P-wave moduli for sand and shale are obtained from $M^r=\kappa^r_{sat}+4\mu^r/3$, and the value for each cell, M^{cell}, is obtained from the harmonic mean of the sand and shale values, weighted by the respective fractional volumes via the Net:Gross ratio. This is valid for vertical propagation in a layered medium (Backus, 1962). Using this, the impedance for a column of cells in the simulation model is calculated:

$$I = \sqrt{<\rho>\left\langle \frac{1}{M} \right\rangle^{-1}} \tag{3.4}$$

where ρ is the bulk density of the cell obtained by averaging the densities of the rock frame and the fluid densities. The brackets < > indicate a vertical volume weighted average over the reservoir interval.

When observed seismic data is in the reflectivity domain and impedances are predicted, the datasets are normalised prior to comparison. It is assumed that the effect of changing pressure and saturation induces an equivalent relative change in the reflectivities and impedance throughout the reservoir. For each domain, the surveys are normalised by subtracting the mean of the baseline survey and dividing by the standard deviation. Predicted impedances can then be compared quantitatively to the observed equivalent seismic attribute without the need for a full inversion.

4D attributes are calculated from the observed data by integrating over the reservoir time interval. Observations consist of relative impedance, so both observed and predicted attributes are normalised, scaling by the spread for each to obtain:

$$a(t,x,y,z) = \frac{A(t,x,y,z) - \gamma^o_A}{\sigma^0_A} \tag{3.5}$$

where A is the raw attribute at time t, observed or predicted, prior to normalisation, γ^o_A is the areal mean of seismic attribute A calculated for the pre-production survey, and σ^o_A is the areal standard deviation of the attribute A calculated for the pre-production survey assuming equivalent pressure and saturation induced changes in both the observed and predicted data.

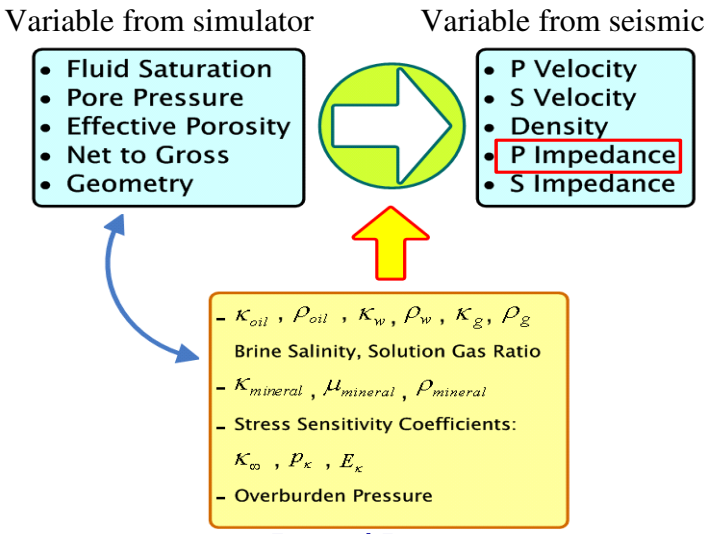

Figure 3.2: *Petro-elastic modelling scheme for seismic comparison (MacBeth, 2004).*

3.2.2 Scale dependence

Integrating simulation and seismic data is difficult because these are two different domains, each with its own geometry and resolution. Seismic grids are fine horizontally and coarse vertically when used as grids in reservoir simulators, as illustrated in Figure.3.3.

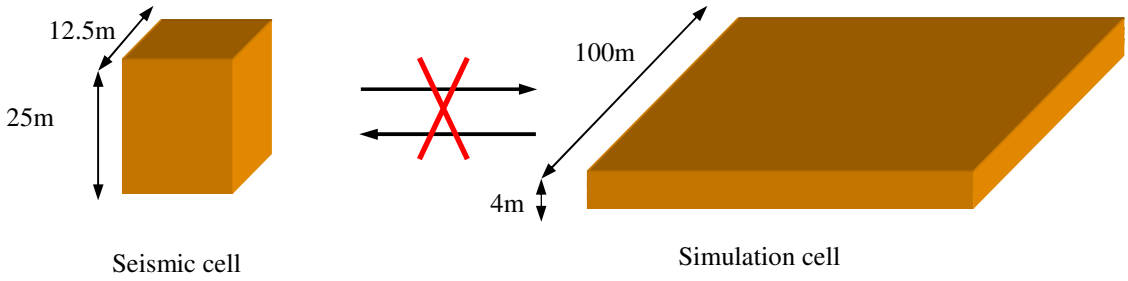

Figure 3.3: *The differences between types of seismic and reservoir simulation cells.*

Upscaling and downscaling is therefore required to bridge the gap between these two scales. Once the flow simulation model results are obtained, the elastic parameters of the reservoir are calculated for each cell through petro-elastic modelling to convert the simulation output into seismic attributes. Vertical upscaling is used (Backus, 1962) then

downscaled into the seismic grid with an inverse exponential distance weighting in order to compute the predicted impedances and compare them with the time-lapse seismic observations (Figure 3.4).

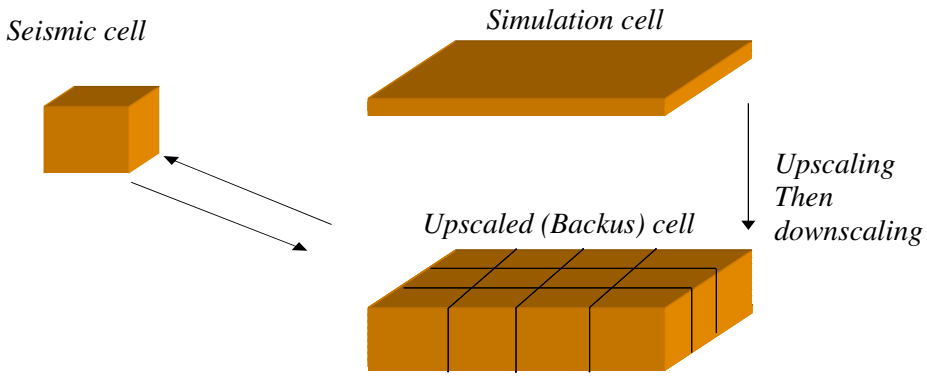

Figure 3.4: *Schematic of the process from the simulation to seismic scale, starting with upscaling synthetic seismic data vertically during petro-elastic transform, then downscaling synthetic data to the seismic grid horizontally.*

The observed seismic data is obtained as a set of points on a grid defined by the acquisition inline and crossline coordinates but also by the bin centre in UTM (Universal Transverse Mercator) coordinates (e.g. Figure 3.5). In this field study, the seismic and model grids are independent, although the latter are aligned at approximately 45° and sub-paralleled in phase II to the former. The bins are typically spaced by tens of metres (12.5 m in our field study), while the wavelet may sample 25 m vertically, the same as the predicted data. Some conversion is therefore required so that predicted and synthetic data can be compared: so far the areas are different but thickness is equivalent. The observed data could be upscaled areally, but it is preferable to interpolate the predicted data using an inverse exponential distance weighting. The interpolated impedance is obtained from:

$$\mathrm{I}_{\mathrm{ij}}^{\mathrm{interp}} = \frac{\sum_{IJ} w_{ijIJ}\, \mathrm{I}_{\mathrm{IJ}}}{\sum_{IJ} w_{ijIJ}} \tag{3.6}$$

$$w_{ijIJ} = \left(\exp(-\beta \left| \underline{r}_{IJ} - \underline{r}_{ij} \right|\right) \tag{3.7}$$

where indices I and J are the x and y indices on the simulation grid, and i and j are equivalent for the finer seismic grid, $w_{ijIJ} = \exp(-\beta(|r_{IJ}-r_{ij}|)$. It is found that $\beta = 0.05$ m^{-1} gives the best results, minimising the representivity error (Stephen *et al.*, 2005).

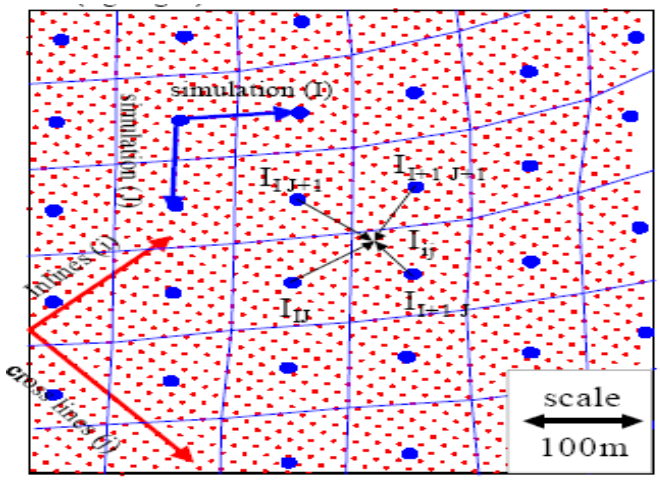

Figure 3.5: *Comparison of the seismic and simulation grids in the present study. Blue lines indicate the simulation cells and large blue symbols the location at which the impedances are predicted. Equation 3.4 is used to interpolate the impedances to obtain values at the small red symbols, i.e. where the observed seismic data is measured. Solid blue and red arrows indicate the principal directions of the simulation axes and seismic grids respectively (Stephen et al., 2005).*

3.3 Observed data

Two groups of seismic data are used. The first group, named Phase I, consists of two P-wave seismic volumes collected for three surveys, gathered in 1993, 1999 and 2000, and the second group, Phase II seismic data, uses 1996 as a baseline, and 2002 and 2004. Well production and injection history data for seven years was also provided by the operator's model, such as oil rate, water rate and gas rate. For more details see Chapter 6.

3.4 Quantifying the model misfit

Once the predicted and observed seismic attribute maps are mapped to a common grid, they are normalised prior to comparison. This normalisation is carried out because the mismatch is evaluated between two attributes that are in different seismic domains to one another.

3.4.1 Evaluating the mismatch

A single misfit objective function is obtained for each model, incorporating a comparison between observed and predicted production and seismic data. For each variable being compared, the following equation is used (Tarantola, 1987):

$$J_i = \left\langle \underline{x}_i^{obs} - \underline{x}_i^{\mathrm{mod}} + \underline{x}_i^{error} \middle| \underline{\underline{C}}_{mi}^{-1} + \underline{\underline{C}}_{di}^{-1} \middle| \underline{x}_i^{obs} - \underline{x}_i^{\mathrm{mod}} + \underline{x}_i^{error} \right\rangle, \tag{3.8}$$

where the x_i is the ith data vector under comparison, with superscript *obs* or *mod* for observed and modelled respectively, and C_{di} is the data covariance matrix capturing data errors, while C_{mi} captures model error covariance, and $\underline{x}_i^{error}$ is the model error.

$$J = \sum J_i \tag{3.9}$$

Seismograms contain data errors from a number of sources, including repeatability of the acquisition components, cross equalisation, tuning and wave interferences, and are difficult to assess. The attribute map obtained from predicted seismic data contains uncertainties from the time-to-depth conversion, the uncertainty of the picked horizons and the process used to calculate the attributes. With all of these sources of data error, it is more efficient to determine the error from our map of the 4D signature (Stephen *et al.*, 2006). To calculate C_{mi}, both seismic and production datasets are band-pass filtered to separate the data error and estimated signal in each case. The data error is then used to determine the data covariance C_{di}. The seismic data covariance is calculated for spatial correlation in the direction of the inlines and crosslines to give two matrices. Soldo (2005) found that the random sampling of a subset of inlines and crosslines can speed up calculations by an order of magnitude (for full details see Soldo, 2005). Otherwise, calculation of the seismic misfit can take as long as the flow simulation. We can thus (i) use the numerical representation of

the matrices, (ii) fit an exponential model (e.g. Deutsch and Journel, 1992) or (iii) if the correlation is low, assume a diagonal matrix using the standard deviation of the noise.

3.5 Parameter space exploration

The neighbourhood approximation (NA) algorithm is a stochastic sampling algorithm. NA was originally developed for solving a seismic waveform inversion problem in earthquake seismology (Sambridge, 1999a), but it has recently been adapted to the problem of generating multiple history matching models in petroleum engineering. The first applications of NA in reservoir characterisation and uncertainty quantification were introduced by Christie *et al*. (2002) and Subbey *et al*. (2002). The NA workflow may be divided into two phases: a search phase, which is implemented to generate an ensample of acceptable solutions of the inverse problem, and an appraisal phase. Figure 3.6 summarises the search phase as follows.

Firstly, an initial set of n_i models are randomly generated in the search space; secondly, for each model, the forward problem is solved and the relevant misfit value is obtained; n_r models with the lowest misfits among all models are determined. Finally, new n_s models are generated by uniform random walk in the Voronoi cell of each of the n_r chosen models. The algorithm returns to the second step, and the process is repeated. The parameters n_s and n_r control the explorative and exploitative behaviour of the algorithm. Exploration is a feature by which an algorithm searches in the parameter space without considering what it has 'learned' from previous sampling. On the other hand, exploitation makes use of the sampling. Large values of n_s and n_r improve the chances of avoiding local minima and should be increased with the dimension of the parameter space (Sambridge, 2001).

The size and shape of the neighbourhoods are not imposed by any external information. They are exactly determined automatically and uniquely by the previous samples. The algorithm requires models to be considered only for their relative fit to the data, because it uses the rank only of the 'misfit to the objective' ratio. This is very useful because

sometimes it is much easier to answer the question 'Is model X a better fit to the data than model Y?' instead of estimating the difference in a specific way (Sambridge, 1999a).

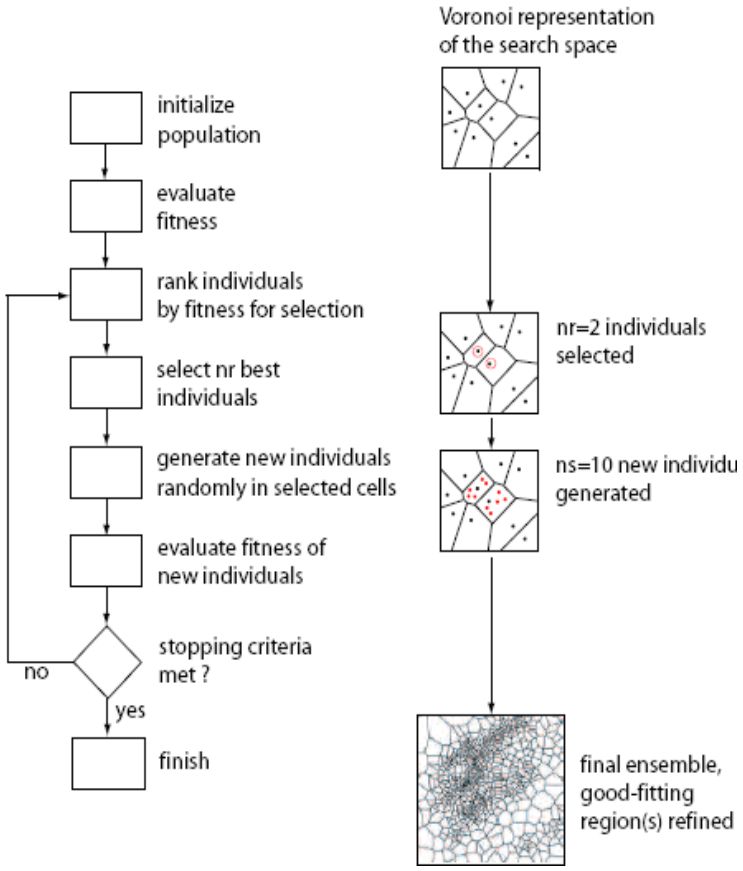

Figure 3.6: *Neighbourhood algorithm workflow in the parameter space where a number of best models are selected, and their neighbourhoods identified using Voronoi cells. New models are distributed randomly in the neighbourhoods of the best models, and new misfits calculated. This process is repeated a number of times until the misfit is reduced (Erbas and Christie, 2007).*

3.6 The Bayesian framework for quantifying uncertainty

Uncertainty analysis can be performed on an ensemble of models and is used to calibrate the range of various data, including water saturation and oil pressure per grid cell, upscaled impedance for each layer, and also the seismic misfit map. For each of the spatial variables, maps or volumes of means and standard deviations may be calculated. This

approach was demonstrated by Stephen and MacBeth (2006) and Stephen (2006). In this study, the misfit is used to estimate the likelihoods of the observed data *O*, given the model *m* and the misfit J_i for the *i*th variable, via:

$$p(O \mid m) \propto 1/\exp\left(\sum_i J_i / 2\right) \tag{3.10}$$

Once we have created sufficient models, the misfits can be used to update model probabilities from the prior $p(m)$ in a Bayesian framework, so the probability of each model *m* can be estimated given observations *O* using:

$$p(m \mid O) = \frac{p(O \mid m)\, p(m)}{\sum p(O \mid m_i)\, p(m_i)} \tag{3.11}$$

where *p (m)* is the prior probability of the model. The PPD (Posterior Probability Density) is then resampled a posteriori as part of the uncertainty analysis of modified parameters (Sambridge, 1999b). The probabilities can then be used to calculate mean and standard deviation properties (L1 and L2 norms respectively):

$$\langle \chi(\mathrm{x,y,z,t}) \rangle = \int \chi \mathrm{p(m \mid O) d}\chi \tag{3.12}$$

$$\mathrm{std.dev.} = \int \chi^2 \mathrm{p(m \mid O) d}\chi \tag{3.13}$$

where χ is a spatially or temporally varying property. For a given ensemble of models, Monte Carlo integration methods can be used for the mean. For example:

$$\langle \chi(\mathrm{x,y,z,t}) \rangle \approx \frac{1}{\mathrm{N_t}} \sum_{\mathrm{ensemble}} \frac{\chi \mathrm{p(m \mid O)}}{\mathrm{h}} \tag{3.14}$$

where $\mathrm{N_t}$ is the total number of models, and h is the density distribution of the samples (normalised so that $\int \mathrm{h d}\chi = 1$).

The probabilities may be estimated if we assume *p (m)* is uniform via relative likelihoods:

$$\langle \chi(x,y,z,t) \rangle \approx \frac{1}{N_t} \sum_{ensemble} \frac{\chi(p(m \mid O) / p(m^{best} \mid O)}{h} = \frac{1}{N_t} \sum_{ensemble} \frac{\chi / \exp(\sum_i (J_i^m - J_i^{best})}{h} \tag{3.15}$$

Alternatively, with sufficient sampling via the NA, we can use the feature that the sample density increases with probability such that we may approximate $p\,(m|O) \approx h$ (Sambridge 1999b), and if we assume a uniform prior distribution and use the likelihoods

$$\langle \chi(x,y,z,t) \rangle = \frac{1}{N_t} \sum_{\text{ensemble}} \chi(x,y,z,t) \tag{3.16}$$

for any cell in the model. We can repeat this for other parameters, such as pressures, impedance and seismic error. A standard deviation can be similarly calculated to estimate the spread of variables over the ensemble, and this is used here to estimate uncertainty.

3.7 Likelihood function and least-square misfit derivation

Data errors in the production history are usually expressed statistically and are incorporated into the likelihood function. For example, Floris *et al*. (2001) assumed that time-series data errors would be distributed independently and follow a Gaussian distribution. These approximations resulted in a well-known form of logarithmic probability known as the sum of the squares of each discrepancy. Although it leads to the popular method of least-squares, it should be emphasised that the justification of the least-squares form for a logarithmic likelihood relies on the assumptions of the independence and Gaussian distribution of data error. Equation 3.11 expresses Bayes' equation for the reservoir model.

We assume that we are using only the water rate measurements as a function of time as the observed data, and that the data measurement errors at any time are Gaussian (Figure 3.7), independent and have identical distribution (all have the same variance) with zero mean error. The simulation errors are also assumed to be zero. Then, at any time the probability that the true value of the observed rate, Q_{obs} is:

$$p(Q_t|m) = \frac{1}{\sigma\sqrt{2\pi}} \exp\left\{ -\frac{1}{2} \frac{(Q_{obs} - Q_{\text{mod}})^2}{\sigma^2} \right\} \tag{3.17}$$

where t is the time step, σ is the standard deviation of the error and Q_{mod} is the model output.

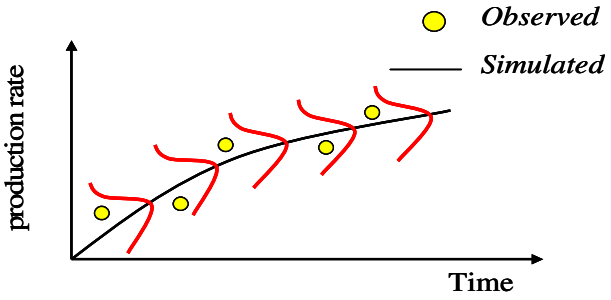

Figure 3.7: *Gaussian assumption to define the likelihood of a reservoir model given the observations.*

If it is assumed that the measurement errors at each time step are independent, the joint probability density, i.e. the likelihood of the model, is given by the product of the probabilities of the individual measurements (Eq. 3.17):

$$p(O|m) = (\frac{1}{\sigma\sqrt{2\mu}})^N \prod_{t=1}^{N} \exp\left\{-\frac{1}{2}\frac{(Q_{obs} - Q_{\mathrm{mod}})_t^2}{\sigma^2}\right\} \tag{3.18}$$

where N is the number of the data points.

Since $(\frac{1}{\sigma\sqrt{2\mu}})^N$ is constant, Eq. 3.18 can be written as:

$$p(O|m) = \alpha \exp\left\{-\sum_{t=1}^{N}\frac{(Q_{obs} - Q_{\mathrm{mod}})_t^2}{\sigma^2}\right\} \tag{3.19}$$

Thus, if we define the misfit M as

$$M = \sum_{t=1}^{N}\frac{(Q_{obs} - Q_{\mathrm{mod}})_t^2}{\sigma^2} \tag{3.20}$$

then the likelihood function is:

$$p(O|m) \;\alpha\; e^{-M/2} \tag{3.21}$$

3.8 Resampling from the posterior

The basic idea of using an ensemble of models to quantify the degree of uncertainty is that the ensemble represents a proper sample of the posterior PDF (Probability Density Function) of the model parameters. This is because the posterior is constructed from a set of data misfit values for a given ensemble amount (Sambridge, 1999b). The quality and the accuracy of the uncertainty quantification will, accordingly, depend on how well-sampled and representative the ensemble distribution of the true PDF is. In this thesis, NA–Bayesian (NAB) algorithm constructs are used as an approximation of the PPD (Posterior Probability Distribution) via a Gibbs sampler. Voronoi cells are used to represent the model space and to interpolate the PPD of unknown points in the high dimensional parameters space. The Voronoi interpolation is done simply by setting the known PPD of each model to constant inside each cell. By means of the interpolation, NAB does not require any forward modelling during the posterior sampling. Figure 3.8 shows how the Gibbs sampler works in two dimensions. The conditional probability density function outside the Voronoi cell is set to zero to generate a new model in the cell. A new x-axis element, x_{aa}, is obtained by a uniform random perturbation from point x_a. This perturbation is restricted to (x_1, x_2). From (x_{aa}, y_a), we generate a new y-axis component by a uniform random perturbation, restricted to (y_1, y_2), to arrive at (x_{aa}, y_{aa}).

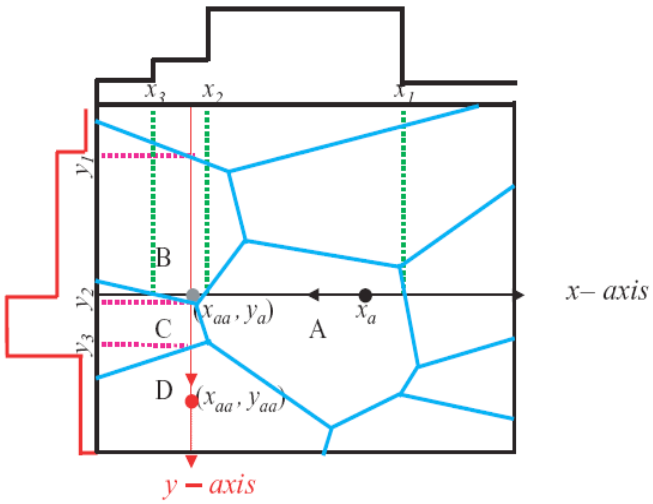

Figure 3.8: *The NA–Bayes Gibbs sampler.*

3.9 Simulation errors

Simulations regularly involve theory, experimental data and numerical modelling, including their intrinsic errors. The accuracy and reliability of a simulation model is questioned as a result of these errors. There are a variety of methods in the literature for analysing and combining the various types of errors that can occur in simulations. The existence of uncertainties heightens the difficulties in making accurate predictions. Theory may be imprecise, or simplified when represented numerically, or input data may be sparse or badly measured. Generally, because we are dealing with complex phenomena, knowledge about the state of the system and the governing physical processes is often incomplete, inaccurate or both. Additionally, the non-linearity of many physical processes of interest can lead to a drastic boost of even small uncertainties in the input, thus leading to large uncertainties in system behaviour. This study focuses on the source of errors, particularly how the theory is represented numerically and from the petro-elastic transform error.

3.9.1 Numerical dispersion

When water enters one side of a simulation grid block, it is directly dispersed throughout the grid block. The water saturation at the far end of the grid block will be instantaneously the same as at the inlet (Figure 3.9a and c). As a result, the water front is smeared, causing early breakthrough in the coarse grid model. This effect is called numerical dispersion. Numerical dispersion, in relation to the effect of the upscaling, is linked to the ratio of the number of grid blocks in the flow direction between the fine and the coarse grid model. For this reason, it is important to start the upscaling at the core plug scale where the SCAL (Special Core Analysis) measurement has been made, with the aim of capturing the effect of numerical dispersion. The simulation errors are correlated in time. This time correlation must therefore be included in assessing model fit to data, otherwise acceptable models are rejected if too many points are included in the time series of production data (Christie 2002).

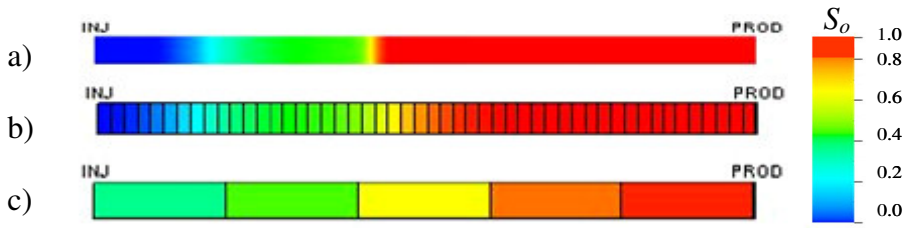

Figure 3.9: *The 1D effect of numerical dispersion explains front resolution error and flow behaviour for different grid sizes. a) Fine grid cells, the closest to the analytical solution, b) coarse grid cells and c) very coarse grid cells.*

3.9.2 Upscaling

Ideally models should be constructed at the finest scale, i.e. core scale. It is difficult to incorporate all the fine-scale data in this model, however, because fluid flow simulations are not feasible, as they would require a large memory and long processing time. In addition, history matching would be a daunting challenge, if not impossible. For simulation purposes, a coarse scale model must be constructed. The thickness of the grid blocks is often around 1 to 10 m. The coarse grid fluid flow model should honour the behaviour at the pore scale. Upscaling allows us to work with larger grid blocks, while the model still reflects the behaviour of the fine-scale model. By upscaling, the fine-scale data, such as that obtained from core plugs and outcrops logs, is then incorporated. For certain properties, upscaling is complex, e.g. permeability, relative permeability, capillary pressure and saturation curves. The available techniques comprise, among others, arithmetic and harmonic means, power law averaging and flow-based methods. Two phase upscaling techniques comprise steady-state (Pickup *et al.*, 2000) and dynamic methods (Barker and Dupouy, 1999; King *et al.*, 1993).

3.9.3 Downscaling of dynamic properties

Commonly, the pressure and saturation data are obtained from the coarse grid flow simulation grids and compared laterally to finer-scale grids. The pressure and saturation values are available in the inactive grid blocks, and large gaps can exist in the coarse simulation grid. These gaps need to be in-filled with realistic saturation and pressure

values during the downscaling process. Sengupta *et al.* (2003) found that the saturation details at the fine vertical scale below seismic resolution can affect the seismic response and that the saturation outputs from flow simulators may be too smooth vertically to construct realistic 4D synthetic data representative of the real seismic response (Doyen, 2007). Castro *et al*. (2006) and Enchery *et al*. (2007) have proposed flow-based downscaling approaches to generate fine-scale saturation and pressure fields from coarse-scale flow simulation grids.

3.9.4 The saturation law

The choice of saturation law equation depends upon the reservoir information available, the assumptions that can be accepted and the accuracy required in the reservoir characterisation study. A good description for finding the best choice for the saturation law has been presented by MacBeth and Stephen (2008). They generalised the saturation law equations for the case of heterogeneous geology in the turbidite reservoirs. They used a synthetic model to represent the majority of turbidite reservoirs that are sand-rich and sheet-like in nature. Each channel sand package was taken to have a vertical thickness roughly equal to a fifth of a seismic wavelength (≈20 m maximum total thickness compared to a wavelength of 100 m), and thus could be treated as a single homogeneous rock mass with an equivalent set of elastic properties defined by effective medium theory. To account for heterogeneity, bed-scale fluctuations in porosity and saturation were defined and added to the mean of the symmetrically distributed porosity and saturation. The perturbation terms are distributed across the reservoir and vary from bed to bed. The desired estimate of the fluid bulk modulus is obtained through application of Backus (1962) and perturbation theory, yielding an adapted harmonic average which is accurate to second order in the saturation and porosity fluctuations.

In Figure 3.10, the laws defined by the homogenous case and the heterogeneous case both represent different ways of determining the fluid bulk modulus K_{eff} in different prospective. They are useful as they can be applied without the need for reservoir information, but they

do require essential assumptions to be applicable: in the homogenous case, this is merely a mathematical limit and does not represent any known physical saturation distribution. The heterogeneous case requires homogeneous and pressure equilibration in the rock volume imaged by the seismic data.

However, in a real reservoir with heterogeneous geology and saturation, such laws do not accurately predict pore-volume weighted average saturation S_w. From Figure 3.10, mainly in MacBeth and Stephen's (2008) case, the saturation errors are mostly constant over large ranges of production time. This finding is connected to the way in which the saturation field changes in the reservoir. The differences in saturation measurements between successive monitor surveys will cancel out the majority of the errors in the S_w estimate, mainly if these surveys are frequently shot. This conclusion is valid provided the change in the spread of the vertical saturation distribution over time is not significantly greater than the change in the average saturation value being detected.

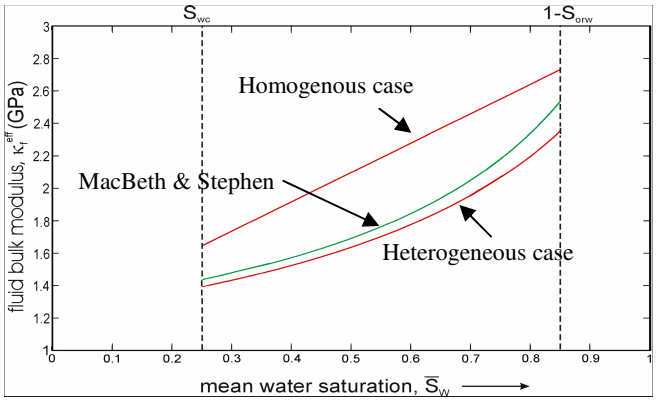

Figure 3.10: *Estimates of the relationship between measured (seismic scale) fluid bulk modulus κ_{eff} and the true pore-volume weighted mean water saturation S_w for a two-phase (oil–water) system under water flooding conditions (increasing S_w) (MacBeth and Stephen, 2008).*

3.10 Summary

Production data used in the process of history matching measures pressure and saturations at discrete well locations, and it is necessary to constrain dynamic reservoir parameters

such as permeability and the effect of faults. Time-lapse seismic analysis has the potential to provide the missing information, but it lacks precise details of the pressure and saturation states. The process of seismic history matching is an effort to merging the benefits of both types of information to improve estimates of the reservoir model parameters.

This study presents a method of combining time-lapse seismic data with production data in an automatic history matching process based on an integrated workflow. The procedure set out aims to determine the uncertainty of the reservoir description parameters.

A multi-model approach to history matching including seismic data has been explained in this chapter, detailing a number of steps necessary to follow in order to put it into practice. A full description for each individual part of a loop was discussed. The neighbourhood approximation (NA) algorithm and its use as a sampling algorithm was presented, along with details about the objective function and a discussion of the application of the Bayesian framework for quantifying uncertainty. The benefit of a Bayesian approach over other traditional methods of uncertainty analysis was presented. This also extended the analysis to higher levels of interpretation, e.g. the rejection of any particular model and the selection of appropriate models. The chapter concluded by presenting the various types of errors from both sides: simulation and seismic.

CHAPTER FOUR

History Matching With Time-Lapse Seismic Data: Will Any Starting Model Do?

The aim of this chapter is to answer two questions: can we use the pilot point method to update permeabilities, and how does the residual error compare to scale-dependent errors? Fine-scale permeability realisations were generated using sequential Gaussian simulation and upscaled by a factor of 5 in each direction. Flow simulations of each model (i.e. at both scales) were used to predict impedances annually for two years for both scales of the models. Each of the coarse-scale models were updated via seismic history matching using the predicted impedances from each coarse-scale model in turn as history data. It was found that the pilot point approach is a good way to modify a permeability field that has a similar degree of spatial correlation to the pilot point separation. The impedances generated from the fine-scale models were then used as the observed data, and the process was repeated to investigate the scale-dependent errors.

4.1 Introduction

Seismic history matching requires a good method of controlling the parameters of the model. It is necessary that the solution space of the problem, defined by the base case model, the parameterisation scheme and the inversion process, contains a reasonable approximation to reality. History matching generally begins after the generation of the base case model, usually an upscaled geological model that has been conditioned to well data (logs, core plug and core images) and 3D seismic data using a geostatistical modelling approach.

Usually, a model is generated that honours the static data (pre-production seismic data, well logs, core plug permeability, well testing and relative permeability from special core analysis) using geostatistical methods (Figure 4.1). This model is then updated to honour dynamic data (usually production and injection rates, but more recently time-lapse seismic). In SHM, there is the possibility that we may choose the wrong starting model or the wrong method of changing it. In the model-building scheme, the geological concepts of the reservoir and available data should be honoured. In this synthetic study, the degree to which we can match a synthetic truth can be determined by considering both dynamic data and the truth model on which these are based. This work is complementary to previous work where the effects of scale-dependent model errors were examined (Stephen, 2007). Flow simulations are often created such that computer resources are optimised and some level of accuracy is sacrificed. Some form of upscaling is required to capture two-phase flow properties such as relative permeability to speed up simulations, but also to represent geological heterogeneity. The upscaling may be oversimplified or ignored. Finally, the petro-elastic transform contributes to the model errors owing to assumptions about saturation distributions, and cross-scaling is required because modelled and observed seismic data are obtained for different volumes. The ultimate aim here is to compare the residual geological parameter error against the scale-dependent errors and hopefully minimise the effect of both.

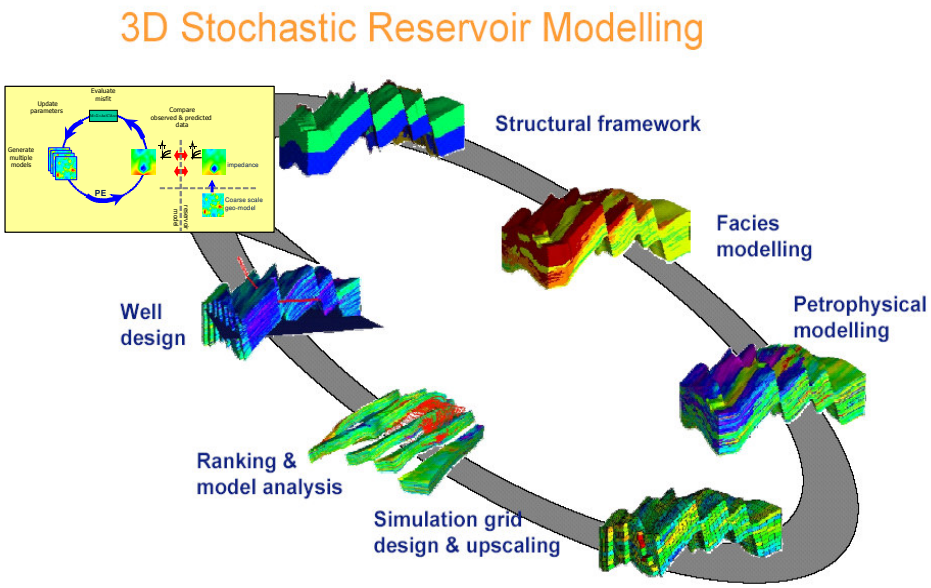

Figure 4.1: *Workflow of reservoir modelling (after Roxar) approach where models are constrained to well logs and seismic data before history matching.*

4.2 The main problems investigated

The choice of starting model in the history matching process may be critical, and so the following questions need to be answered:

- Can any realisation be updated with our parameterisation scheme to obtain a good match?
- How good is the prediction?
- Do we know that there will be a model error, both in terms of flow simulation and geological modelling?
- Can we reduce the latter by history matching, or will the model error be determined anyway?

4.3 Method of study and application

The Seismic History Matching workflow (Figure 4.2) presented previously (Stephen *et al.*, 2006; Stephen, 2007) is used and applied to a synthetic field. The 'observed' impedances are derived from flow simulations at different time steps. For the truth case, simulations on both a typical coarse grid as well as a fine grid are considered. History matching simulations are performed using coarse-scale models using a finite difference simulator (Schlumberger Geoquest, 2007). We modify the coarse-scale models using pilot points with Kriging (de Marsily *et al.*, 1984) (for more details see Appendix A) to alter permeability, and compare the predicted impedance to the equivalent from the truth case. We ignore the influence of model errors in the history matching process to avoid being dominated by the model error. These can be important, however, as they can affect the convergence rate, leading us to incorrect models. The errors arise because we make simplifications in the simulation process, as discussed in Christie *et al.*, 2005.

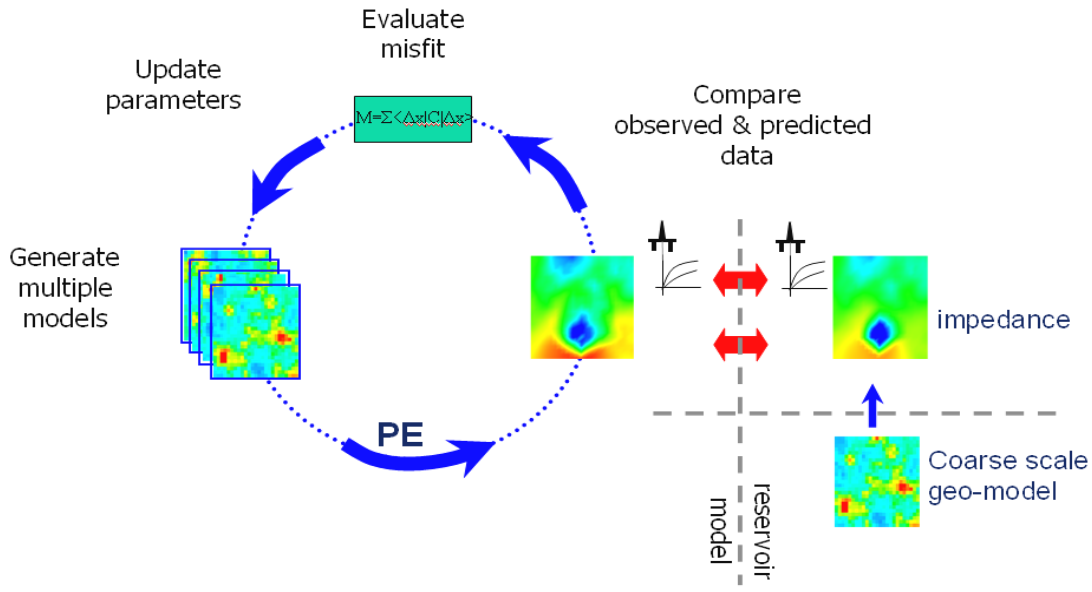

Figure 4.2: *Schematic of the iterative automatic history matching process. Multiple of simulations are run simultaneously and converted to predicted change in acoustic impedance. These are compared to observed data via a misfit. We then use the neighbourhood algorithm (Sambridge, 1999a) to select parameters for a new set of models.*

A set of fine-scale models is generated as synthetic truth cases for study where each is constrained to the same synthetic well logs and 3D seismic data. In this chapter, we perform all combinations of history matching where each coarse-scale model is used as a starting model (base case) and modified to match each of the 'truth' impedance differences (Figure 4.3). We begin by investigating whether we can use the pilot point method to update permeabilities as well as the quality of the best model predictions. Finally, we compare the residual error to scale-dependent errors.

4.4 Descriptions of the models

4.4.1 Fine-scale model

We build a fine-scale model by distributing Net:Gross and permeability (horizontally, it is isotropic and independent of Net:Gross). Vertical permeability is a function of Net:Gross, and the porosity of the sand is uniform, as in our Schiehallion field study (Stephen *et al.*, 2006a). Properties are distributed using sequential Gaussian simulation (SGS) using GSLIB (Deutsch and Journel, 1992).

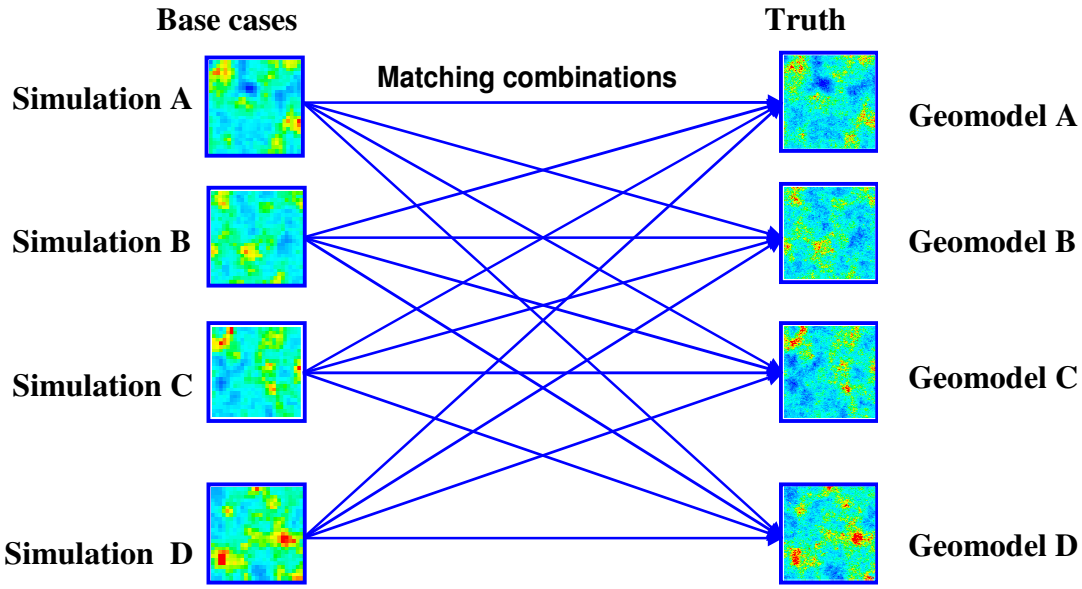

Figure 4.3: *All possible combinations of history matching where the coarse-scale models are used as starting models against each truth impedance difference.*

We generate multiple realisations of the permeability with values at the wells conditioned from the first realisation. Fine grid geomodels are created with cell sizes of 20×20×1.5 m cells. We use a Net:Gross distribution that is generated by SGS rather than an object model at this stage. We fix Net:Gross (Figure 4.4a) and assume that this is known from pre-production seismic analysis. The porosity value is fixed at the true value of 0.28 in every grid block.

4.4.2 Coarse-scale model

We use PETREL (PETREL Manual, 2007) to upscale the fine grid model by a factor of 5 in each direction. We flow two-phase simulations with a horizontal producer and vertical injector using the ECLIPSE simulator (Eclipse Manual, 2006). Figure 4.5 illustrates the oil saturation distributions, and Figure 4.6 shows the pressure map for the fine and the coarse scale. The difference between the flow simulation outputs is related to the effect of the upscaling and numerical dispersion (see Chapter 3). The petro-elastic transform is used with the parameters in tables 4.1 and 4.2 to calculate the base-case maps of impedance for each model at both scales. The coarse grid impedances are interpolated so that a comparison can be made at the fine scale. Figure 4.7 shows the impedance change at various time steps for the fine and the coarse-scale model. Figures 4.8, 4.9 and 4.10 show the residual model errors for the base-case model against its equivalent upscaled model. The difference is due to the upscaling effect and petro-elastic transform after one year of production for the fine and coarse-scale models.

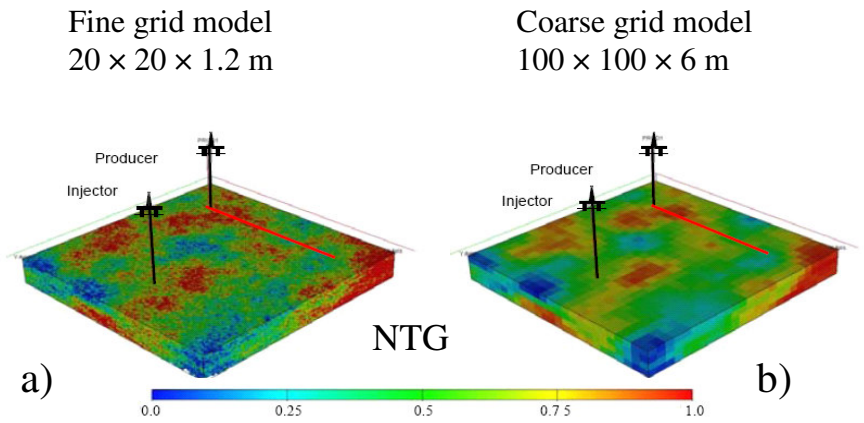

Figure 4.4: ExampleExample Net:Gross (a) fine grid geo-model and (b) upscaled equivalent. The fine grid geo-model measures 20 x 20 x 1.2 m while the upscaled grid is 100 x 100 x6 m.

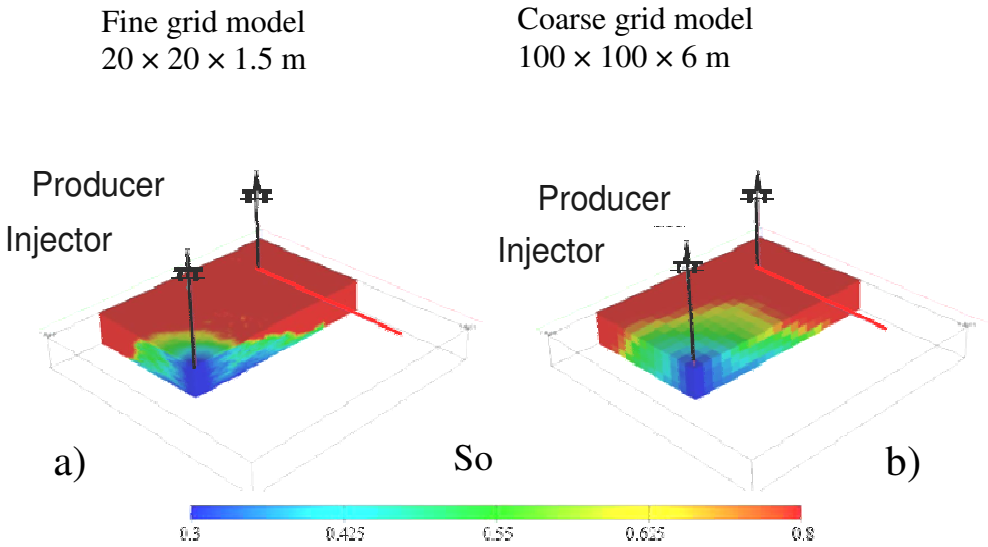

Figure 4.5: *Oil saturation in a) the fine grid and b) the coarse grids. The difference between both is related to the upscaling effect and numerical dispersion.*

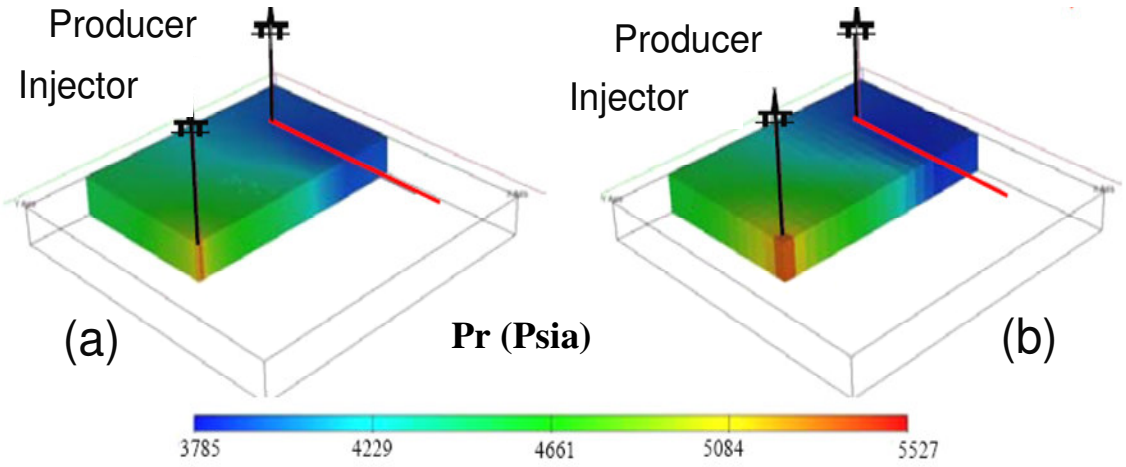

Figure 4.6: *Pressure in a) the fine grid and b) the coarse grid.*

Symbol	Value
$k_{\inf}$	9.78 GPa
E_k	1.0
P_k^{sand}	17.1 MPa
P_k^{shale}	1.45 MPa
$\mu_{\inf}$	6.28 GPa
E_μ	1.0
P_μ^{sand}	17.1 MPa
P_μ^{shale}	1.45 MPa

Table 4.1: *Default petro-elastic transform parameters for the dry bulk modulus obtained from history matching (Stephen et al., 2006c) and lab data for Schiehallion (MacBeth, 2004).*

Symbol	Value
k_{gr}	37 GPa
k_w	2.58 GPa
k_o	1.18 GPa
k_g	0.035 GPa

Table 4.2: *Petro-elastic transform parameters for Gassmann's equation. The fluid bulk moduli are functions of pressure, temperature, etc. Full details of the calculation can be found in Soldo (2005), which follows Batzle and Wang (1992).*

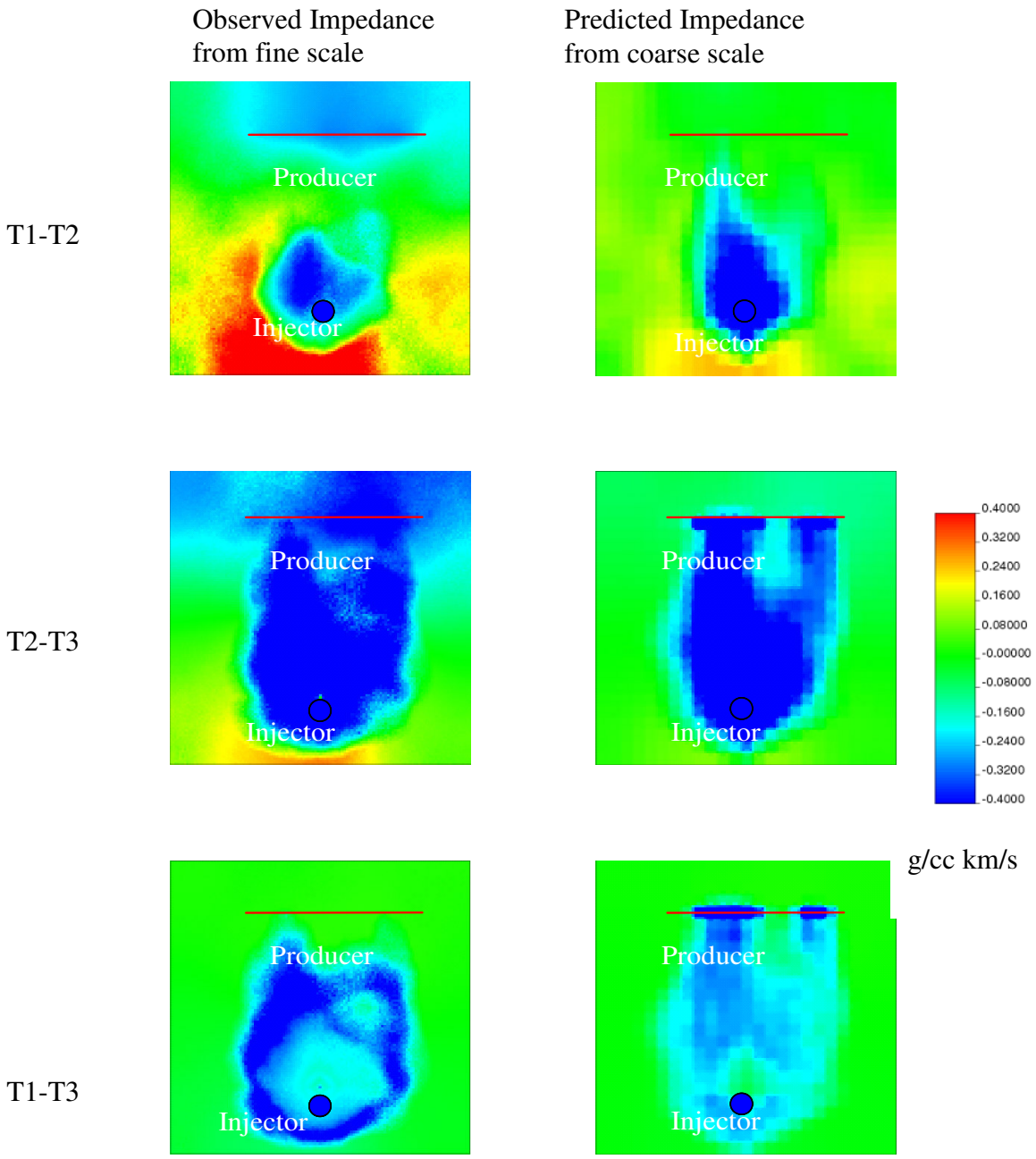

Figure 4.7: *Maps of calculated impedance differences (baseline minus survey) during two years of production for the fine grid geomodel (left column) and the coarse upscaled equivalent after interpolation (right column). For the base case of geomodel B, T refers to time steps. Old –new that give you positive number corresponding to a decrease in effective pressure, which is an increase in the pore pressure. Positive impedance is therefore linked to an increase in the reservoir pressure (pore pressure) negative impedance is either liked to a decrease in pressure or increase in water saturation.*

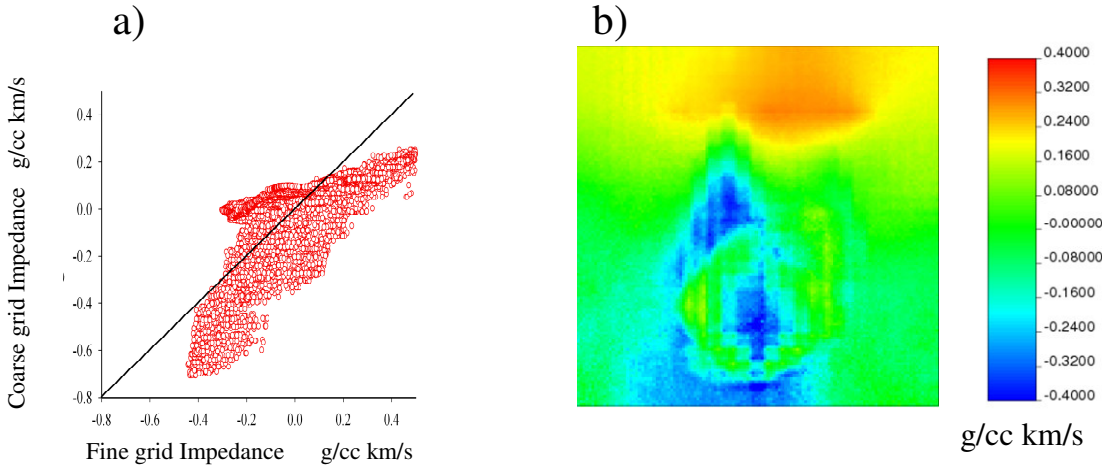

Figure 4.8: *Impedance differences (second minus first year). (a) Cross-plot of fine and coarse grid and (b) map of impedance differences.*

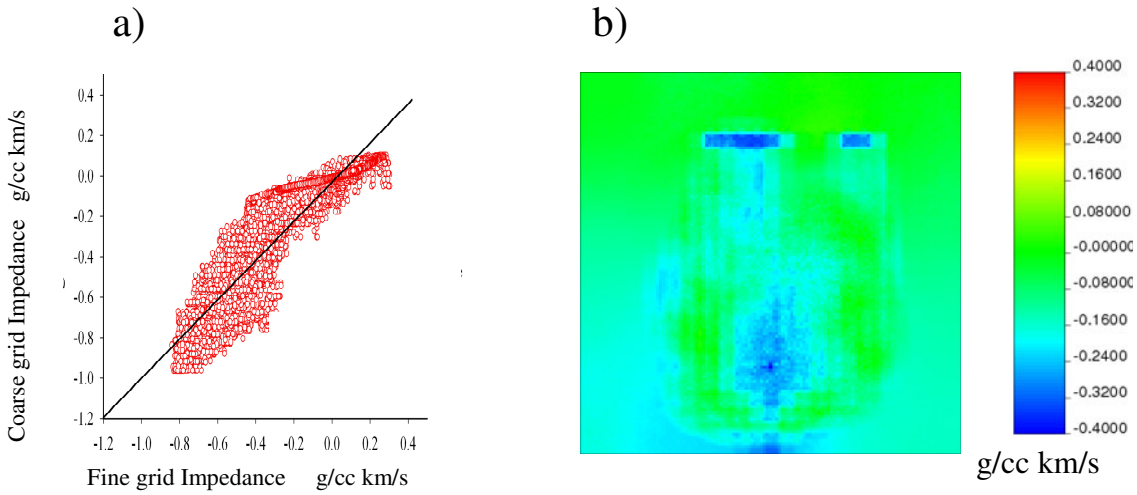

Figure 4.9: *Impedance differences (third minus second year). (a) Cross-plot of fine and coarse grid and (b) map of differences.*

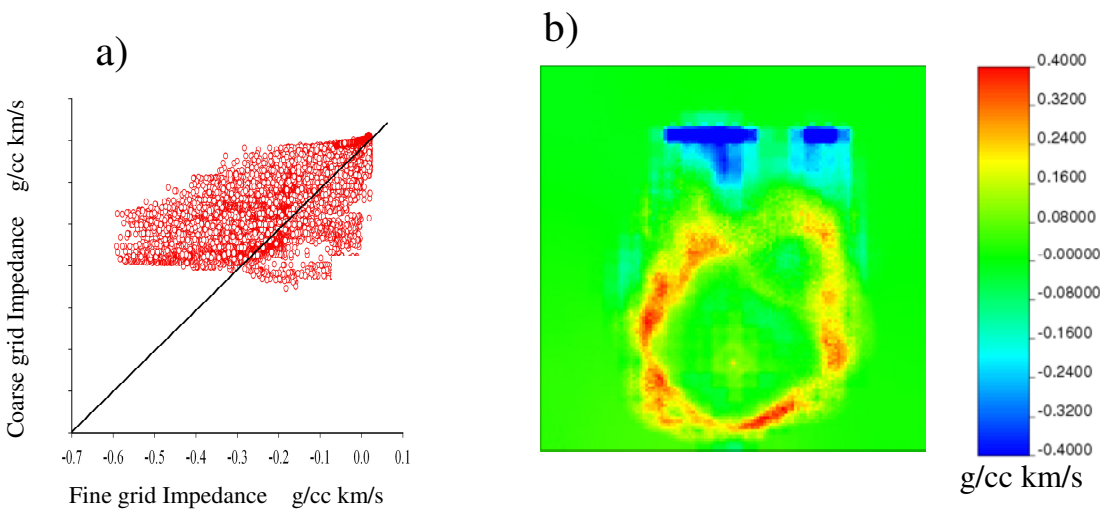

Figure 4.10: *Impedance differences (first minus third year). (a) Cross-plot of fine and coarse grid and (b) map of differences.*

4.5 History matching with time-lapse seismic data: starting models

4.5.1 Can any realisation be updated to obtain a good match?

All combinations of history matching are performed, as shown in Figure 4.3, where the coarse-scale models are used as starting models against each of the four truth impedance differences.

The simulation grid measures 25 × 25 × 4 cells. On top of this, we place a grid of pilot points measuring 4 × 4 × 1 cells, as shown in Figure 4.11. In the picture, the eight pink points are varied by history matching, and the rest are fixed with multipliers of 1. The multipliers are interpolated using Kriging with a variogram range of 625 m, the separation of the pilot points. We populate the initial ensemble of models by randomly sampling eight-dimensional parameter space such that the multipliers of the pilot points are able to vary from 0.1 to 10.

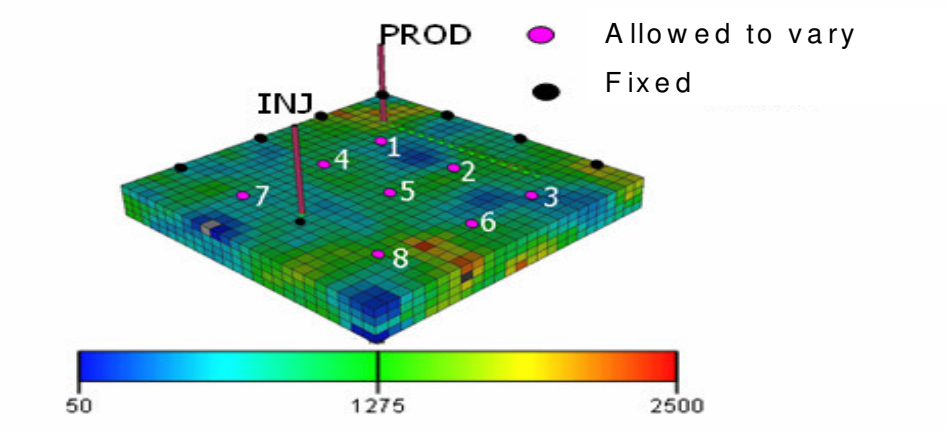

Figure 4.11: *Pilot point locations. An eight-dimensional parameter space has been defined (permeability multipliers) to adjust the permeability around the injector.*

In this case, the truth case is shown in geomodel B, and the best models after SHM are shown when each of the four models, A–D, is used as a starting model against geomodel B (Figure 4.12).

An initial sample of 400 models was used, followed by 80 per iteration (ns=80) of the NA routine. The best 40 (nr) models are then resampled (ns/nr=2), generating 2400 models in each case. A single misfit objective function is obtained for each model, incorporating a comparison between observed and predicted seismic data, only because we ignore the production data in this case. For each variable being compared, we use Eq. 3.7 for the misfit evolution as we update each base-case model. In all four cases, we reach a point where the misfit cannot be reduced any further, as shown in Figure 4.13. We note that, as simulation models A and C are quite similar, the misfits are also similar. Figure 4.13b shows the parameter evolution for one of the pilot points which controls permeability as a multiplier.

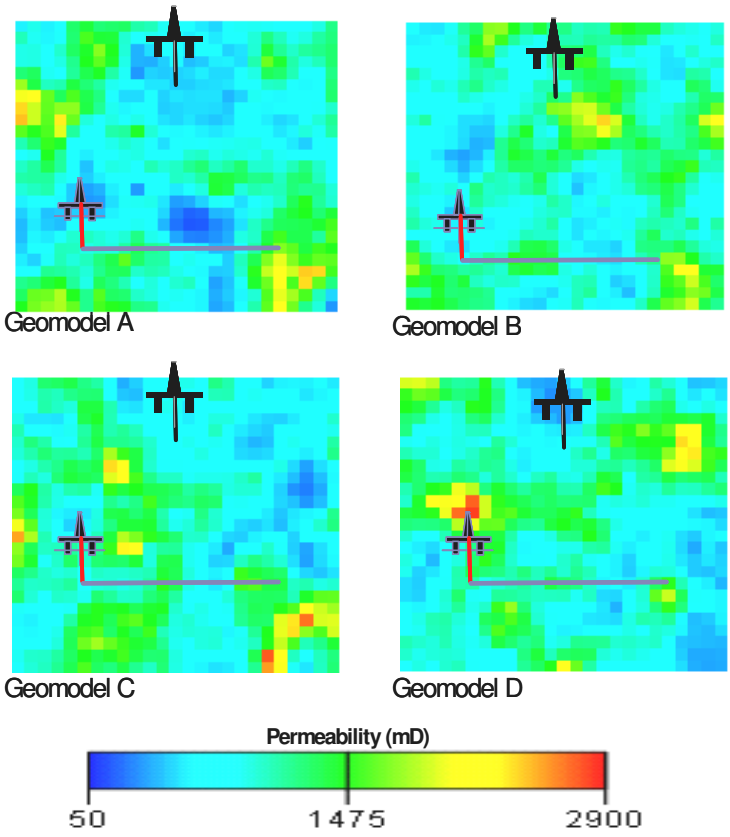

Figure 4.12: *Top view of the model permeability realisations via SGS. Permeability is conditioned at the wells.*

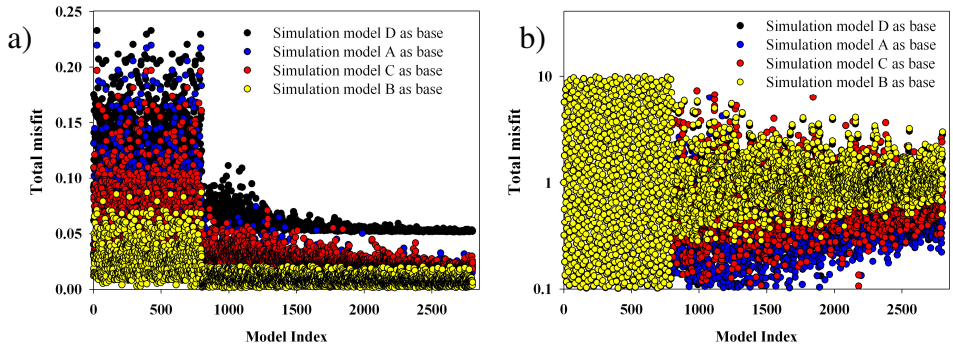

Figure 4.13: *a) Misfit evolution during history matching of simulation models A, C and D using B as a truth case and b) evolving permeability multiplier values for pilot point 5 (see Figure 4.11).*

In the vicinity of the pilot points, the permeability resembles the truth case quite closely (Figure 4.14). Quantitatively, the estimated permeability for the best case after SHM is better than before when we use the base-case permeabilities as shown in Figure 4.15. We apply the same approach using models A, C and D as truth cases in turn and then update the remaining three by history matching. We find that in each case the misfit could be reduced and a reasonable representation of the truth is obtained.

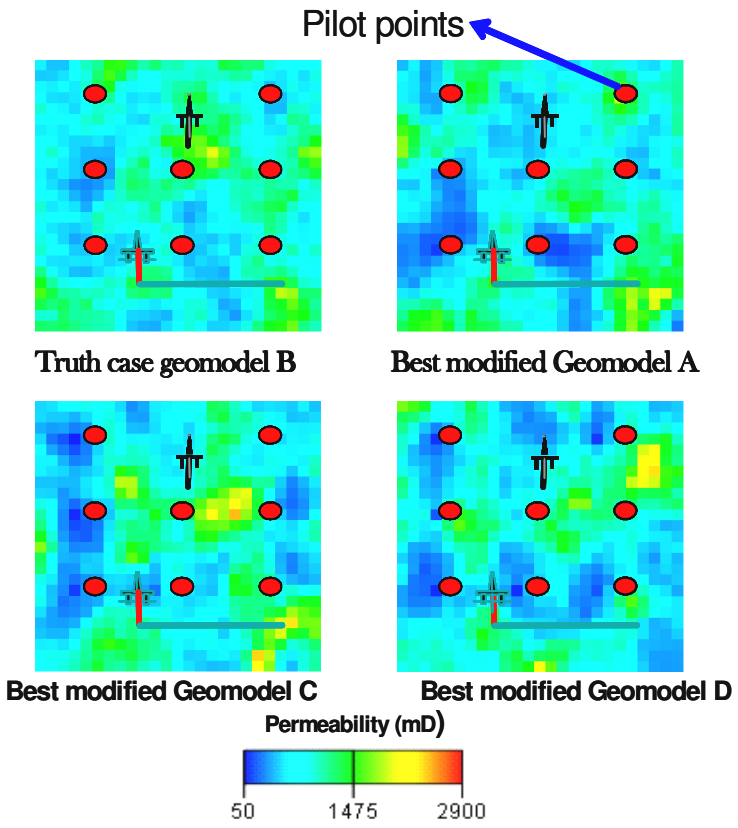

Figure 4.14: *Comparison of truth case model B and best model after history matching with three other models as the base case.*

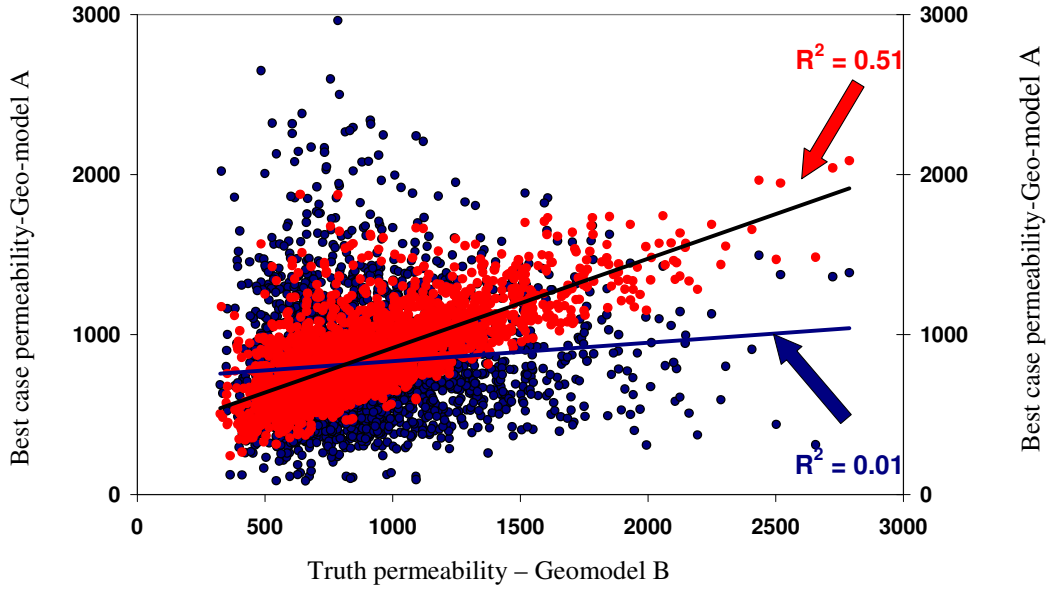

Figure 4.15: *Permeability comparison before SHM and after SHM (matched to seismic data only). The pilot point method improves the permeability representation against the truth case. Blue dots are the base case permeability and the red dots are the best model permeability after history matching.*

4.5.2 Model forecasting

We can also see the quality of the forecast after history matching when using the best models in the above cases. This is because the producer well is rate controlled and water has yet to break through during the history-matching period. We can see that the recovery factor is not sensitive to the choice of starting model (Figure 4.16), while water cut is slightly more sensitive to the starting model (Figure 4.17).

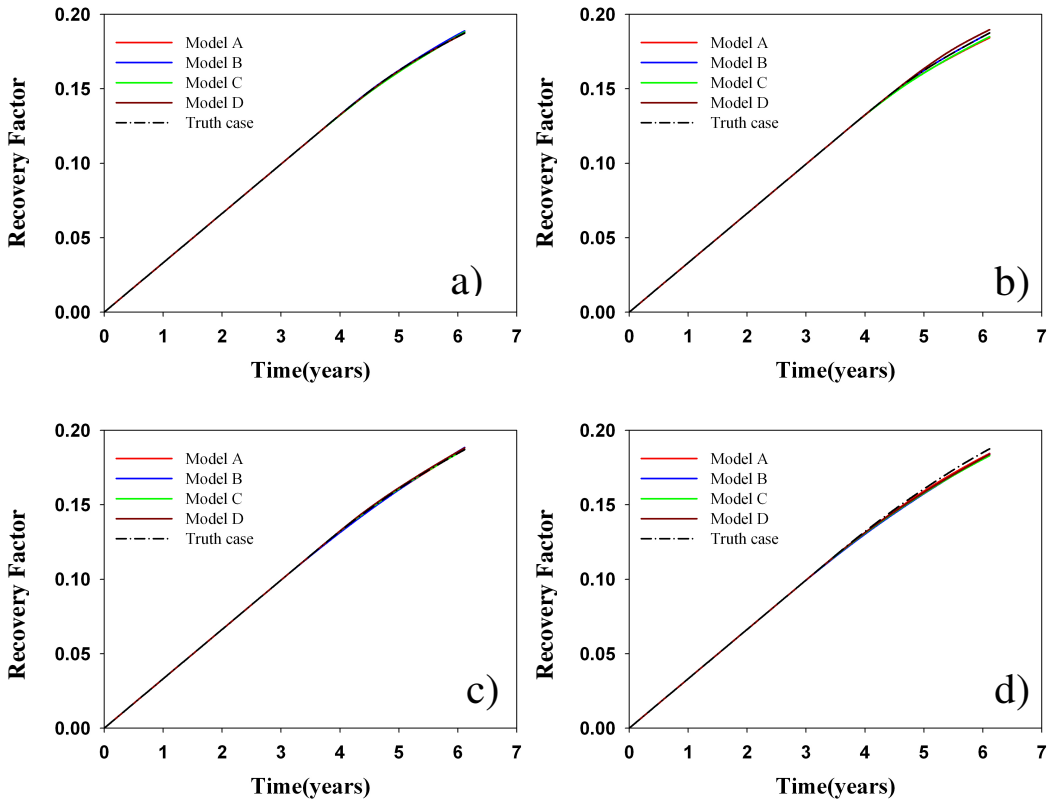

***Figure 4.16**: Prediction of the best models for recovery factor after seismic history matching the truth from a) model A, b) model B, c) model C and d) model D.*

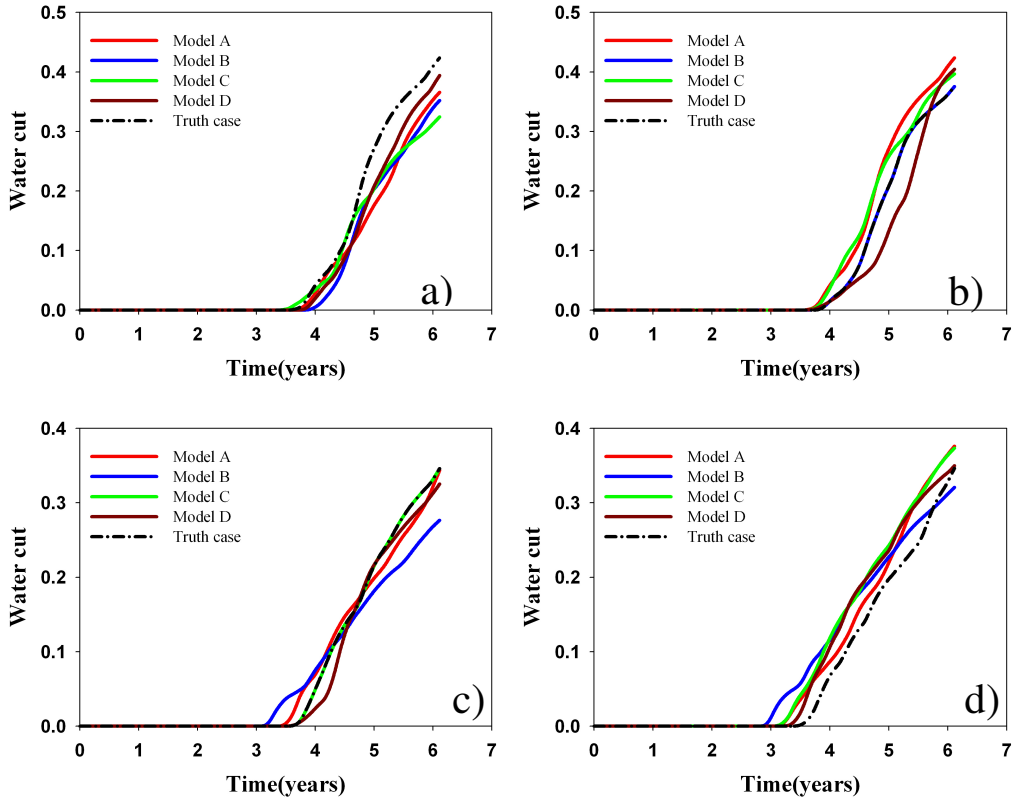

Figure 4.17: *Prediction of the best models for water cut after seismic history matching where model B is used as truth from a) model A, b) model B, c) model C and d) model D.*

4.6 Quantifying the scale error

In this section, we quantify the errors that arise when we use our coarse-scale geomodel as input to the simulation process, and compare it to a fine-scale model assumed to be the truth. We synthesise the observed data by using impedances calculated from a fine grid flow simulation model with cells measuring 20 × 20 × 1.2 m. During history matching, we run simulations on a coarse-scale grid measuring 100 × 100 × 6 m. The predicted impedance is therefore obtained at a coarser scale compared to what we observe. To enable comparison, we must either upscale the observed data or downscale the predicted impedances. It is preferable to keep our observed data as intact as possible and interpolate the predicted seismic from Figure 4.18. As can be seen from the figure, the observed and predicted seismic data grids are parallel to one another.

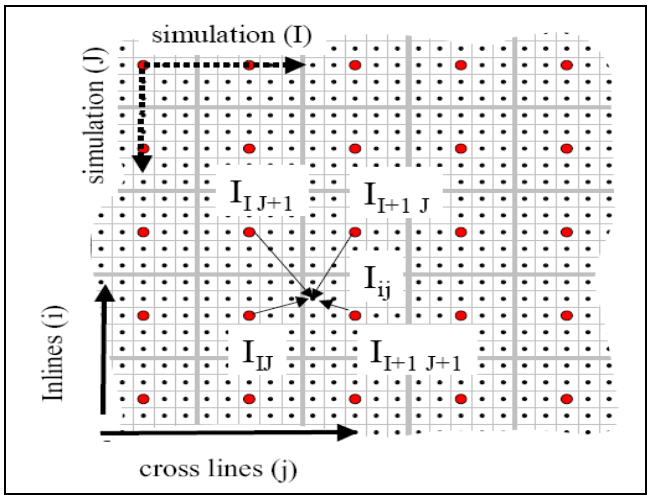

Figure 4.18: *Comparison of the coarse and fine grids used in the study. Thick grey lines indicate the coarse cells, while large circles show the location at which the impedances are predicted. Equation 3.6 is used to interpolate the impedances to obtain values at the small black circles, i.e. where the observed seismic data would normally be measured. Broken and solid arrows indicate the principal directions of the coarse (simulation) and fine (seismic) grids respectively. (Stephen, 2005)*

The coarse-scale models are used as starting models in history matching. We modify the coarse-scale model using pilot points to change permeability, and compare the predicted impedance to the equivalent from the fine-scale model. We ignore the production data, although it is fairly well matched. All combinations of history matching are performed, as shown in Figure 4.3.

Using geomodel B as a truth case, three other geomodels are updated to match the impedance change. Figure 4.19a shows the misfit evolution as we update, starting with each base-case model. In all three cases, we reach a point where the misfit cannot be significantly reduced any further. It is noted that geomodels A and C are quite similar, therefore the misfits are also similar. Figure 4.19b shows the parameter evolution for one of the pilot points which controls permeability as a multiplier and is restricted to a range of

0.1 to 10. All three geomodels are updated so that a moderate change to permeability is required, though some uncertainty remains.

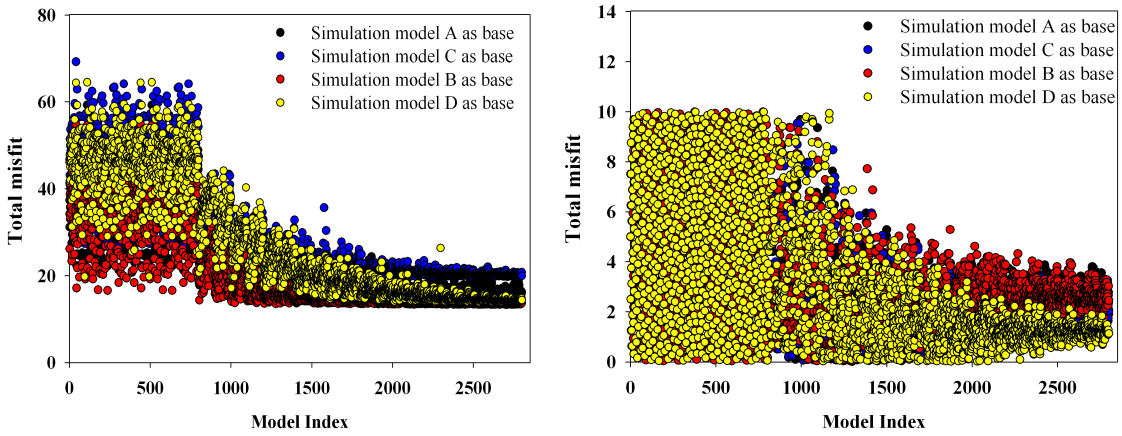

Figure 4.19: *a) Misfit evolution during history matching of simulation models A, C and D using geomodel B as a truth case, and b) evolving permeability multiplier values for pilot point 5 in Figure 4.11.*

Figure 4.20 shows statistics (mean and standard deviation) for the inverted values, that is the eight parameters case for all of the four cases as base cases against geomodel B as truth; the uncertainty for each parameter is represented in terms of standard deviation. Figures 4.21 and 4.22 shows the impedance change after one year of production for fine and coarse-scale models. The impedance is reduced around the injector owing to pore pressure increase, but impedance increases as water invades the pore space, thereby stiffening the medium. Qualitatively, the match is quite good, although some fine grid details are lost in the coarse grid model (see figures 4.23 and 4.24).

The numerical dispersion error, apparent from Figure 4.23, may actually be comparable to the physical dispersion induced by the heterogeneity. Alternatively, the relative permeability curves may have captured the effect of sub-grid heterogeneity with appropriate upscaling. The waterfront would then be spread out physically as well as numerically, and the coarse-scale simulation will then be closer to the truth.

Figure 4.25 shows that the residual error after updating is much smaller when coarse-scale models are used to generate observed data (i.e. there is no scale-dependent error). The scale-dependent errors dominate, however, and make finding a good model difficult. Further analysis on a wider range of geological models and updating procedures is required. When we consider the scale error, this error is due to the upscaling effect and the use of a different realisation as a starting model. In the case of ignoring the scale errors, the residual error is much smaller. We can measure this error and include it as a weighting factor in the SHM workflow.

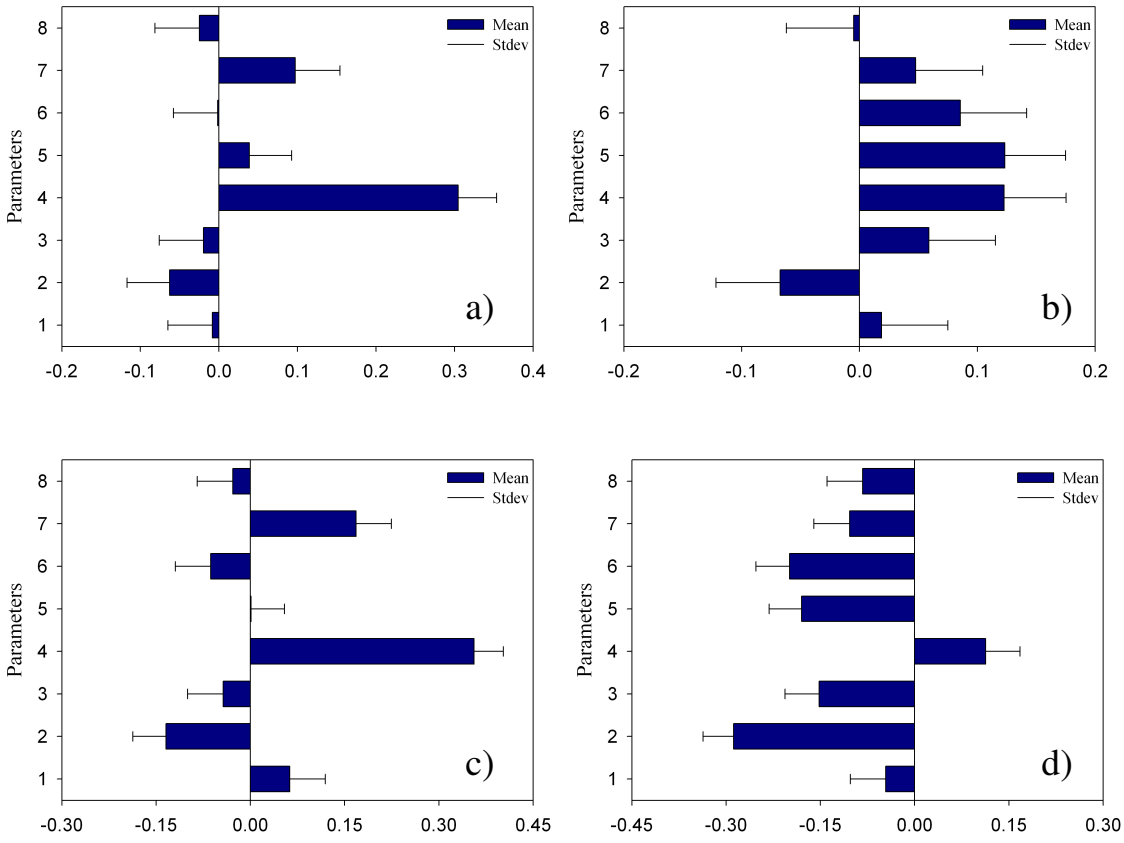

Figure 4.20: *Statistics (mean and standard deviation) for a) simulation model A as base case, b) simulation model B as base case, c) simulation model C as base case and d) simulation model D as base case against geomodel B as truth case.*

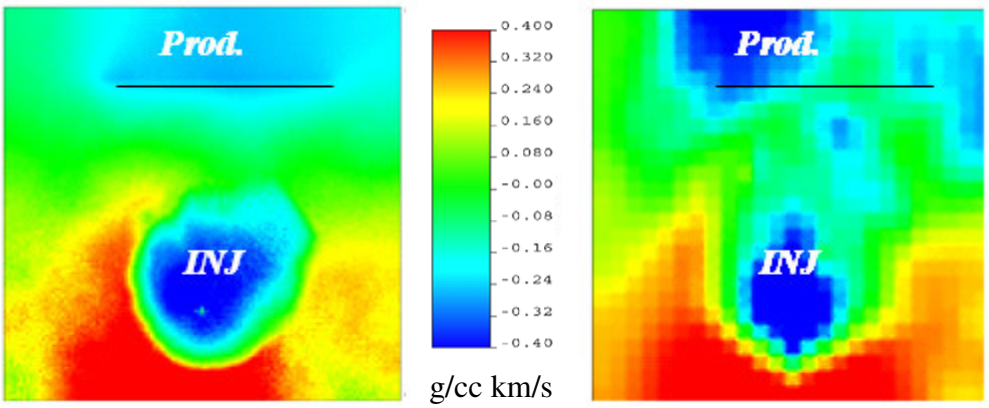

Figure 4.21: *Calculated impedance changes (baseline minus monitor survey) after the first year of production for (a) fine grid geomodel B and (b) upscaled version from geomodel A.*

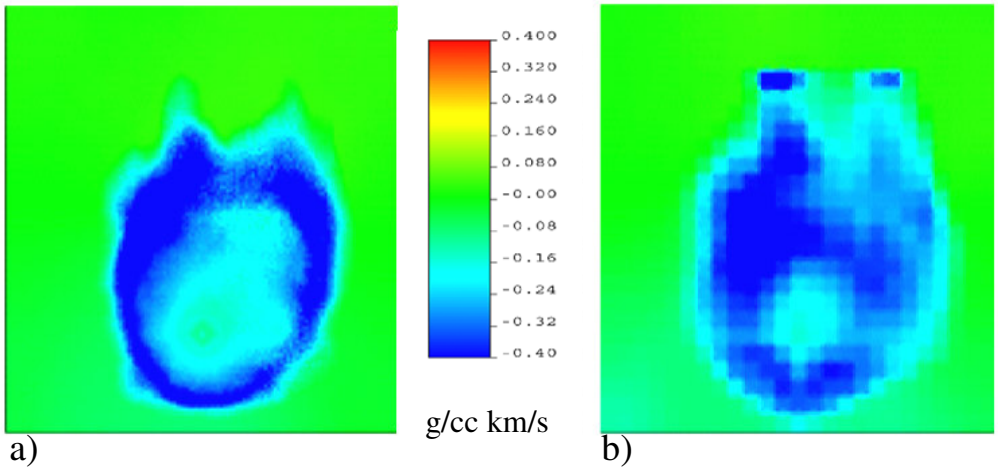

Figure 4.22: *Calculated impedance changes (baseline minus monitor survey) after the second year of production for (a) fine grid geomodelB and (b) upscaled version from geomodel A.*

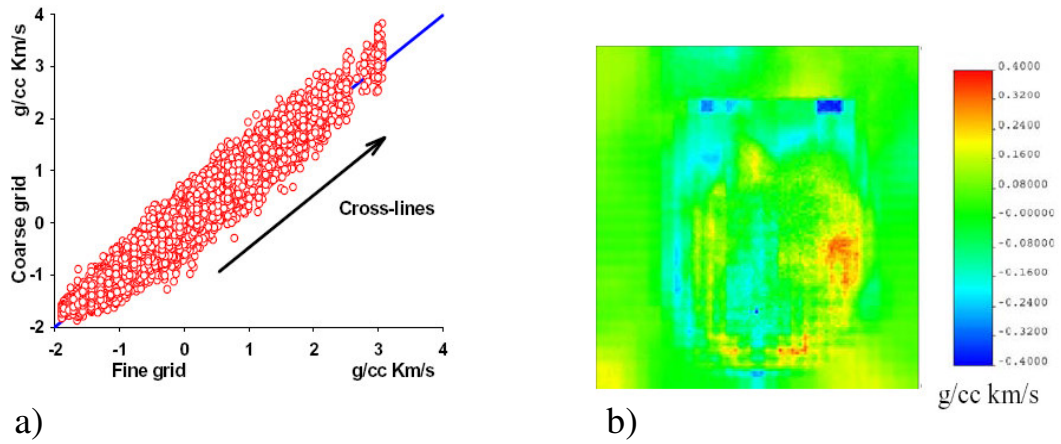

***Figure 4.23**: Impedance difference (first minus second year) from Figure 4.21 as (a) cross-plot of fine and coarse grids and (b) map of differences.*

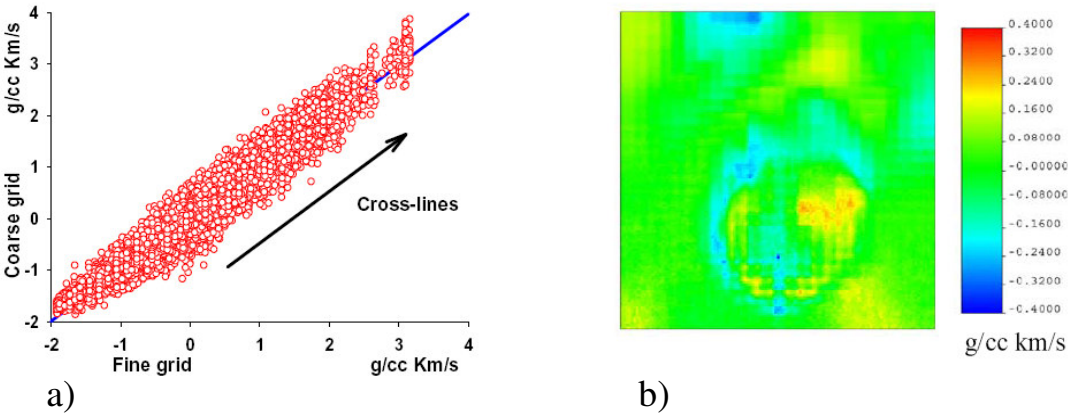

***Figure 4.24:** Impedance difference (second minus third year) from Figure 4.22 as (a) cross-plot of fine and coarse grids and (b) map of differences.*

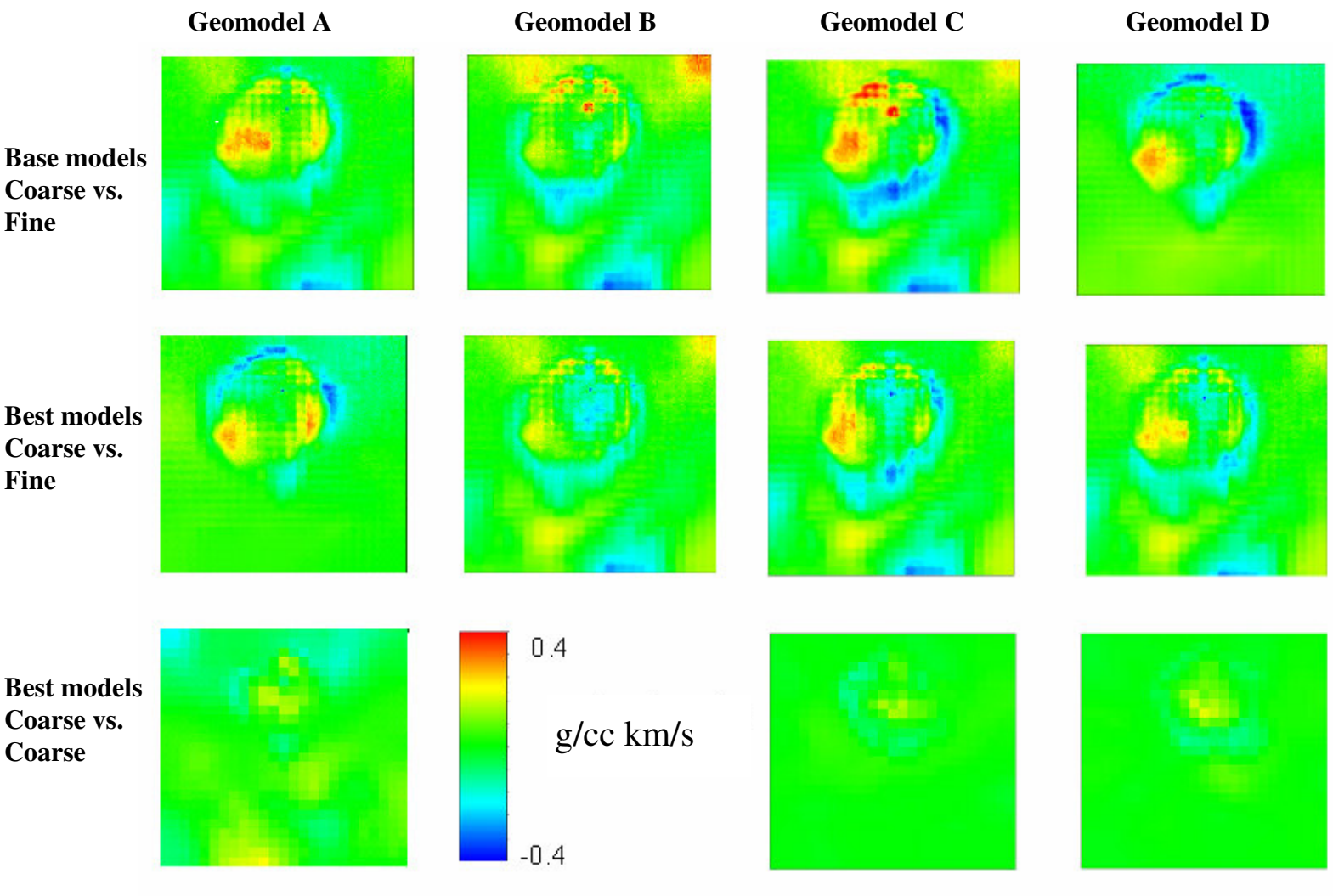

Figure 4.25: *Residual error is much smaller if we ignore the scale errors. The pilot point approach is a good way to modify a permeability field with a similar degree of spatial correlation as the pilot point separation. The scale-dependent errors dominate history matching, however, and can prevent a good model being found in some cases.*

The permeability resembles the truth case quite closely in the vicinity of the pilot points. There will still be some error in the comparison of seismic and production data as a result. In addition, the pilot point method modifies the permeability at a scale defined by the range of the variogram used in Kriging. Below this scale, differences remain and will add to the misfit.

4.7 Discussion

Two issues have been addressed in this study: whether we can use the pilot point method to update permeabilities, and how the residual error compares to scale-dependent errors.

To address the first issue, we generated fine-scale permeability realisations using sequential Gaussian simulation, which were upscaled by a factor of 5 in each direction. This was conducted using the synthetic model. It was found that the pilot point approach is an efficient way of modifying a permeability field that has a similar degree of spatial correlation to the pilot point separation.

As we move from finer to coarser-scale simulations, the waterfront becomes more spread out. The changes in permeability, such as at faults or at the edges of high permeability zones from facies transitions, may, however, still have a large model error. This would be the case particularly if permeability transitions are not coincident with the edges of grid cells.

The coarse grid should be defined relative to the faults before the geomodel is built, and this is often the case. It is, however, more difficult to avoid intra-coarse grid transitions of permeability during facies modelling. To do so requires that the facies transitions be modelled deterministically, perhaps constrained by 3D or even 4D seismic data. We have not here addressed the impact of applying different levels of noise to the observed data in terms of reducing the ability to find better models. Stephen (2007) discusses this, stating that, if the level of data error is much larger than we have observed, it may not be worthwhile spending time calibrating the model error.

4.8 Summary and final observations

We began by describing four equally probable realisations for a synthetic reservoir. We used each in turn to generate four time-lapse seismic signatures as separate truth cases. The four models were then upscaled and used as starting models in the history-matching process so that all sixteen combinations of starting model and truth case were considered. It was shown that the SHM process (using pilot points to control permeability) was able to match the time-lapse signatures such that the base-case model was updated to resemble the truth case.

For these types of models investigated here (defined by the range of the variogram used in SGS and by the pilot point separation), any realisation can be updated to obtain a good match. The pilot point approach is a good way of modifying a permeability field with a similar degree of spatial correlation as the pilot point separation, but eventually a point was reached at which the misfit could not be improved.

Finally, scale-dependent errors dominate history matching and can prevent a good model being found in some cases. The error may depend on the parameters of the system that we vary during history matching. The error in the models used here has a significant impact on the history-matching result and is unavoidable without seriously increasing the detail that we must consider which in turn would reduce our ability to search the parameter space adequately. We can accept the error provided that we compensate for it in the misfit calculation so that we have a better measure of how close our predictions are to reality. We have shown that it is possible to correct for the errors in the modelling described here, to enable us to find more accurate models. Of course, the effect of the model error must be considered relative to the data error, which, if large, may dominate the history-matching process. In addition, a good model prediction can be seen from the best models, along with their closeness to the truth.

CHAPTER FIVE

Schiehallion: Reservoir Evaluation and Management

This chapter provides a full description of the Schiehallion field. This includes geological settings, reservoir development, management, and static modelling. Seismic amplitude attributes maps are used by the operator's model to demonstrate the external structural design of the channelised sands and to describe time-lapse seismic applications such as the importance of assessing lateral connectivity in this field and improving reservoir management. The main source of uncertainty in this field is discussed, together with its importance. In addition, understanding the origin of this uncertain parameter provides useful lessons for achieving good SHM.

5.1 Schiehallion overview

The Schiehallion field is situated on the Atlantic margin of the UK Continental Shelf (UKCS), about 200 km to the west of Shetland, and holds most of the hydrocarbon reserves in that area. A partnership of BP (operator), Shell U.K., Amerada Hess, Murphy Petroleum, OMV, and StatoilHydro (U.K.) currently own the field. Together with the Foinaven and Loyal fields (all of them BP operated), they comprise the biggest and deepest water UKCS subsea development in water depths of up to 500 m (see Figure 5.1).

The Schiehallion Paleocene turbidite reservoir sands lie at a depth of 1800–2064 m (~1800–2000 ms TWT). Horizontal wells must be steered through the four 10–50 m thick

sand bodies to ensure that 300–1000 m of net rock is contacted to produce at a sufficiently high rate (Walder *et al.*, 1999).

The oil is close to bubble point, and to prevent significant gas breakout and deliver sweep, sub-vertical water injectors are employed. However, the effective use of the water flood demands a high level of connectivity between injectors and producers. This is a significant issue in a turbidite system that is inherently heterogeneous. The field has been producing since 1998 through subsea horizontal wells, which are tied back to the Schiehallion FPSO (Floating Production Storage and Offloading vessel).

The multiple reservoir sands are siliciclastic turbidites, with seismic interpretation and attribute mapping revealing them to be highly channelised units. Reservoir quality varies in character from thinly interbedded sands to massive sands (Lancaster *et al.*, 2000), with the massive sands being of better quality. Classically, the sands are fine to medium grained, with 23–30% porosity and 250–2000 mD permeability. The Schiehallion reservoir fluids are geochemically mixed source oils, with oil gravity in the range of 22–28° API. It has been estimated that high levels of gas have come out of solution in some areas, particularly early on in field life. Several seismic surveys have been acquired in Schiehallion (pre-production in 1993 and 1996, as well as monitor surveys in 1999, 2000, 2002, 2004, 2006 and 2008). The static seismic image for the field is good; the subtleties of the barriers and baffles to flow remain ambiguous.

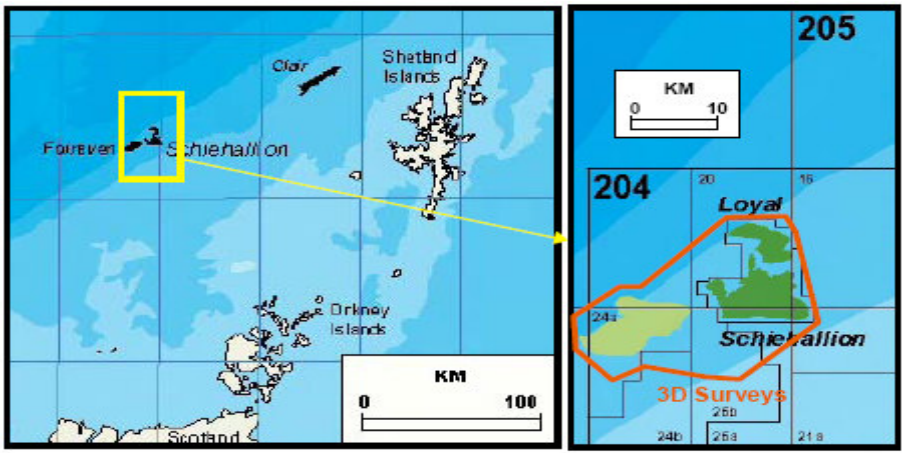

Figure 5.1: *Location of the Schiehallion field.*

5.2 Geology, reservoir characterisation and management of the field

The operator refers to the Paleocene–Early Eocene sequence in the West of Shetland as the 'T-sequence'. More comprehensive and detailed descriptions of the Paleocene deep-water sandstones can be found in Lamers and Carmichael (1999). This convention is used in this thesis in order to refer to the reservoir. The description of the T-sequence has been developed over the last ten years by incorporating seismic and well log data constrained by biostratigraphical analysis (see Figure 5.2). The Schiehallion reservoir is encapsulated within the T30 Paleocene Sequences, which are equivalent to the Andrew Member according to the North Sea lithostratigraphy and are represented as siliciclastic turbidite sandstones that are the result of the erosion of the uplifted Scottish Massif in the southeast. The T30 interval is also subdivided into a number of sequences (e.g. T31, T32), based upon well log and seismic data interpretation. Within these sequences, three different sets of episodes of sandstones depositions are known in the Schiehallion field, namely T31, T34 and T35, and contain the main reservoir of the field. Reservoir sand quality increases from thin interbedded sands to massive sands. The sandstone packages are fine to medium grained, and porosity ranges from 23% to 32%, with structure dip of 2–3° to the northwest, crossed by a series of east–west faults dividing the field into four structural segments as shown in Figure 5.3.

In April of 1995, an Extended Well Test (EWT) was carried out in a high-angle well drilled in main channel sand in the T31 sequence to identify possible flow barriers at the edge of the identified channels (Richardson *et al.*, 1997). From the interpretation of the EWT, it was concluded that the reservoir is quite well connected throughout the main channel sands, with good communication of fluids within each segment defined by the structural interpretation. There also appeared to be some degree of decrease in the transmissibility in the areas around channel edges.

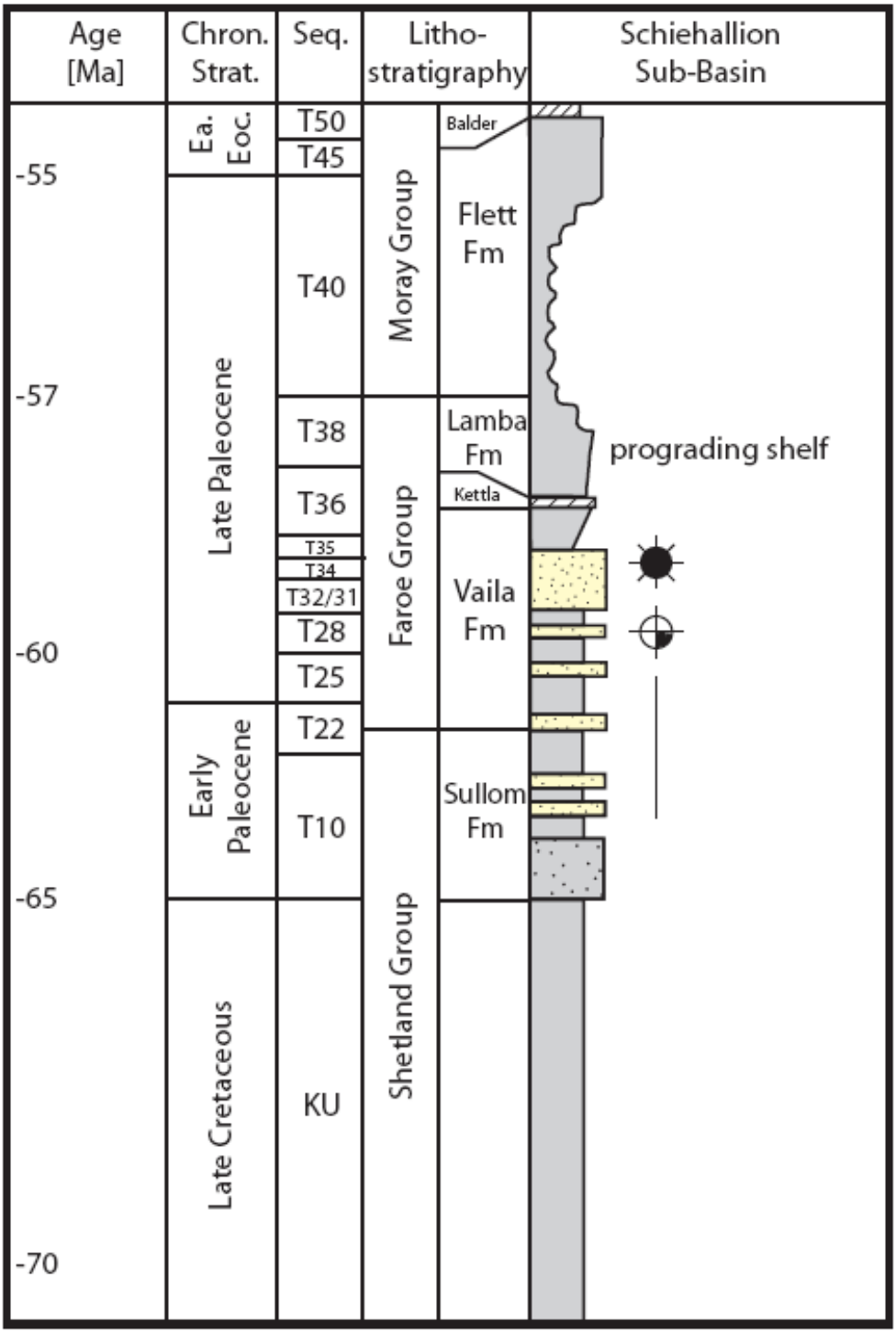

Figure 5.2: *Paleocene stratigraphy template for the Schiehallion field and its relationship with the operator's regional stratigraphic sequence, after Lamers and Carmichael (1999).*

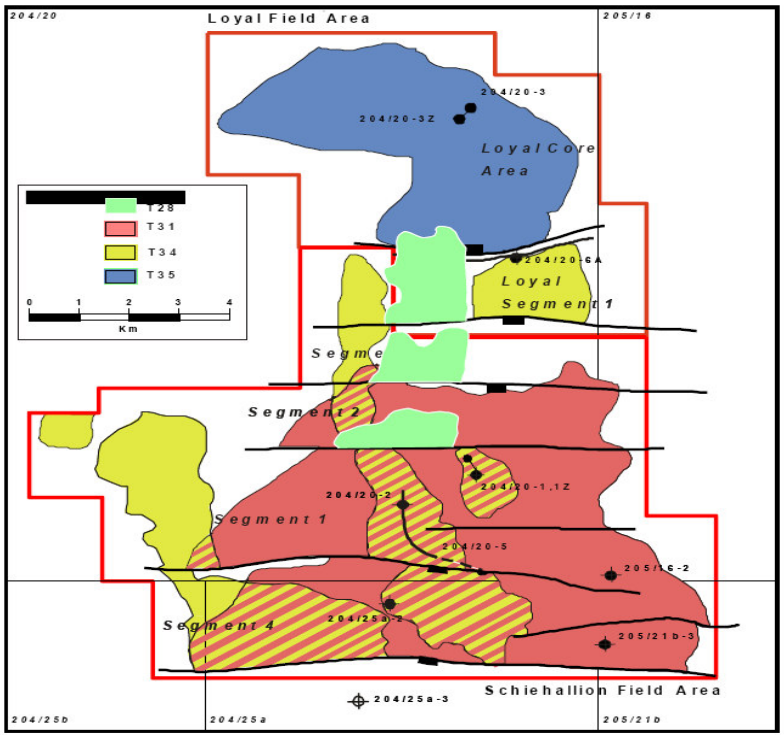

Figure 5.3: *Schiehallion field outline T31 is presented in Segment 4, Segment 1 and Segment 2.*

As a result of the 3D seismic interpretation by the operator (Leach *et al.*, 1999), three types of seismic facies have been presented in this field as follows:

1. Channelised Seismic Facies: This is typical basal erosion with elongated shape geometry. Based on well and core log information, the channels are interpreted as massive sandstone structures with the laminated sandstone on the tops of the bed preserved (Figure 5.4). The depositional environments are interpreted as a submarine slope channel system. The channels are up to 70 m thick and vary in width between 100 and 1000 m.

2. Parallel Seismic Facies: These seismic facies are observed as parallel top and base sandstone reflections. The top event has a moderate seismic amplitude response. The gross thickness is around 20–40 m. No wells have been drilled in this facies, and as a result, the

exact nature reservoir architecture is currently uncertain. 1996 3D seismic data suggests these facies have a more channelised character.

3. Chaotic Seismic Facies: These seismic facies are observed as a low to moderate seismic amplitude. They are probably generated because of a submarine slope failure. No wells have been drilled in these facies. The NTG (Net:Gross) is very low or zero, and the reservoir connectivity is very poor or absent.

The southern part of the Schiehallion field is sealed by an east–west normal fault. This fault exceeds the reservoir thickness and links the Schiehallion T31 and T34 sandstone reservoir against the overlying T35 mudstone. The trap in the eastern part of the field is a result of the pinch out of the T30 reservoirs against a north–south Paleocene intrabasin structural high (figures 5.5 and 5.6). The regional structural dip creates the trap to the north and west.

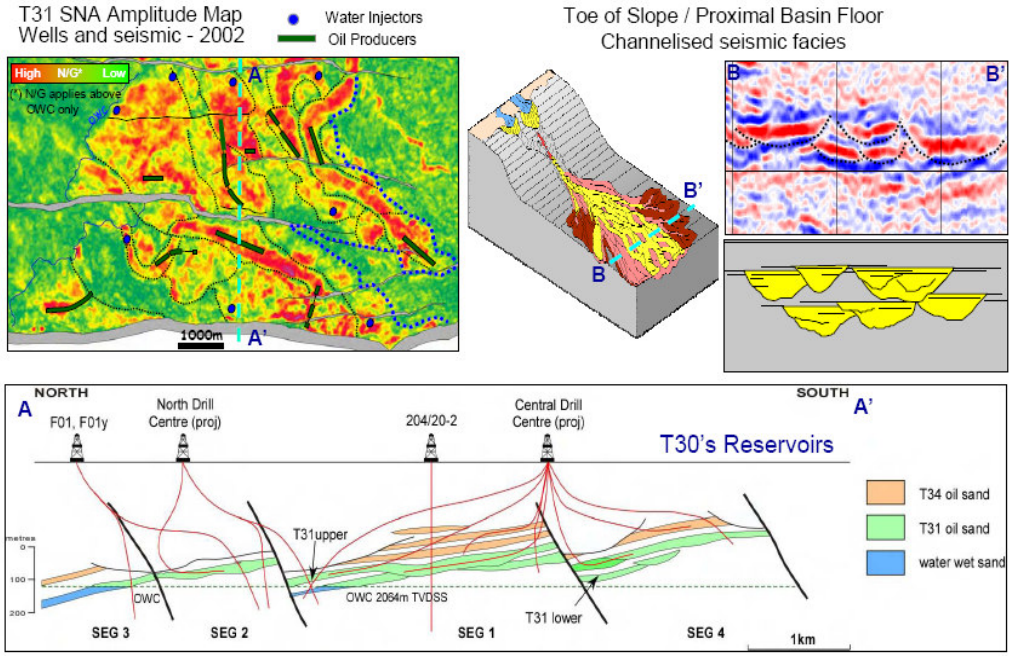

Figure 5.4: *Schematic geological model for the Schiehallion field (after Gainski et al., 2008) showing two different cross sections. A–A' is north–south and shows the four segments in the field and the different T-sequence distributions. B–B' shows the channelised seismic facies and their orientations.*

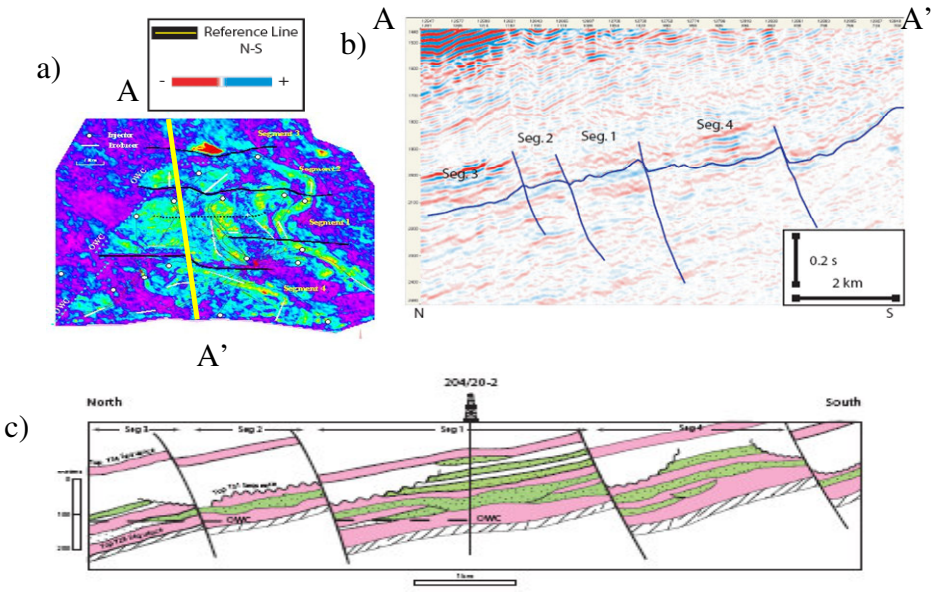

Figure 5.5: *(a) Location of the cross section in the field, (b) North–south cross section of the Schiehallion field, showing the reservoir segmentation through a normal fault system and . (c) schematic north–south cross section of the Schiehallion field, showing the reservoir segmentation through normal fault system. (After Leach et al., 1999)*

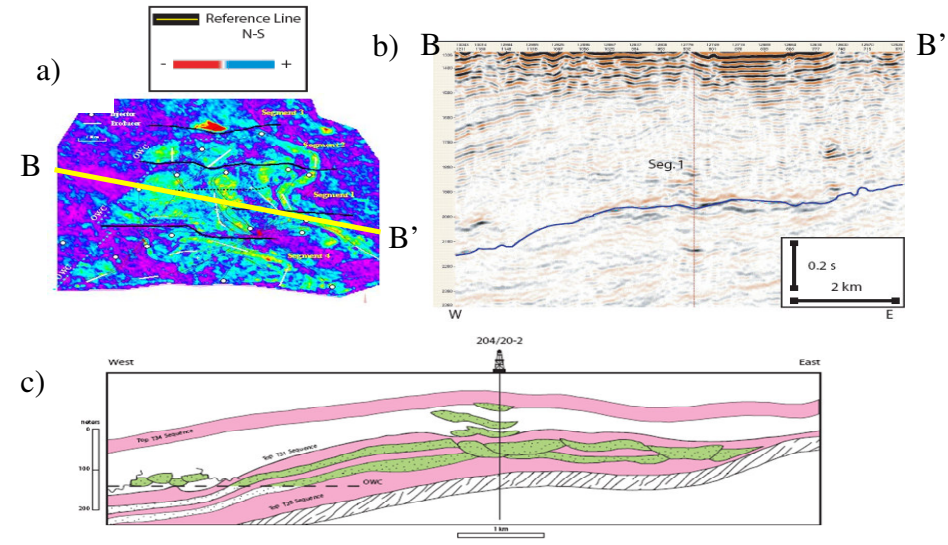

Figure 5.6: *(a) location of such as cross section in the field (west–east cross section of the Schiehallion field, (b) West–east cross section of the Schiehallion field showing the seismic quality for Segment 1, and (c) the reservoir segmentation through a normal fault system. (After Leach et al. 1999)*

5.2.1 Reservoir faulting and barriers

Schiehallion is crossed by east–west faults, which divide the reservoir into four major Segments (1–4, Figure 5.7). Most of the mapped oil in place is contained in Segment 1 and Segment 4. The degree of connectivity across the faults on a production timescale is uncertain. In 1996, wells drilled in Segment 1 encountered depletion from the 1995 EWT, whereas wells in Segment 4 were not depleted, which suggests that the connectivity between the two segments is limited.

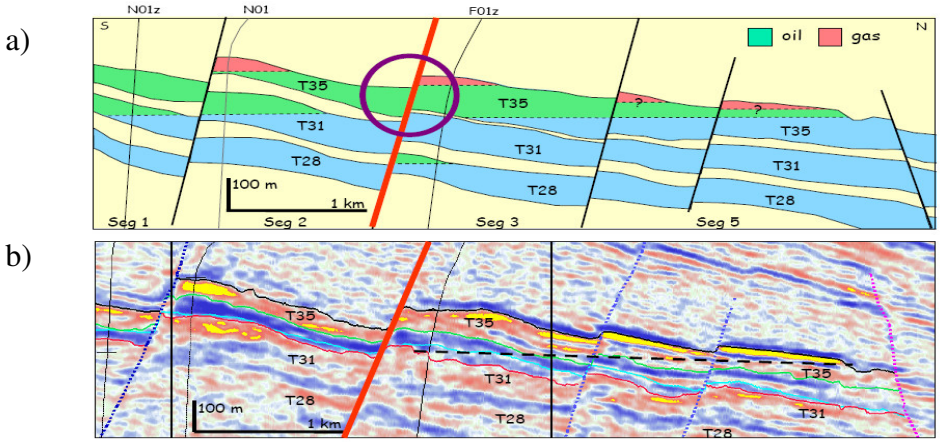

Figure 5.7: *Section a and b along North Channel. Also shown is the faults and barriers system in Schiehallion field (after Miranda, 2007).*

5.3 Base 3D seismic interpretation

The first 3D survey was acquired in 1993 and confirmed the distinction between the high-amplitude, oil–sand response and nearly invisible water-wet sands. Localised, primary gas caps were subsequently found to have the highest amplitudes. The acquisition and interpretation of this data was used to determine the extension of the fields within this sub-basin and to plan the well location and appraisal approach for a later field development.

In T31, the hydrocarbon bearing intervals are represented by a decrease in acoustic impedance, and a trough-over-peak assuming zero phase and normal SEG polarity (Leach *et al.*, 1999) therefore represents the top and the base of the reservoir intervals. In general,

the impedance contrast is weak in the non oil-bearing regions of the reservoir, but as we enter the mineralised zone, this contrast is stronger. The seismic signature in the Schiehallion field can be clarified by classical bright spot technology, where constructive physics situation are presented within the reservoir. Seismic reflection can produce effects that can be captured – for example, local decreases in amplitude creates what are called dim spots, while a local wave shape change can be identified as a polarity reversal or local phasing (Sheriff, 1992; Brown, 1999). This type of physical phenomena depends on the impedance difference being present in the background of the reservoir. For a water-saturated reservoir rock with lower acoustic impedance than the surrounding rock, the presence of hydrocarbons usually increases the contrast, and a high-amplitude bright spot results. This is a very common situation for Tertiary clastics (see Benabentos *et al.*, 1975; Huston and Backus, 1998; Benabentos *et al.*, 2002) and has been applied in 4D interpretations (Watts *et al.*, 1996; Parr and Marsh, 2000). In consequence of this seismic characteristic, a window-based attribute extraction technique was used to interpret the spatial distribution of reservoir properties in the reservoir.

5.4 Reservoir fluid properties for Schiehallion

The Schiehallion reservoir fluid has three phases (oil, gas and water) with gravity in a range of 22 to 28° API. The initial reservoir pressure is 2907 psia at a datum depth of 1940 m TVDss. Typical values for the gas–oil ratio (GOR) and saturation pressure are 342scf/bbl and 2677 psia respectively. High wax content results in high viscosities ranging from 1.5 to 4.5 cp. PVT properties have a high uncertainty, derived from the difficulty in obtaining single-phase samples, because the reservoir pressure is close to bubble point pressure (Leach *et al.*, 1999).

5.5 Production history and field development

The initial reservoir pressure in Schiehallion is close to bubble point. The field was developed with horizontal producers and near-vertical water injectors to provide sweep and

maintain pressure. Based on seismic attribute analysis, the horizontal wells were drilled in the core of the channels, where high pay reservoir properties (Figure 5.8) were expected.

The original development strategy aimed to avoid placing injectors and producers in the same channel, in order to avoid early water breakthrough and therefore to maximise sweep. However, owing to the poor connectivity, especially in the east part of the field, it quickly became clear that many of the producers did not achieve the pressure support from the injector wells. For the first 3–4 years, the reservoir management plan was largely about gas management, with a focus on the infill drilling of water injectors to recover reservoir pressure and reduce GOR production (Figure 5.9).

Water cut has increased, and the field water cut is now around 30%, and the reservoir management focus has moved to managing the water cut problem. The Schiehallion field and Loyal field produced over 2 billion barrels of oil in situ and have produced at rates of 140 MStb/d of oil. The Schiehallion field alone had produced 212 MMstb by the end of 2004 (Fletcher *et al*., 2005).

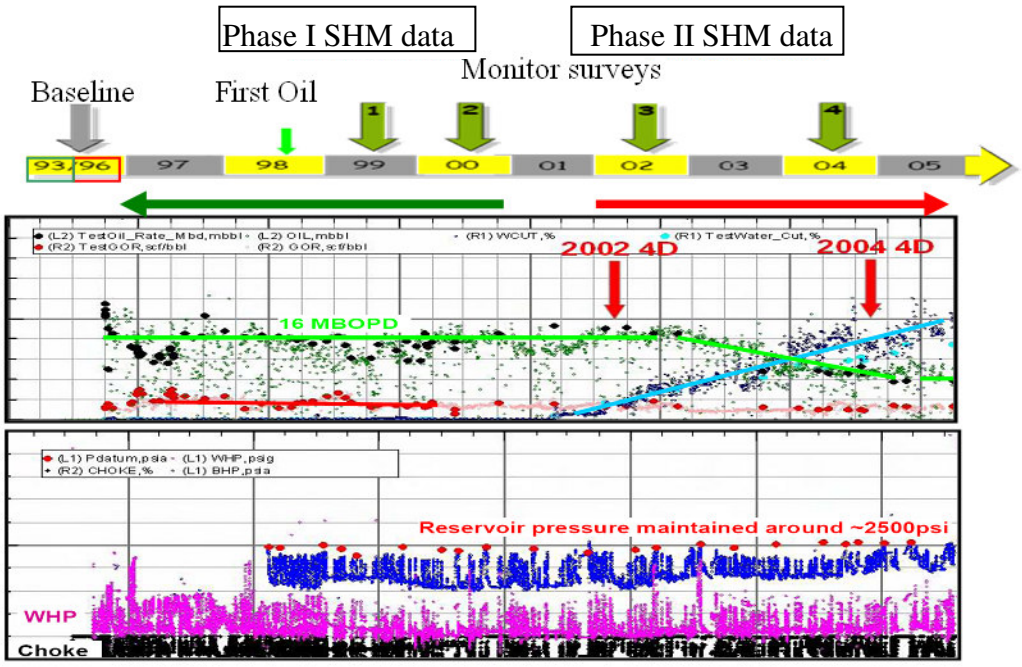

Figure 5.8: *The monitoring surveys during Schiehallion's life show the trend in pressure and GOR (after Miroslow G. et al., 2008). Phase I includes seismic data from 1993 as baseline, 1999 and 2000, and Phase II data includes seismic data from 1996 as baseline, 2002 and 2004.*

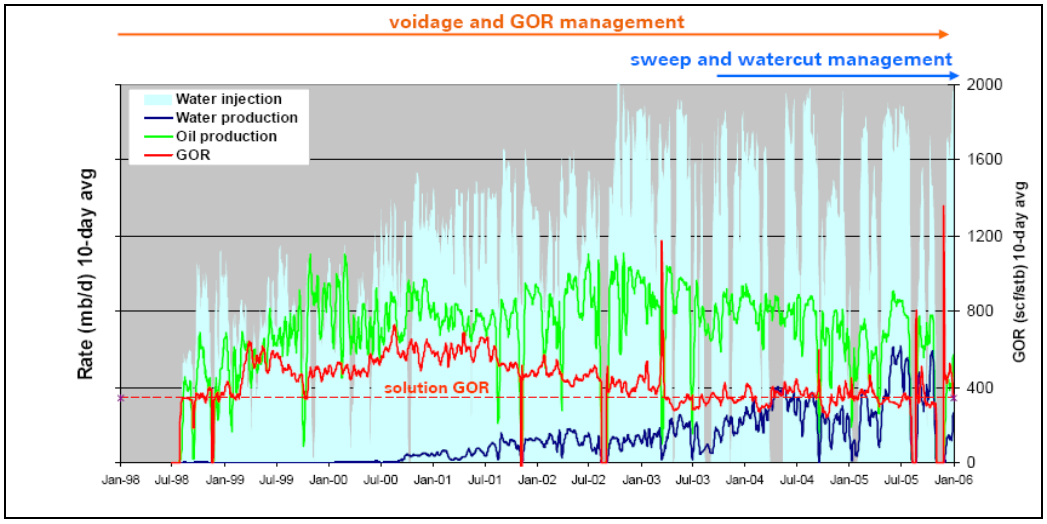

Figure 5.9: *Production profile including GOR, oil rate, water production rate and water injection rate for Schiehallion (after Govan, 2006).*

5.6 4D seismic for reservoir monitoring

The successful 1999 4D (time-lapse 3D) programme and depletion has played an important role in the improvement of reservoir management and well planning.

Acquisition was repeated during the summer of 2000, when data was obtained over 390 km^2 of Quad 204 in the UKCS Atlantic Margin. The data covers all three BP-operated producing fields to the West of Shetland.

The 1998 study established that the acquisition differences in the 1993 and 1996 surveys could still deliver a high level of repeatability (~6% in RMS amplitude) when processed in an identical way (Parr *et al.*, 1999). The 1999 data was processed through the exact same sequence as the earlier reprocessed pre-production surveys. An identical approach was taken with the 2000 data.

A comparison of two pre-production surveys across the Schiehallion field (1993 and 1996) demonstrated the repeatability of surface-towed data, given the same acquisition alignment and processing through an identical sequence (Parr *et al.*, 1999; Cooper *et al.*, 1999b and Kristiansen, 2000). A priority volume across the Schiehallion field was processed on board, and interpretation volume was delivered within fourteen days of the last shot. Monitor surveys were acquired in 1999 and 2000, both being referenced back to the 1993 pre-production baseline survey, and another two surveys in 2002 and 2004 being referenced back to the 1996 pre-production baseline survey. The effective uses of these 4D seismic surveys and pressure data acquisition have led to a successful infill drilling campaign. The reservoir pressure has recovered in several areas, and the producing GOR has been reduced to close to the solution values. As the Schiehallion field has matured, water production has inevitably increased, and the field water cut is now around 30% (Govan *et al.*, 2005). The reservoir management focus has shifted to managing sweep and water cut. Therefore, a new seismic survey was planned for 2004 in order to help identify zones swept by water. However, feasibility studies have shown the 4D signal expected for water flood is smaller

than the 4D signal for gas breakout. To optimise the potential for the detection of weak 4D signals over Schiehallion, the 1996 dataset was used as the baseline, thereby taking advantage of the acquisition improvements between the 1993 and 1996 datasets (Figure 5.10 and Figure 5.11).

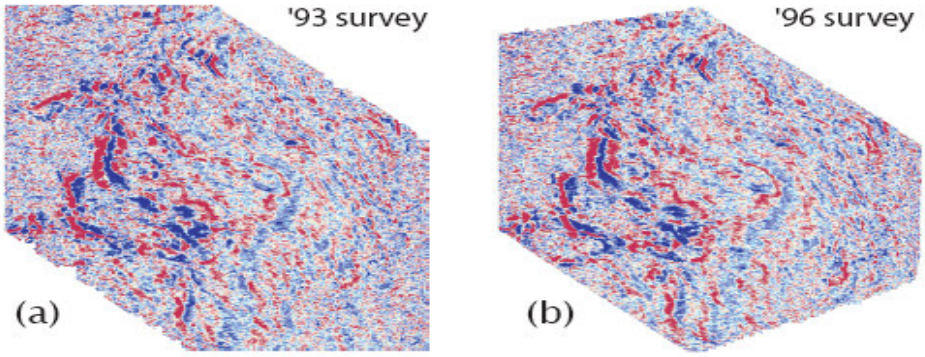

Figure 5.10: *Time slices for (a) 1993 and (b) 1996 seismic surveys at 2000 ms (after Altan et al., 2001).*

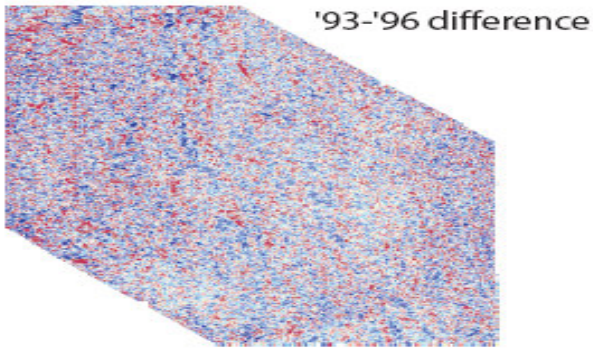

Figure 5.11: *Time slices at 2000 ms for the difference between the 1993 and 1996 seismic surveys (after Altan et al., 2001).*

New 4D repeat/monitor towed streamer surveys provided a significant improvement in 4D repeatability. This was achieved after careful pre-survey planning to repeat the source and receiver positioning to within 100 m or less. Figure 5.12 shows the water saturation change. Figure 5.13 shows the shot/receiver repeatability for the 2002 and 2004 surveys

with respect to the 93/96 baselines. In the Schiehallion field, the reservoir rocks are acoustically softer than the overlying shales. This contrast will increase if something occurs to make the rocks softer than the AI (Acoustic Impedance), and so the 'brightness' will increase. This will reduce the net effective stress on the rock frame because of the increase in the pore pressure, which will make the matrix 'softer'. A much more compressible fluid is introduced into the pore space by the evaluation of the gas well, significantly reducing the overall fluid hardness. An opposite effects reverse of the processes presented above because of a reduction in the pore pressure, and resolution of gas. In addition, a hardening effect arises in reservoir rocks owing to water injection, because the compressibility of the hydrocarbon is higher than that of the water.

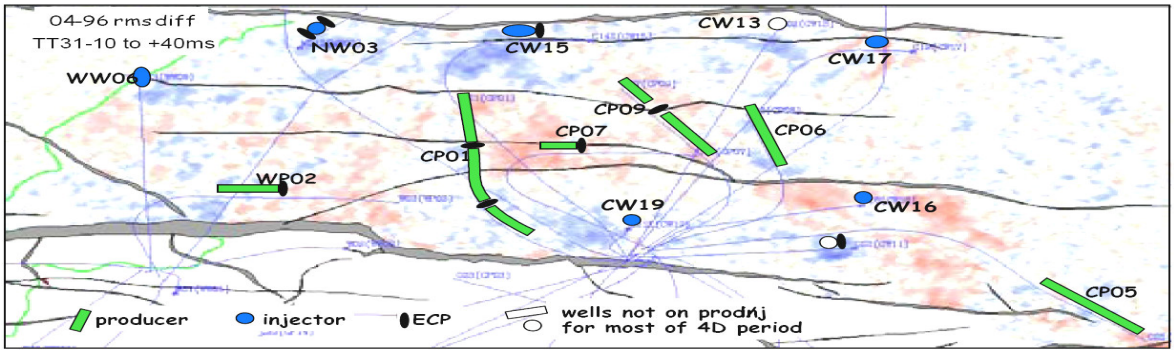

(blue = increased Sw, red = increased Sg or increased P)

Figure 5.12: *Differences map (2004–1996) showing clearly the water saturation change (after Govan et al., 2005).*

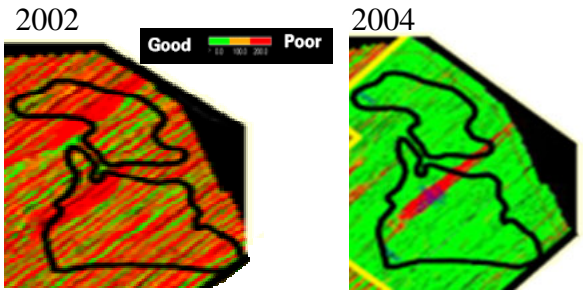

Figure 5.13: *Maps showing geometrical repeatability after acquisition – baselines/2002 monitor (left), baselines/2004 monitor (right). After Campbell et al. (2005).*

5.6.1 Feasibility study for 2004 time-lapse seismic data

Floricich (2007) introduced a full feasibility study to estimate the possible 4D signal expected between the 2004 and 1996 seismic surveys. A stochastic fluid replacement procedure was used to examine the impedance changes due to fluid saturation changes in the reservoir. The mean and standard deviation for the fluid properties are taken from the published literature for the Schiehallion area. Batzle and Wang's (1992) equations are used to compute the density and bulk modulus of the different fluids (water, oil and gas).

Floricich (2007) concluded that the variations in acoustic impedance are due to the combined effect of changes in water saturation and reservoir pressure for the Schiehallion area in a rock of 27% porosity.

An increase in reservoir pressure has an opposite effect to an increase in water saturation on the acoustic impedance change (Figure 5.14). In the case of Schiehallion, an increase in pressure of 500 psi could reduce the acoustic impedance change due to water flood to half the value if no change in reservoir pressure is present. Most importantly, an increase in reservoir pressure of 1000 psi or more could mask the change in acoustic impedance due to water flood. The 4D signal is a combination of both effects, and separating and quantifying these production effects would provide additional value to the field reservoir management (Floricich, 2007).

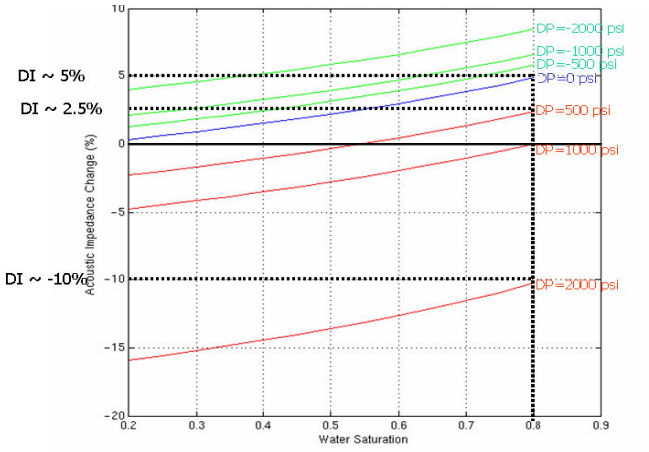

Figure 5.14: *Estimated changes in acoustic impedance due to change in water saturation and reservoir pressure. (Floricich, 2006)*

5.7 Seismic data-derived barriers

Production data and 4D seismic surveys have shown that the Schiehallion field is compartmentalised: fluid is strongly impacted by barriers. A total of 215 (Macdonald *et al.*, 2004) such barriers were mapped from the coherency data (Figure 5.15). It is difficult to convert the seismic coherency picks into surfaces with a sufficient number of points on them to be able to definitely 'snap' the surfaces to the correct faces of the simulation grid cells: the coherency data picks tended to be inclined, and not vertical, making the surfaces true three-dimensional objects. To avoid this problem, barriers have been represented vertically (in a simulation k-direction) and by discretising them areally, so that they stair-step through the simulation grid at the top of the T31 reservoir.

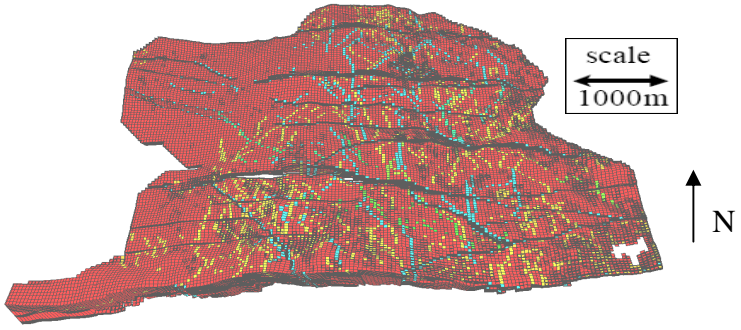

Figure 5.15: *Top-view picture showing the x-direction barriers in the T31 reservoir.*

5.8 Static reservoir model

The static reservoir model provided by the operator is an updated version of the Phase I model. The main differences are the network of faults and barriers in terms of the location and the density. The new model has more faults and barriers than the Phase I model, and the new model has been updated since additional wells and reprocessed seismic data is included. Incorporating new production and pressure data suggests a high degree of compartmentalisation. In this new model, the seismic data was used more effectively by matching the NTG maps (Figure 5.16) derived in 2004. The porosity trend is clear throughout the field, increasing towards the southeast. Nevertheless, the range in the porosity values is high, and varies from 0.25 in the west flank to 0.32 to the southeast of the reservoir (Figure 5.17). The new model has been built to improve planning of the field development. It is also needed for planning future seismic surveys. The facies modelling is constrained by the facies interpretation conducted for each well and is stochastically driven by the depth-converted coloured inverted stack volume (Lancaster and Whitcombe, 2000). The volumes have been used in two ways. Firstly, seismic volumes have been used to separate large-scale channels over bank regions in the model. Secondly, correlations between facies type and seismic amplitude have been used to guide the stochastic facies modelling.

Cross checks between the geologically interpreted cross section and analogues (Brushy Formation outcrops analogues (see Borer *et al.*, 2003; Borer, 2003; Leiphart and Hart, 2002) show a good correlation, and its estimations have been proven to be robust.

The final model was built in a fine grid scale vertically (typical cell size is 100 m × 100 m × 0.5 m) in order to obtain a detailed description. For the simulator to be used for field management, upscaling was applied to decrease computational run time. Generally, for this model, there is no correlation between external geometry distribution and lithofacies, e.g. a high sandstone proportion can be found in channelised systems as well as in sheet-like systems.

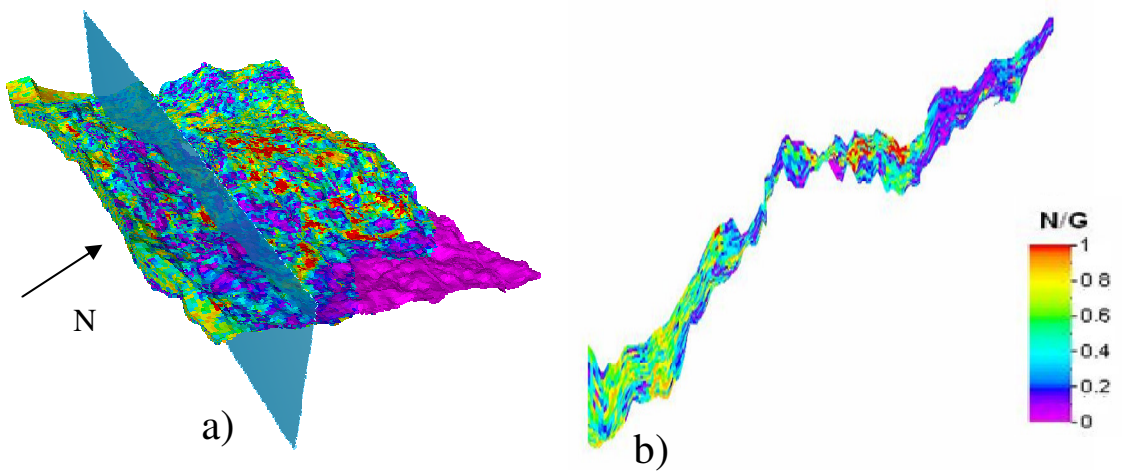

Figure 5.16: *NTG reservoir static model for Schiehallion field. In (a) we can see a vertical average map of the simulator NTG model. b) A north–south cross section of the reservoir model, showing the vertical distribution of NTG around T31 sequence. Note also the well path penetrating the high NTG zone.*

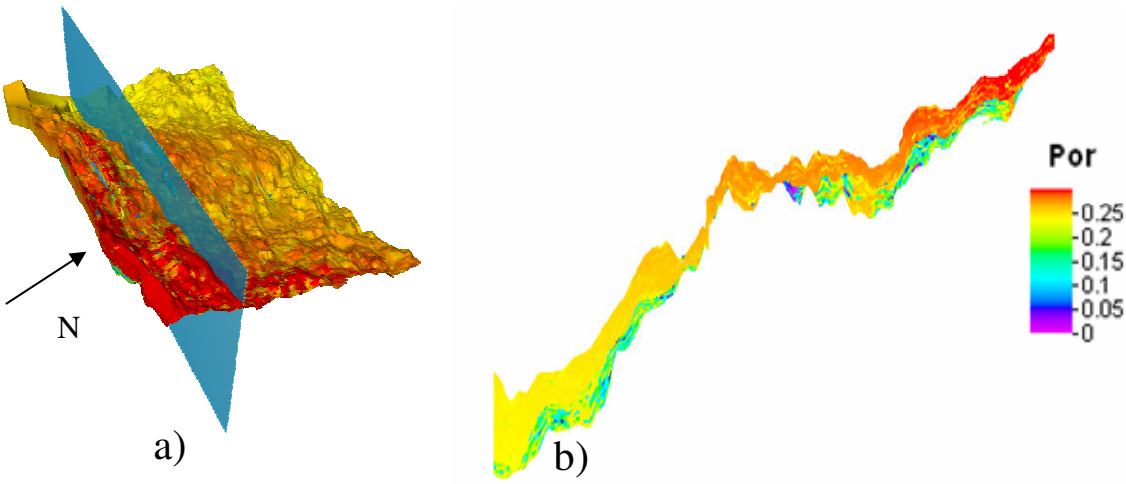

Figure 5.17: *Map showing the modelled average porosity distribution in the Schiehallion field. East–west cross section for T31 in the Schiehallion. In (a) we can see a porosity map of the reservoir model. b) A north–south cross section of the reservoir model, showing the distribution of Porosity around T31 sequence.*

5.9 Aquifer representation

Initially, the operator applied an infinite radial analytical aquifer model to the western side of the model to provide aquifer support (Figure 5.18) with 8 mD effective permeability. Subsequently, a numerical aquifer has been used on the western side of the model that has water-bearing cells with increased pore volumes, to provide aquifer support. These aquifer cells have an NTG ratio of 1, a permeability of 8 mD and a porosity of 20% (Macdonald *et al.*, 2004).

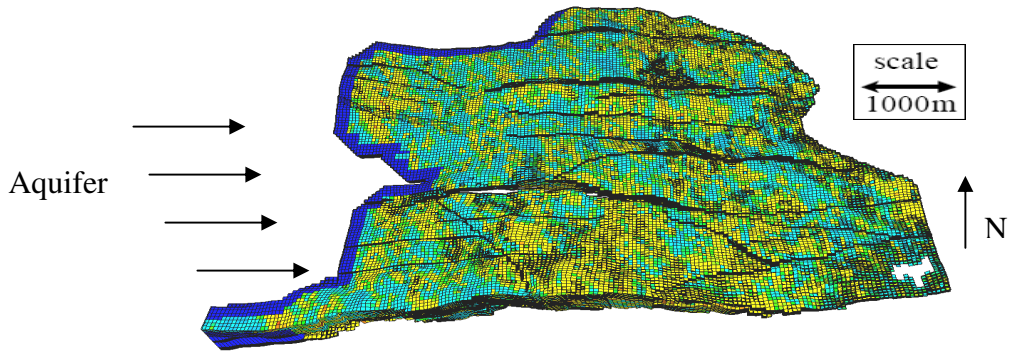

Figure 5.18: *Location of aquifer cells (blue band on western side of model).*

The Schiehallion model is run through a simulator to predict the three-phase flow changes and pressure changes (Figure 5.19) from the production time obtained in 1998 (figures 5.20 and 5.21).

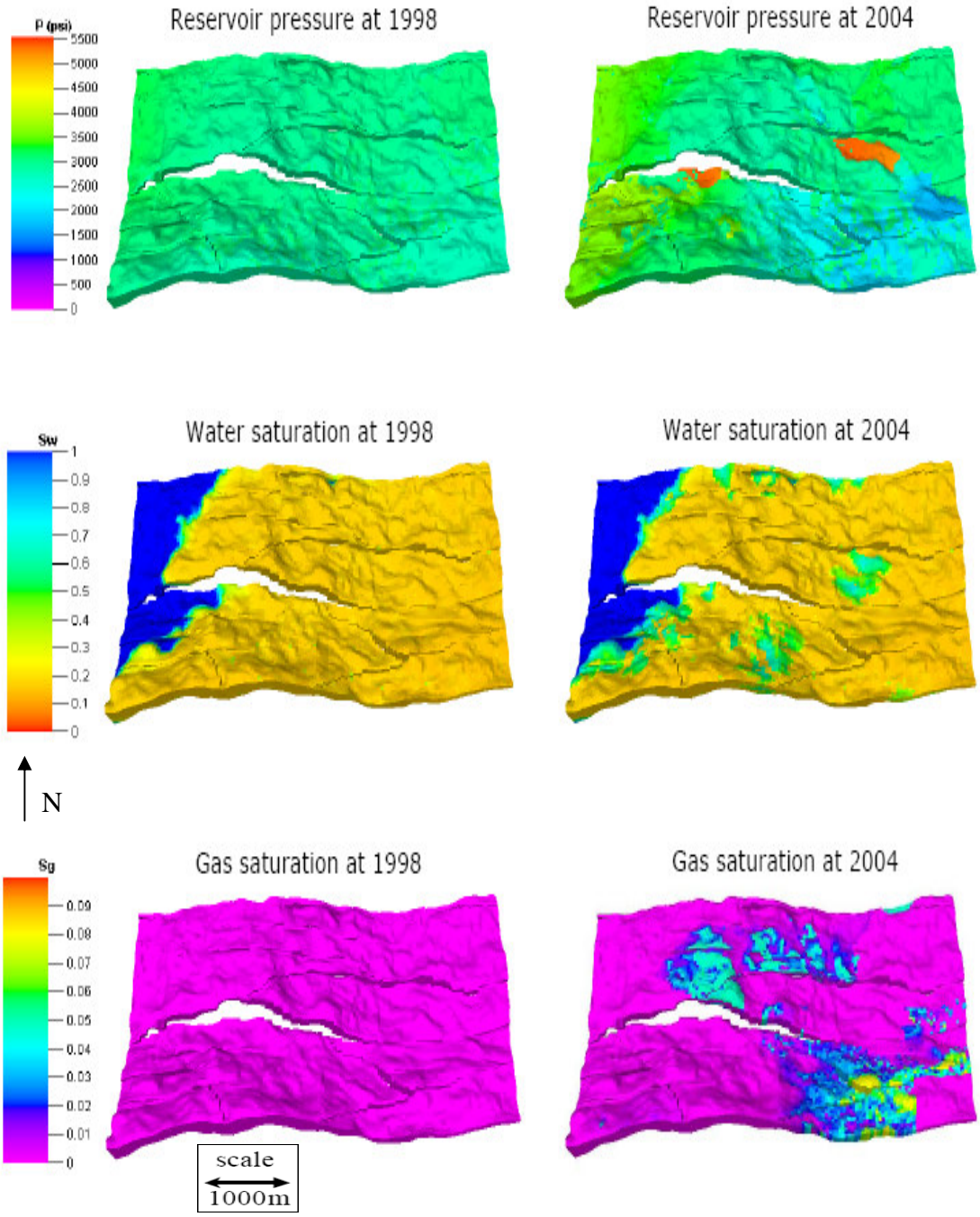

Figure 5.19: *Pressure, water saturation and gas saturation predictions from the reservoir simulation model for the initial pre-production conditions and for 2004.*

a)

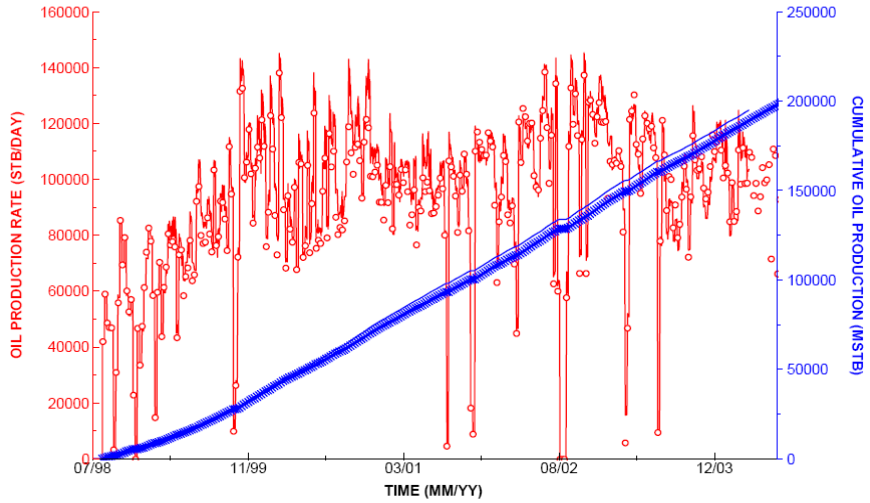

(b)

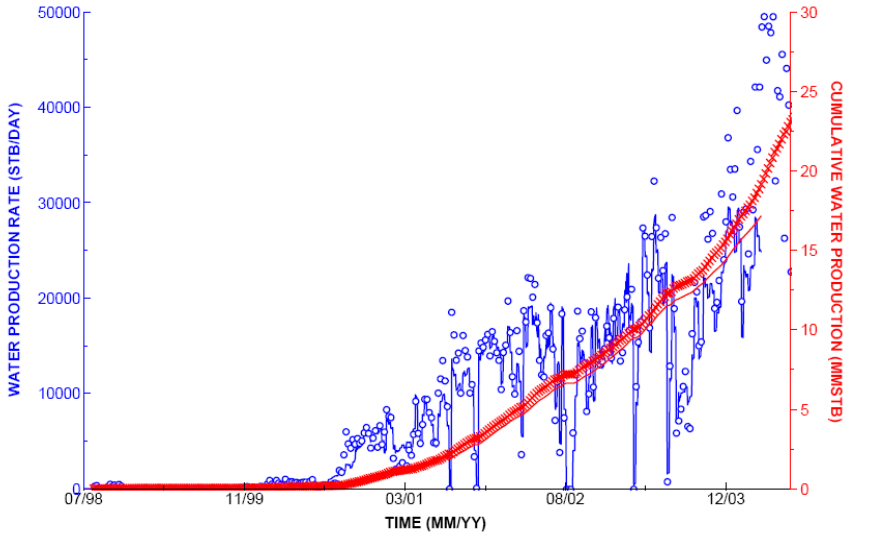

Figure 5.20: *Production profile observed and estimated for the best operators obtained realisations of the model up to 2003. a) Oil production rate and cumulative oil production. b) Water production rate and cumulative water production. (Macdonald et al., 2004)*

(a)

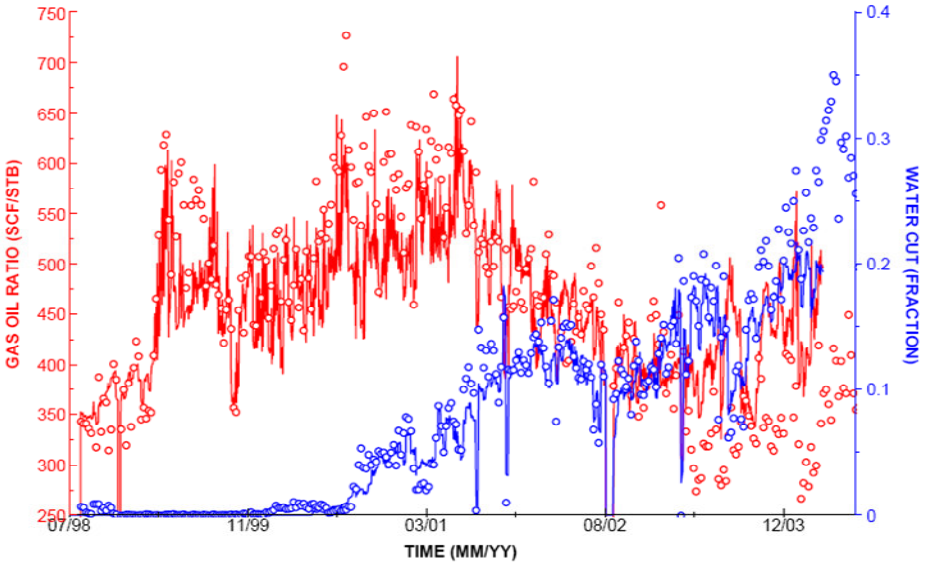

(b)

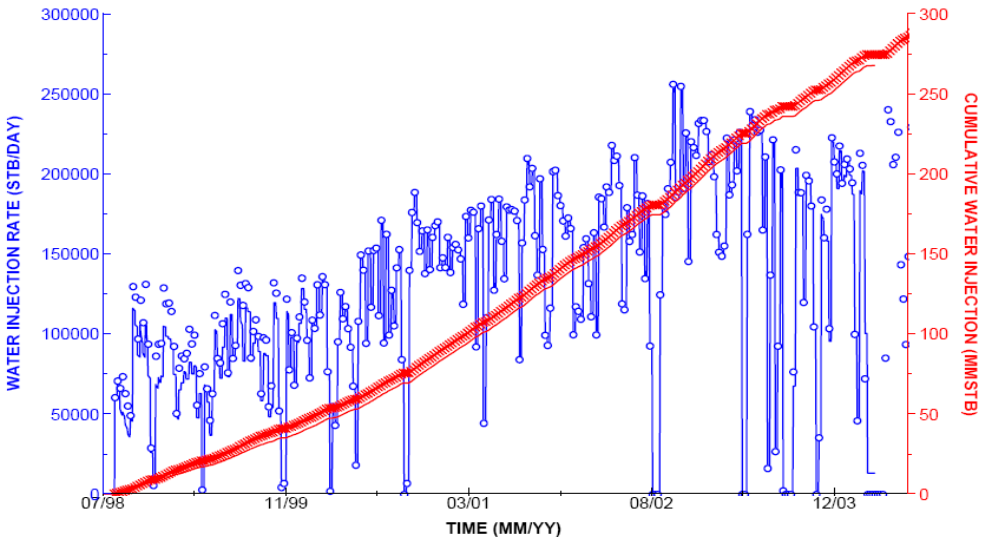

Figure 5.21: *Production profile observed and estimated of the best operators obtained realisations of the model up to 2003. a) Gas–oil ratio and water cut. b) Water injection rate and cumulative water injection. (Macdonald et al., 2004)*

5.10 Identifying key reservoir uncertainties

Many parameters can be used for the parameter space because of the high level of uncertainty, such as permeability, porosity between the wells, and any lab measurements that represent a small scale, such as relative permeability. In the Schiehallion field, the physical barriers to flow still present a major uncertainty after ten years of production. From the operators understanding, they define some uncertain parameter as shown in Figure 5.22. In our case, we have made the decision to consider the fault transmissibility, permeability and NTG to be the most uncertain parameters because at the time we did not have this specific information about the degree of uncertainty of the various parameters for the Schiehallion field.

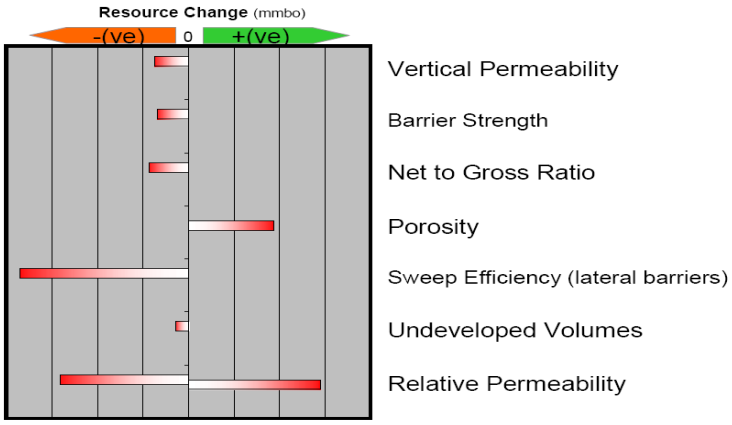

Figure 5.22: *Identifying key reservoir uncertainties. (After Gainskiet et al., 2008)*

5.11 Summary

A full description of the Schiehallion field has been given in this chapter. This included geological settings, reservoir development, management, and static modelling. Seismic amplitude attributes maps were used in order to demonstrate the external structural design of the channelised sands. A full detailed section on time-lapse seismic response, acquisition characteristics and 4D signature analysis was also given to confirm that the seismic data acquired in this field could provide a qualitative data for interpretation and monitoring. Additionally, the operator demonstrated that the Schiehallion field is a good candidate for seismic history matching as a static reservoir model.

CHAPTER SIX

Inspection of Selected Area for Seismic History Matching Application

This is an overview for the Segment 4 area selected for Seismic History Matching application. A set of examples of the 4D response in the two main reservoirs is also given, as well as a description of the data analysis (production and seismic), particularly for measuring the data error. A comprehensive description is given concerning the application of the wavelet transform as a tool for measuring the data error. Finally, we end this chapter by presenting a summary of the previous work and the main results obtained in this segment.

6.1 Reservoir simulation model Segment 4

To reduce CPU time and the number of variables that should be varied for such a large model, we focused on a smaller independent sector of the reservoir which represents the T31 layer. To make sure that the full field model and the sector are both compatible, we made a comparison between well profiles in both cases. For example, the GOR (gas–oil ratio) for well P3 (Figure 6.1) in both cases has the same trend as shown in Figure 6.2. Additionally, other variables gave us confidence to use this sector, such as pressure and saturation, as illustrated in Figure 6.4 and Figure 6.5 respectively.

The sector is enclosed on three sides by faults and pinches out on the fourth side; some of the non-Segment 4 cells have been retained, merely to keep the extraction simple (Figure 6.6). Five producers (Figure 6.7) and six injectors (Figure 6.8) were active between 1998 and 2004. The reservoir quality varies in character from thinly interbedded sands to massive sands, with the massive sands being of better quality.

Typically, the sands are fine to medium grained, with 23–30% porosity and 250–2000 mD (Figure 6.9) permeability, as shown in Figure 6.10. The Schiehallion reservoir fluids are geochemically mixed source oils, with oil gravity in the range of 22–28° API. Figure 6.11 shows the upscaled reservoir simulation model predictions of the pressure, water saturation and gas saturation for the initial pre-production conditions and for 2004. In the Segment 4 reservoir model, eleven wells were completed in the T31 sandstone sequence (see Table 6.1). The production from this segment again started in 1998, and continues to the present. The base-case model was upscaled vertically by a factor of 4 using arithmetic averaging for NTG and porosity and geometric averaging for permeability to speed up simulation time. The CPU time was halved for a two-year simulation, as shown in Figure 6.3a. The field water cut of the original and the upscaled models were quite close, as presented in Figure 6.3c, as is also the case for the reservoir pressure and gas–oil ratio, as shown in Figure 6.3 (b and d). Similarly, saturation and pressure distributions were preserved by upscaling.

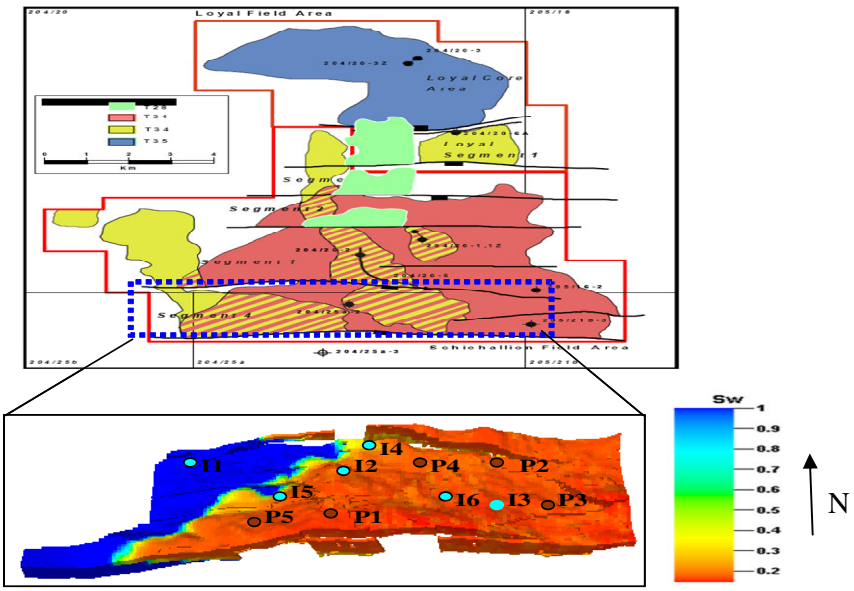

Figure 6.1: *Location of Segment 4 for the Schiehallion field.*

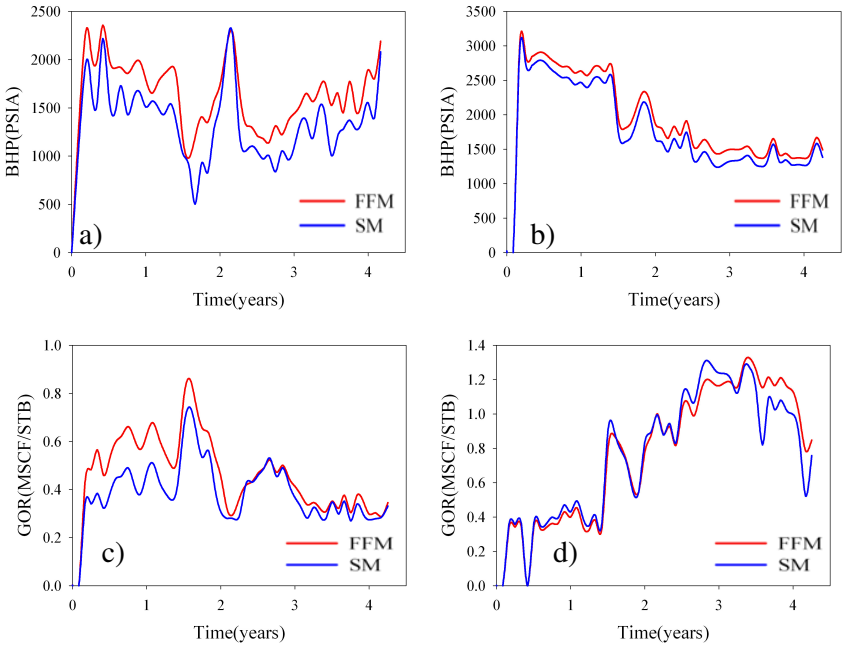

Figure 6.2: *Comparison between well profiles in both cases: the FFM (Full Field Model) and the SM (sector model). a) BHP for well P2, b) BHP for well P3, c) GOR for well P2 and d) GOR for well P3.*

Well Name	Type	Active Since
P2	Producer	July 1998
I6	Injector	July 1998
P4	Producer	July 1998
I3	Injector	September 1998
I2	Injector	November 1998
I1	Injector	May 1999
P3	Producer	December 2001
I4	Injector	May 2003
P1	Producer	June 2002
I5	Injector	June 2002

Table 6.1: *Well list for Segment 4 in the Schiehallion field.*

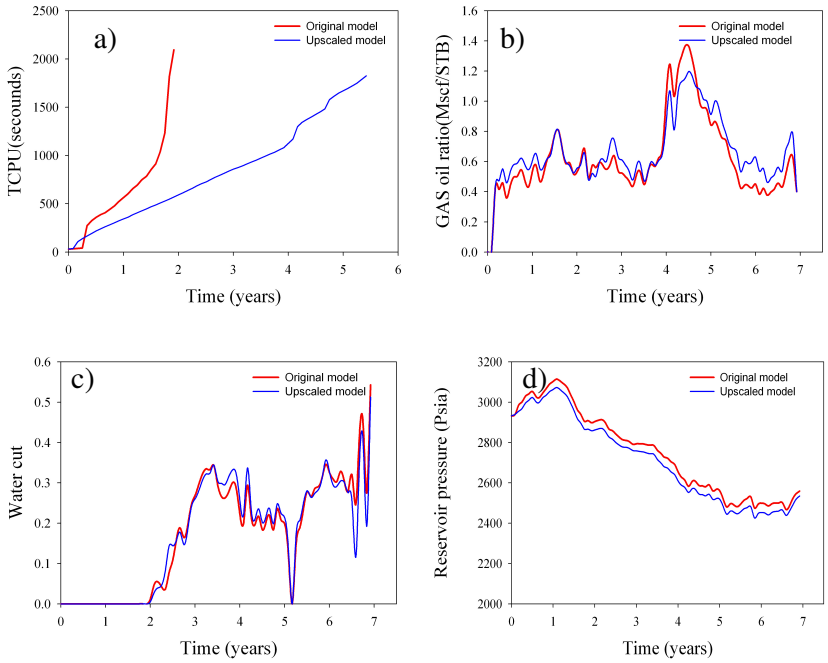

Figure 6.3: *Comparison between the upscaled model (Segment 4 sector) and the original model in terms of a) TCPU time, b) gas–oil ratio, c) water cut and d) Reservoir pressure.*

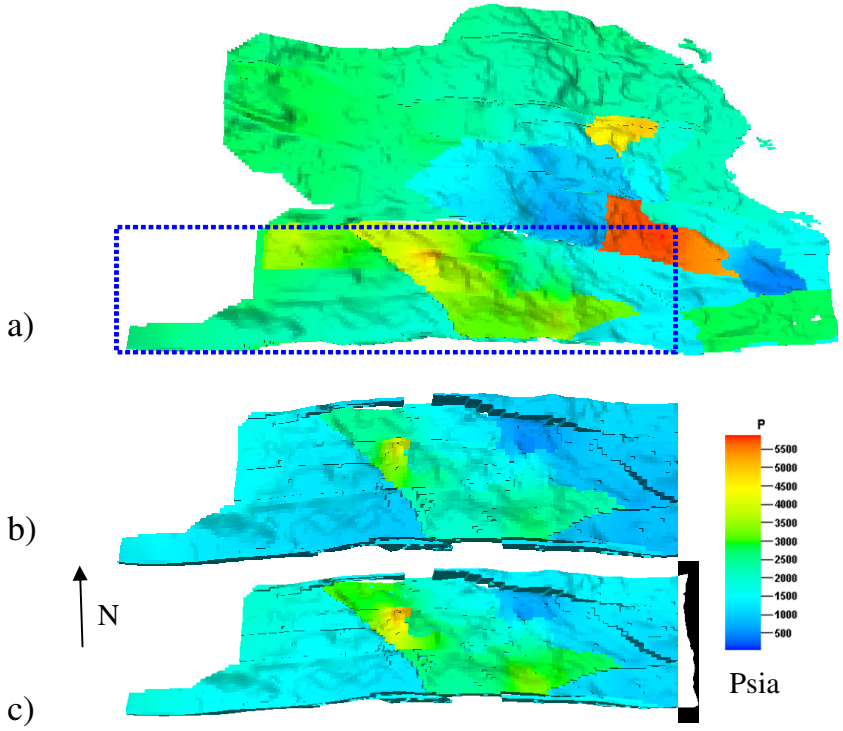

Figure 6.4: *A comparison of pressure distribution for a) full field model, b) sector model for Segment 4 and c) upscaled model.*

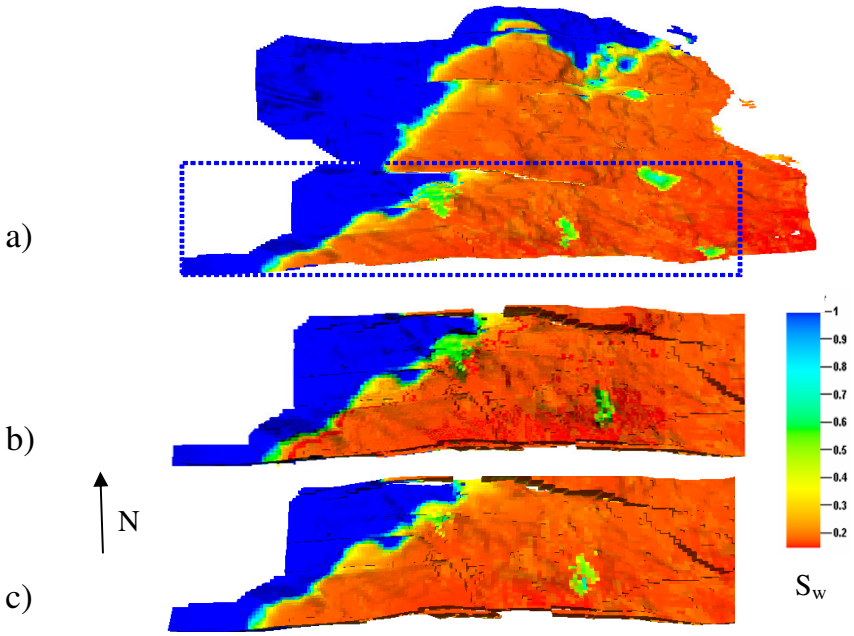

Figure 6.5*: A comparison for water saturation distribution for a) full field model, b) sector model for Segment 4 and c) upscaled model.*

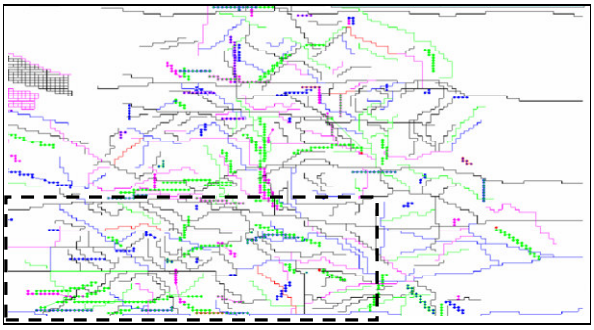

Figure 6.6: *Faults and barriers used in history matching Segment 4.*

This sector measured 146 × 44 × 7 after up scaling the original model by a factor of 4 (26616 active cells typically measuring 100 × 100 × 6 m). Note that the sector was mostly four cells thick vertically, but to the west-left side of our maps it extended to eight cells in the aquifer. To run one model through SHM workflow, from updating models step to misfit calculation, took twenty minutes, including six years of production, on a single 1.26 GHz processor of our cluster with 3 GB of RAM.

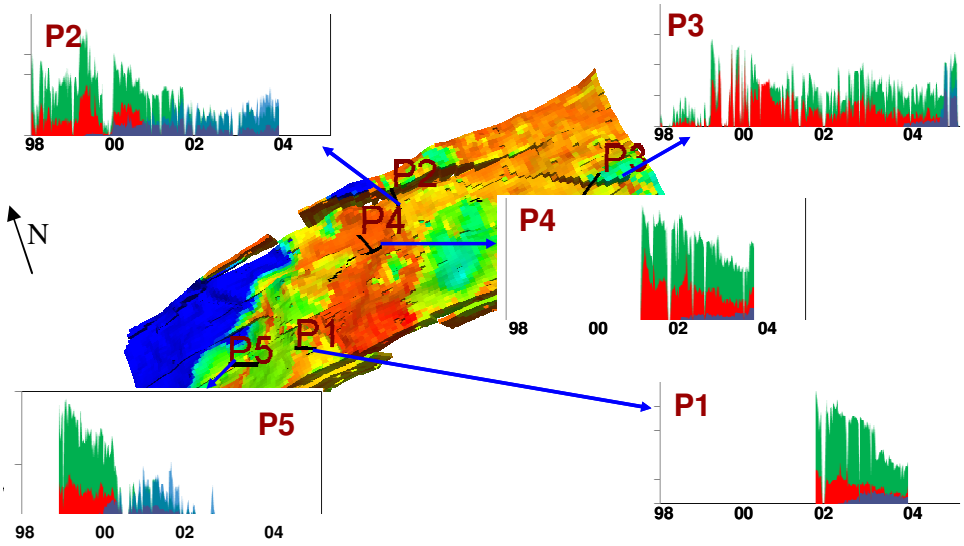

Figure 6.7: *Production well locations for Segment 4 and the production rate profile for each well, where green indicates the oil production rate, blue indicates the water production rate and the red indicates the gas production rate.*

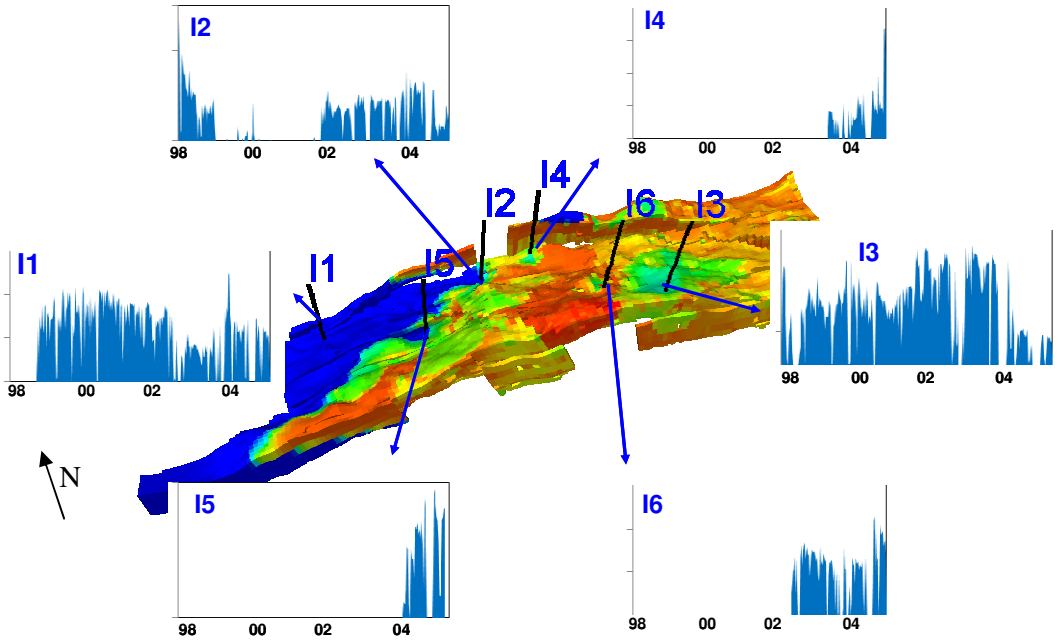

Figure 6.8: *Injection well locations for the Schiehallion field Segment 4 and the injection rate profile for each well.*

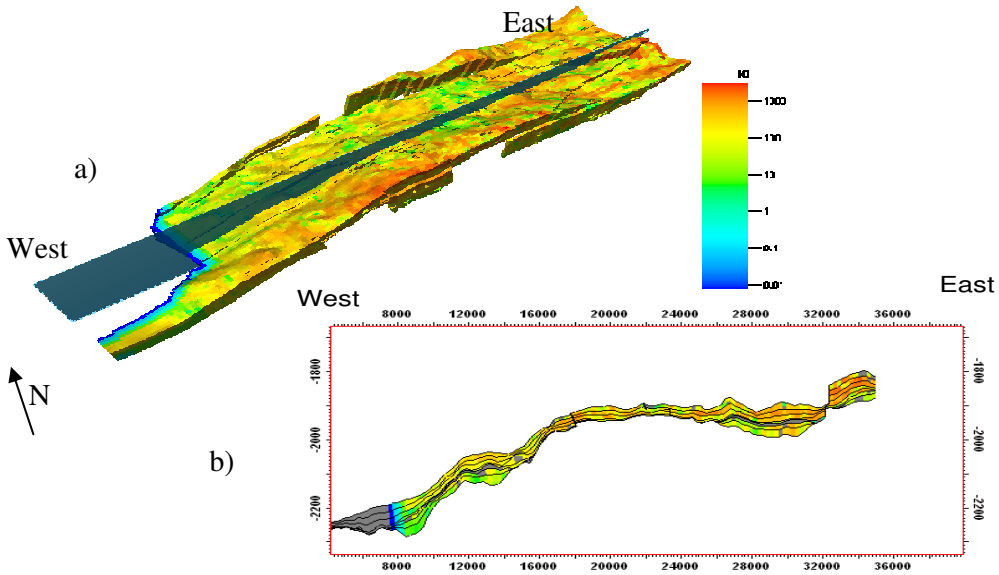

Figure 6.9: *(a) A vertical average map of the modelled permeability, and (b) west–east cross section of the reservoir model, showing the vertical distribution of permeability (mD) in the T31 sequence.*

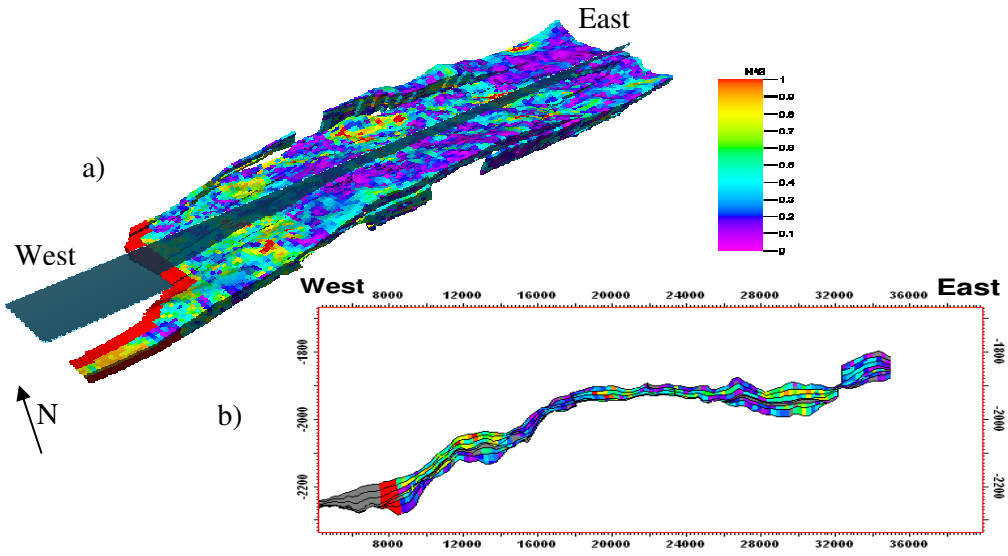

Figure 6.10*:(a) A vertical average map of the modelled NTG, and (b) west-east cross section of the reservoir model, showing the vertical distribution of NTG in the T31 sequence.*

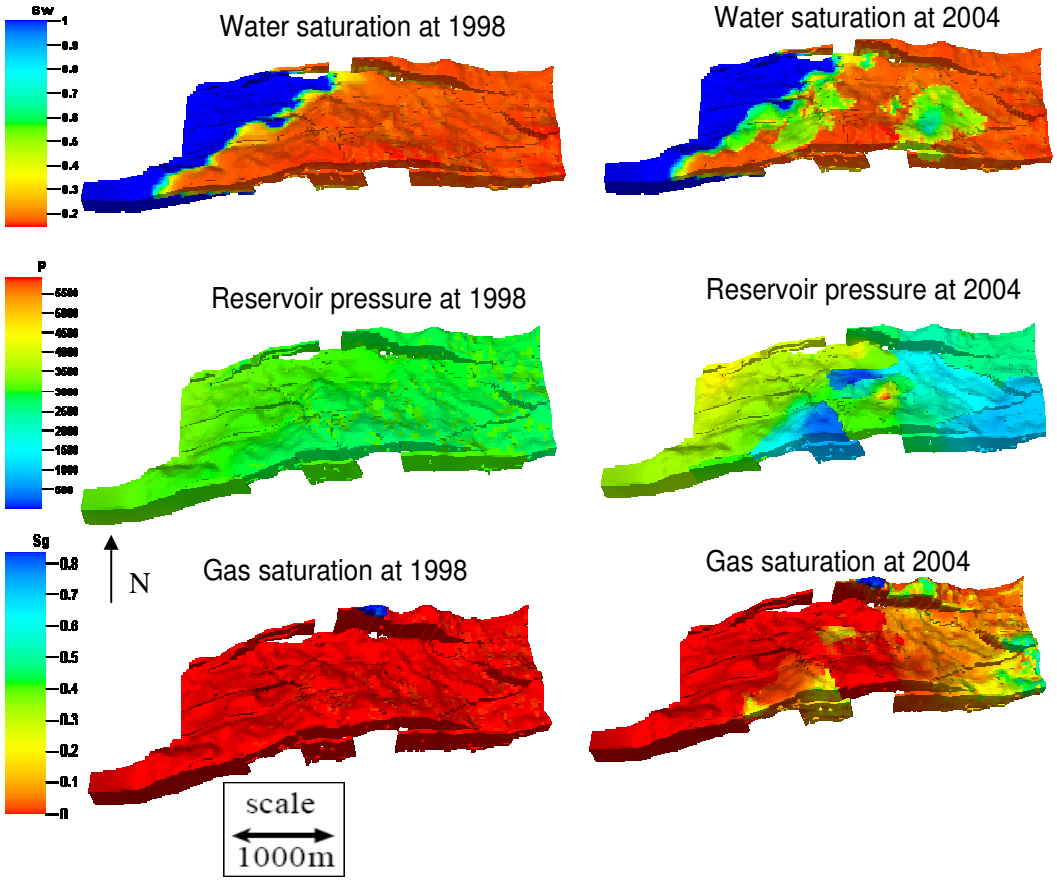

***Figure 6.11**: Pressure, water saturation and gas saturation predictions from the reservoir simulation model for the initial pre-production conditions and for 2004.*

6.2 Seismic attributes used in this study

The seismic dataset consisted of two P-waves of seismic volumes – Migrated Stack Fore Phase I seismic and coloured Inversion Stack – collected for three seismic surveys (1993 as baseline, 1999 and 2000). The process of cross-equalisation, calibration and transformation of Migrated Stack was performed by the operators by a combination of phase rotation and filtering, to produce the Coloured Inversion Stack. Time-to-depth conversion and the location of the reservoir horizon was provided by the operators and used to generate a map of Root Mean Square (RMS) amplitudes from the Migrated Stack by integrating the signal over a suitable time window, following Leach *et al.* (1999). After this, the pre-production RMS amplitudes were mapped to Net:Gross (NTG), given the almost uniform porosity of the sand (Stephen *et al.*, 2006). Based on the operator's guidance, a second attribute, the Sum of Negative Values, was obtained

by summing the negative amplitude in the Coloured Inversion stack from the picked horizon to 20 ms below (Figure 6.12 and Figure 6.13).

Phase II 4D seismic attributes (96 as baseline, 02 and 04 as monitors) was obtained using the RMS amplitudes of the migrated stack, obtained by integrating the signal from 5 ms above the picked horizon to 25 ms below (Figure 6.12).

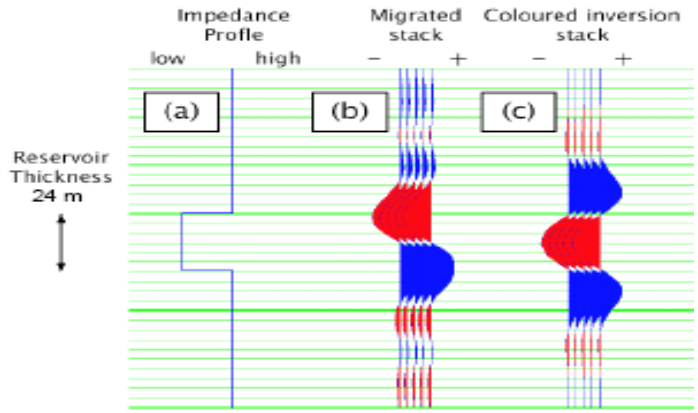

Figure 6.12: *Coloured inversion schematic, showing (a) a P-wave impedance profile with a thickness of 24 m (approximate thickness for our reservoir), (b) the zero-angle seismic stacks and (c) the coloured inversion stack. The reservoir is located between the two zero crossings in the case of the coloured inversion stack, and the shape of the wavelet is similar to that of the impedance profile. (Soldo, 2005)*

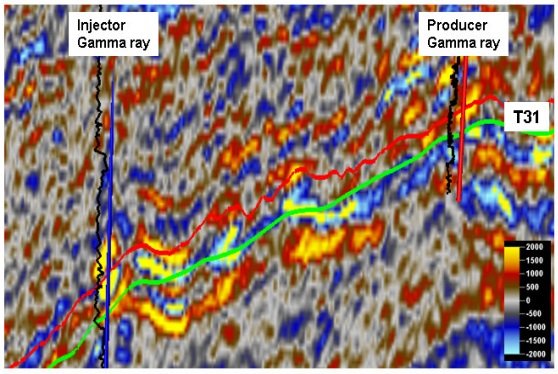

Figure 6.13: *Coloured inversion product for the full offset migrated stack from 1996. The green and red lines indicate the top and bottom of the T31a sand respectively. (Edris et al., 2008)*

Both attributes (Phase I and Phase II) were used as a pseudo-impedance to detect pressure and saturation effects via the time-lapse map (Figure 6.14 and Figure 6.15). Figure 6.14 shows the time-lapse seismic differences between all the surveys for the Phase I dataset. The attribute maps are also normalised to the baseline (by subtracting the mean and dividing by its standard deviation) to gain a comparable change in magnitude and signs between surveys. Softening occurs around I2 (Figure 6.14a) in the first year of production, followed by hardening when the well is switched off (Figure 6.14c). We also see the effect of two years of production near wells P2 and P3. Assuming that cross equalisation has been applied to the seismic data, some shadowing production effects in the upper sandstones possibly cause the anomaly around P1 in Figure 6.14, e.g. T34 sequence (for more details see Soldo, 2005). By simple visual interpretation, there is clearly a high degree of compartmentalisation and heterogeneity, perhaps due to a combination of faulting and channelised structures in the reservoir, which is recognisable by 4D differencing. For more details, see Stephen *et al.*, 2005.

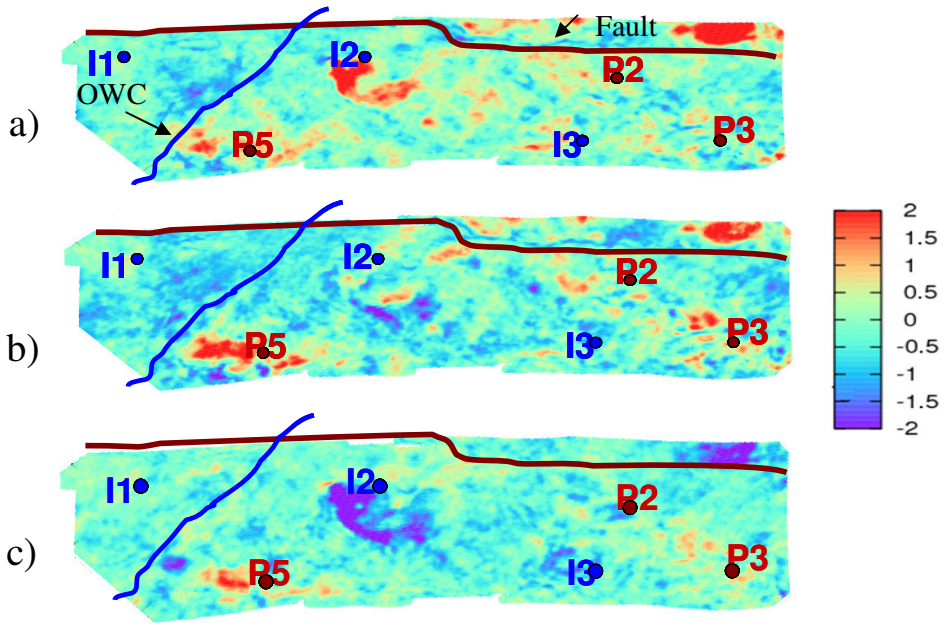

Figure 6.14: *Map view of the three differences of time-lapse seismic attributes for Phase I data for (a) 1993–1999, (b) 1999–2000 and c) 1993–2000. Prior to differencing, the attributes for each survey were normalised by subtracting the mean for 1993 and dividing by its standard deviation. The colour bar is the same for all the images and is in units of the 1993 standard deviation. Old –new that give you positive number that corresponds to decrease in effective pressure which is increase in the pore pressure positive .A positive number may also represent decrease in water saturation or increase in gas. (The brown line indicates a sealing fault – no activity was simulated to the North of this and blue indicates water saturation increase).*

Figure 6.15 shows a map view of the differences of the time-lapse seismic attributes for Phase II data. Similar to Phase I, prior to differencing, the attributes for each survey were normalised by subtracting the mean for 1996 and dividing by its standard deviation.

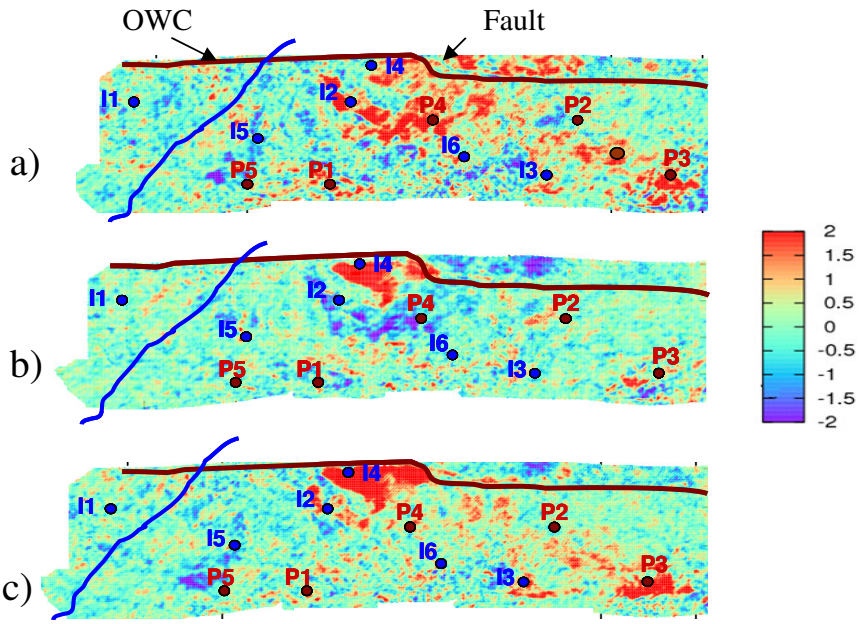

Figure 6.15: *Map view of the differences of time-lapse seismic attributes for Phase II data for (a) 1996–2002, (b) 2002–2004 and c) 1996–2004. Prior to differencing, the attributes for each survey were normalised by subtracting the mean for 1996 and dividing by its standard deviation. The colour bar is in units of the 1996 standard deviation.*

6.2.1 Shadowing effects

The shadowing effects around well P5 have been pointed out previously (e.g. see Abriel *et al.*, 1992; Castagna *et al.*, 2003; Al-Maskeri *et al.*, 2003). The main cause of this effect is an unexpected change in the elastic properties of the sediments, which leads to a reduction in the energy of the seismic wavelet. Towards the south-west of Segment 4, there is a clear signal which cannot be explained in terms of reservoir production activities for the T31 sequence. Figure 6.16 shows such a feature in a map view, where the magnitude of the amplitude anomaly around the highlighted box is comparable with the real time-lapse seismic signal around injector I2.

In this case, production from the upper sequence (T34) at well P5 could be the origin of the 4D signature in the area, since depletion may generate a release of gas that could create an amplitude shadow detectable in time-lapse seismic interpretation. Picking the horizons incorrectly may also cause the same effects shown in a time-lapse seismic cross section (Figure 6.17) that passes across the amplitude map anomaly around well

P5, where the main two time horizons (top T34 and top of T31) of the Schiehallion field are displayed. Time-lapse anomalies do not exist in the upper layers of T34, indicating that other type of anomalies such as acquisition footprints can be leftover, since there is no continuation of the effect either upwards or downwards across the reservoir time window zone. Alternatively, this might be due to vertical connectivity between the two sands. This is another important type of time-lapse effect that is not captured in the predicted 4D amplitude maps and that will prevent the misfit between the predicted and the observed seismic from reaching the minimum value. Soldo (2005) suggested that the problem could be tackled by computing the predicted time-lapse seismic response in the pre-stack seismic reflectivity domain, since the ray path will take into account any change in fluid in the upper proximity of the zone of interest and involves full 3D modelling.

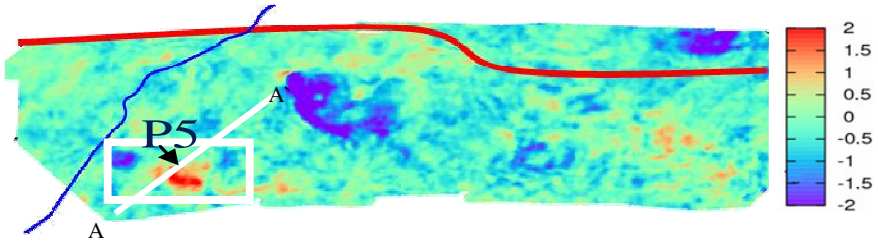

Figure 6.16: *An amplitude map of horizon T31. A change in amplitude at well P5 occurs even though there is no recorded production from the T31 sequence.*

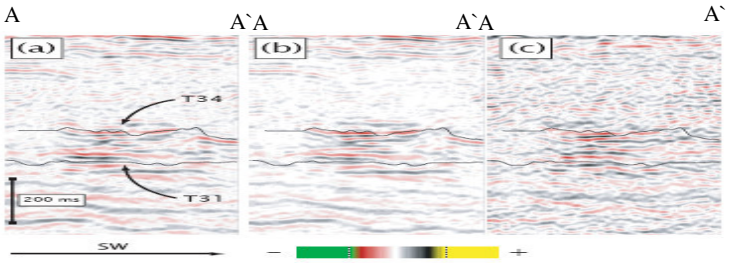

Figure 6.17: *Seismic cross section near producer well P5 showing the shadowing effect. In (a), the 1993 coloured inversion stack, (b) the monitor seismic stack respectively with the top horizons of T34 and T3 and (c) a strong 4D seismic difference anomaly at well P5 in the layer above, which has an effect on the lower layer. The upper picked horizon shown in the top of the T34 sequence, while the lower time horizon is the top of T31 sequence. Note the strong 4D signature around the well due to production on the upper layers of the field and how this time-lapse effect is influencing the amplitudes in the surroundings of the T31 sequence (Soldo, 2005).*

6.2.2 4D seismic anomalies due to well activities in the T31 sequence

As we can see, there is a relationship between the well activities and the seismic response – for example, the main signal in Phase I seismic data is due to the injector I2, whereas I3 and I1 are less obvious (Figure 6.18). For Phase II data (Figure 6.19), the main signal in this data is created around the injector I4. As the production continues, the response of P1, P2 grows stronger; but I1, I2 and I3, constantly injecting water into the reservoir, still have no clear response. Around P3, we see a signal caused by the effect of the gas coming out of the solution.

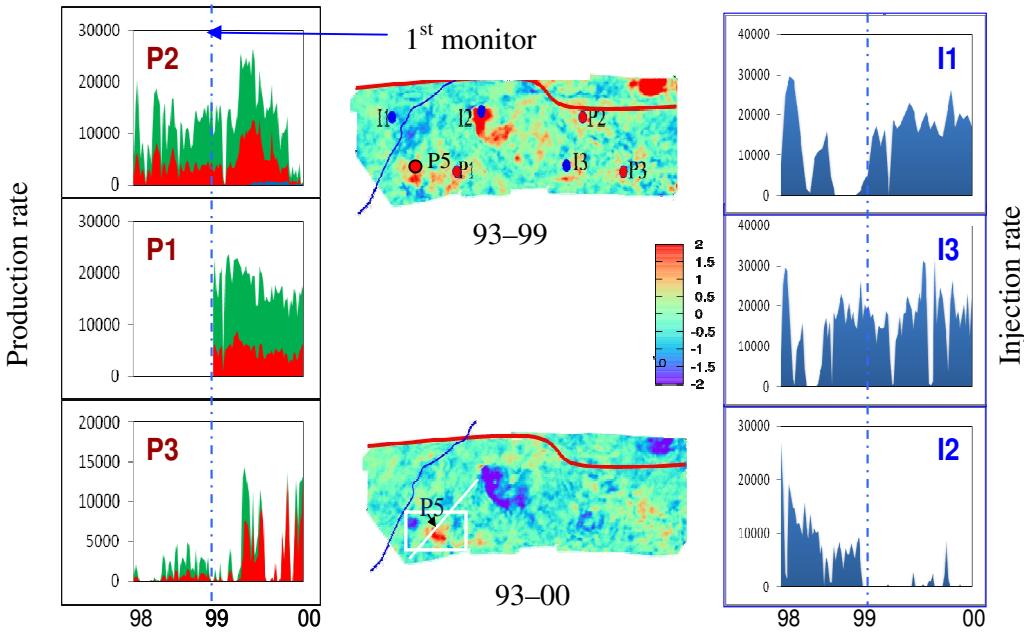

Figure 6.18: *Comparison of well activities and 4D attributes behaviour for Phase I time-lapse data.*

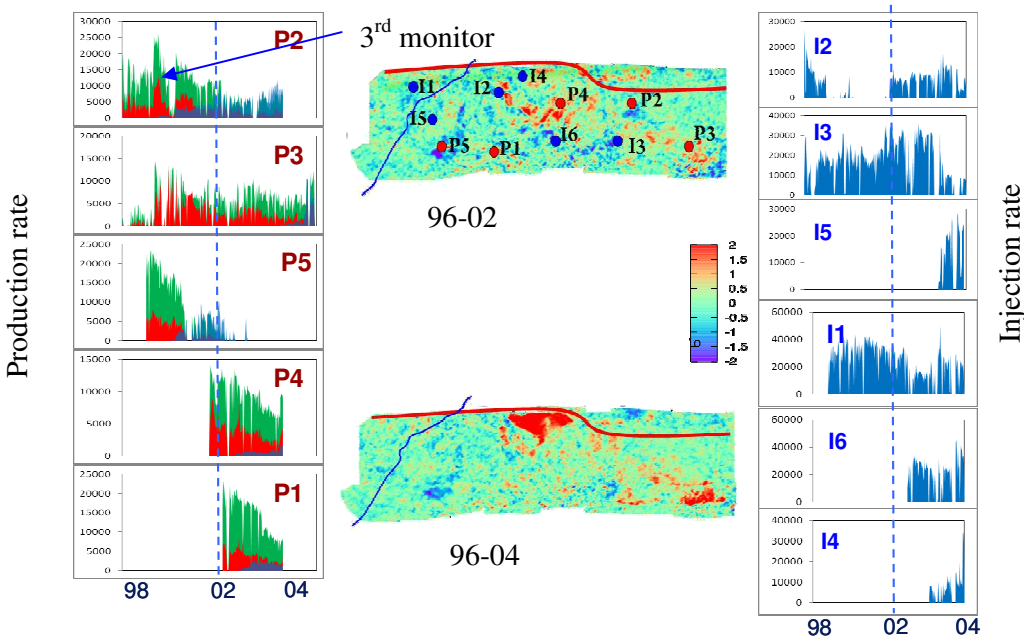

Figure 6.19: *Comparison of well activities and 4D attributes behaviour for Phase I time-lapse data. As the production continues, the response of P1, P2 becomes stronger. I1, I2 and I3, which are constantly injecting water into the reservoir, still have no clear response. Around P3, a signal caused by the effect of the gas coming out of the solution can be seen.*

6.2.3 Seismic data error

The seismic data error has been presented by Soldo (2005), in which the amplitude attribute of each individual survey and their corresponding differences are analysed in terms of the covariance function in the two main seismic acquisition directions (inline/crossline).

It is assumed that the covariance matrix could be represented as $\sigma_0^2 I$. The same type of covariance function structure (behaviour of the covariance as a function of lag (Figure 6.20) is observed in Gosselin *et al.* (2003). The same analysis is repeated for all of the seismic data (1993, 1999 and 2000 and their corresponding differences). For Phase II seismic data, we assume that we have the same level of data error. (For more details, see Soldo, 2005).

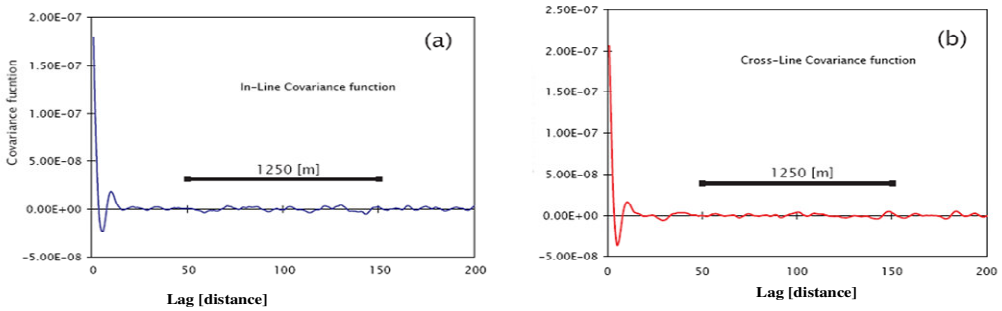

Figure 6.20: *Covariance functions for seismic data. The covariance function in this case is built taking into consideration all possible pairs of data in the inline direction and in the crossline direction. (a) Represents the covariance function in the inline direction, while in (b) the same function in the crossline direction can be observed. Note that the stationary condition is reached at lag=5. (Soldo, 2005).*

6.3 Production data analysis

In Schiehallion, there was no information about production data error, which is an important issue for the misfit calculations. A single misfit objective function is used for each model that we create, incorporating a comparison between observed and predicted production and seismic data. For each variable being compared, we use the following equation:

$$J_i = \left\langle \underline{x}_i^{obs} - \underline{x}_i^{\mathrm{mod}} \middle| \underline{\underline{C}}_i^{-1} \middle| \underline{x}_i^{obs} - \underline{x}_i^{\mathrm{mod}} \right\rangle \qquad (6.1)$$

where $\underline{x}_i$ is the *i*th data vector under comparison, with superscript *obs* or *mod* for observed and modelled respectively, and *C* is the covariance matrix capturing data and model errors. It is important to measure the data error for more accuracy in the calculation of the seismic misfit – for more details see Chapter 3.

A least-squares filter (Yilmaz, 1987) has previously been used (Soldo, 2005). The problem with this, however, is that it cannot detect a high frequency signal, and so we do not know what should be the right level of filtering. The power spectrum of the signal, filtered data and noise are shown in Figure 6.21 for the producer well P2. Note the very good discrimination between signal and noise in the power spectrum domain.

On the other hand, the histogram of the noise data is plotted in order to show that Gaussian approximation holds for this type of data. There are some problems with this method, however: some real signals can be interpreted as noise because there are no filtering levels to define for this method.

To measure the data error, in the next section we use the wavelet transform.

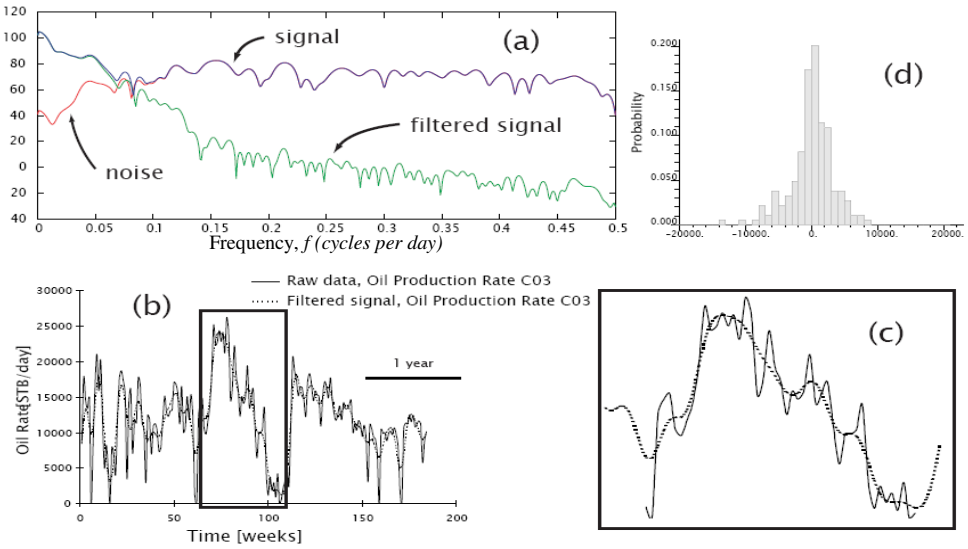

Figure 6.21: *Power spectrum decomposition and data analysis for well P2. (a) The power spectrum of the three signals (measured, filtered and noise) plotted as a function of time frequency. (b) The filtered and measured signal transformed back in the time domain after inverse Fast Fourier Transform. (c) Zoom view for the original signal and extracted noise. The extracted noise shows a Gaussian behaviour in (d) (Soldo, 2005).*

6.3.1 Wavelet transforms as a filtering tool

The wavelet theory was developed by Grossman (Grossman and Morlet, 1984), Daubechies (Daubechies, 1988) and Walnut (2003). For an example, see Figure 6.22. A wavelet is a mathematical function used to split a given function or continuous-time signal into different frequency components and to study each component with a resolution equivalent to its scale. These properties allow the wavelet to be appropriate for the analysis of non-stationary data.

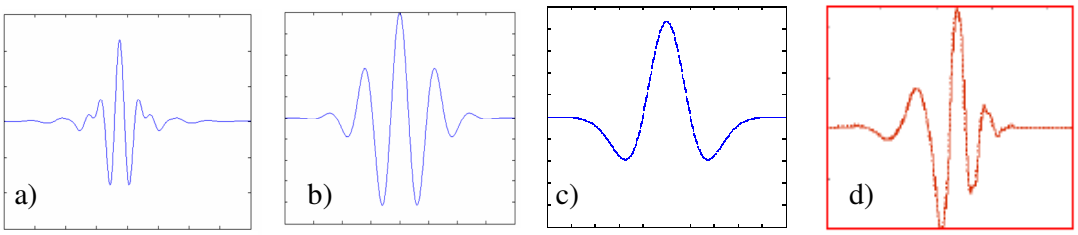

Figure 6.22: *(a) Meyer, (b) Morlet wavelet, (c) Mexican Hat wavelet and (d) the Daubechie 4 wavelet, which we use in this work.*

The multi-resolution (low and high frequency) wavelet analysis method for data processing was proposed by Morlet in 1988. Later, Daubechies (1988) created a set of basic wavelet functions that have wide application in signal processing, image compression, data de-noising and other areas.

Figure 6.23 shows the filtering process at its most basic level. The original data {signal(S)} is passed through two filters yielding firstly the approximate (A) and then the detailed (D) components. This process, called wavelet decomposition, is an established method for outlier and noise extraction (Polikar, 2001).

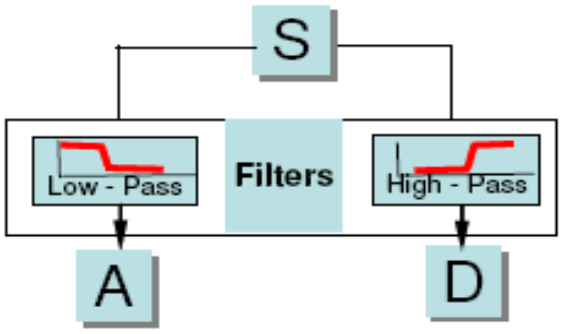

Figure 6.23: *The filtering process at its most basic level (Polikar, 2001).*

The Continuous Wavelet Transform (CWT) achieves the above multi-resolution by time-scaling and time-shifting a prototype function (t), often called the mother wavelet. For example:

$$\psi_{a,b}(t) = \frac{1}{\sqrt{|a|}} x(t)\psi\left(\frac{t-\tau}{a}\right)\delta\ t \qquad (6.2)$$

The above equation shows that the transformed signal can be a function of two variables: the translation (τ) and the scale (a) parameters. The signal is transformed by x (t), the mother wavelet. Examples of mother wavelets include the Haars, the Daubechies (consisting of ten wavelets) (Daubechies, 1988), the Gaussian (consisting of eight wavelets) and Coiflets wavelet family (consisting of five wavelets). The CWT is continuous in terms of shifting the wavelet smoothly over the full domain of the analysed data. In addition, CWT is also said to be continuous because of the set of scales (from that of the original data up to some maximum scale that is determined by trading off the need for detailed analysis with available computational power) and the positions at which it operates.

The procedure of filtering means the decomposition process can be iterated, with successive approximations being decomposed in turn. For this reason, one signal is broken down into many lower resolution components. Figure 6.24 demonstrates the process of multi-level decomposition if we have any time series. In this work, high-pass and low-pass filters of the Daubechies 4 wavelet were used to filter the data. The chosen wavelet, Daubechies 4, is known to offer a wide range of flexibility for this type of analysis. Aggrey (2007) has reported successfully using Daubechies 4 in a high-density data to filter out the non-signal components from the real signal for pressure data recorded from some smart wells in the North Sea. In Figure 6.24, $\mathbf{d_1}$, $\mathbf{d_2}$, $\mathbf{d_3}$ and $\mathbf{d_4}$ are the details of the original signal **s** at each decomposed level, and $\mathbf{a_1}$, $\mathbf{a_2}$, $\mathbf{a_3}$ and $\mathbf{a_4}$ are the approximations of the signals after decomposition. The greater the resolution, the finer the detail that can be accessed by taking into account the high frequencies of **s**. The decomposition procedure can be presented as:

$$S = a_5+d_1+d_2+d_3+d_4+d_5 \tag{6.3}$$

In general, after a number of decompositions, the approximated signal (s) is defined as

$$S = a_j + \sum d_j \tag{6.4}$$

where j is the decomposition level (Burrus *et al.*, 1998; Walnut, 2001; Daubechies, 2004; Weeks, 2006; Matlab™).

The determinant for the most appropriate wavelets and level of decomposition is based on visual assessment and the experience of the analyst. For this study, we use the available pressure data, relating it to the changes in production profile, such as oil rate for the wells, and define key points where the changes in pressure appear unnatural. Excessive filtering or decomposition tends to wipe out valuable information. Figure 6.25 shows that increasing the level of decomposition with the Daubechies 4 wavelet beyond level 6 destroys the valuable contents of the data series. In this case, the recommended level of data approximation will be a_2.

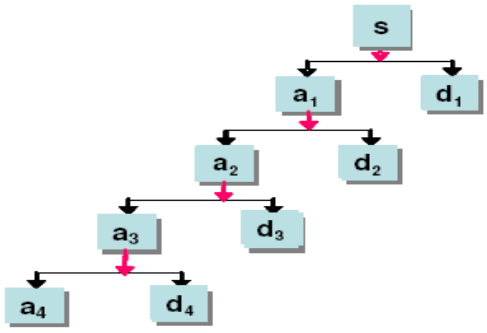

Figure 6.24: *The process of the multi-level decomposition of multiple decomposition levels.*

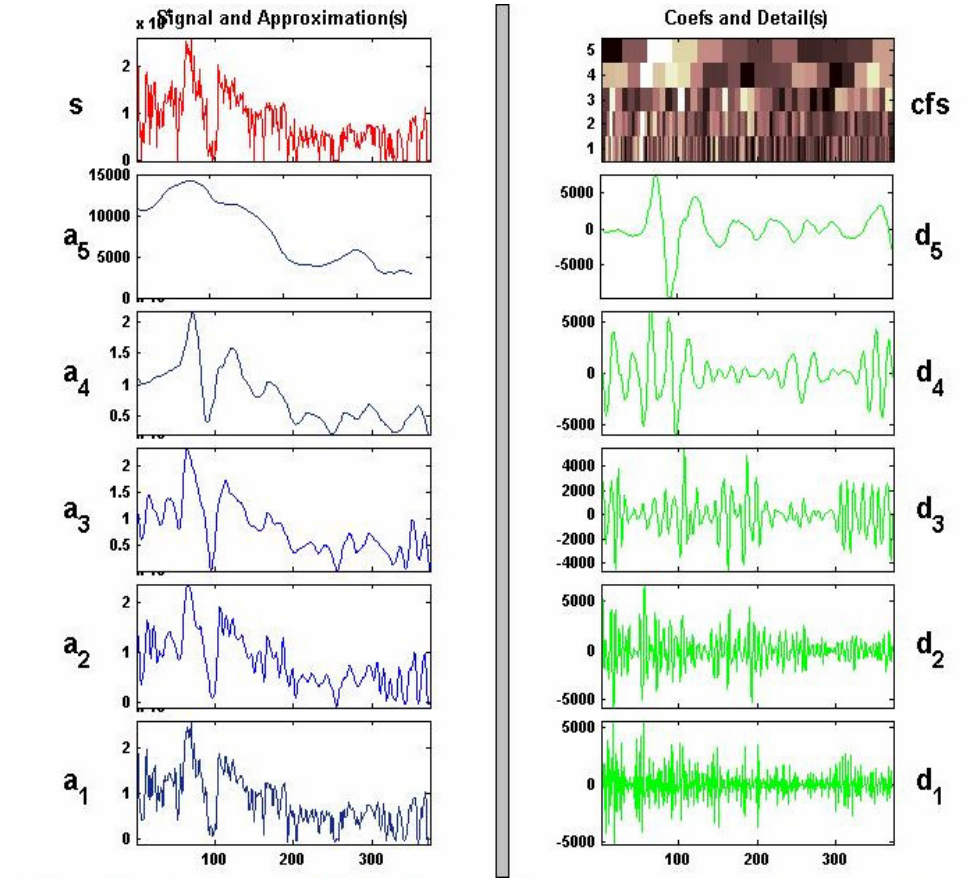

Figure 6.25: *The wavelet decomposition of oil production rate data. The data error is illustrated along with the original oil production rate data at different nodes with increasing level of detail. It indicates that an optimum decomposition level exists ahead of which valuable information will be lost.*

6.3.2 Application to Schiehallion field production data

The idea of using the wavelet transform is to measure the data error in the production data and use that to calculate the covariance for each data component as presented in Figure 6.26. We use the whole dataset including the pressure and GOR (gas–oil ratio) to define the truth signal from the noise, so we use this as reference to define the correct level, as shown in Figure 6.27. After decomposition and the detailed statistics of standard deviation, the mean can be obtained as outlined in tables 6.2, 6.3 and 6.4.

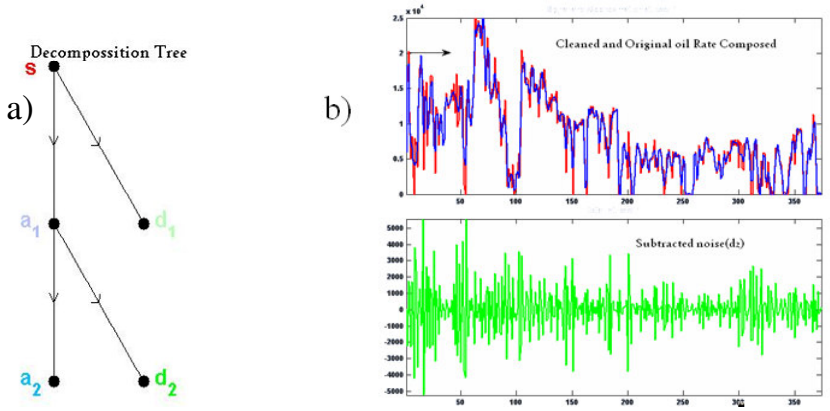

***Figure 6.26**: (a) The workflow for wavelet decomposition of oil production rate for well P3 illustrated along with the original oil rate (s) and the approximated pressure data (a2) (d1 is up to level 2). (b) The approximated data (blue) and the original data (red) compared (upper panel) and the total subtracted noise d2 (lower panel).*

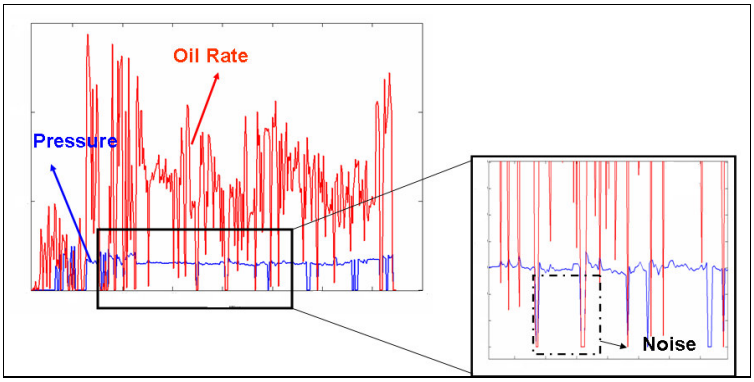

***Figure 6.27:** Defining the correct level of measuring the data error for production data. In this case, we use pressure data for well P3 to study the production data signal and define some key points for using them to define the correct level of measuring the data error.*

WELL	LEVEL	STD.	MEAN
P1	1	1384.460	4.167
P2	2	2241.759	16.416
P3	2	2006.451	1.281
P4	1	1061.082	-0.696

***Table 6.2:** The level of measuring the data error and the mean for the oil production rate for each well in Segment 4.*

WELL	LEVEL	STD.	MEAN
P1	1	420.935	1.075
P2	2	838.4331	-1.3040
P3	2	1301.807	-0.085
P4	1	464.725	-0.495

Table 6.3: *The data error and the mean for the gas production rate for each well in Segment 4.*

WELL	LEVEL	STD.	MEAN
P1	1	682.402	-0.487
P2	2	1414.28	-2.271
P3	2	474.010	-0.459
P4	1	217.2707	-0.242

Table 6.4: *The data error and the mean for the water production rate for each well in Segment 4.*

WELL	LEVEL	STD.	MEAN
I1	1	4607.283	-1.365
I2	1	1690.147	-5.868
I3	1	3295.802	0.95
I4	1	1779	0.569
I6	1	3006.531	0.9
I5	1	5463.3	8.7220

Table 6.5: *The data error and the mean for the water injection rate for each injection well in Segment 4.*

6.3.3 The covariance function for production: an example

The covariance of the time and space series is estimated after extracting and identifying the data noise. Figure 6.28 shows the covariance of oil production for Schiehallion, with Segment 4 as a function of lag. The covariance function is reached after lag = 3 weeks. Since the time step in the reservoir simulator is 1 week, the data errors are uncorrelated, and these correlation coefficients need to be included within the covariance matrix (Figure 6.29).

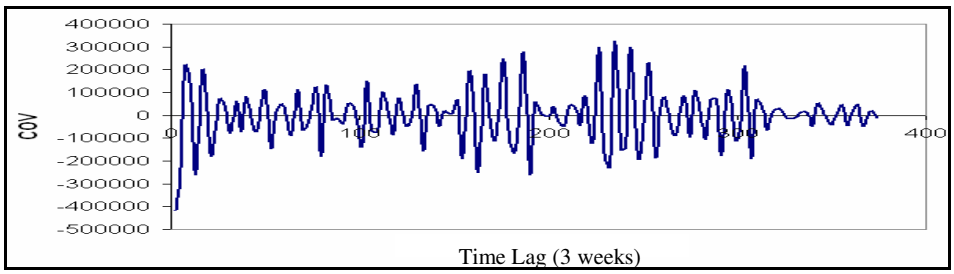

Figure 6.28: *Covariance function for data error for oil production rate.*

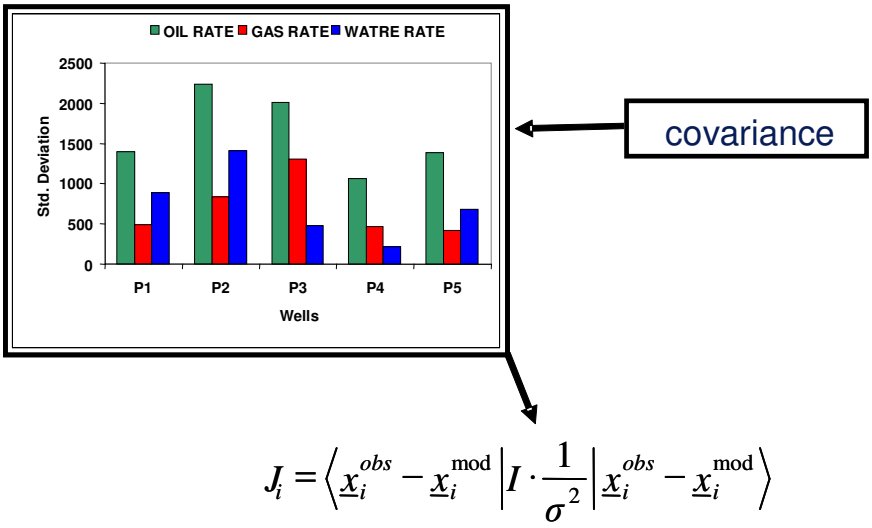

Figure 6.29: *The workflow including production data error.*

6.4 An overview of previous Phase I seismic history matching

Previous studies have identified that the petro-elastic transform parameters, particularly those for stress sensitivity, should be included in the history matching process (Stephen *et al.*, 2005). In our previous studies, we also found that only some pilot points and faults had significant impact on the misfit (Stephen *et al.*, 2005), reducing our parameter space. Good matches between predicted and observed seismic data, allowing for noise and some anomalies in the data (Figure 6.30), have been achieved. The match to well data was also improved, particularly at the injectors. Some observations have been made: for example, the fact that the static geological model should be constrained to the baseline survey, in particular where NTG is obtained from RMS amplitudes. The simultaneous updating of several parameters was possible, including permeabilities,

barrier transmissibilities and the petro-elastic transform parameters, obtained by SHM (Stephen *et al.*, 2006). The accuracy of these parameters has been confirmed in a separate study using well data (Floricich *et al*., 2006). In Figure 6.30, vertical injectors I1, I2 and I3 are indicated by blue circles. Horizontal producers P1, P2 and P3 are indicated by red lines and red circles. Producer P1 is inactive in this period. Red indicates a softening of the reservoir due to pressure build-up or gas evolution, while blue indicates stiffening due to a pressure drop or a water saturation increase (Stephen *et al.*, 2007).

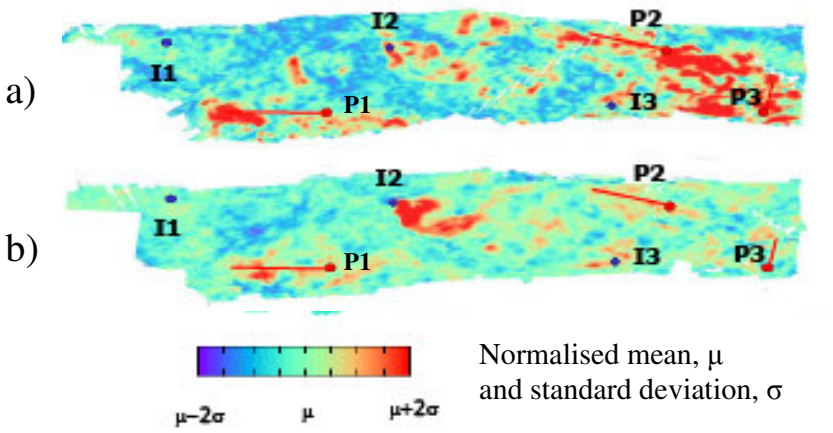

Figure 6.30: *Comparison of a) observed and b) predicted 4D seismic attributes for a sector of our field study reservoir after history matching. Both datasets have been normalised to the monitor surveys and represent the difference between surveys taken prior to and after the first year of production (Stephen et al., 2006).*

Inverting for sand or shale regression coefficients (see Section 3.2.1 for the petro-elastic equations) indicate that the greater the proportion of sand, the more sensitive the system is to pressure changes. Conclusions are thus drawn concerning the degree of spread in the estimates. In Figure 6.31, the dry rock frame parameters, E_k sand and E_k shale, are those presenting the largest uncertainty, and P_k sand and P_k shale are those with a lesser degree of uncertainty. Fault transmissibility multipliers have an intermediate spread in the estimations (Stephen *et al.*, 2005).

6.5 Base-case seismic prediction

Petro-elastic transform is used with the parameters in tables 6.6 and 6.7 to convert the output of the simulation run to predicted seismic data (Sim2seis). In this study, maps of impedance have been generated.

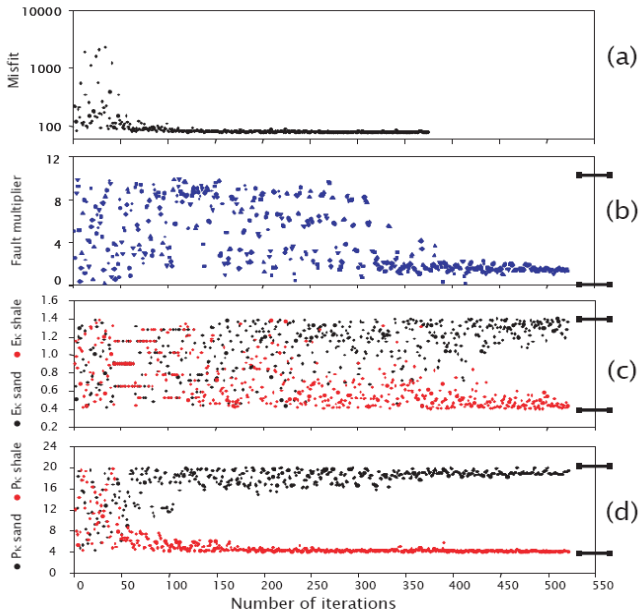

Figure 6.31: *Seismic history matching using the sum of negative values (coloured inversion domain). The misfit function is shown in (a). (b) Shows that the fault multiplier has an intermediate spread. (c) and (d): The spread of petro-elastic transform, such as the dry bulk moduli coefficients* P_k^{sand} *and* P_k^{shale} *when used as parameter space to vary. Right bars indicate the limits for each parameter (Soldo, 2005).*

Symbol	Value
$k_{\inf}$	9.78 GPa
E_k	1.0
P_k^{sand}	17.1 MPa
P_k^{shale}	1.45 MPa
$\mu_{\inf}$	6.28 GPa
E_μ	1.0
P_μ^{sand}	17.1 MPa
P_μ^{shale}	1.45 MPa

Table 6.6*: Default petro-elastic transform parameters for the dry bulk modulus obtained from history matching (Stephen et al., 2006c).*

Symbol	Value
k_{gr}	37 GPa
k_w	2.58 GPa
k_o	1.18 GPa
k_g	0.035 GPa

Table 6.7*: Typical petro-elastic transforms parameters for Gassmann's equation. The fluid bulk moduli are functions of pressure, temperature, etc., and full details of the calculation can be found in Soldo (2005), which follows on from Batzle and Wang (1992).*

Figure 6.32a–c and Figure 6.33a–c show the predicted impedance changes for the base-case model. Near the injector, the values are too high, allowing pressure leakage to extend far from the injectors for Phase I and Phase II seismic data. We use the operator's initial estimation of barriers in most cases. However, for some, we have no data and make a guess at 0.001 for the barrier transmissibility.

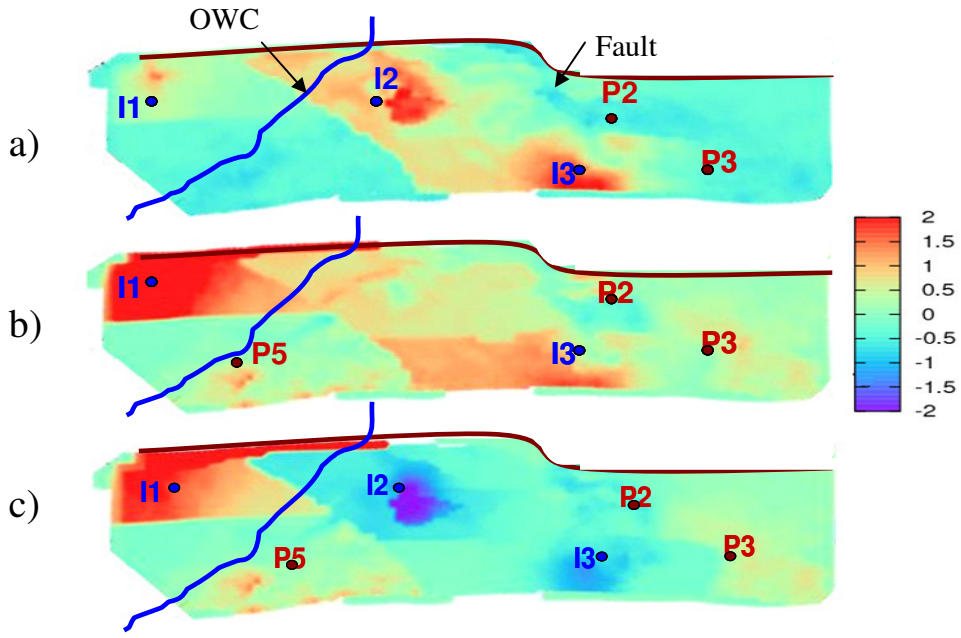

Figure 6.32: *Predicted change in impedance obtained for the base model before history matching for (a) 1993–1999, (b) 1999–2000 and (c) 1993–2000.*

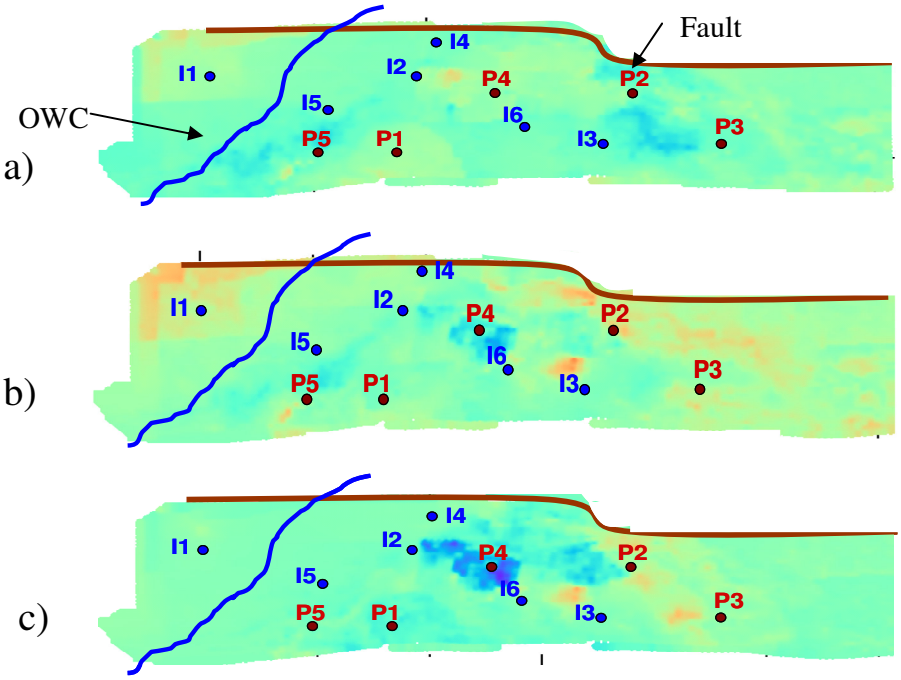

Figure 6.33: *Predicted change in impedance obtained for the base model before history matching for (a) 1996–2002, (b) 1996–2004 and (c) 2002–2004.*

6.6 Summary

A description of Segment 4 of the Schiehallion field has been presented, including geological settings, reservoir development and management and static modelling. A detailed section on time-lapse seismic response, acquisition characteristics and 4D signature analysis, providing a full interpretation of the main seismic anomalies, was presented, including definitions of both phases of the project. Examples illustrated the relation between the well activities, and the 4D seismic signature was also reported. Measuring the production data error has also been described. Examples of using power spectrum decomposition and data analysis and the wavelet transform as tools to measure the data error have also been outlined.

6.7 Challenges

From the operator's understanding of the Schiehallion field, we have defined some uncertain parameter, as shown in Figure 5.22. In our case, we have ignored the relative permeability and porosity variation, because we initially found that the degree of uncertainty was very large and that therefore the output uncertainty was very large. The physical barriers to flow remain a major uncertain parameter after ten years of production. One of the challenges is to improve the representativeness of the barriers by varying their transmissibilities. It would also be advisable to identify an appropriate history-matching scheme that would make the most of the seismic data, and to identify its values. History matching can be performed by using all available data simultaneously. Alternatively, dynamic data can be added to the process as the model is modified so that short simulations can be run initially to sample the parameter space quickly. The best model can then be used as a base case as new data is added. Investigating the value of seismic data in reducing forecasting uncertainty is another challenge in this thesis. During Phase II of the project, the Phase I model for Schiehallion was history-matched using either production, seismic or a combination of both. We plan on testing whether the seismic data will have a significant impact in the uncertainty reduction for this well. With the Phase II model, we have in our possession the production data for the well, with which we can test our forecast uncertainty. The new model requires a different set of parameters, but fault/barrier transmissibilities and reservoir permeability data were modified as before.

CHAPTER SEVEN

Appropriate Seismic History Matching Strategies: Schiehallion Field, Segment 4

In this chapter, we focus on appropriate history-matching strategies. For a field with several years of production and time-lapse history, it is necessary to select the most suitable method of finding the best models. Two possible history-matching strategies will be presented in the following pages. In the first approach, dynamic data can be added to the process as the model is modified so that short simulations can be run initially to sample the parameter space quickly. The best model can then be used as a base case as new data is added. Within a second, all parameters are modified to match all data simultaneously.

7.1 Updating Schiehallion reservoir model using 4D seismic and production data in various scenarios

During the lifetime of a field, data is continually gathered and can be used to constrain reservoir models used in reservoir management. In the model-building stage, the reservoir model is constructed using 3D seismic data from a number of wells. This data is often referred to as static data and includes well logs and core measurements. Once the field is in production, additional data is acquired, such as the production data. In addition, time-lapse (4D) seismic monitoring may be carried out. Time-lapse (4D) seismic analysis is particularly good at picking out pressure discontinuities in heavily faulted reservoirs where high pressure build-up occurs. Two possible history-matching strategies are presented in Figure 7.1. The first approach has the advantage that it allows us to learn about the parameter space, and the model has initially very fast simulations. We may also reduce the parameter space if we know that certain areas of

the reservoir are unperturbed early in the life of the reservoir.

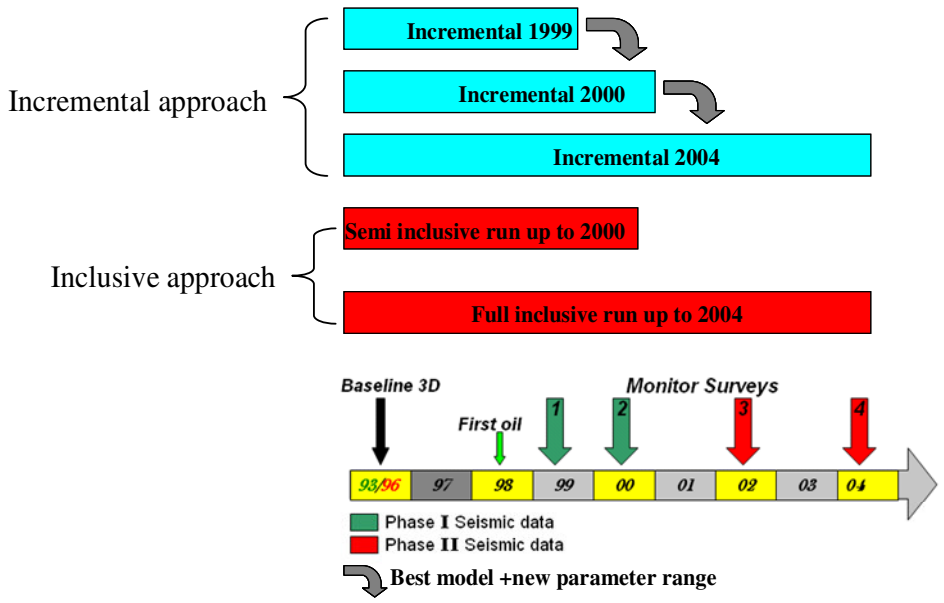

Figure 7.1: *Seismic history matching approaches. For incremental run 1, the 1998–1999 4D map is matched. The best model is used as the base case for incremental run 2000, along with any modified parameter ranges, and also in incremental run 2004. The inclusive runs use all data up to the 2000 or 2004 surveys.*

7.2 Parameterisation

To perform history matching, we must define a parameter space. We history match by changing the transmissibilities of some selected barriers, shown in Figure 7.2. The barriers used for each run are listed in Table 7.1. It was observed that these barriers strongly control the mismatch between predicted and observed 4D signatures.

Barrier transmissibilities may be estimated from the geological model properties using the Shale Gouge Ratio (Manzocchi *et al.*, 1999). These are inevitably uncertain because relationships between observed barrier permeabilities and shale content show order-of-magnitude variations. Estimated transmissibilities are therefore useful starting points for history matching and may provide insight into the uncertainties. History matching, particularly if time-lapse seismic data is available, can then be used to reduce uncertainties in the barrier transmissibility. We control the transmissibility by taking the base-case barrier values and multiplying that number by our control parameter. We

therefore vary multipliers of the transmissibility values. The interpreted barriers and baffles define some degree of reservoir compartmentalisation that can be validated by production and pressure data. These could be useful to estimate which areas of the reservoir have not been drained, suggesting possible infill opportunities. The integration of the interpreted barriers and baffles with the outcome of the 4D seismic inversions and the geology and production data has been used to aid infill opportunities and reservoir management decisions at the Schiehallion field (Floricich *et al.*, 2008).

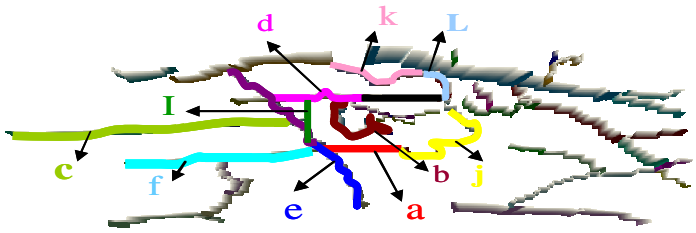

Figure 7.2: *Barriers and faults system in Schiehallion field Segment 4 (Edris et al., 2008)*

Barriers	Incremental run 1999	Incremental run 2000	Incremental run 2004	Semi-inclusive run 2000	Full inclusive run 2004
a	√	√	√	√	√
b	√	√	√	√	√
c	√	√	X	√	√
d	√	√	√	√	√
e	√	√	X	√	√
f	√	√	√	√	√
	√	√	√	√	√
h	√	√	√	√	√
j	√	√	√	√	√
k	x	x	√	x	√
L	x	x	√	x	√

Table 7.1: *Barriers modified in each run for the incremental, semi-inclusive and inclusive runs.*

7.3 Preliminary seismic history matching

The need for a new barrier may satisfy the 4D or the production data or a combination of both. 4D may allow for the spatial position of a barrier to be identified, whereas production data alone may not allow this. The base case and observed data are quite different, indicating the need for the extra fault. However, it is dangerous to justify a barrier addition without cross-checking 3D seismic data to gain an idea of whether there is any evidence of a barrier. In this case, we add an additional barrier based on 4D

seismic data (Figure 7.3). This barrier reduces the misfit values (Figure 7.4), and a similar interpretation of this barrier has recently been agreed by BP, which we received after we had reached our own decisions (Macdonald *et al.*, 2004).

Observed seismic	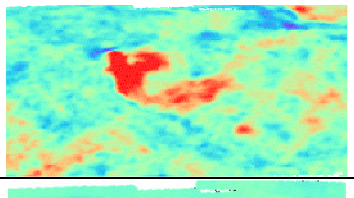
Predicted seismic without added barriers	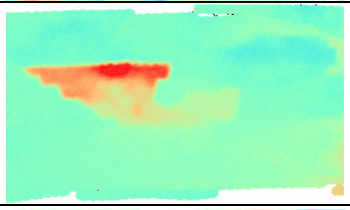
The differences between the best model without the barriers and the observed seismic	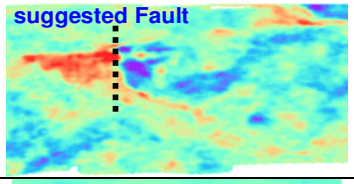
Predicted seismic with the added barrier	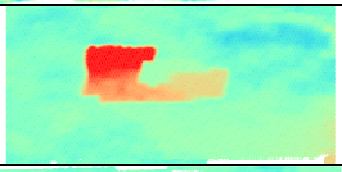
Predicted seismic with the added barrier in a different position	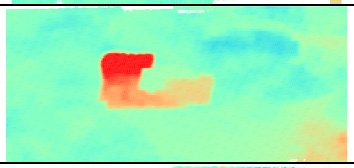
Difference between the observed signal and the predicted after shifting the barrier	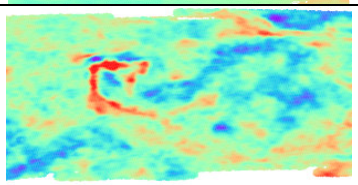
Barrier network and the added barrier position	
Agreement from the operators about the existence of the barrier	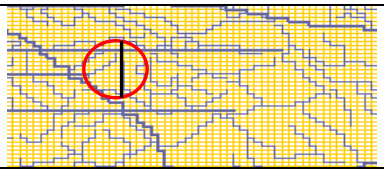

Figure 7.3: *Barrier position based on the 4D seismic data. We add an additional barrier based on 4D seismic data. Recently, the existence of this barrier has been confirmed by BP.*

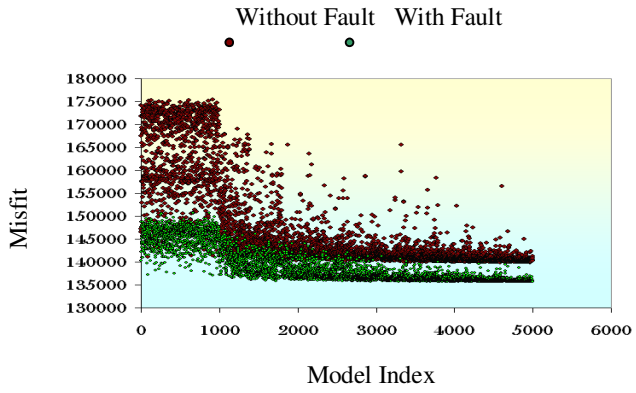

Figure 7.4: *The impact of the added barrier on the misfit.*

7.4 History-matching results

7.4.1 Prior uncertainties

We start with 0.001 as initial barrier transmissibilities values for all parameters. There is a maximum physical limit of 1.0 for the transmissibility multiplier and a lower limit of10^{-3}. The SHM workflow presented in Chapter 3 is applied to perform the history matching. The petro-elastic transform (see Chapter 3) is then used with the parameters in tables 6.5 and 6.6 to calculate the maps of impedance. An initial sample of 1100 models is used, followed by 80 per iteration (ns=80) of the NA routine. The best 40 (nr) models are then resampled, ns/nr=2, generating 3400 models in each case.

7.4.2 Incremental history matching

Incremental run 1**:** We began by simulating the first year of production and matched the difference between the first monitor and the baseline. A good seismic prediction was achieved from this SHM run (Figure 7.5) compared to the observed data in Figure 6.14a. A priori, we require a large uncertainty to ensure we span as wide a range of values as possible. We are able to reduce that uncertainty before continuing with Steps 2 and 3, however. Ten parameters are used in the SHM workflow during the automated modification of barrier transmissibility multipliers around injector well I2. Figure 7.6 illustrates how parameters change as convergence is obtained. This plot suggests that most of the improvements to the model are a result of increases in the barrier transmissibility – for example, for the following parameters, I and g, the direction of

convergence suggests a decrease in the barrier transmissibility. Parameters h, c, f, a and j in the direction of convergence suggest an increase in the transmissibility for the barriers to allow more flow through these barriers. For parameter d, the results suggest that the multiplier is acceptable. Parameter e is not sensitive to these changes.

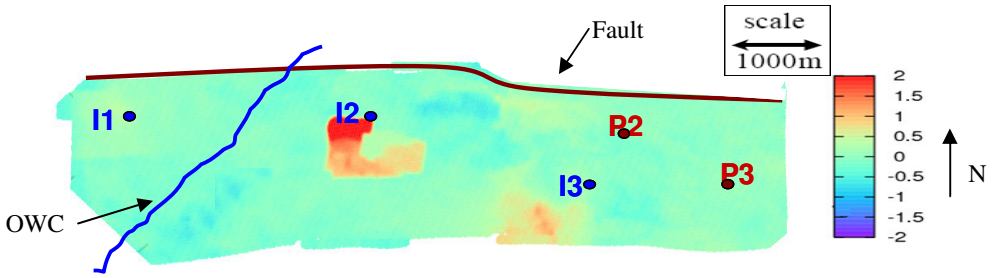

Figure 7.5: *The predicted impedance changes for 1993–1999 for the best model after incremental run 1. A good seismic prediction was achieved from this run compared to the observed data in Figure 6.14a.*

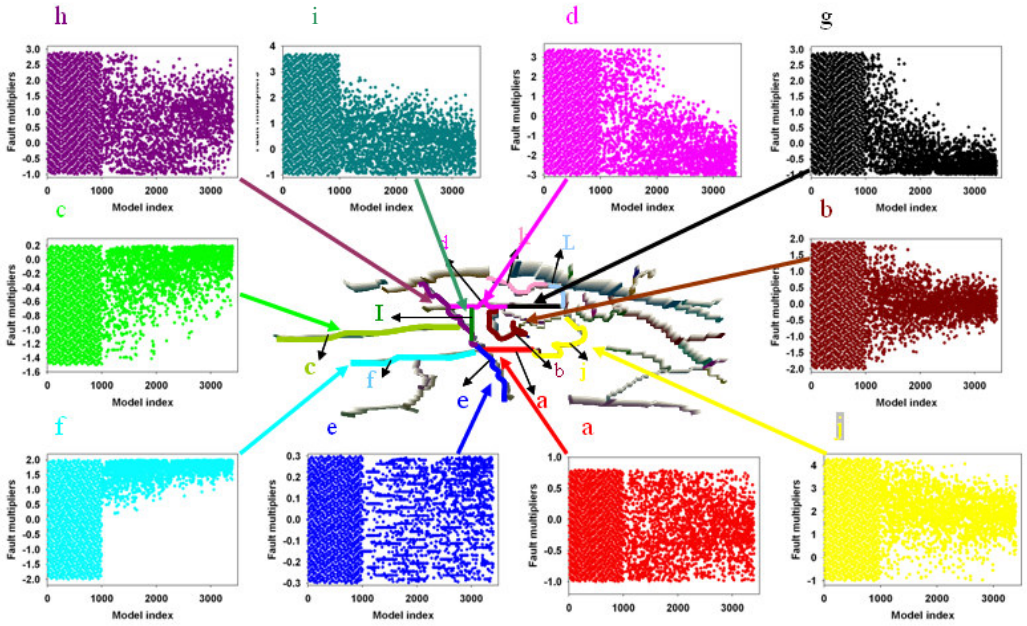

Figure 7.6: *Change in parameters during SHM. Ten parameters are used in the workflow, where the y-axis is log10 of multiplier (barrier transmissibility multipliers around injector well I2).*

Incremental run 2: We use the best model from incremental run 1 as a base case and then simulate the first two years of production (all simulations are restarted, as it is too costly to store restart files for thousands of models, particularly for many of the models that are unnecessary). We also modify the parameter ranges for the barrier multipliers (Table 7.2). The misfit is obviously larger now, because we have included the extra data. Again, we find that we obtain a reasonable match between the predicted and observed seismic differences over the first two years of production (Figure 7.7) compared to the observed seismic data in Figure 6.14.

Barrier multiplier (MULTFLT)	Range		Barrier
	min	max	
0.101	-1	0.98	a
0.343	-1	1.9	b
0.001	-0.4	0.5	c
0.616	-0.5	2.9	d
0.001	-0.7	0.21	e
0.010	-1	2	f
0.001	-1	3	g
0.002	-1	2.6	h
0.00001	0.5	6	I
0.001	0.5	3.3	j

Table 7.2: *Best barrier transmissibility values and the log10 of the parameter limits used in incremental run 2. Colours indicate the barriers in Figure 7.2.*

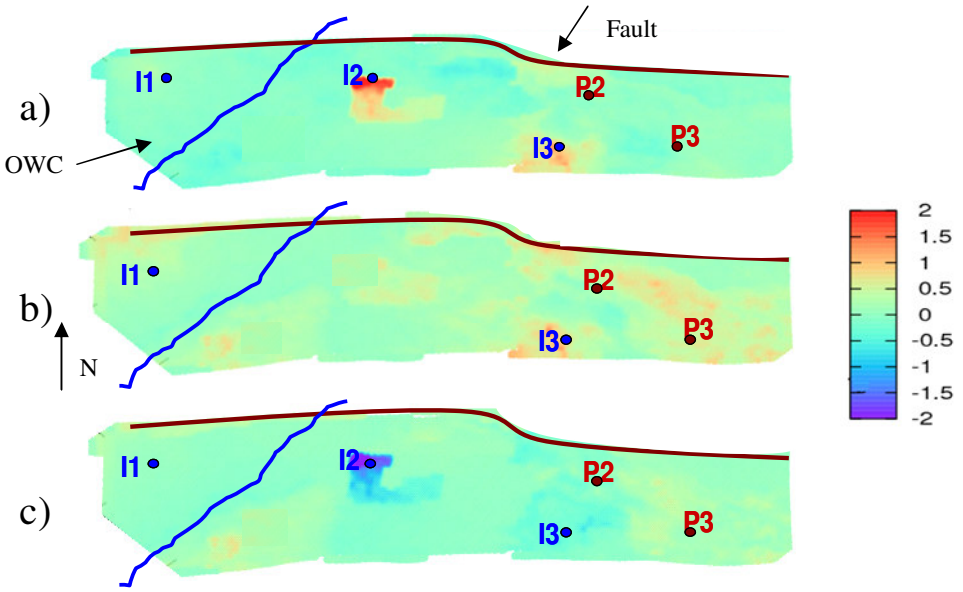

Figure 7.7: *Predicted change in impedance obtained for the best model using the incremental history match up to 2000 for (a) 1993–1999, (b) 1999–2000 and (c) 1993–2000. Compare with Figure 6.14 a, b and c respectively.*

Testing the model's predictability

a) In terms of seismic data

We use the best model from incremental run 2 as the base case using the barrier multipliers in Table 7.2 and predict Phase II seismic data (2002 and 2004). We find that this model is not a good predictor for the Phase II seismic data (Figure 7.8), however, as we cannot match the main 4D signature around the injector I4 (Figure 6.15). The main reason for this is that the transmissibility multipliers for the barriers around that well are not included in our parameter space.

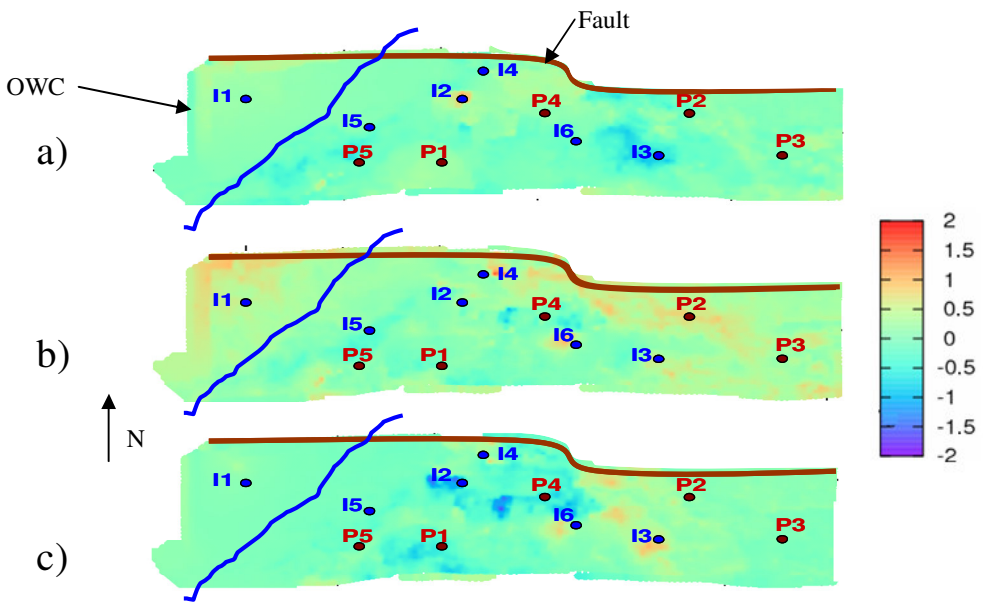

Figure 7.8: *Predicted change in impedance obtained for the best model of incremental run 2 for (a) 1996–2002, (b) 1996–2004 and (c) 1999–2000. Compare with Figure 6.15 a, b and c respectively.*

b) In terms of production

We obtain a good history-matching result, even without matching to production data during SHM (Figure 7.9). A good match for gas production is obtained up to 2002, but the forecast is not satisfactory, because we do not include the parameters that can affect the flow close to the main anomaly in the 1996–2004 4D seismic data. However, the water cut is not sensitive to these parameters.

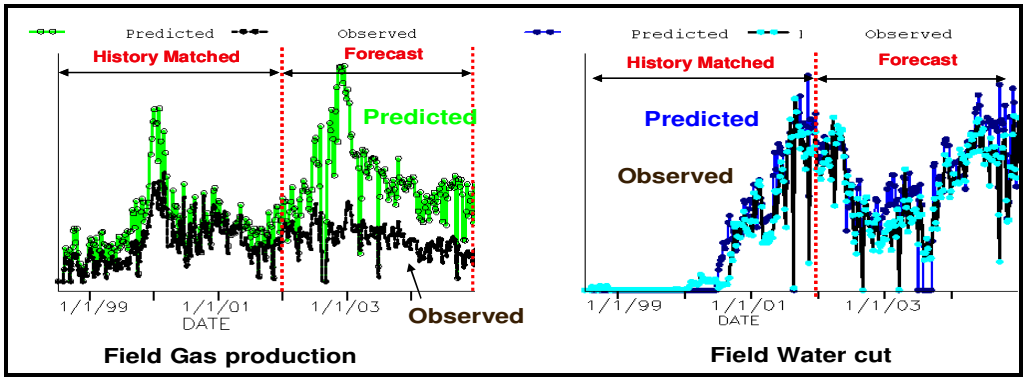

Figure 7.9: *History matching and prediction for GOR profile, on the left, and water cut profile for the field, on the right.*

Incremental run 3: Additional barriers are added to the parameter space when the Phase II seismic data (an additional two surveys covering four more years of production) are included. We perform an SHM run, adding barriers K and L (Table 7.3 and Figure 7.10). We fix two barriers (c and e) that are apparently less important for flow impact owing to the wide range of parameter value changes, and for the other parameters, we use the best values of transmissibility multipliers from previous history-matching runs. The best model is now significantly improved (Figure 7.11) compared to the observed seismic data in Figure 6.15.

Barrier multiplier (MULTFLT)	Range		Barrier	
	min	max		
0.043	-1.3	1.3	a	
0.184	-1	0.7	b	
0.947			c	
0.493	-0.5	0.3	d	
0.356			e	
0.004	-1	2.4	f	
0.010	-1	2	g	
0.162	-1	0.8	h	
0.002	1	2.7	I	
0.004	1	2.4	j	
0.321	-1	0.5	k	
0.134	-1.5	0.9	L	

Table 7.3: *Best barrier transmissibility values and the $\log_{10}$ of the parameter ranges from Step 2.*

Figure 7.10: *The new area considered to match Phase II seismic data by changing the barrier transmissibility of barriers K and L.*

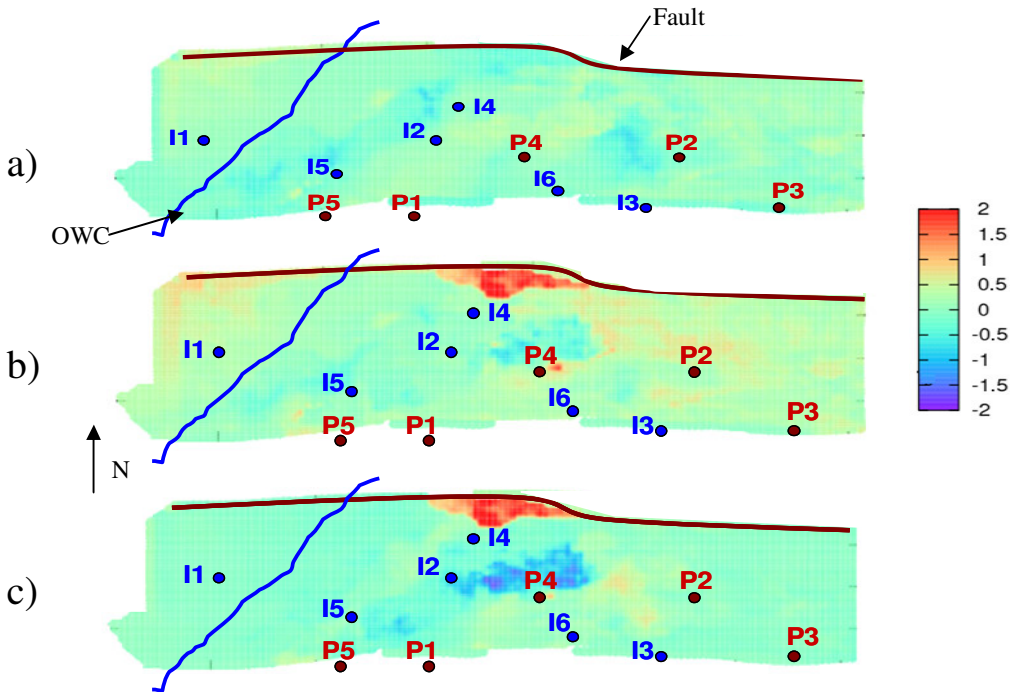

Figure 7.11: *Predicted change in impedance obtained for the best model using the inclusive history match up to 2000 for (a) 1996–2002, (b) 1999–2000 and (c) 1996–2004. Compare with Figure 6.15a, b and c respectively.*

7.4.3 Inclusive history-matching

Semi-inclusive run to 2000: In this case, we include all the Phase I seismic data, simulating the first two years of production. The best model predicting impedance (Figure 7.12 a, b and c) is improved significantly for the two observation periods compared to the observed pseudo-impedance (Figure 6.15 a, b and c). Figure 7.13 shows how parameters change as convergence is obtained.

This plot suggests that most of the improvements to the model are a result of increases in the barrier transmissibility. For example, in the parameters h, g, c, b, e and a, the direction of converges suggest an increase in the transmissibility for these barriers, but for parameter f, the degree of converging suggests a decrease in this barrier transmissibility. For parameters I and d, the greater spread has two possible causes, but the most likely is an increase in these barriers' transmissibility. Parameter j is not sensitive to the changes.

We perform some sensitivity analyses on the misfit to the parameters and find that, when changing one parameter at a time, the shape of the misfit is asymmetric (Figure 7.14.

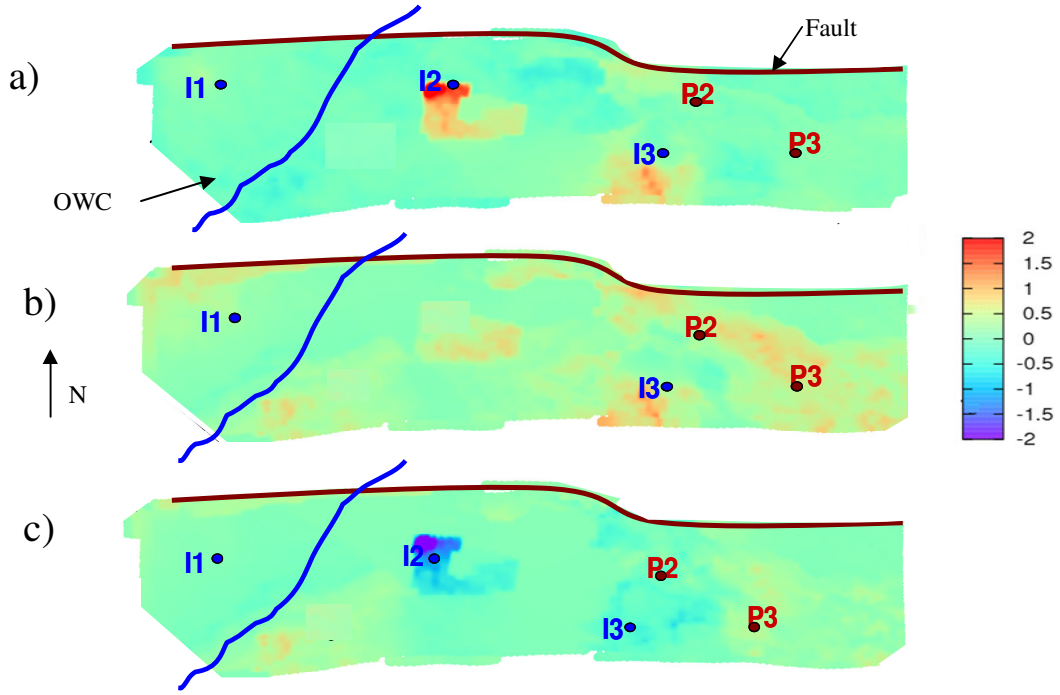

Figure 7.12: *Predicted change in impedance obtained for the best model using the inclusive history match up to 2000 for (a) 1993–1999, (b) 1999-2000 and (c) 1993-2000. Compare with the observed data in Figure 6.14a, b, and c respectively.*

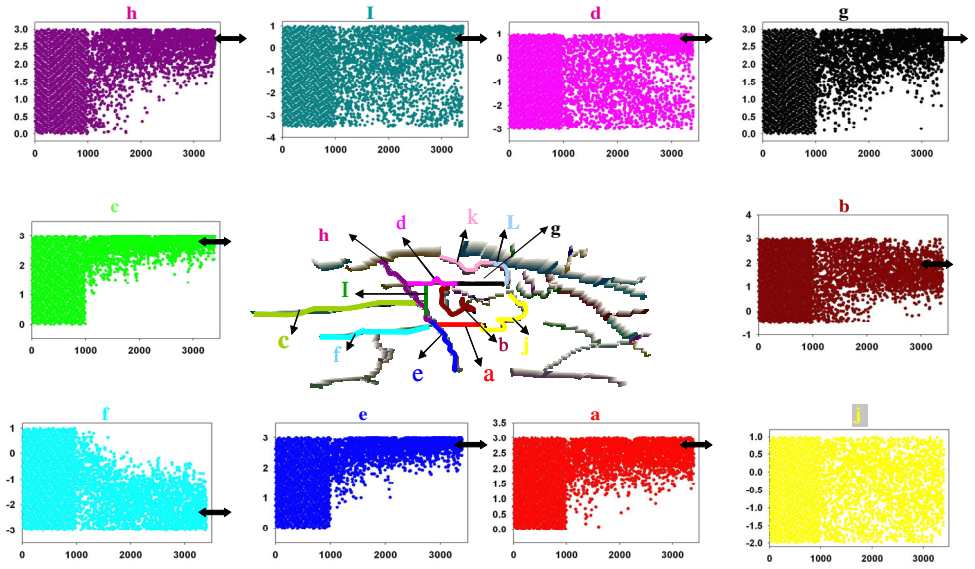

Figure 7.13: *The change in the parameters used in the inversion workflow after the automated modification of barrier transmissibility multipliers around injector well I2. The distribution plots are colour-coded according to the barriers in the central figure. The black arrows indicate the most likely value for each parameter.*

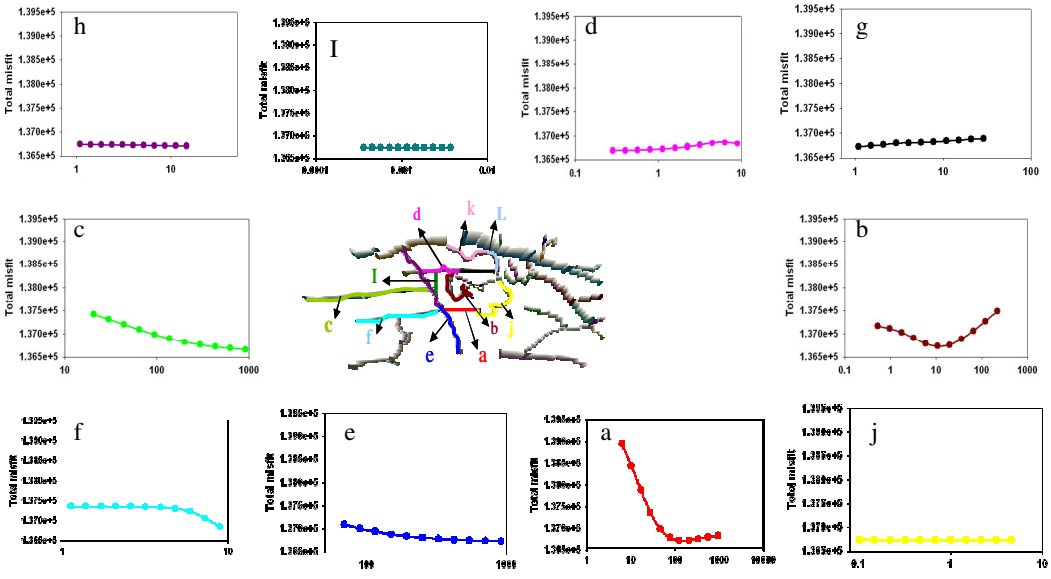

Figure 7.14: *Sensitivity analysis by changing one parameter at a time. The x-axis is the parameter value, which is the log of the barrier multiplier, and the y-axis shows the total misfit. The sensitivity plots are colour-coded according to the barriers in the central figure.*

A reduction in the misfit is obtained from the incremental runs compared to the semi-inclusive run, as shown in Figure 7.15. This is the case when we compare the semi-inclusive run to 2000 to incremental run 2 using the incremental run 1 approach, as illustrated in Figure 7.16. It is possible that the new data may result in an old history match being lost if we use the same data in a different order and obtain better results compared to the best models.

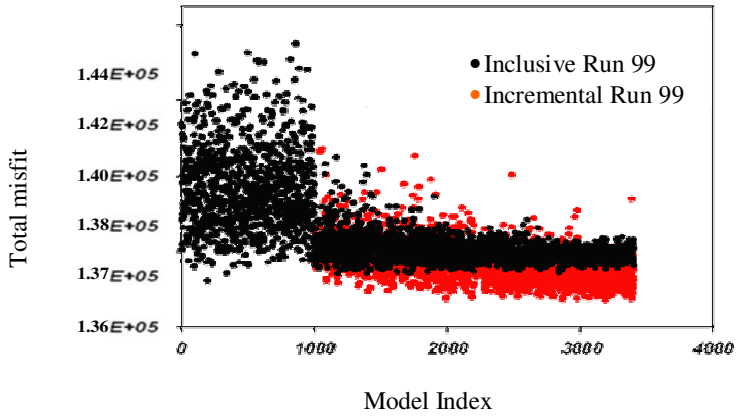

Figure 7.15: *Misfit evolution during incremental run 1 and for the 1998–1999 contribution to the seismic misfit for the inclusive run up to 2000.*

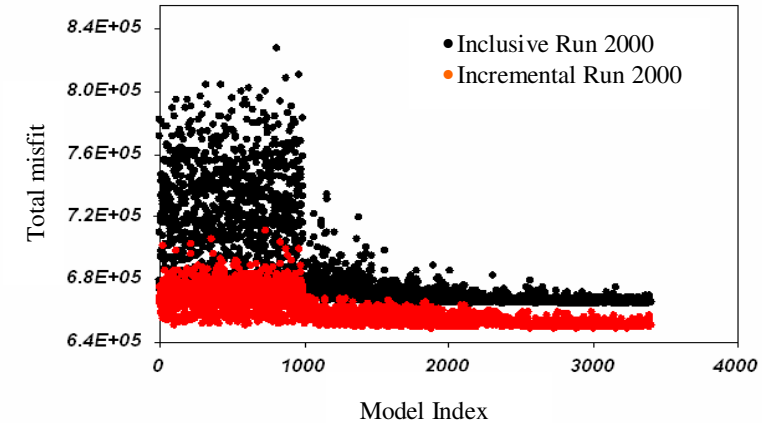

Figure 7.16: *Misfit comparison between the incremental run and the inclusive run up to 2000.*

Figure 7.17 shows the probability distribution of the parameter space after Markov chain Monte Carlo resampling of the posterior probability density (Sambridge, 1999b). We can see two groups of parameters showing different degrees of sensitivity to the

addition of data. The less sensitive group includes faults a, b, c, e, i and j, which have similar parameter distributions. The second group (d, f, g and h) is sensitive, showing a hysteresis effect due to injector I2 pressuring up the fault compartment in the first year and then relaxing in the second. These parameters also have less effect on the misfit. Fault b does not have an impact despite being close to the injector well, because it is isolated from the injector by a very low Net:Gross area.

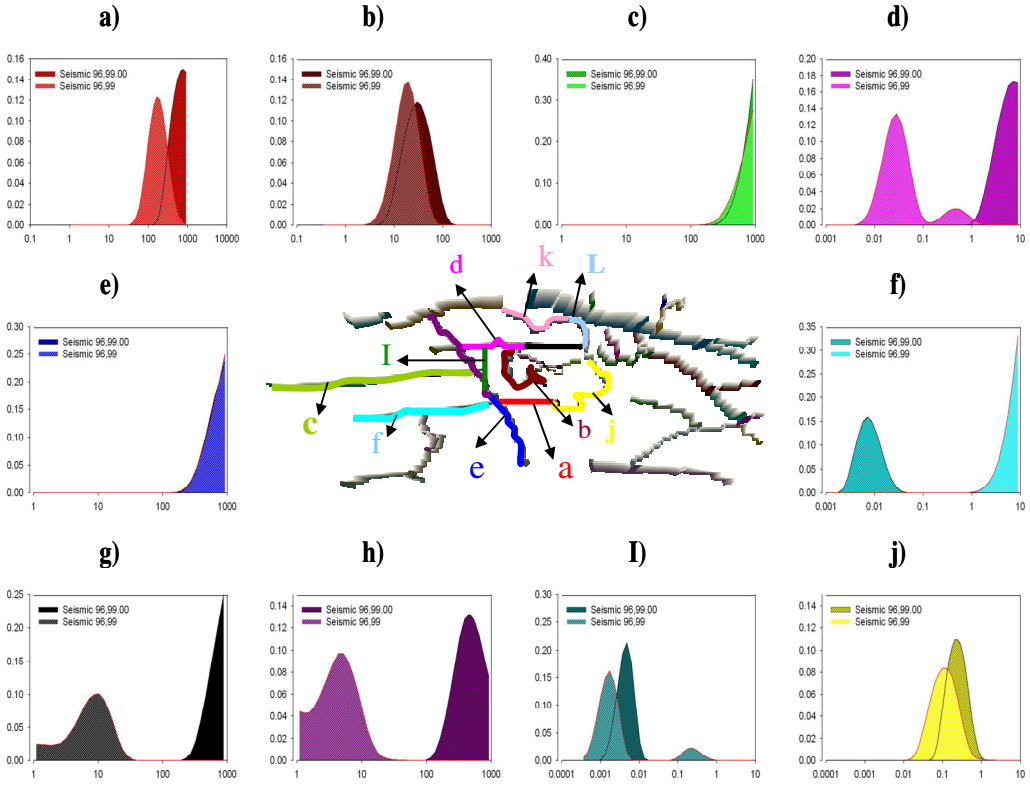

Figure 7.17: *Probability distributions of the parameters for the semi-inclusive run and incremental run 1. The distribution plots are colour-coded according to the barriers in the central figure.*

Uncertainty analysis

To understand the uncertainty of the reservoir model, we adopt a similar approach to analyse saturation, pressure, impedance and misfits by volume and maps. The PPD (Posterior Probability Density) is then resampled as part of the uncertainty analysis of modified parameters (Sambridge, 1999b). These probabilities can also be used to infer uncertainty in predictions (Stephen, 2006). Variables such as saturations, pressures and

impedances for each grid cell can be averaged over the ensemble of models, weighted by the model probability. We can then determine the most likely simulation result and its uncertainty (see Chapter 3). We calculate standard deviations using equation 3.16 to quantify the variable uncertainty (Stephen *et al.*, 2006). We find that the pressure and saturation uncertainties were significantly reduced in the case of 2000 data, where we use the best model 99 as base in this run misfit. Saturation uncertainty is low here in all cases (Figure 7.18). Time-lapse seismic data measures some combination of saturation and pressure change in the reservoir and reduces the non-uniqueness. In a reservoir where time-lapse is saturation-dominated, the influx of water can be detected, thereby improving characterisation at the water front. With pressure-dominated time-lapse, pressure build-up and, to a lesser extent, draw-down, can be determined, enabling the identification of flow barriers and pathways. In the sector of the Schiehallion field, the time-lapse signature is pressure-dominated and helps to quantify a number of parameters some distance from the producing wells, including the transmissibilities of faults near one of the injectors.

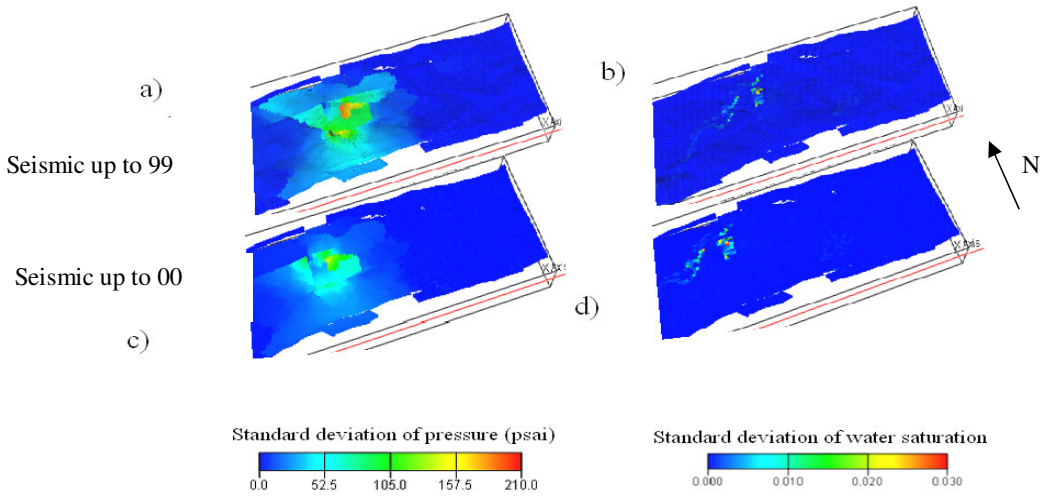

Figure 7.18: *Prediction uncertainty: (a) Seismic 99 for pressure, (b) Seismic 99 for water saturation, (c) Seismic 2000 for pressure and (d) Seismic 2000 for water saturation close to the matched area.*

Full inclusive run to 2004: In this case, we include all the Phase I and Phase II seismic data simultaneously, simulating all six years of production. We use the same prior range for each parameter as used for incremental run 1 and the semi-inclusive run to 2000. In addition, we add more barriers to the parameter space around the main seismic signature around well I2 and I4.

The best predicted model is improved. Figure 7.19 a and b and Figure 7.20 a and b for the Phase II dataset are compared to the observed data in Figure 6.14 a and c and Figure 6.15 a and c respectively.

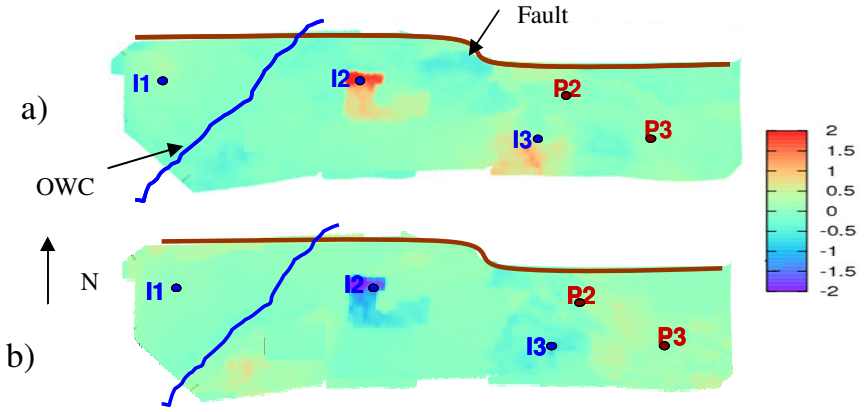

Figure 7.19: *Predicted Phase I changes in impedance obtained for the best model using the inclusive history match up to 2004 for (a) 1993–1999 and (b) 1999-2000. Compare with Figure 6.14 a and c.*

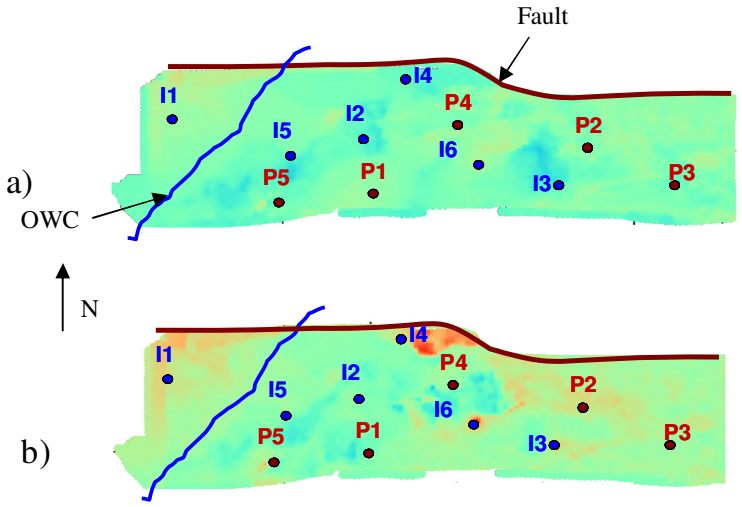

Figure 7.20: *Predicted change in impedance obtained for the best model using the inclusive history match up to 2004 for (a) 1996–2002 and (b) 2002–2004. Compare with Figure 6.15 a and c.*

Probability distributions for each parameter are calculated and show that the most likely values for barrier transmissibilities a, b, c, e, h, I and k suggest an increase. In Figure 7.21, d, f, j, and L suggest a decrease in the transmissibility of these barriers. In Figure 7.21, g is not sensitive to the changes. Figure 7.22 shows statistics (mean and standard deviation) for the inverted values. In the twelve parameters case for the inclusive run 2004, the uncertainty for each parameter is represented in terms of standard deviation.

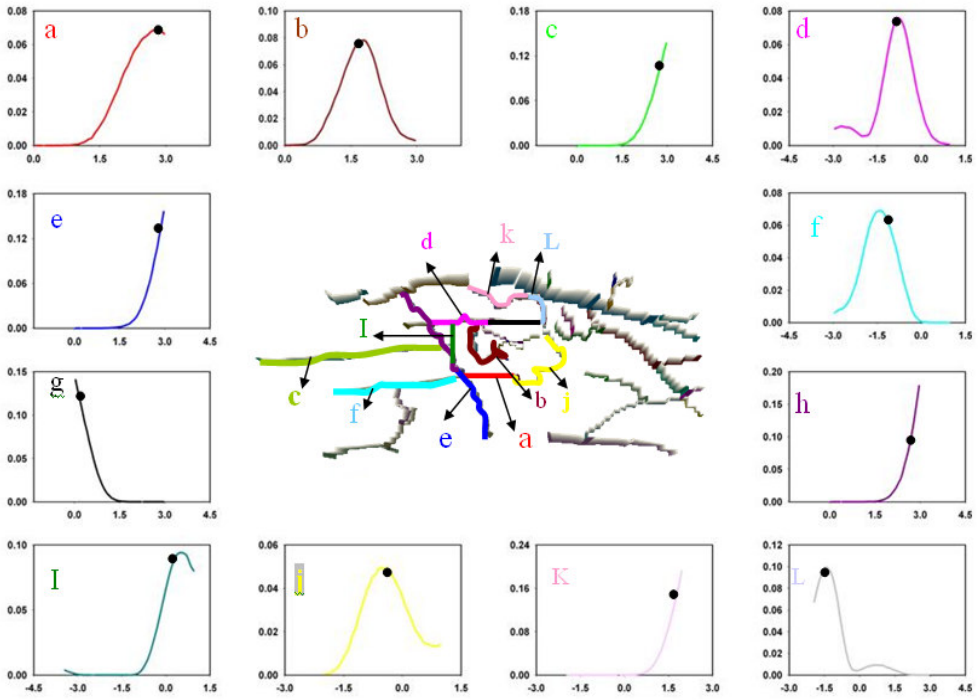

Figure 7.21: *Probability distributions after resampling the PPD for the inclusive run up to 2004. The distribution plots are colour-coded according to the barriers in the central panel. Black points indicate the best model multipliers. X axis is log10 of barriers multiplier and Y axis is probability.*

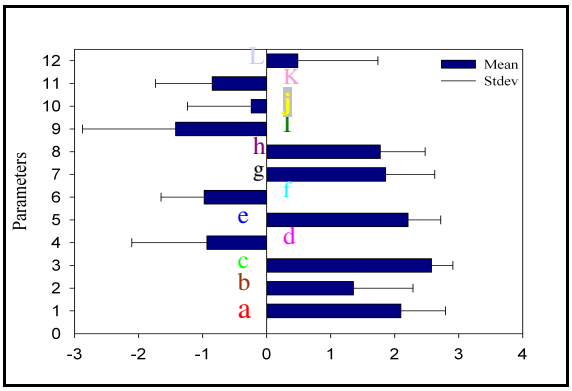

Figure 7.22: *Statistics (mean and standard deviation) for the inverted values, twelve parameters case for the inclusive run 2004.*

7.5 Discussion

The more data that we include in the history match, the stronger the constraints, and therefore the harder it can be to find a match. This makes it more difficult to determine how better off we really are. The curse of dimensionality affects history matching as too many unknown parameters can lead to many unnecessary simulations. We then seek to reduce dimensionality as much as possible. In a field such as Schiehallion, different areas are produced (or injected into) at different times. We may therefore use this information to identify parameters separately at different stages in the lifetime of the reservoir. We can find the most appropriate values for parameters that affect its early life with quick simulations, and we can then use those values to look at other parameters later. Finally, all inclusive runs may be performed as a cross check. We found that there is an apparent hysteretic effect in some of the barriers due to pressure increasing then decreasing. We carried out a number of applications of history matching with time-lapse seismic data to reduce the uncertainty of barrier transmissibilities in the Schiehallion field. We found that we were able to obtain a reasonable match to the observed data (within data noise limits).

History matching with just one year of data leads to different preferred results compared to when the second monitor survey is included. It may be that these barriers are mechanically active or, alternatively, that the transmissibility is dynamically active.

These barriers are close enough that the free water level has not invaded the barrier pores, as has happened in the neighbouring reservoir rock. As the barrier compartment around injector I2 pressures up, the barrier rock containing mobile water will act as a dynamic barrier to the flow of oil. We can see the impact of adding more data to SHM, our selected parameter, because of the influence of flow during the production time and also of the method of using the data. History matching incrementally leads to more control over the parameter range. We can learn about the uncertainty of the parameters and understand their importance by submitting short runs first. The incremental approach can be compared to the EnKF (ensemble Kalman filter) method where the latest production data is assimilated without rerunning the simulator from the initial conditions. This leads to many problems such as when the EnKF tends to transform multi-modal permeability distributions to a more normal or Gaussian distribution over a sequence of many updates. This transformation leads to a loss of structure in the permeability field. Another common difficulty experienced when using the EnKF is known as the filter variance. The effect of filter divergence is such that the distribution produced by the filter drifts away from the truth. Filter divergence normally occurs because the prior probability distribution becomes too narrow and the observations have progressively diminishing impact on the Kalman gain. Moreover, a change in the parameter behaviour, such as a diminishing importance from the early life of the field onward, cannot be considered in EnKF, but the incremental run allows the parameters to be switched on and off.

7.6 Observations and summary

In this chapter, two possible history-matching strategies have been presented. In the first, dynamic data can be added to the process as the model is modified so that short simulations can be run initially to sample the parameter space quickly. In the second approach, all parameters can be modified to match all data simultaneously. The best model can then be used as a base case as new data is added. Successive updating produced a better result, however. Additional barriers had to be modified when the Phase II seismic data (an additional two surveys covering four years of production) was included. Successive updating enabled these to be added without increasing the parameter space too much, while giving a result that was actually better than the

inclusive approach. The second approach gave a reasonable improvement when ten barrier transmissibility multipliers were updated using the first two monitor surveys (as used in Phase I of the project). We can therefore summarise this chapter as follows:

- Appropriate updating strategies were investigated, comparing an all-inclusive approach to one in which data was gradually added and the prediction period extended.
- Whichever approach was used, a good match to the predicted data was obtained provided that all parameters affecting the misfit were included.
- Slightly better models were obtained if the parameter space was explored first with short simulations. Unnecessarily long history-matching runs could be avoided in this case.

CHAPTER EIGHT

Reducing Forecasting Uncertainty Using SHM in Schiehallion

This study investigates the value of seismic analysis in reducing forecasting uncertainty, where 4D seismic is added to the history-matching procedure. First, SHM is carried out. Then some of the best models are taken, and the behaviour of an infill well is predicted. The accuracy of forecasting that follows history matching is quantified, and the impact of time-lapse seismic data for infill well placement is analysed.

8.1 Introduction

The accurate prediction of reservoir behaviour via simulation models greatly helps field planning and management. Static models are often created using low-resolution 3D seismic along with log and core data from wells that may be widely separated. These geomodels are then converted into simulations for predictions, which are compared to history (production) data. The models are modified, often manually, to improve the match, and suffer from non-uniqueness due to data sparseness such that numerous combinations of parameters give the same result. This inevitably affects the accuracy of subsequent forecasts, which may be accurate for a few months at best. Time-lapse (4D) seismic analysis has been adopted in a number of fields to detect changes in pressure and saturations and is now used in an almost routine manner (Parker *et al.*, 2003). An obvious application is to use this data in the history-matching process. Most applications of time-lapse data have been qualitative, however, and to be used as a constraint in history matching, a more quantitative approach is required.

8.2 Combination of permeability and barrier or fault transmissibility for parameterisation

We have assessed the benefits of using seismic data as part of history matching in the Schiehallion UKCS field. The Phase I model for Schiehallion was history matched using either production, seismic or a combination of both. Then an infill well was considered and its behaviour predicted for a set of models that matched the history. This study was repeated using the Phase II model, except that in this case we had under our control the production data for the well, with which we could test our predicted uncertainty. The best model from the last incremental run (Chapter 7) was used as the base case. The new model required a different set of parameters, but fault/barrier transmissibilities and reservoir permeability data were modified as before. We started with the best model history matched to seismic data. The production data from wells P2 and P3 was included, as presented later. Our method is based on many hundreds of simulations which allow more thorough analyses. We showed that seismic data reduces parameter uncertainty, particularly in the inter-well region and near injectors. Forecasts of field pressures are also improved, resulting in reduced uncertainty, while saturation distributions are well constrained.

Six pilot points and four fault multipliers (Figure 8.1) were used. The pilot points were located between the producers P2, P3 and the injector I3 to modify the original permeability locally through multipliers applied to the column of cells. In this study, we sampled parameters evenly over a $\log_{10}$ scale, and each parameter was allowed a range of two orders of magnitude relative to the base-case value. Moreover, for fault transmissibility, the maximum physical limit of T_m=1 was considered.

We history matched using the Phase I seismic data (93, 99 and 00) and production data up to 2002 (from wells P2 and P3 only, given the location of the parameters) both separately and together in the misfit.

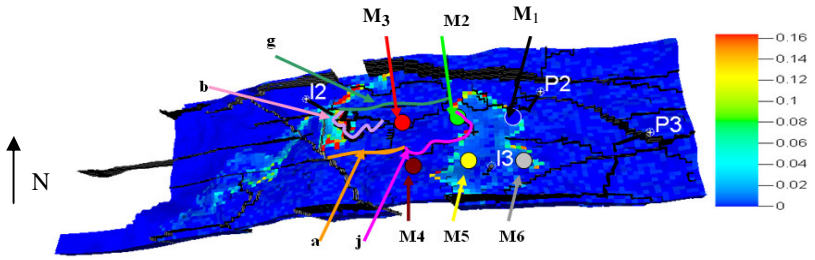

Figure 8.1: *Parameterisation: the coloured circles indicate variable pilot points. Thin coloured lines indicate faults, while thicker coloured lines indicate faults with variable transmissibility.*

We history matched using the seismic data of Phase I (93, 99 and 00) and production data up to 2005 (from wells P2 and P3 with parameters gas production rate, water production rate and GOR only, given the location of the parameters) both separately and together in the misfit. In the three cases, 2700 models were generated, and Figure 8.2 shows the misfit for each model as these were generated. The multipliers are interpolated using Kriging with a variogram of 500 m, the separation of the pilot points. An initial ensemble of 1100 (n_i) models was chosen to properly sample the parameter space so that Voronoi cells were not connected throughout the eight-dimensional parameter spaces. The same initial sample was used for each combination of history data. Resampling took place at 64 (n_s) models per cycle located around the best 32 (n_r). We identified the best model from each ensemble and compared predicted to observed data. Figure 8.3c shows that, when we included just production data in the misfit, the predicted seismic did not match the observed data (Figure 6.14a). With seismic data included in the misfit, predictions are much improved, although without matching some of the noise in the data.

The production data was matched equally well (or badly) regardless of which history data was used in the misfit. We found a good match in the case of the gas production over a period of three years (1998–2002). For the case of GOR, a good match was obtained when the seismic and production data were combined (Figure 8.4) in the case of the whole of Segment 4 model. Figure 8.5 and Figure 8.6 for the individual wells P2 and P3. Water production rate is less sensitive to changes in the selected parameter (figures 8.7 and 8.8). Increasing the density of pilot points between I3 and P2 and

ignoring faults did result in improved GOR when matching to production only.

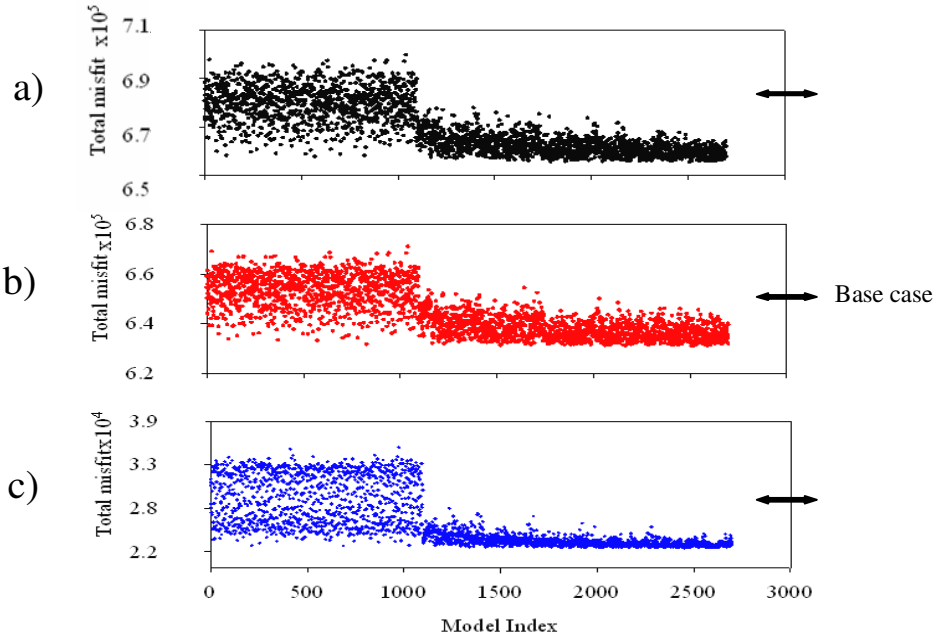

Figure 8.2: *Misfits calculated for an ensemble of 2700 models. The first 1100 models are sampled randomly from the parameter space for a) seismic and production data, b) seismic and c) production only.*

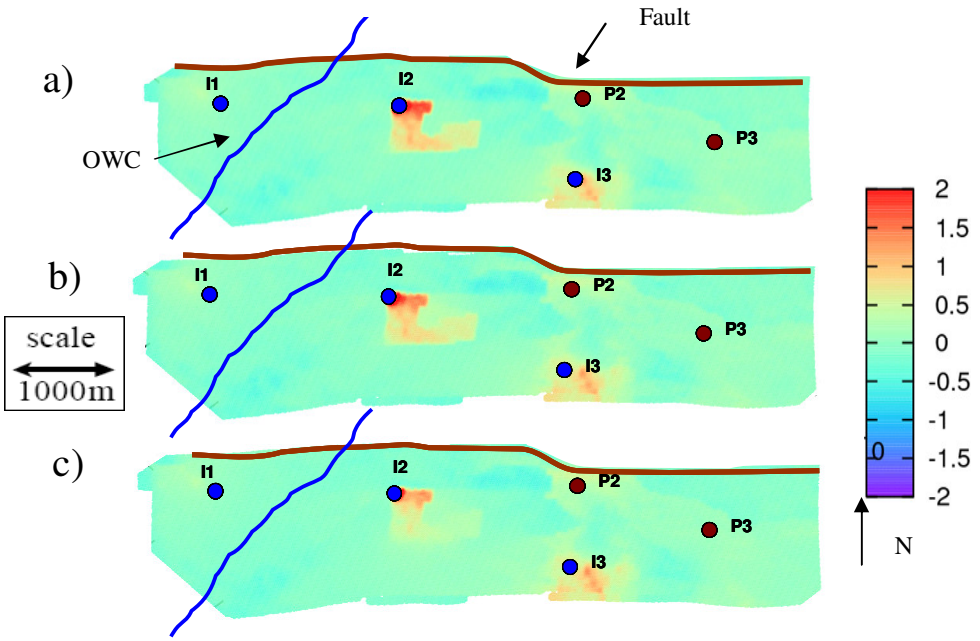

Figure 8.3*: The impedance changes for 1993–1999 (old–new) for the best modelling case of (a) seismic and production data, (b) seismic only and (c) production only. Compare with Figure 6.14a.*

We predicted the behaviour of the model for the next three years using the best 100 models with the lowest misfit value. We found a good match for the case of the gas production for a period of 3.25 years, but the prediction was inadequate. For the case of GOR, a good prediction was obtained when the seismic and production data were combined. Seismic-only matching gives a set of models that are similar to whole Segment 4 models. Gas production rate is sensitive for the prediction period because we did not include some parameters which seem important in the late period. However, water production rate is less sensitive to the changes in the selected parameter, and the choice of pilot point locations has a significant impact on improving or changing the behaviour of the selected parameters, such as controlling the breakthrough time and the flow (figures 8.9 and 8.10).

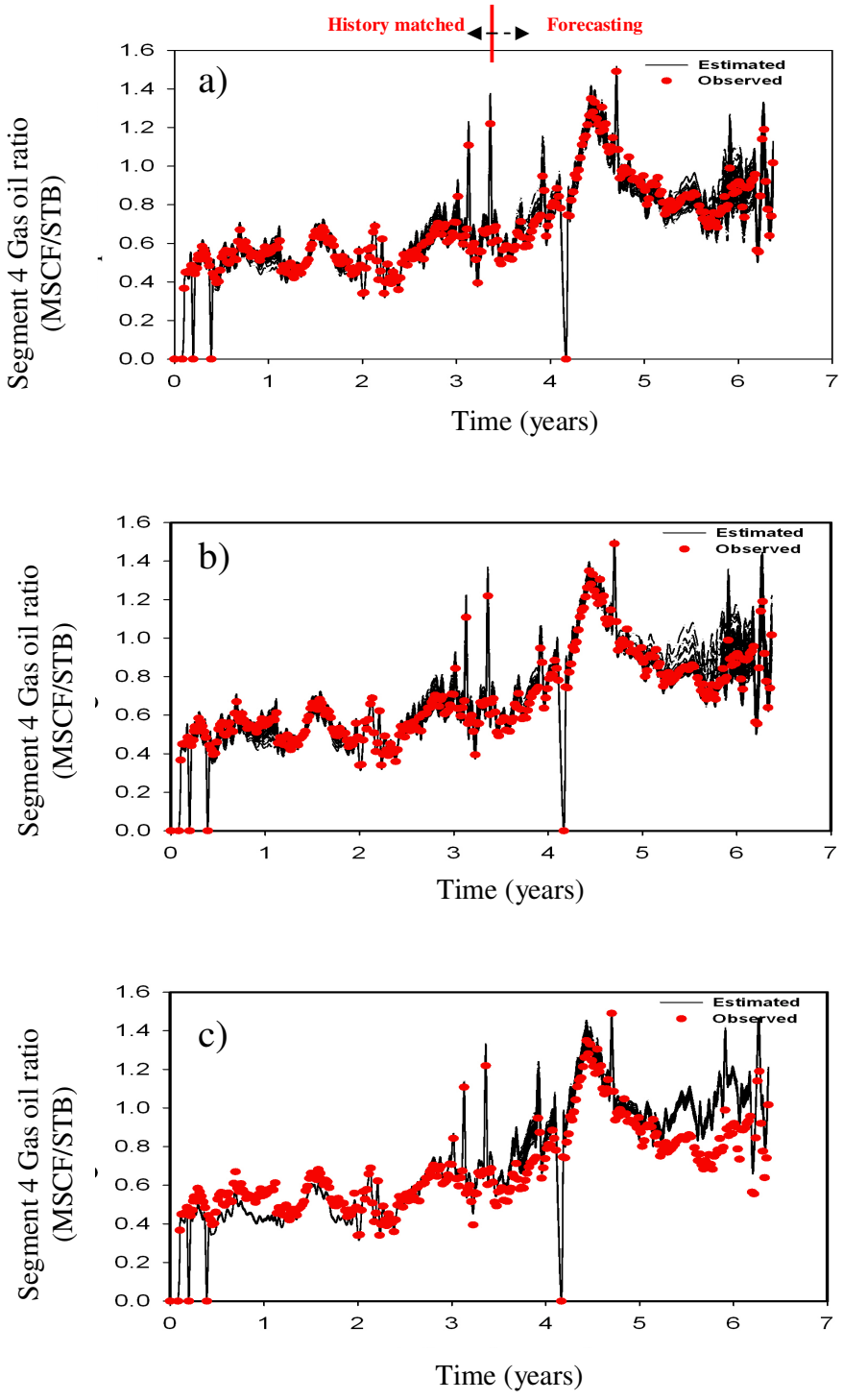

Figure 8.4: *The history-matched and forecasts of GOR (red line is the observed) for the whole of Segment 4 using the best 100 models from history matching, where the misfit included (a) seismic and production data, (b) production only and (c) seismic only.*

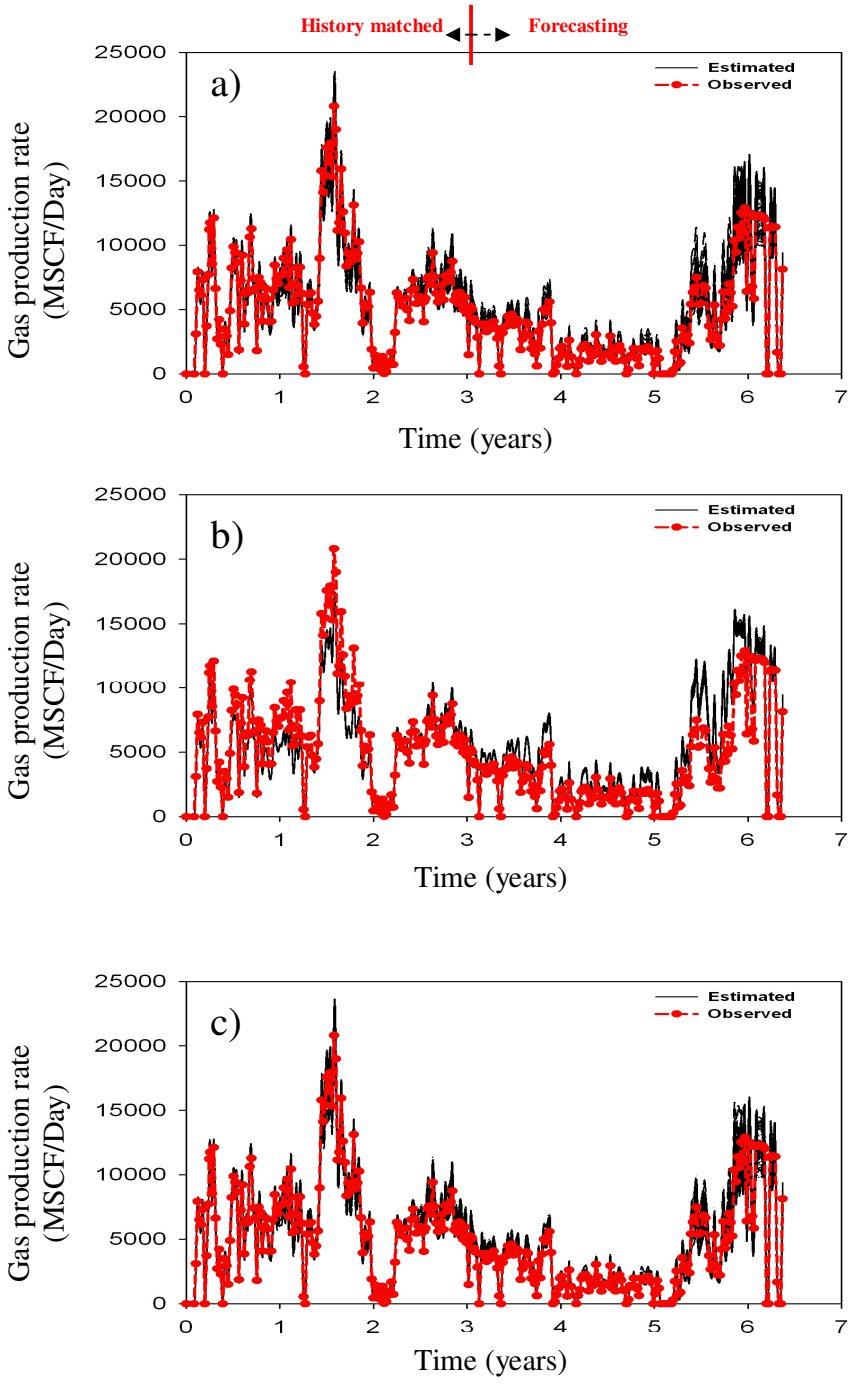

Figure 8.5: *The history and forecasts of gas production rate (red line is the observed) for well P2 using the best 100 models from history matching, where the misfit included (a) seismic and production data, (b) production only and (c) seismic only.*

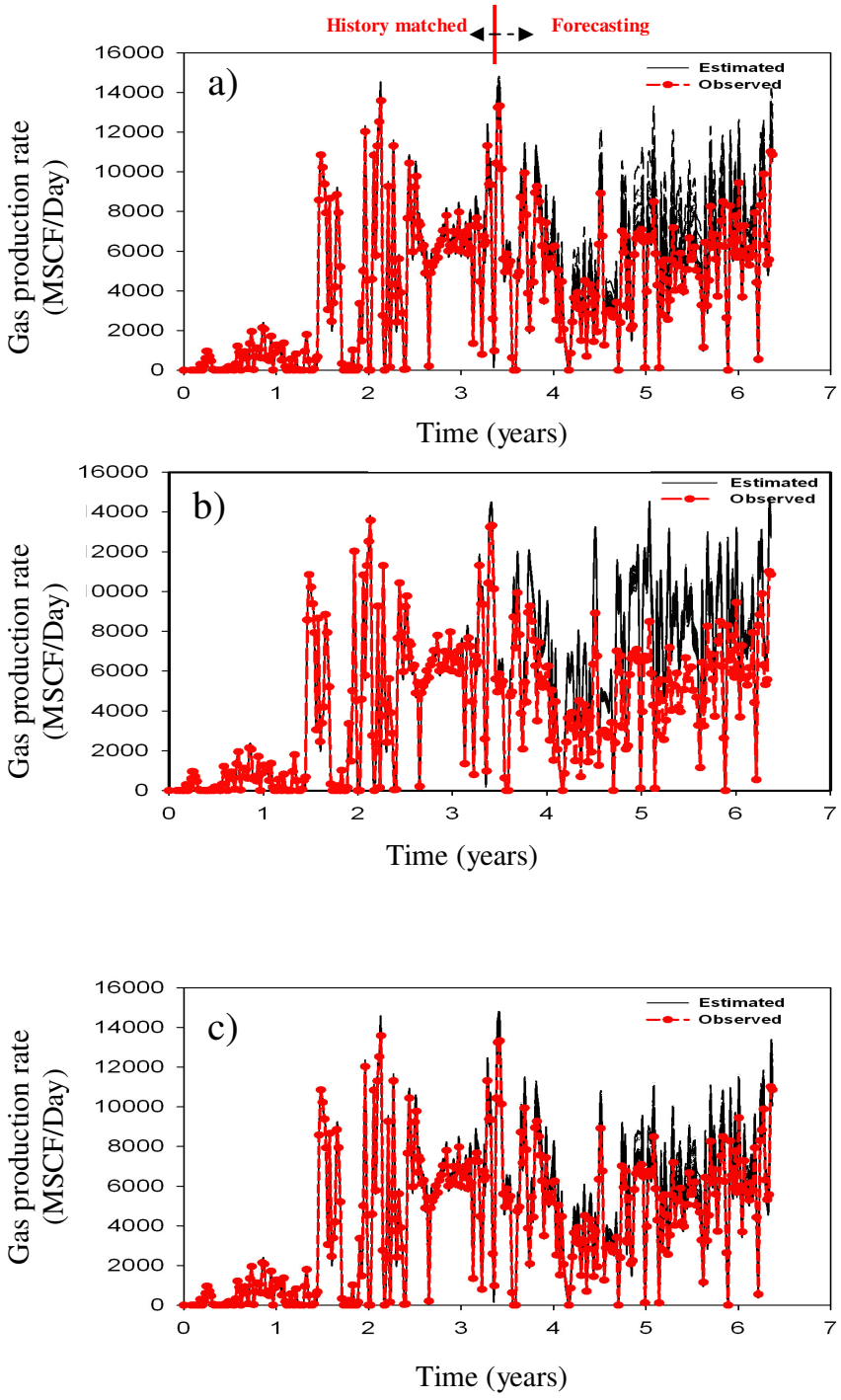

Figure 8.6: *The history and forecasts of gas production rate (red line is the observed) for well P3 using the best 100 models from history matching, where the misfit included (a) seismic and production data, (b) production only and (c) seismic only.*

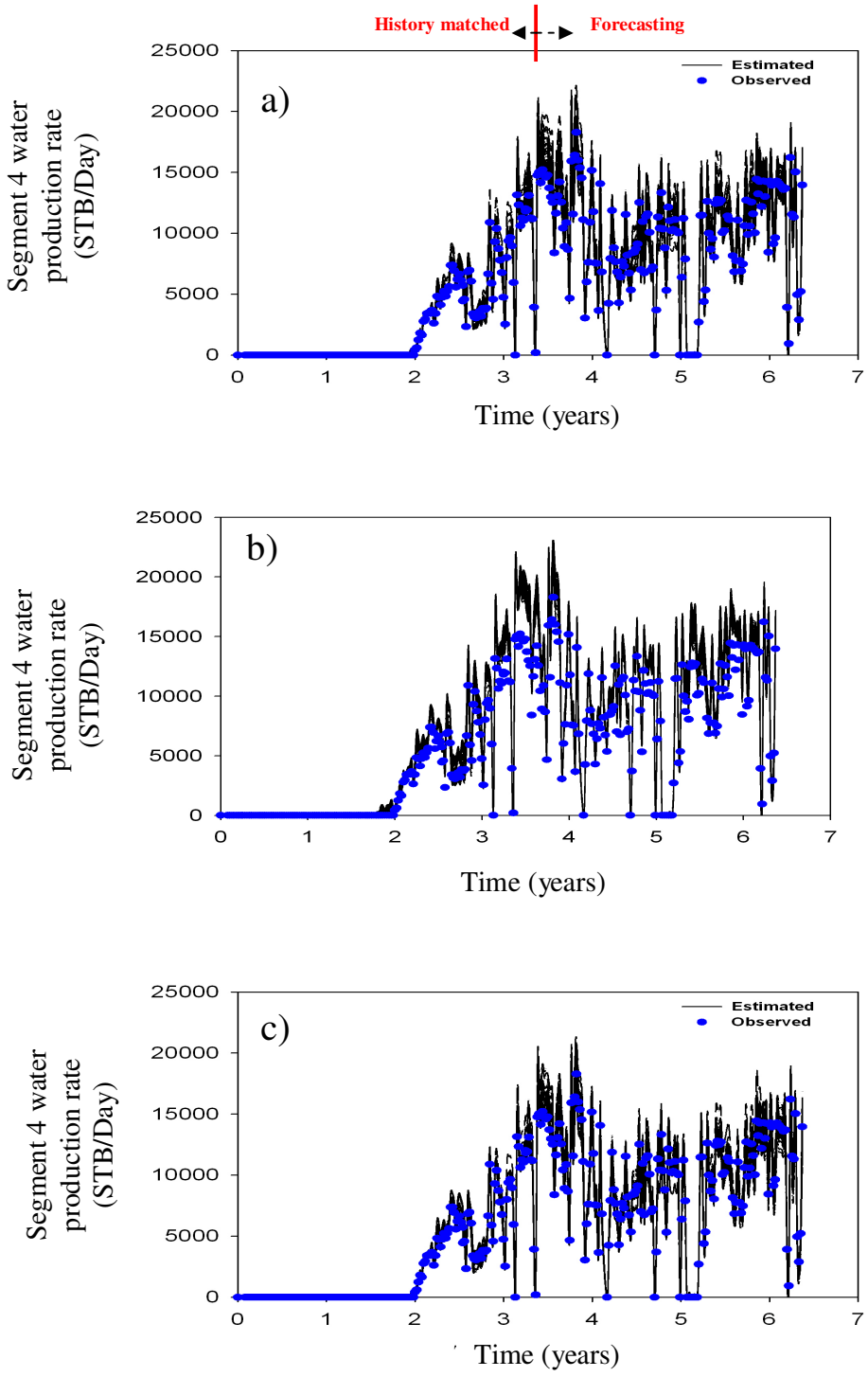

Figure 8.7: *The history and forecasts of water production data (blue line is the observed) for the whole of Segment 4 reservoir using the best 100 models from history matching, where the misfit included (a) seismic and production data, (b) production only and (c) seismic only.*

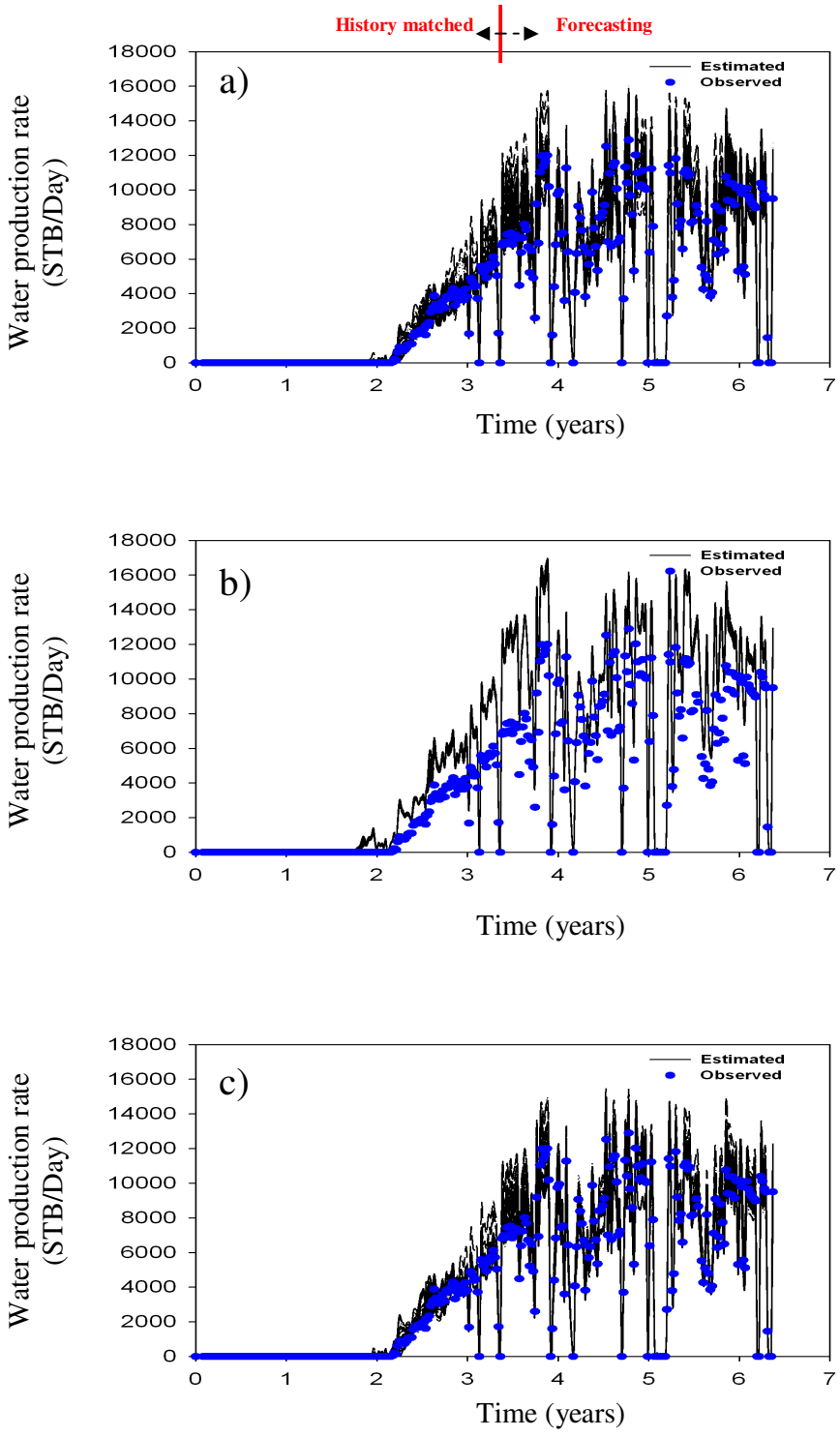

Figure 8.8: *The history and forecasts of water production rate (blue line is the observed) for well P2 using the best 100 models from history matching, where the misfit included (a) seismic and production data, (b) production only and (c) seismic only.*

We used Markov chain Monte Carlo methods to resample the PPD (Posterior Probability Density; Sambridge, 1999b) for each ensemble and obtained the probability distributions for each parameter. Distributions (Figure 8.9, m_1 and j) for the central fault nearest P2 were similar irrespective of whether seismic or production data were used in the misfit. In Figure 8.9, m_2 and m_3, show that the most likely value for the pilot point nearest the injector P3 is much larger if seismic data is used in the misfit, compared to using just production data from P2 and P3. We may have to alter the stress sensitivity function in this region, as found in Floricich *et al.* (2006). Figure 8.9, m_4, m_5 and m_6, suggest that the remaining pilot point did not affect the production, as the uncertainty of the multiplier was quite large. The pilot point lies in a separate fault-defined flow region where permeability affects only pressure, which is detected by seismic analysis. The remaining faults (g, b and a) lie far from well P2, and their multiplier distributions depend strongly on whether seismic or production data is used in the misfit.

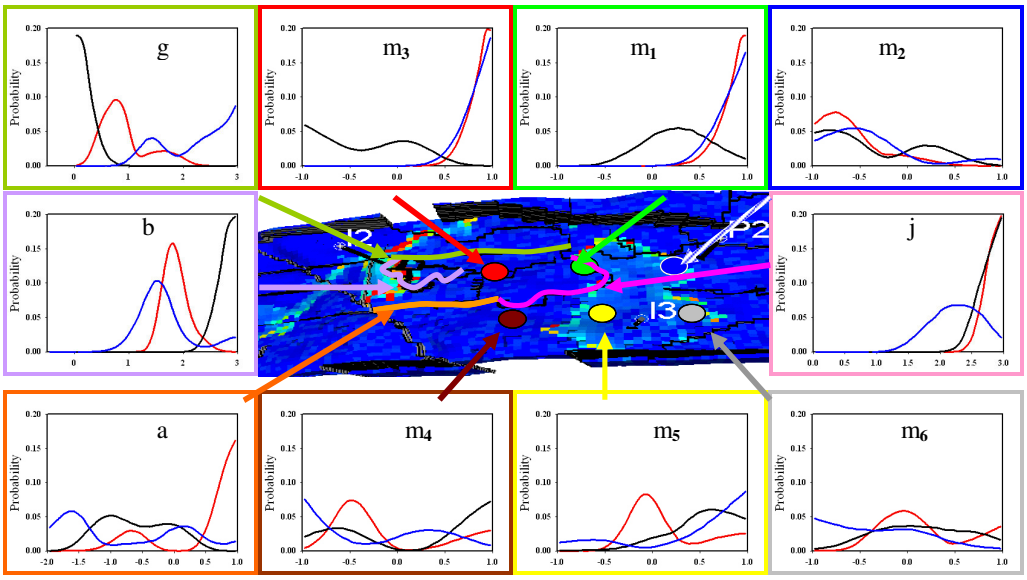

Figure 8.9: *Probability distributions (1D marginals) after resampling the PPD. Arrows point to the location of the pilot point or faults. The colours indicate the data used in the simulation. Seismic with production data are in red, seismic only in blue and production only in black.*

Figure 8.10 shows statistics (mean and standard deviation) for the inverted values; ten parameters were used in this case, with the uncertainty for each parameter represented in terms of stranded deviation.

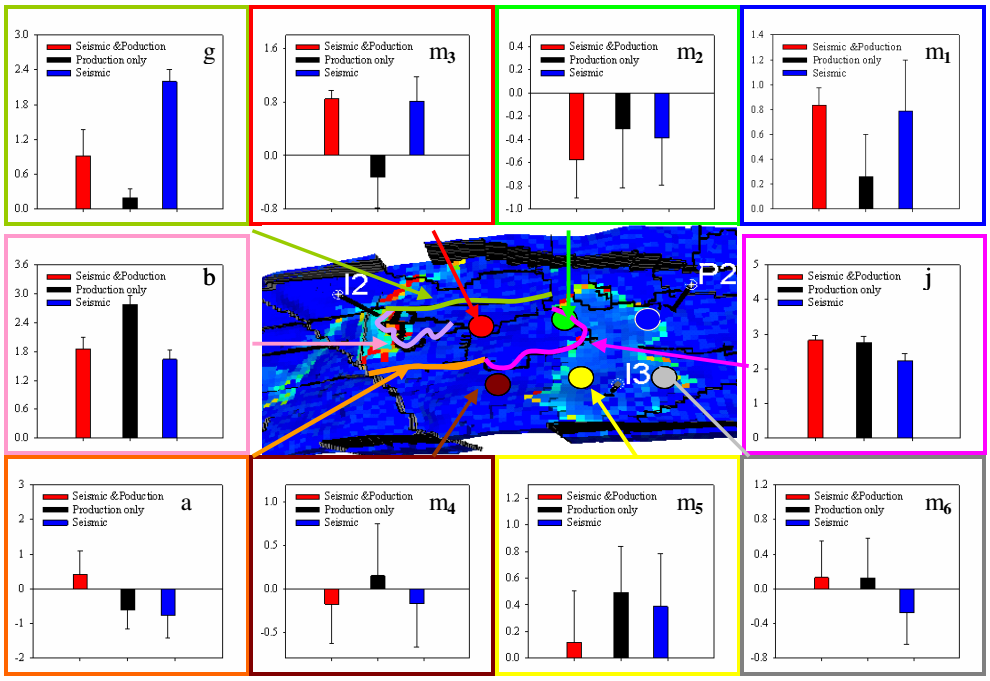

Figure 8.10: *Statistics (standard deviation and mean, calculated from Eqs 3.11 and 3.12 respectively) for ten parameters.*

To understand the uncertainty of the reservoir model, we can adopt a similar approach to analyse saturation, pressure, impedance and misfits by volume and maps. The PPD is then resampled a posteriori as part of the uncertainty analysis of modified parameters (Sambridge, 1999b). These probabilities can also be used to infer uncertainty in predictions (Stephen, 2006; see also Chapter 3).

The uncertainty of pressure and saturation distributions was also analysed. We presented a means of quantifying this information by using the model misfits to weight the average and standard deviations using equation 3.16. Both are invaluable for determining the location of fluid fronts, but also fluid pressures, mainly if gas evolution is expected. The evolution of saturation and pressure uncertainty can be used to determine the value of adding further models to the ensemble by predicting the point at which the uncertainty reaches zero (Stephen, 2006).

The pressure and saturation uncertainties change only around I2 and I3 (figures 8.11 and

8.12), with a pressure response at I2, but no saturation response; a significant reduction was obtained when seismic and production data were both included in the misfit. Saturation uncertainty is quite high here in all cases, however. The uncertainty of impedance (figures 8.13 and 8.14) shows a reduction when seismic and production data are combined.

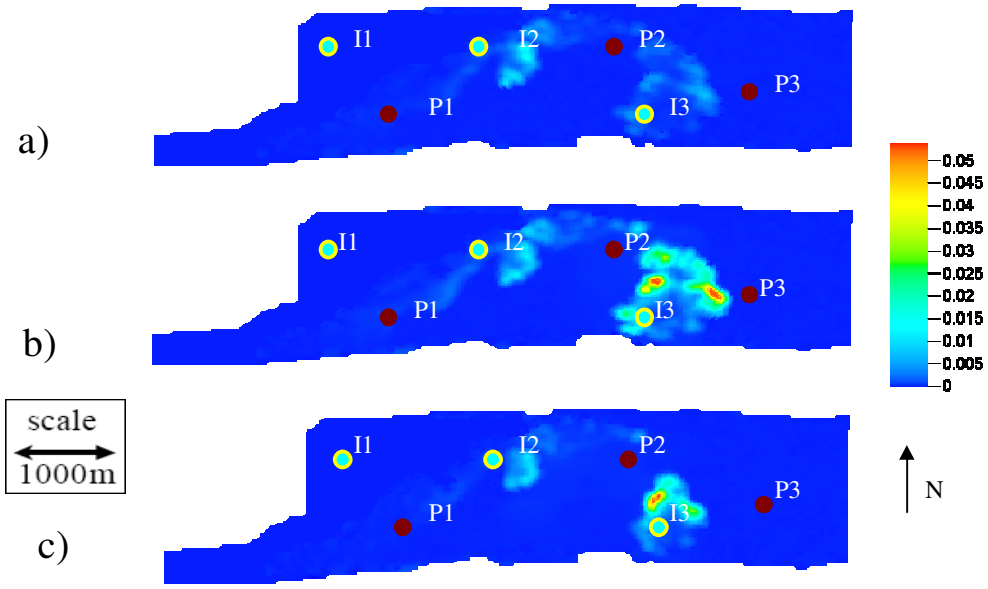

Figure 8.11: *Prediction uncertainty via the standard deviation of the water saturation when matching to a) seismic and production data, b) production only and c) seismic only.*

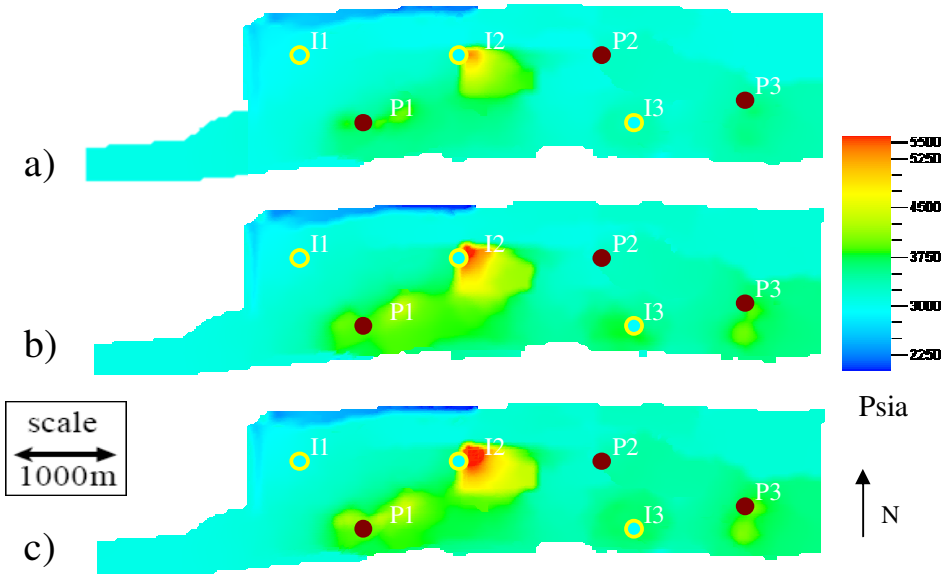

Figure 8.12: *Prediction uncertainty via the standard deviation of the pressure when matching to a) seismic and production data, b) production only and c) seismic only.*

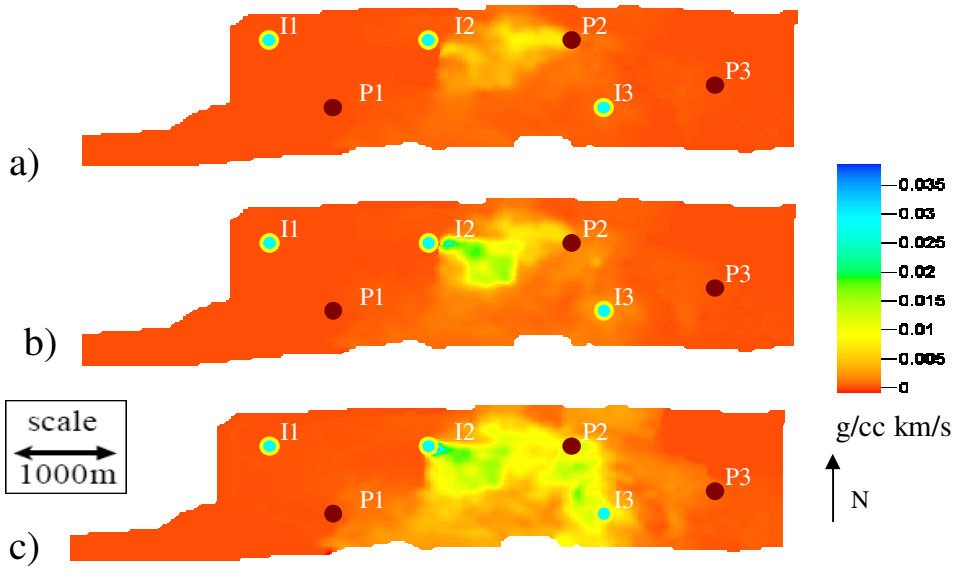

Figure 8.13: *Prediction uncertainty via the standard deviation of the impedance when matching to a) seismic and production data, b) production only and c) seismic only.*

8.3 Quantifying the accuracy of history-match predictions and the impact of time-lapse seismic data for an infill well

We investigated the impact of seismic data on subsequent predictions using the best 100 models from each of the three history-matched ensembles. Well P3 produced a significant amount of water after nearly four years, and infill well P4 was placed by BP between wells I2 and I3 (Figure 8.14) to drain the by-passed region and revive injector well I2.

Using seismic data in the misfit with production data clearly reduces uncertainty in the gas rate (Figure 8.15b), but not in the case of water rate (Figure 8.16), which is very sensitive. If production data alone is used in the history-matching process, water rates are generally significantly higher, and the uncertainty in the breakthrough time is doubled from four to six months compared to using seismic data alone. The high variation between models prediction and the observed data shown in Figure 8.16 a, b and c can be explained by Figure 8.17, where we can see that most parameters are sensitive to the combined case (seismic and production data), except m_1, m_3 and j. The changes in these parameters are sensitive to the three cases (matching to production, seismic and both). In the SHM cases of seismic and production data considered separately, there were fewer parameters controlling the change. Parameters g, m_1, m_3 and j have small effect, and all are quite far from well P4, but in the case of both types of data being used (seismic and production), which has less variation, all the parameters showed an effect, which led to a reduction in the uncertainty.

The best 100 history-matched models had a low saturation uncertainty, and we have shown that seismic data also reduces the pressure uncertainty using equation 3.16. This can be very useful for determining the location of fluid fronts, but also for that of fluid pressures, particularly if gas evolution is expected (Figure 8.18). This may be because seismic misfit and production misfit cancel each other, which may also explain the reduction in the uncertainty map in figures 8.18 and 8.19.

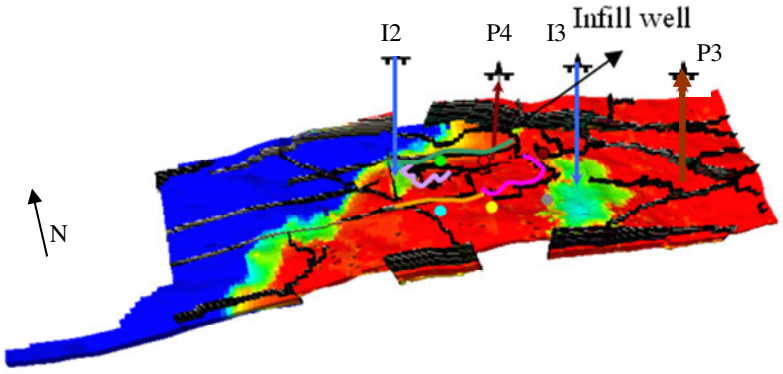

***Figure 8.14**: Average oil saturation over all models after five years of production.*

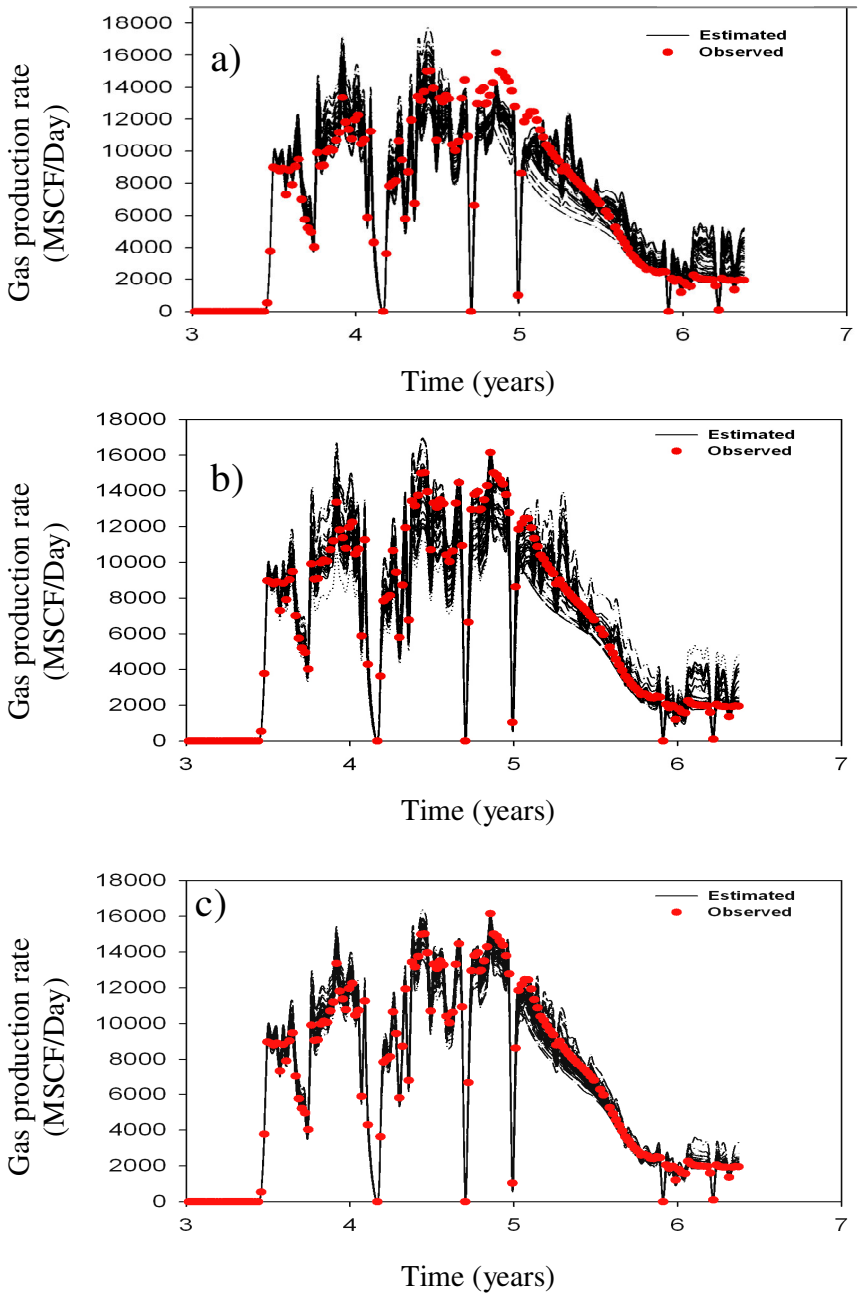

Figure 8.15: *Forecasted and observed (red points) gas production for the infill well P4, using the best 100 models from history matching, where the misfit included (a) seismic and production data, (b) seismic data only and (c) production data only.*

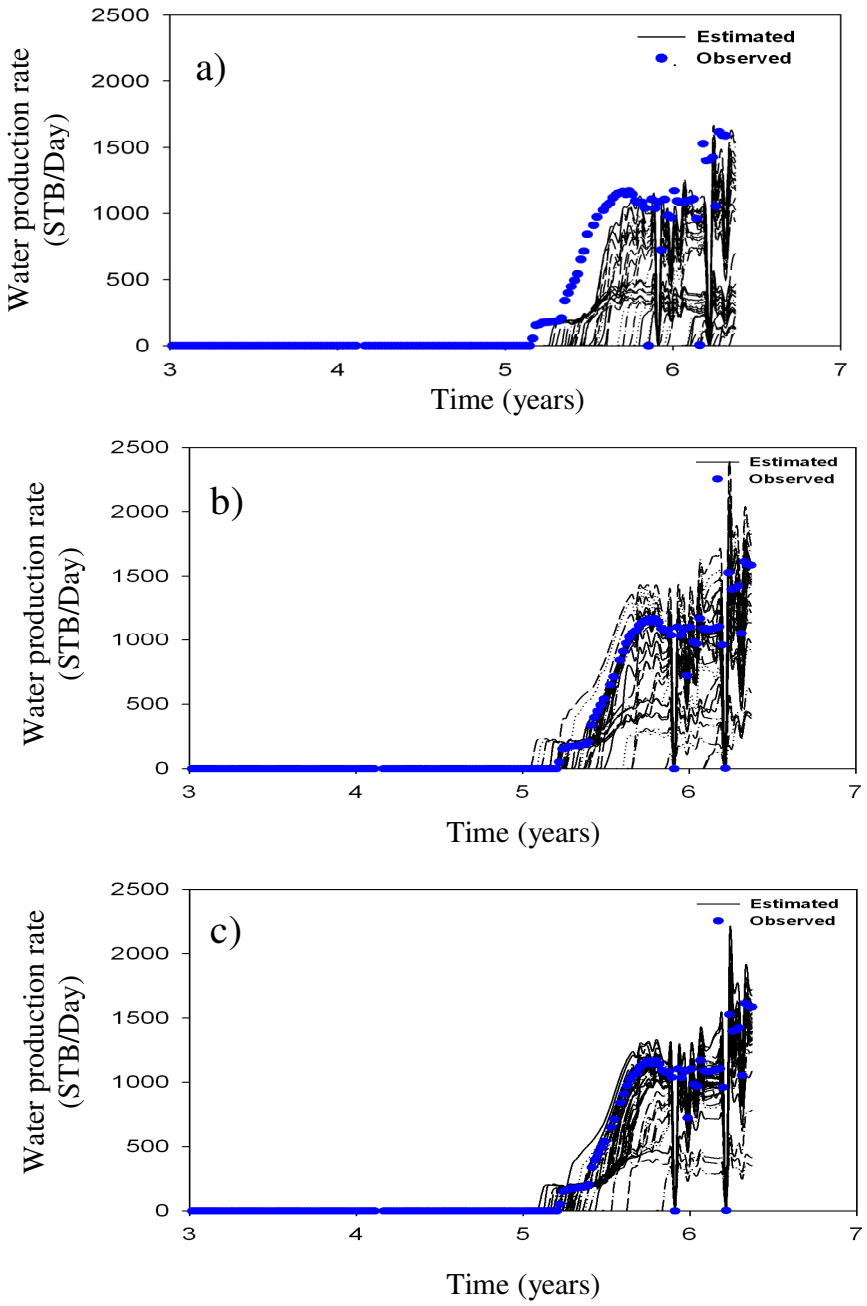

Figure 8.16: *Forecasted and observed (blue points) water production rate for the infill well P4, using the best 100 models from history matching, where the misfit included (a) seismic and production data, (b) production data only and (c) seismic data only.*

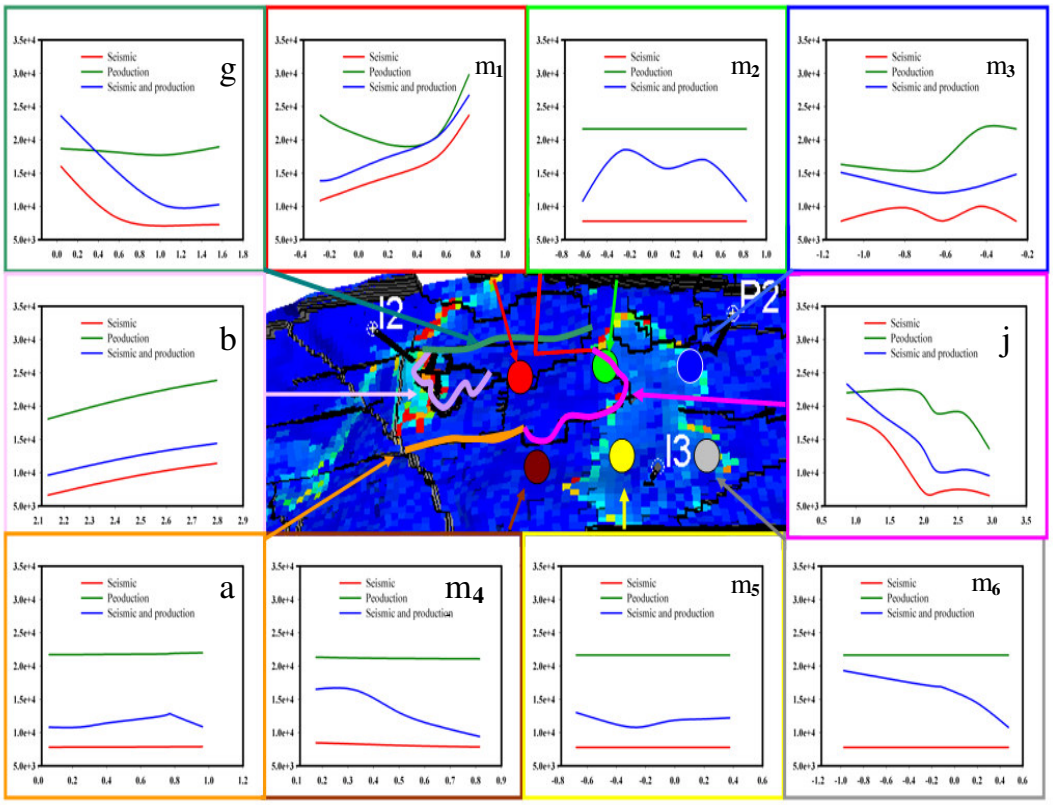

Figure 8.17: *Sensitivity analysis by changing one parameter over time. The x-axis is the parameter value, which is the log_{10} of the barrier multipliers, and the y-axis shows the prediction misfit.*

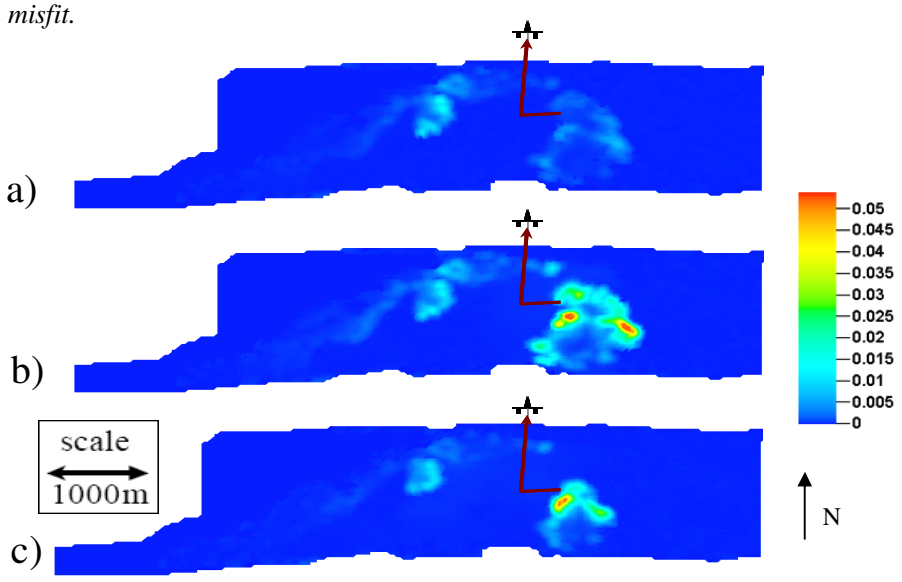

Figure 8.18: *Prediction uncertainty via the standard deviation of the water saturation when matching to a) seismic and production data, b) production only and c) seismic only, for the year 2000.*

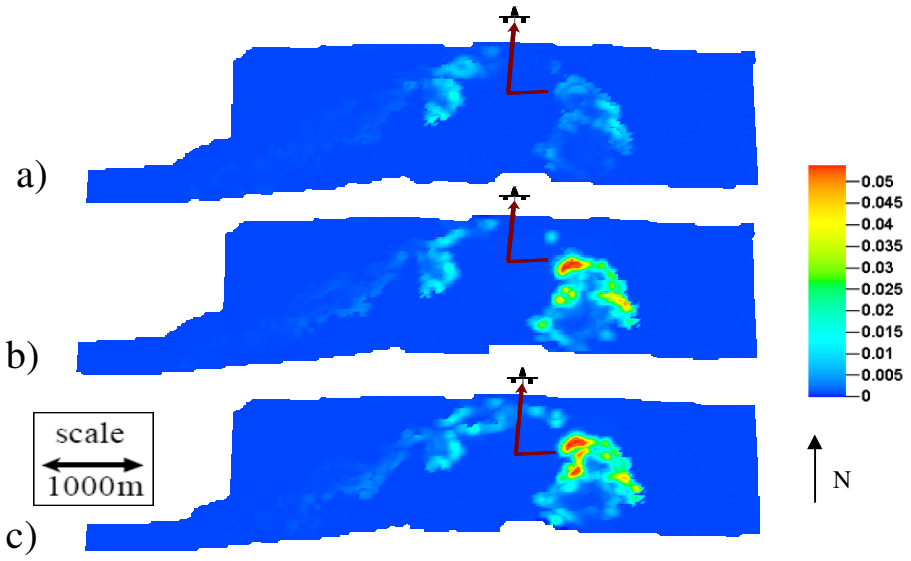

Figure 8.19: *Prediction uncertainty via the standard deviation of the water saturation when matching to a) seismic and production data, b) production only and c) seismic only, for the year 2005.*

It is much more challenging to find models that honour both types of observations simultaneously. This is shown schematically by the Venn diagram in Figure 8.20, where the region of intersection corresponds to only a small subset of the total reservoir uncertainty space.

The quality of the match to conventional well data at the time of the 4D survey for Phase I seismic data (93 as baseline, 99 and 00) is largely controlled by the misfit between observed and simulated parameters for our case. We use the gas production rate and water cut to predict the behaviour of well P4. Figure 8.21 shows the prediction match quality based on history period misfit and prediction period misfit, where well P4 is included (gas production rate and water cut for the infill well up to 2005). A good history match and forecast quality will plot toward the bottom left of the figures, and is a known value for the asset team in choosing reservoir models for further study.

Figure 8.21c shows the impact of including 4D seismic data: it reduces the variance between the predicted misfit and the history misfit. When 4D seismic data is included in a history match, there is a significant and positive impact on the predicted outcomes relative to the conventional case where forecasts are based on history matches to well

data only.

Walker *et al.* (2007) discussed the quality of the match to conventional well data. The quality of the match is largely controlled by the misfit between observed and simulated data.

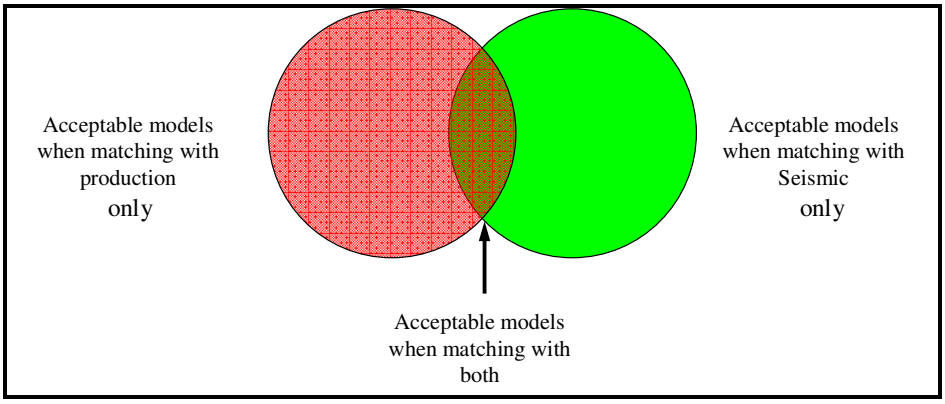

***Figure 8.20**: Diagram illustrating a small subset of models honouring both well data and time-lapse data as the intersection of two constraints (adopted from Walker et al., 2006).*

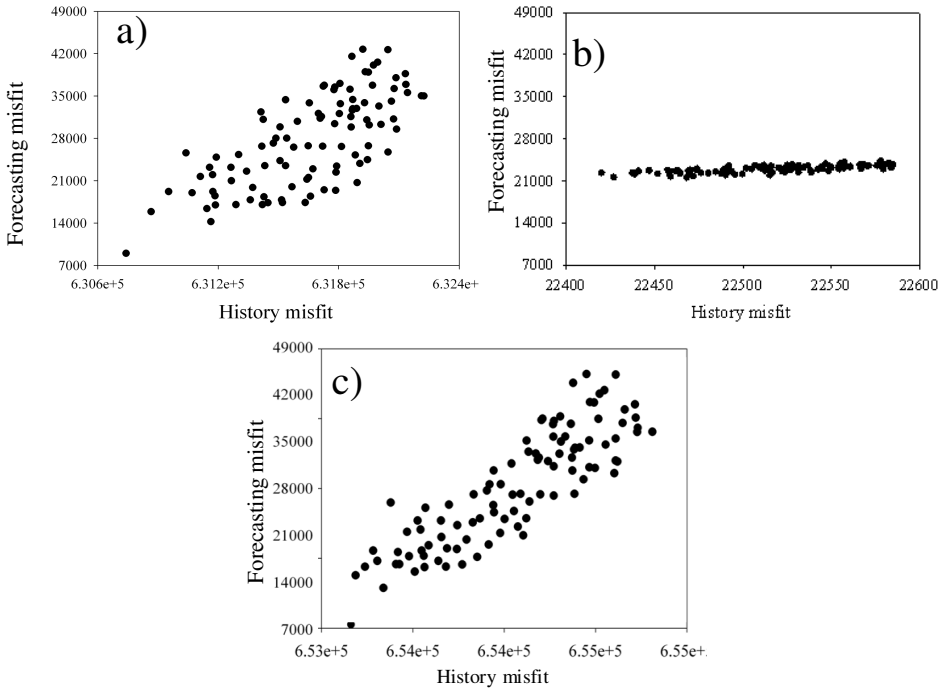

***Figure 8.21:** Comparison of forecasting and history-matching misfits for well P4, where the misfit data is from a) seismic data only, b) production and c) seismic and production.*

A similar study (Stephen *et al.*, 2006b) shows that increasing the density of pilot points between I3 and P2 and ignoring faults resulted in improved GOR when matching to production data only. Table 8.1 compares Stephen's (2006) study with the present study. It was reported that the use of seismic data significantly reduced the uncertainty. We have in our possession the production data for the well, with which to test our forecast. The model in the present study requires a different set of parameters, but fault/barrier transmissibilities and reservoir permeability data were modified as before. We show that the use of 4D seismic in the misfit reduces the prediction uncertainty in this model, as it performed better than previously. Seismic and production data are best used together because each parameter controls the seismic and production misfits to different degrees. The uncertainty of the forecasted well is reduced by using seismic data, and we find that better matched models are better predictors. The degree of uncertainty is increased compared to the previous study, but in the present study, we modified parameters in the area around the infill well. Parameters were modified close to the production well or the area dominated by seismic data.

	Stephen, 2006	***Present work***
****Model***	Phase I model	Phase II model
Seismic data	93,99,00	93,99,00
Production data	3 years	5 years
No. of parameters	8 4 Faults + 4 pilot points to change permeability locally	10 4 Faults + 6 pilot points to change permeability locally
No. of best models	128	100
Achievements	• Seismic data provides information about areas not yet affected by production. • Less forecast uncertainty. • Reasonable forecasts. • The quality of prediction not tested.	• Seismic data continues with the same information. • Forecast uncertainty is greater. • Better forecasts. • Tested.

**Different fault network*

Table 8.1: *Comparison between Stephen's (2006) study and the present case study.*

8.4 Discussion

History matching is required when we are unsure of model parameters that are often spatial in nature. The data we use to constrain our match is also spatially variable. Production and injection data is most sensitive to flow properties in the vicinity of active wells. Flow properties in the inter-well region also have an impact, although non-uniqueness means that there are many more ways of assigning these to obtain the same behaviour.

Time-lapse seismic analysis measures some combination of saturation and pressure change in the reservoir and reduces the non-uniqueness. In a reservoir where time-lapse data is saturation-dominated, the influx of water can be detected, thereby improving characterisation at the water front. With pressure-dominated time-lapse, pressure build-up and, to a lesser extent, draw-down, can be determined, enabling the identification of flow barriers and pathways.

In the sector of the Schiehallion field studied here, the time-lapse signature is pressure-dominated and helps to quantify a number of parameters some distance from the producing wells, including the transmissibilities of faults near one of the injectors. These faults have a negligible impact on the producer wells operating early in the field lifetime.

The evolution of saturation uncertainty can be used to determine the value of adding further models to the ensemble by predicting the point at which the uncertainty reaches zero (Stephen, 2006). The saturation uncertainty maps were very similar for the separate use of production and seismic data in history matching. When seismic and production are combined, the result is much lower. The level of uncertainty (i.e. the data error) will affect these. The uncertainty, as shown above, measures the degree of similarity of the best models rather than the quality of their match. This may mean that there are a small number of models that satisfies both seismic and production data, but it is possible that the uncertainty is not reduced.

We see a better agreement between seismic and production data in Schiehallion; even though the seismic signal is quite weak around the producer, the data are

complementary. The field differences may be related to the fact that we have pressure- rather than saturation-dominated signals.

Most changes are pressure- rather than saturation-related owing to the low spatial frequency of changes to the flow parameters. The weighting applied during the averaging process is important because it allows us to assess properly the impact of a range of models by down-weighting highly unlikely models. Understanding the posterior parameter distribution curves is a challenge when the match to seismic data completely alters the production match. The seismic data provides us with additional information, so we should consider that something is wrong with the model even if the production match is good. It is advisable to take the models that match the production data and look at how each of these also matches to seismic data: do they lie in the envelope of the seismic uncertainty? Seismic data is more likely to be controlled by global parameters such as, fault transmissibility whereas production is based on local parameters for example, permeability, porosity and NTG. If we start with production and then move onto seismic matching, we may lose the production match. If we start globally, we may obtain a better match, then we can update locally for production data.

The best reservoir simulation models are those that predict reservoir performance accurately, which minimises the uncertainty associated with the history match predictions. On the basis of new surveillance information, some of the history-matched models will likely be rejected, while others can be retained, allowing for more rapid integration of the surveillance data. Time-lapse seismic surveys have the potential to identify changes between wells and provide advance warning of events such as water breakthrough before a production signature is observed at a well. There is also an expectation that time-lapse seismic analysis will improve the predictive capability of our reservoir models (Stephen *et al.*, 2005). However, a major difficulty is the time required to integrate the spatial information from a 4D seismic survey with the reservoir model. If the integration process takes too long, then value would be lost if a predictable event actually occurs before the 4D interpretation is complete. One efficient way of predicting future reservoir performance and evaluating prediction uncertainty is to have a portfolio of potential modelled outcomes which provides reasonably accurate forecasts for the reservoir.

In general, there are multiple reservoir descriptions that might satisfy available observation constraints. One of the largest uncertainties is the shape of the flow paths between wells. While well-based observation (pressures, rates) do not often provide us with much insight here, seismic observation has the potential to supply this spatial information.

An infill well, drilled later, is affected, however, and time-lapse seismic analysis has been shown to reduce uncertainties in predicted liquid rates. Seismic analysis has also reduced the water breakthrough uncertainty in post-breakthrough production rates by a similar degree. We wanted to show that seismic analysis provides us with something, but in fact it often reduces the match quality. We can, however, change the model locally to fix the seismic match, as seen in Schiehallion. Looking at the parameter distributions, there is quite a difference.

8.5 Observation and summary

In this chapter, we have enhanced the reservoir description of the Schiehallion UKCS field by improving the match to seismic data. Much of the improvement is found close to the injectors, while around the producers, the use of 4D seismic in the misfit has been shown to reduce the prediction uncertainty in this model as it did previously. Seismic and production data are best used together because each parameter controls the seismic and production misfits to differing degrees. The uncertainty of the forecasted well is reduced by using seismic data, and we find that better matched models are better predictors, which can lead to good management decisions, for example regarding replacing an infill well that must be located away from the high-uncertainty area. The degree of uncertainty is increased compared to the previous study, but in the present study, we modified parameters in the area around the infill well. Previously, parameters were modified close to the production well or the area dominated by seismic data. Additionally, we found that the combination of different parameters has a significant impact on the misfit and model quality. We can improve our estimates of prediction uncertainty by identifying the parameters that are relatively unimportant. Saturations and pressures are predicted with low uncertainty for the parameters varied here, offering confidence to future reservoir management, including the identification of unswept regions.

CHAPTER NINE

Seismic History Matching in the Schiehallion Field: NTG calibration

The model provided by the operator is adopted for modifications and possible improvements. At the first stage of the analysis, the objective function of the base seismic survey was larger than the objective function for the two monitor surveys, and therefore the misfit was always biased and the optimum state could not be reached. One of the main causes of this discrepancy is the NTG (Net:Gross) characterisation of the static reservoir model used for simulation, since there is no evident large variation in porosity.

9.1 Introduction

The input data for the model, such as NTG, should be consistent with the seismic data – otherwise the objective function for the baseline seismic will be larger than the monitor's seismic data. The main factor for this difference is the NTG characterisation of the static reservoir model used as input data for simulation.

The integration of the geological outcrop templates, seismic cross-section diagrams and non-quantitative propagation driven by seismic amplitude attribute maps were used to build the original NTG distribution. Figure 9.1 demonstrates the robustness of the method used. The final product of the calibration is a link between the seismic attribute and the hydrocarbon pore thickness in the entire reservoir (Leach *et al.*, 1999), leading to an important reduction in the uncertainty usually related to any development strategy after the exploration and appraisal stages. The NTG map is

obtained from the RMS attribute map by assuming a linear correlation between the attribute map and NTG (Stephen *et al.*, 2006), given by:

$$\overline{NTG(x,y)} = NTG_{\min} + \frac{RMS(x,y) - RMS_{\min}}{RMS_{\max} - RMS_{\min}} \left(NTG_{\max} - NTG_{\min} \right) \qquad (9.1)$$

where $NTG(x, y)$ is the vertical averaged NTG, and $RMS(x, y)$ is the seismic attribute map. NTG_{max} and NTG_{min} are obtained from the operator's reservoir model, while the values of the seismic attribute, RMS_{max} and RMS_{min}, are selected in order to ensure the same NTG range of values as in the original operator's model.

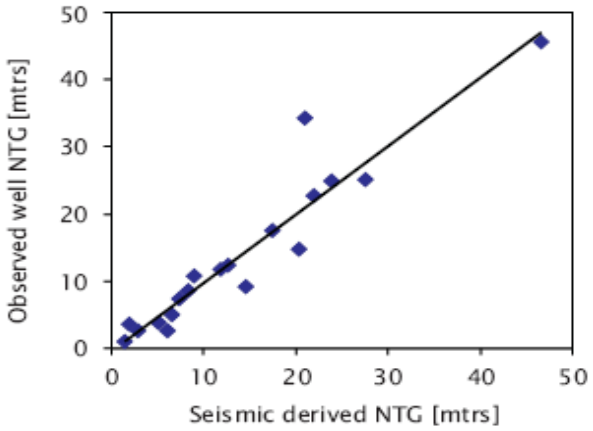

Figure 9.1: *The calibration of NTG-to-seismic attribute for the original reservoir static model. This calibration is performed for the first set of exploration and appraisal wells (after Leach et al., 1999).*

In this study, we predict the NTG using two different baselines, seismic 1993 and 1996 seismic, using Eq. 9.1. Before history-matching to dynamic data, we first modify our model to match the observed baseline RMS amplitudes of the migrated stack quantitatively. Leach *et al.* (1999) showed that RMS amplitudes are a good indicator of NTG, so we began by modifying this parameter first, and eventually obtained a new three-dimensional model of NTG with predicted impedance (Figure 9.2a) that agreed much more closely with the baseline RMS amplitudes for seismic baselines 1993 and 1996 (Figure 9.2 b and c). The importance of this step is to determine the correct location for the pilot point when we use NTG as parameter space.

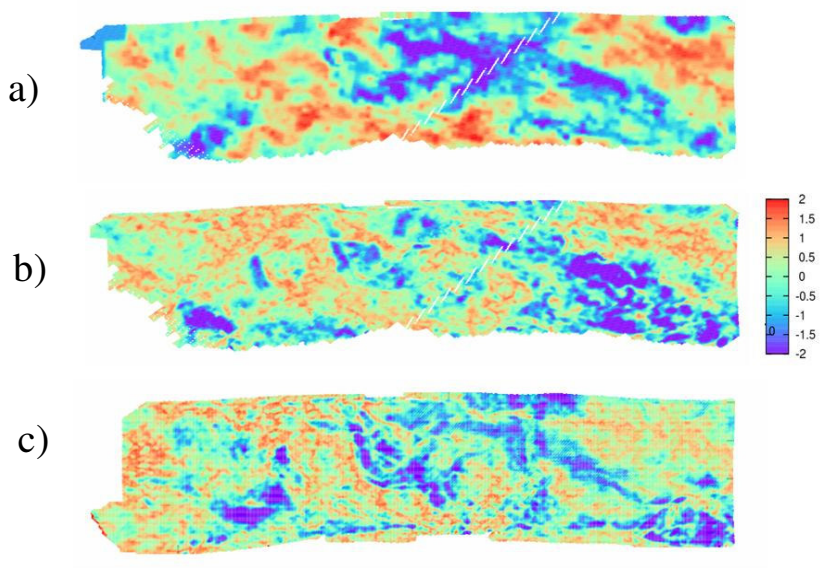

***Figure 9.2**: Predicted baseline impedance for (a) the base-case model, (b) observed RMS amplitudes of the migrated stack for the baseline of 93 and (c) observed RMS amplitudes of the migrated stack for the baseline of 96.*

9.2 Permeability and NTG combination as parameter space

There is a mismatch in some regions between the predicted NTG from seismic data and the NTG from our model. This information is used to place several master pilot points to obtain an improvement in NTG.

The master pilot point is used as a parameterisation tool in this case, which can control a group of individual pilot points to the changes regarding the permeability locally between the injectors and the producers. We group them as master pilot points to change the NTG in the area of mismatch, as illustrated in Figure 9.2. The location of the pilot points is identified based on the pre-production data, as shown in Figure 9.3. The multipliers are interpolated using Kriging with a variogram of 150 m as the separation of the pilot points to avoid any interference between the pilot points.

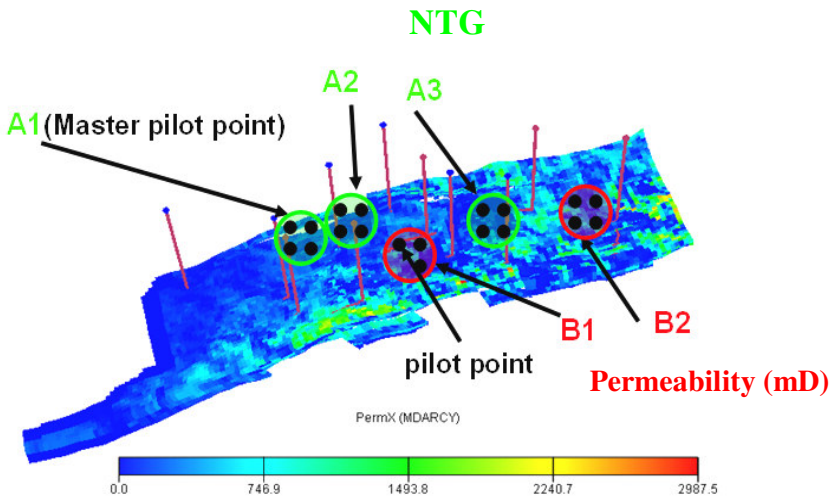

Figure 9.3: *Location of A1, A1 and A3 pilot point groups used to vary the NTG. B1 and B2 are used to vary permeability. Arrows point to the location of the master pilot point.*

Nineteen pilot points were used in total and distributed as shown in Table 9.1. We assigned three master pilot points, each of which has four pilot points to control changes to the NTG, and two master points to modify permeability (the first has three individual pilot points, and the second has four individual pilots, as outlined in Table 8.2), located between the injector wells I3 and I6 and the producers P2 and P3.

Master pilot point	***No. of individual pilot points***	***Parameter to change***
A1	4	NTG
A2	4	NTG
A3	4	NTG
B1	3	Permeability
B2	4	Permeability

Table 9.1: *Pilot point distributions for each master pilot point.*

We sampled parameters evenly over a $\log_{10}$ scale, and each parameter was allowed to decrease by an order of magnitude and increase by the same range relative to the original value. The maximum physical limit of NTG was considered. Seismic history matching was then carried out using Phase I seismic data (93 as baseline, 99 and 00)

and production data (from wells P2 and P3, given the location of the parameters), both separately and together in the misfit. In the three cases, 1500 models were generated. An initial ensemble of 500 (n_i) models was chosen to properly sample the parameter space, so that Voronoi cells were not connected throughout the five-dimensional parameter space. The same initial sample was used for each combination of history data. Resampling took place at 80 (n_s) models per cycle located around the best 40 (n_r). We identified the best model from each ensemble and compared predicted to observed 4D seismic data, as shown in Figure 9.4. When we included just production data in the misfit, the predicted seismic was good compared to the observed data (Figure 6.14a) because the parameters that were varied change the behaviour of the model geographically.

When seismic data is used in the misfit, predictions are much improved, although without matching there is some noise in the data. Production data is matched equally well (or badly in the case of GOR) regardless of which history data is used in the misfit.

The best models are used to predict the behaviour of the model for the next 3.5 years. We find a good match in the case of the gas production, but in the prediction it was not good enough, because we excluded the parameters that could affect the flow strongly. For the case of Segment 4 GOR (Figure 9.5) and water production rate (Figure 9.6), a good prediction is determined when the seismic and production data are combined, while the opposite is the case for the individual well P2 (Figure 9.7 and Figure 9.8 respectively).

We used Markov chain Monte Carlo methods to resample the PPD (Sambridge, 1999b) for each ensemble and obtain the probability distributions for each parameter (Figure 9.9). In Figure 9.9, A1 shows that decreases in the NTG are required, but the remaining master pilot points which control changes in NTG (A2 and A3) suggest an increse in the NTG. The master pilot points which change the permeability (B1, B2) affect only pressure and are detected by seismic data, both suggesting that the increase in the permeability as well as that in the original permeability is quite low.

The statistical variables, mean and standard deviation of the inverted values, are also shown. Figure 9.10 shows the degree of uncertainty for each parameter, represented by the standard deviation bar; for the selected parameters, the degree of uncertainty is low. Figure 9.11 illustrates the final NTG distribution for the best model, showing that it is improved compared to the observed RMS amplitudes of the migrated stack minimum (Figure 9.2).

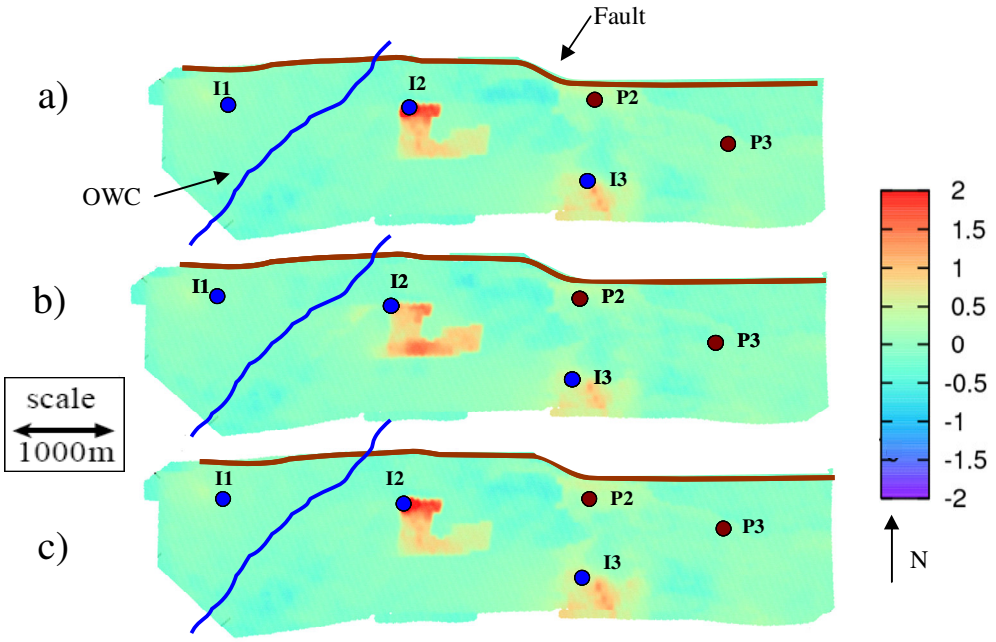

Figure 9.4: *Impedance changes for 1993–1999 for the best modelling case of (a) seismic data only, (b) production only and (c) seismic and production. Compare with Figure 6.14a.*

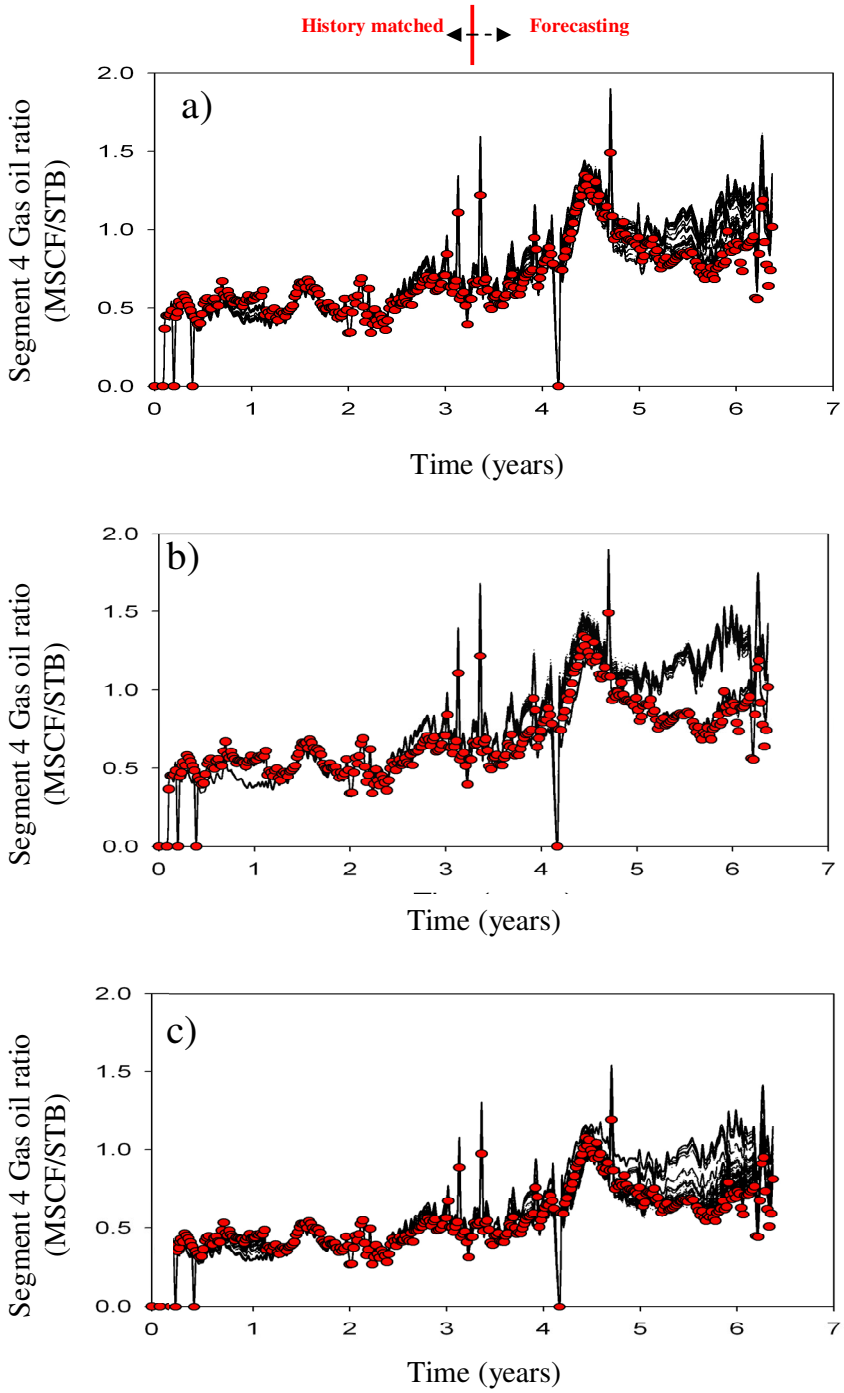

Figure 9.5: *History and predictions of GOR for the entire Segment 4 reservoir, using the best 100 models (history matching for 3.5 years and prediction for 3.5 years) from history matching using (a) seismic and production data, (b) production only and (c) seismic only.*

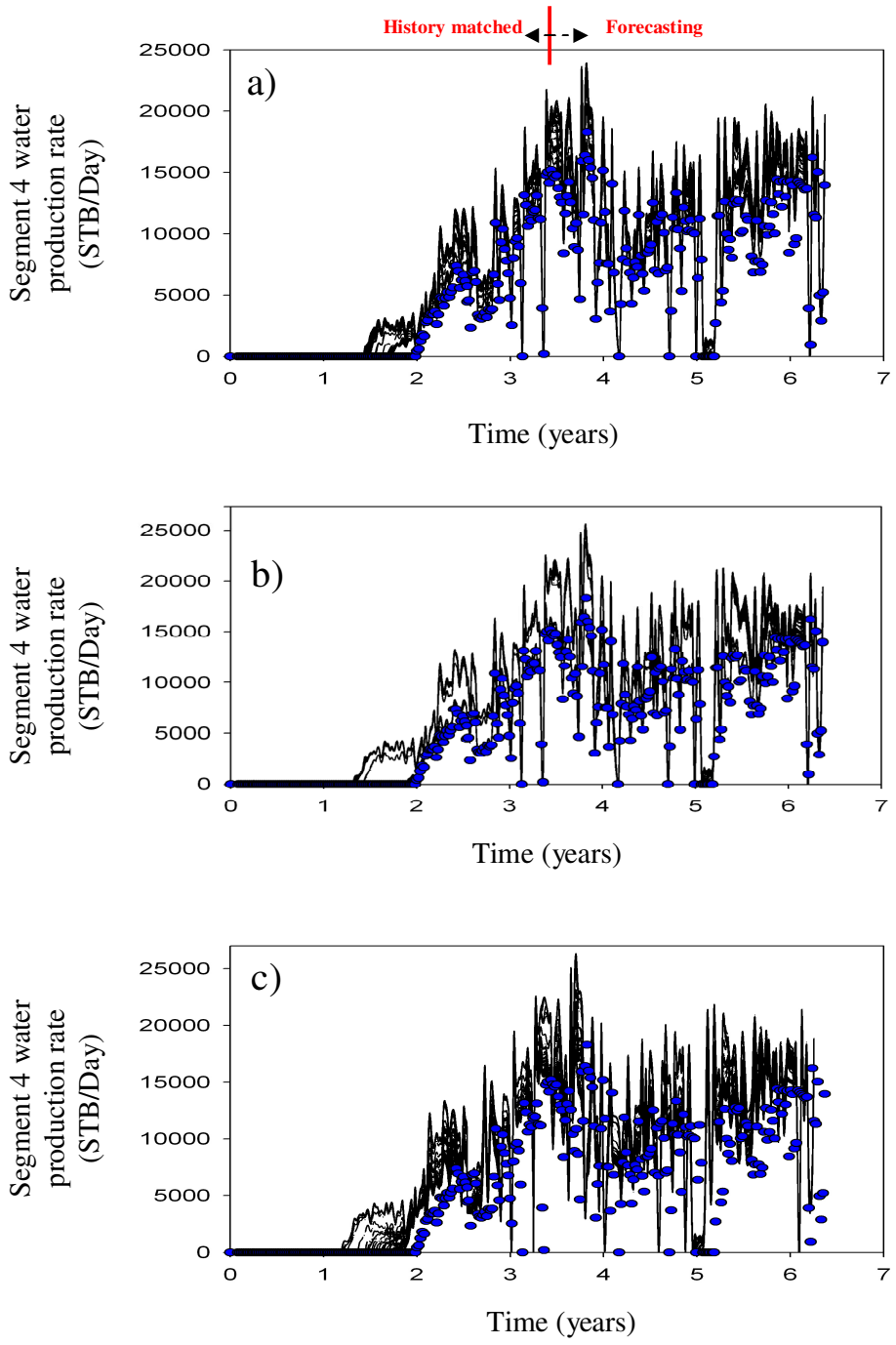

Figure 9.6: *History and predictions of water production rate for the entire Segment 4 reservoir, using the best 100 models (history matching for 3.5 years and prediction for 3.5 years; blue points are the observed water production rate) from history matching using (a) seismic and production data, (b) production only and (c) seismic only.*

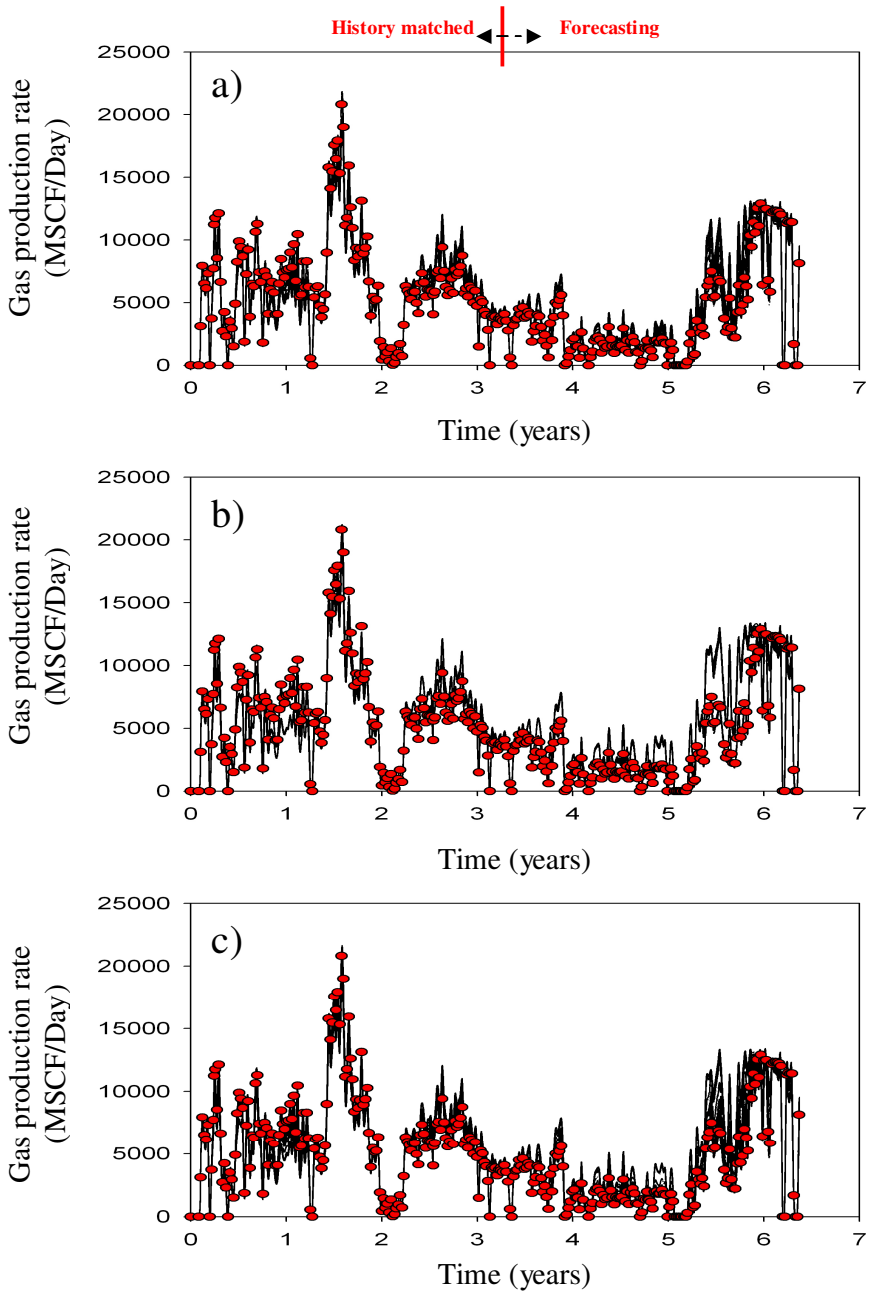

Figure 9.7: *History and predictions of gas production rate for well P2, using the best 100 models (history matching for 3.5 years and prediction for 3.5 years; red points are the observed data) from history matching using (a) seismic and production data, (b) production data only and (c) seismic data only.*

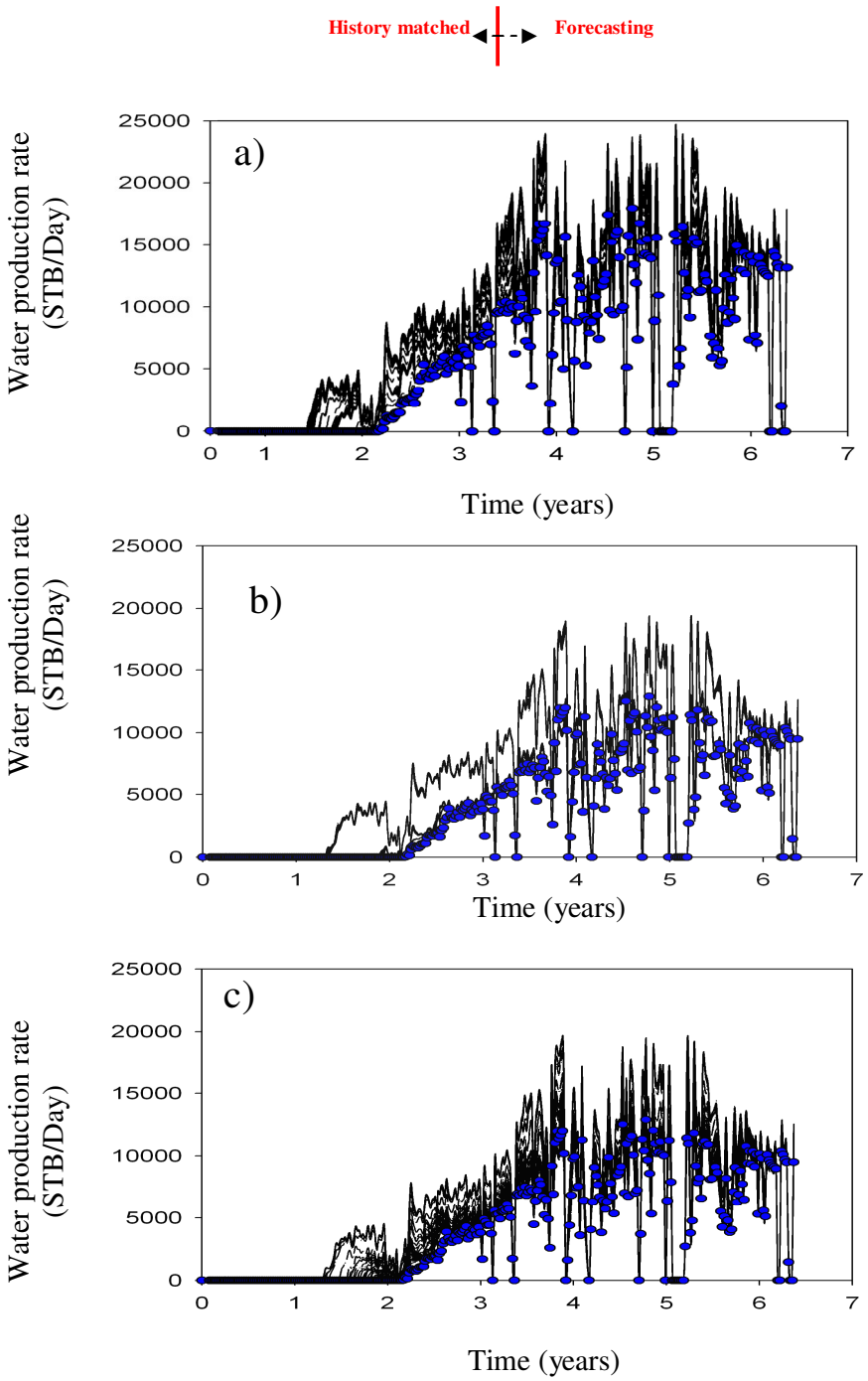

Figure 9.8: *History and predictions of water production rate for well P2, using the best 100 models (history matching for 3.25 years and prediction for 3.25 years; blue points are the observed water production rate) from history matching using (a) seismic and production data, (b) production data only and (c) seismic data only.*

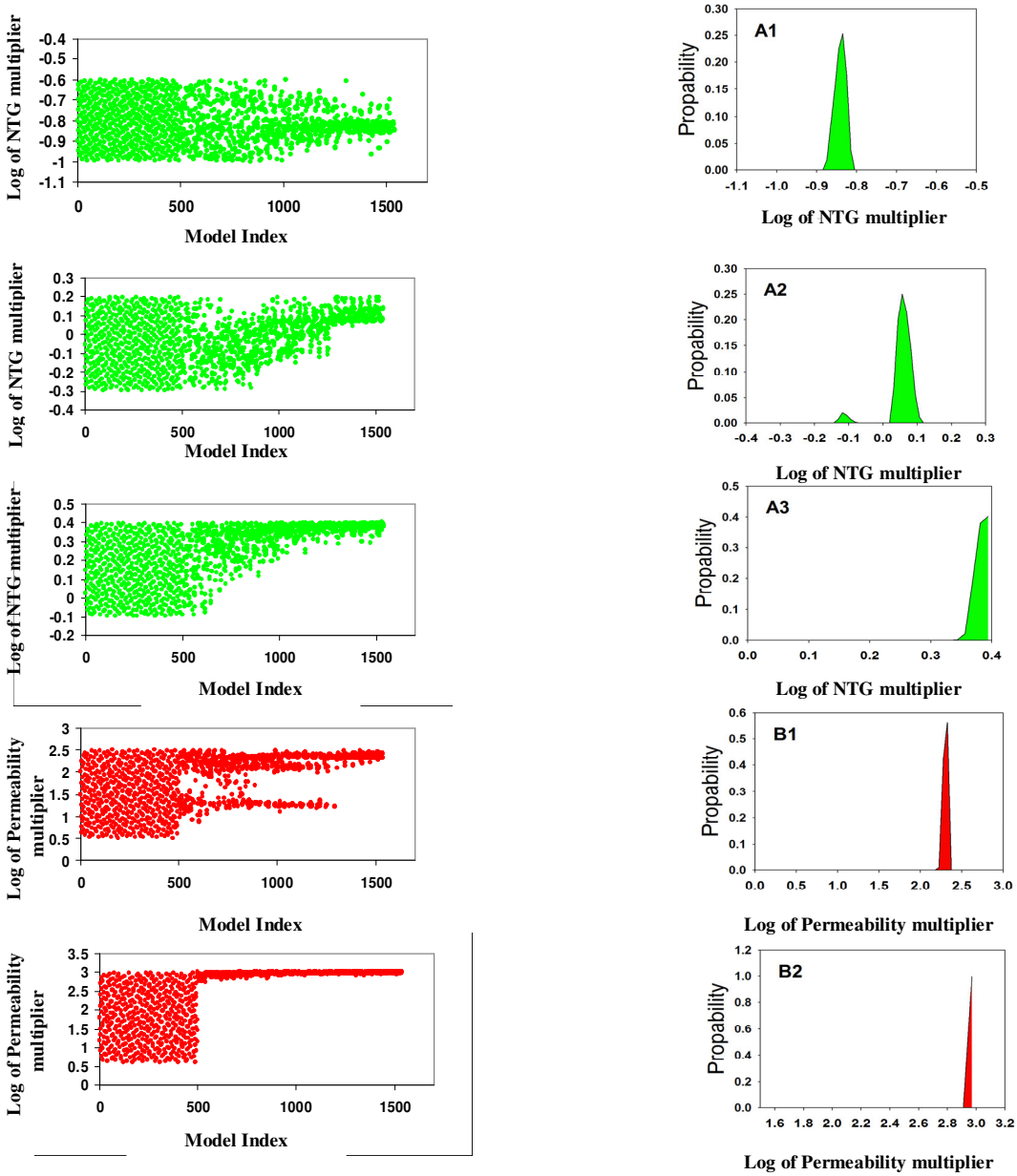

Figure 9.9: *Parameter evolution and probability distributions (1D marginal) after resampling the PPD.*

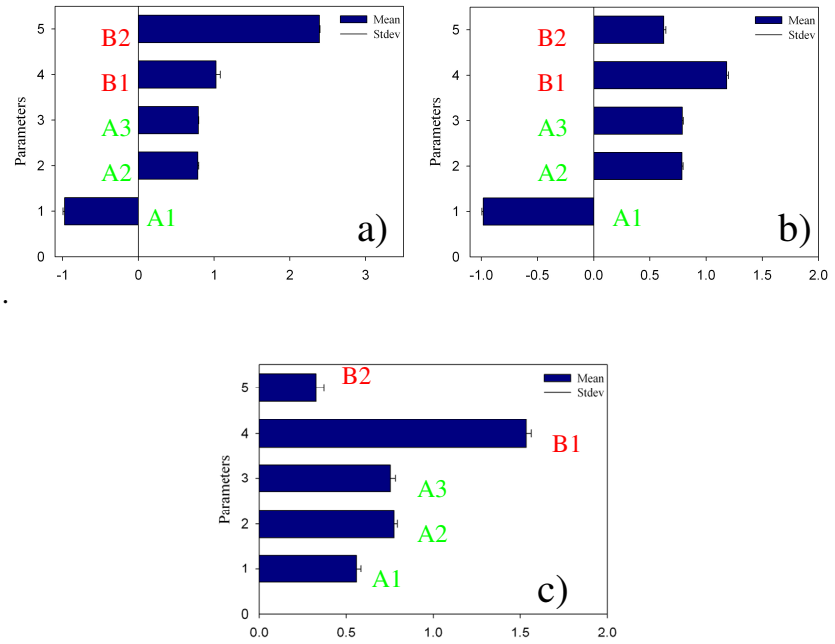

Figure 9.10: *Statistics, mean and standard deviation, for the inverted values of five parameters when matching to a) seismic data only, b) production and seismic and c) production data only.*

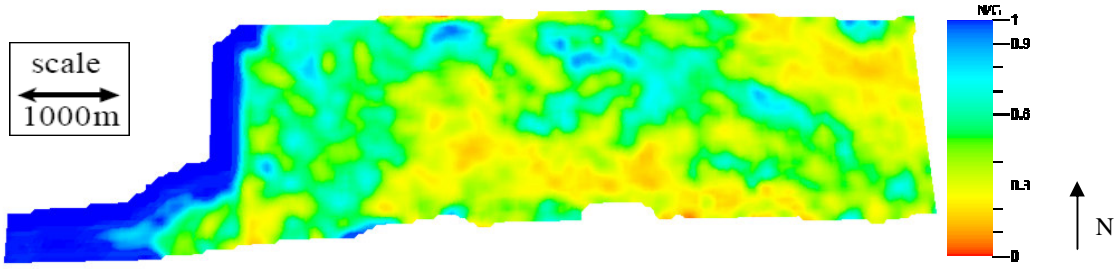

Figure 9.11: *Final NTG map after history matching with one pilot point.*

We calculate standard deviations for the water saturation to quantify variable uncertainty, using equation 3.16. We find that, over the whole ensemble, the uncertainty does not depend on the choice of history data. When we select the best 100 models, however, we find that saturation uncertainties (figures 9.12 and 9.13) were significantly reduced when seismic and production data were both included in the misfit. The uncertainty, as shown above, measures the degree of similarity of the best models rather

than the quality of their match. Saturation uncertainty is low here in all cases, however. We find that the uncertainty decreases for both variables when seismic data is included in the misfit, but that it reaches a minimum when production data alone is used. We then investigated the impact of seismic data on subsequent predictions using the best 100 models from each of the three history-matched ensembles.

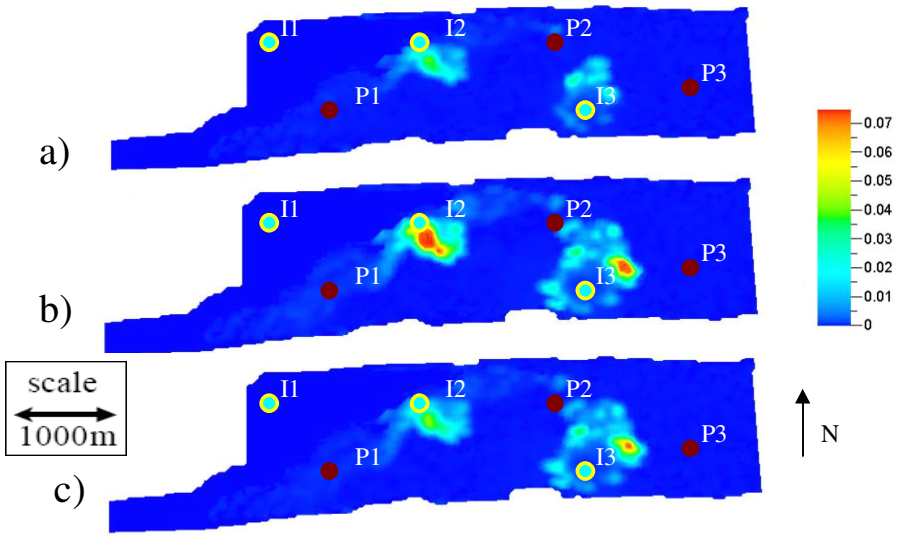

Figure 9.12: *Prediction uncertainty of water saturation when matching (standard deviation) when matching (a) seismic and production data, (b) production data only and (c) seismic data only.*

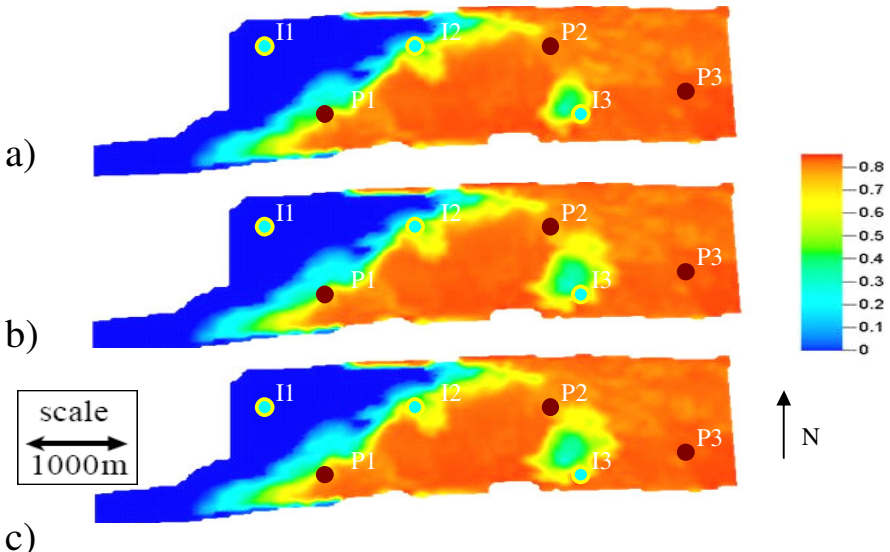

Figure 9.13*: Prediction uncertainty of water saturation when matching (mean) to (a) seismic and production data, (b) production data only and (c) seismic data only.*

9.3 Discussion

We observed RMS amplitudes over each simulator grid cell and normalised the data to obtain an estimated NTG map assuming a linear relationship (the same as found when predicting impedance). The RMS amplitudes were slightly truncated to give a NTG distribution that respected the average and spread more precisely (Stephen *et al.*, 2005). We chose to vary the model Net:Gross (NTG) as the model porosity was specified for the sand and was approximately uniform, although some depth dependence was clear, along with the permeability in some selected areas, with low permeability values between the wells. The master pilot points approach was tested, which allowed more control if Kriging conditions such as the Kriging range and spacing between the points were well defined.

9.4 Summary

In this chapter, a first approach to seismic history matching in a selected sector for Segment 4, Schiehallion field has been presented, and the need to change the reservoir NTG static model based on the integration of seismic attributes using geostatistics has also been addressed. This approach led to a large improvement in terms of base seismic misfit function, and in the total seismic misfit function to a lower degree.

CHAPTER TEN

Summary, Conclusions and Future Work

10.1Summary

Geological model errors

Seismic history matching requires an efficient method of controlling the parameters of the model, which in practice means we may choose the incorrect starting model or the incorrect method of altering it. The aim of this part of the project is to address two issues: can we use the pilot point method to update permeabilities, and how does the residual error compare to scale-dependent errors?

To address these issues, we generated fine-scale permeability realisations using sequential Gaussian simulation, which were upscaled by a factor of 5 in each direction (this was conducted using a synthetic model). Coarse-scale truth impedances are used to determine how good the pilot point method is so that we can avoid scale-dependent model errors. We updated the coarse-scale models via seismic history matching (SHM) using the predicted impedances from each coarse-scale model in turn as history data. We found that the pilot point approach is a good way of modifying a permeability field that has a similar degree of spatial correlation to the pilot point separation. We then used the impedances generated from the fine-scale models as the observed data to address the second issue (scale-dependent errors) and repeated the process. The residual error after updating is much smaller when coarse-scale models are used to generate observed data (i.e. there is no scale-

dependent error). The scale-dependent errors dominate, however, which means it is difficult to find a good model.

Schiehallion: appropriate updating schemes

We have focused on appropriate history matching strategies using the Phase II model (Chapter 7). For fields with several years of production and time-lapse history, it is important to choose the most appropriate method of finding the best models. Inclusive runs were carried out to match the entire history period in one go. The disadvantage to this approach is that we had to consider all parameters simultaneously, leading to uncontrollable numbers of time-consuming simulations. We thus need to develop an understanding of how parameters affect flow at different times. An alternative incremental approach may be used to update the model by improving the prediction of the first part of the history period very quickly with shorter simulation times. Then, with information about the best models and uncertainty information, we can add more data and parameters, if necessary, and continue. This approach may lead to a biased result, of course, if we are not careful about which parameters we include at each stage. Both approaches led to a good match to the observed seismic data up to 2000. Matching the Phase II seismic data was more difficult with the inclusive run, as more parameters were required owing to new wells accessing the reservoir. In the incremental run, some parameters that affected early seismic data could be fixed when simulating later production time, and we obtained a good seismic history match.

Reducing forecasting uncertainty by using SHM and assessing the value of 4D seismic data

Fault/barrier transmissibilities, reservoir permeability in the first case and additional parameters, including Net:Gross (due to mismatches in the predicted and observed baseline impedances), were combined with permeability. In this study, we have reported that the use of 4D seismic data in the misfit reduces the prediction uncertainty in this model, as it also did previously. Seismic and production data are best used together, because each parameter controls the seismic and production misfits to differing degrees. An infill well was considered, and its behaviour predicted for a set of models that matched history. It was

reported that the use of seismic data significantly reduced the uncertainty in this well. The uncertainty of the forecasted well is reduced by using seismic data, and we found that better matched models are better predictors.

10.2 Main conclusions on seismic history matching

Several lessons have been learnt from the application of the SHM technique to several (synthetic and real) cases. Based on this, the following steps are suggested for the application of the technique to other data cases:

- In Schiehallion, simulator speed was increased by taking sectors and upscaling.
- Three main parameters were inverted: a) fault transmissibility multiplier scaling factors, b) Net:Gross and c) permeability pilot point multipliers. In terms of the fault transmissibility multipliers' scaling factor and the permeability pilot points, both parameters have an intermediate spread in the estimations. The misfit function was reduced throughout the different approaches in the inversion scheme.
- There were a number of anomalies in the Phase I Schiehallion data which were never addressed. In Phase II, there was a smaller number. In all cases, the noise in the data was largely unresolved, although we took some steps to calibrate it.
- We were able to develop model acoustic impedance relatively easily. This appears to be the most appropriate attribute to the model. Cross-scaling was addressed by downscaling the predicted attributes in Phase I and Phase II. It is not clear whether this is the best approach.
- Two types of history-matching strategy were presented. In the first approach, dynamic data can be added to the process as the model is modified so that short simulations can be run. In the second, all parameters can be modified to match all data simultaneously.
- History matching using the baseline survey with the first monitor ('99) enabled a quick scan of the parameter space, and the range was adjusted (either reduced, if too large, or enlarged, if the limits were reached).

- Additional faults had to be modified when the Phase II seismic data (an additional two surveys covering four years of production) was included.
- The estimation of uncertainty was improved by identifying the most important and relatively unimportant parameters in the Schiehallion field faults that proved to be the dominant uncertainty.
- Production data errors were captured in Phase II of Schiehallion using wavelet analysis. This appears to be more effective than the frequency analysis of Phase I.
- To understand the uncertainty of the reservoir model, a similar approach was applied to analyse saturation, pressure, impedance and misfits by volume and maps and to analyse the distributions of the well data. This is essential for forecasting.
- The combination of different parameters has a significant impact on the misfit and model quality.
- The uncertainty of the forecasted well is reduced by using seismic data, and it was found that better matched models are better predictors, which can lead to better management decisions.
- We can improve our estimates of prediction uncertainty by identifying those parameters that are relatively unimportant.

10.3 Future work and major challenges

- The problem of dimensionality may be addressed by considering updating separately in different locations and at different times. Seismic data may be used to provide information on the large-scale properties of the reservoir, while wells are more local.
- The convergence of global assisted history-matching methods may be improved by using misfit sensitivities. All global methods combine some degree of exploitation (information about the misfit surface may be used to improve parameter choices) with exploration (the width of a search). Exploitative methods require more elaborate estimates of sensitivities but are susceptible to being trapped in local

minima. While explorative methods are computationally expensive, the aim is to consider a diverse set of models.

- Comparison in the time domain (i.e. before depth conversion) is attractive because the model-based prediction of seismic data may be compared to observations by using changes in amplitude, impedance/attribute or pressure and saturation. We currently have the option of comparing in the following domains: the time domain, the impedance/attribute domain and the pressure and saturation domain.
- A comparison of seismic data on the simulation grid must be undertaken.
- We still must address how to better update the model so that the conceptual geological model is honoured.
- The balance between production and seismic misfits can be addressed only by calibrating the data error. We have made inroads into production data error, but much remains to be done on the seismic side. Improved seismic misfit is essential because, when the predicted and observed seismic data are compared, it is often quite difficult to determine the data error. As yet, the noise is assumed to be uncorrelated with the signal and can therefore be determined by spectral analysis. Examining the type of noise that the seismic contains will improve the misfit evaluation and enhance forecasting.
- More updating strategies need to be investigated to determine how best to sample the parameter space of the model, by deriving measures of model diversity to prevent over sampling of the parameter space in volumes where negligible new information is obtained. Such measures are linked to misfits but also to other variables such as saturations, pressures and permeabilities. Time-lapse seismic data will reduce the non-uniqueness of such indicators.

Appendix A

Kriging

Kriging-based techniques are widely used for interpolating reservoir properties. The Kriging technique was developed in the 1960s by Georges Matheron (Matheron, 1971). Simple Kriging is mathematically the simplest: it assumes the guess of the random field to be known and relies on a covariance function. However, in most cases, neither the prospect nor the covariances are known in advance. There are different types of Kriging. We present here a brief description of these types of Kriging techniques. For more detailed information, see Cressie (1993), Hassani Pak (1998) and Doyen (2007).

Simple Kriging

Simple Kriging is mathematically the most straightforward, since it assumes the guess of the random data is known and relies on a covariance being known beforehand. Simple Kriging relies on many assumptions, such as the wide-sense stationarity of the field and a zero expectation everywhere; it also assumes that the covariance function is well known. The basic idea of simple Kriging is shown in Figure A.1 and Figure A.2 in the context of predicting an unknown rock property x_o. In our approach, we use this type of Kriging to interpolate between the pilot points.

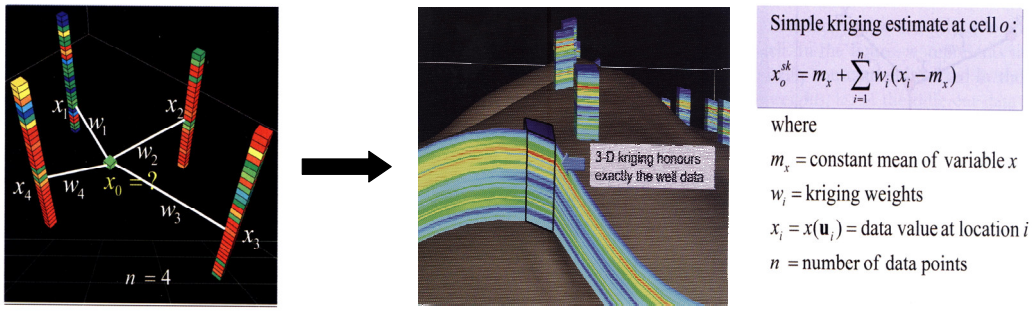

Figure A.1: *Simple Kriging in 3D (Doyen, 2007).*

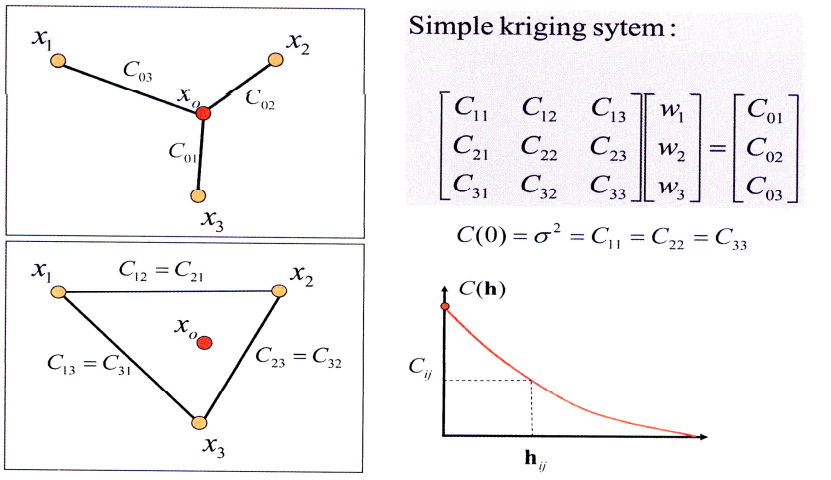

Figure A.2: *Definition of a simple Kriging system (Doyen, 2007).*

Ordinary Kriging

Ordinary Kriging is a variety of Kriging which assumes that the local means are not necessarily closely related to the population mean, and which therefore use only the samples in the local neighbourhood for the estimate. Ordinary Kriging is one of the most common techniques used in geological modelling.

Point Kriging

Point Kriging estimates the value of a point from a set of nearby sample values. This is used to account for the presence of trends in the data, such as a vertical porosity compaction trend or a real trend linked to lithology variations.

REFERENCES

Aanonsen, S., Aavatsmark, I., Barkve, T., Cominelli, A., Gonard, R., Gosselin, O., Kolasinski, T., and Reme, H. (2003). *Effect of Scale Dependent Data Correlation in an Integrated History Matching Loop Combining Production Data and 4D Seismic Data* (SPE79665). SPE Annual Technical Conference and Exhibition, Houston, Texas.

Aanonsen, S., Cominelli, A., Gosselin, O., Aavatsmark, I., and Barkve, T. (2002). *Integration of 4D Data in the History Match Loop by Investigating Scale Dependent Correlations in the Acoustic Impedance Cube*. European Conference on the Mathematics of Oil Recovery, Freiberg, Germany.

Abriel, W., Stefani, J., Shank, R., and Bartel, D. (1992). *3D Depth Image interpretation*. In Brown, A. (editor), Interpretation of Three-Dimensional Seismic Data., volume 9 of *Investigation in Geophysics*, pages 435–474. Society of Exploration Geophysics, Tulsa, Oklahoma.

Aggrey, G. H. *A Study of Intelligent Oil and Gas Fields' Real Time Optimisation and its Value Quantification*. PhD thesis (2007). Heriot-Watt University.

Al-Maskeri, Y., Fulton, J., and MacBeth, C. (2003). *Model-Controlled Quantitative Interpretation of 4D Signatures in Turbidite Reservoirs*. International Congress of The Brazilian Geophysical Society, Rio de Janeiro, Brazil.

Altan, S., Zhu, X., Dillon, G., McArdle, J., Walker, C., Parr, R., and Westwater, P. (2001). *Schiehallion 4D: From Time-Lapse Repeatability Study to Reservoir Monitoring*. SEG International Exposition and Annual Meeting, San Antonio, Texas.

Anderson, R., Boulanger, A., He, W., Xu, L., Flemings, P., Burkhart, T., and Hoover, A. (1997). *4D Time-Lapse Seismic Monitoring in the South Timbalier 295 Field, Gulf of Mexico*. SEG International Exposition and Annual Meeting, Dallas, Texas.

Arenas, E., Van Kruijsdijk, C., and Oldenziel, T. (2001). *Semi-Automatic History Matching Using the Pilot Point Method Including Time-Lapse Seismic* (SPE71634). SPE Annual Technical Conference and Exhibition, New Orleans, Louisiana.

Aziz, K. and Settari, A. (1979). *Petroleum Reservoir Simulation*. Applied Science Publishers Ltd., London, UK

Backer, J. W., Cuypers, M., and Holden, L. (2001). Quantifying uncertainty in production forecasts: Another look at the PUNQ-S3 problem. *Soc. Petrol. Engr. Jour*. 433–441.

Backus, G. E. (1962). Long-wave elastic anisotropy produced by horizontal layering. *J. Geophysical Research*, 67 (11), pp. 4427–4440.

Barker, J. W. and Dupouy, P. (1999). An analysis of dynamic pseudo-relative permeability methods for oil-water flows. *Petroleum Geoscience* 5, 385–394.

Batzle, M. and Wang, Z. (1992). Seismic properties of pore fluids. *Geophysics*, 57(11):1396–1408.

Benson, R. and Davis, T. (1998). *Time-Lapse Seismic Monitoring and Dynamic Reservoir Characterization, Central Vacuum Unit, Lea Country, New Mexico* (SPE49292). SPE Annual Technical Conference and Exhibition, New Orleans, Louisiana.

Bissell, R. C., Sharma, Y., and Killough, J. E. *History Matching Using the Method of Gradients: Two Case Studies*. SPE 28590. Presented at the SPE Annual Technical Conference and Exhibition, New Orleans, LA, 25–28 September, 1994.

Bogan, C., Johnson, D. Litvak, M. and Stauber, D. *Building reservoir models based on 4D seismic & well data in Gulf of Mexico oil fields*, SPE 84370. SPE Annual Technical Conference and Exhibition, 2003.

Brouwer, D. R., Jansen, J. D., van der Starre, S., Van Kruijsdijk, C. P. J. W., and Berentsen, C. W. J. *Recovery Increase through Water Flooding with Smart Well Technology.* Paper SPE 68979 presented at the SPE European Formation Damage Conference, The Hague, The Netherlands, 21–22 May 2001.

Brouwer, D. R. and Jansen, J. D. *Dynamic Optimization of Water Flooding with Smart Wells Using Optimal Control Theory.* Paper SPE 78278 presented at the SPE 13th European Petroleum Conference, Aberdeen, Scotland, UK, 29–31 October 2002.

Brouwer, D. R., Naevdal, G., Jansen, J. D., Vefring, E. H., and Van Kruijsdijk, C. P. J. W. *Improved Reservoir Management through Optimal Control and Continuous Model Updating.* Paper SPE 90149 presented at the SPE Annul Technical Conference and Exhibition, Houston, TX, 26–29 September 2004.

Caers, J. Efficient Gradual Deformation Using a Streamline-Based Proxy Method. *Journal of Petroleum Science and Engineering*, 39, 57–83, 2003.

Campbell, S., Ricketts, T., Davies, D., Slater, C., Lilley, G., Brain, J., Stammeijer, J., and Evans, A. (2005). *Improved 4D seismic repeatability – A West of Shetlands towed streamer acquisition case history*. SEG International Exposition and Annual Meeting, Houston, Texas.

Carter, R. D., Kemp, L. F., Pierce, A. C., and Williams, D. L. Performance Matching with Constraints. *Soc. Petrol. Eng. J.*, 14(4), 187–196, 1974.

Castagna, J., Sun, S., and Siegfried, R. (2003). Instantaneous Spectral Analysis: Detection of Low-Frequency Shadows Associated with Hydrocarbons. *The Leading Edge*, 22(2):120–127.

Castro, S., Caers, J. and Durlofsky, L. (2006). *Improved modelling of 4D seismic response using flow-based downscaling of coarse grid saturations.* Paper A024 presented at the 10th European conference on the mathematics of oil recovery, Amsterdam, The Netherlands, 4–7 September.

Chen, W. H., Gavalas, G. R., Seinfeld, J. H., and Wasserman, M. L. A New Algorithm for Automatic History Matching. *Soc. Petrol. Eng. J.*, 14(12), 593–608, 1974.

Chavent, G. M., Dupuy, M., and Lemonnier, P. History Matching by Use of Optimal Control Theory *Soc. Petrol. Eng. J.,* 15(1), 74–86, 1975.

Christie, M. A. and Blunt, M. (2001). Tenth SPE comparative solution project: A comparison of upscaling techniques. *Soc. Petrol. Engr. Reservoir Evaluation & Engr.* 4(4), 308–317.

Christie, M., MacBeth, C., and Subbey, S. (2002). Multiple History Matched Models for Teal South. *The Leading Edge*, 21(3):286–289.

Christie, M., Demyanov, V., and Erbas D. Uncertainty Quantification for Porous Media Flows. *Journal of Computational Physics*, 217, 143–158, 2006.

Cominelli, A., Seymour, R., Stradiotti, A., and Waggoner, J. (2002). *Integrating Time-Lapse Seismic Data in the History Match of a Gas-Condensate Reservoir*. EAGE Conference and Technical Exhibition, Florence, Italy.

Cooper, M.,Westwater, P., Thorogood, E., Kristiansen, P., and Christie, P. (1999b). *Foinaven Active Reservoir Management :Towed Streamer and Buried Sea-Bed Detectors in Deep Wter for 4D Seismic*. In SEG International Exposition and Annual Meeting, Houston, Texas.

Corana, A., Marchesi, M., Martini, C., and Ridella, S. (1987). Minimizing multimodal functions of continuous variables with the simulated annealing algorithm: ACM. *Trans. of Math. Soft.* 13, 262–280.

Cressie, Noel A. C. (1993). *Statistics for Spatial Data.* USA: John Willey & Sons Inc.

Daubechies, I. (1988) Orthonormal Bases of Compactly Supported Wavelets. *Communications on Pure Applied Mathematics*, XLI, 901–996.

Deutsch, C. and Journel, A. (1992). *GSLIB Geostatistical Software Library and User's Guide*. Oxford University Press, New York, U.S.A.

Dong, Y., Gu, Y. and Oliver, D. S. Sequential Assimilation of 4D Seismic Data for Reservoir Description Using the Ensemble Kalman Filter. *Journal of Petroleum Science and Engineering*, 53(1-2), 83–99, August 2006.

Doyen, P. M. (2007). *Seismic Reservoir Characterization. An Earth Modelling Perspective*. EAGE 2007.

Edris, N. and Stephen, K. D. (2008). *History matching with time-lapse seismic: will any starting model do?* Presented at the SPE Europec/EAGE Annual Conference and exhibition held in Rome, Italy, 9–12 June 2008.

Edris, N., Stephen, K. D., Shams, A. and MacBeth, C. (2008). *Updating Fault Transmissibilies in Simulations by Successively Adding Data to an Automated Seismic*

History Matching Processes: A Case study. SPE113557. SPE Europec/EAGE Annual Conference and Exhibition held in Rome, Italy, 9–12 June 2008.

Enchery, A. C., Ravalec-Dupin, M. and Roggero, F. (2007). *An improved pressure and saturation downscaling process for better integration of 4D seismic data together with production history*. Paper D003/SPE 107088 presented at the 69th EAGE conference and Exhibition, London, UK, 11–14 June.

Erbas, D. and Christie, M. (2006). *How does sampling strategy affect uncertainty estimations?* Oil & Gas Science and Technology -Revue de l'IFP (under review).

Erbas, D. and Christie, M. *Effect of Sampling Strategies on Prediction Uncertainty Estimation.* Paper SPE 106229 presented at the 2007 SPE Reservoir Simulation Symposium, Houston, TX, and 26–28 February 2007.

Evensen, G. Sequential Data Assimilation with a Non-Linear Quasi-Geostrophic Model Using Monte-Carlo Methods to Forecast Error Statistics. *J. Geophys Res.*, 99 (C5), 10143–10162, 1994.

Evensen, G., Hove, J., Meisingset, H. C., Reiso, E., Seim, K. S. and Espelid, Ø. *Using the EnKF for Assisted History Matching of a North Sea Reservoir Model.* Paper SPE 106184 presented at the 2007 SPE Reservoir Simulation Symposium, Houston, TX, 26–28 February, 2007.

Ewing, R. (1983). Problems arising in the modelling of process for hydrocarbon recovery. In Ewing, R. (editor), *The Mathematics of Reservoir Simulation*, 3–34. Society for Industrial and Applied Mathematics, Philadelphia.

Favergik, K., Lygren, M., Valen, T., Hetlelid, A., Berge, G., Dahl, G., Sønneland, L., Lie, H., and Magnus, I. (2001). *A Method for Performing History Matching of Reservoir Flow Models Using 4D Seismic.* SEG International Exposition and Annual Meeting, San Antonio, Texas.

Fletcher, J., Seymour, G., Flynn, T., and Burchell, M. (2005). *Formation pressure testing while drilling for deepwater field development* (SPE 96321). SPE Offshore Europe Conference, Aberdeen, UK.

Fletcher, R. (1987). *Practical methods of optimisation*. Wiley.

Floricich, M. *An engineering-consistent approach for pressure and saturation estimation from time-lapse seismic data*. PhD thesis (2006). Heriot-Watt University.

Floricich, M., Evans, A., McCormick, D., Jenkins, G., and Stammeijer, J. (2008). *Adding the Temporal Coherence Dimension to 4D Seismic Data - Assessing Connectivity in the Schiehallion Field.* Presented at the SPE Europec/EAGE Annual Conference and exhibition held in Rome, Italy, 9–12 June 2008.

Floris, F., Bush, M., Cuypers, M., Roggero, F., and Syversveen, A. R. (2001). Methods for quantifying the uncertainty of production forecasts: a comparative study. *Petroleum Geoscience* 7(SUPP), 87–96.

Foster, D. (2008). *Lessons Learnt from over 20 Years of 4D Deployment*. Presented at Indian oil and gas technical conference and exbibition held in Mumbai, India, 4–6 March 2008.

Gainski, M., Freeman, P., MacGregor, A., Nieuwland, F. and Fletche, J. (2008). *Detection of reservoir compartmentalisation and identification of new infill targets using 4D seismic surveys and dynamic production data*. Presented at AFES Rock Physics Seminar Aberdeen, April 8th 2008.

Gassmann, F. (1951). Uber die elastizitat poroser medien. *Vier. Der Natur. Gesellschaft*, 96, 1–23.

Gavalas, G. R., Shah, P. C., and Seinfeld, J. H. Reservoir History Matching by Bayesian Estimation. *Soc. Petrol. Eng. J.,* 16(6), 337–350, 1976.

Goldberg, D. E. (1989). *Genetic algorithms in search, optimization and machine learning*. Addison Weasley, Reading, MA.

Gómez-Hernánez, J. J., Sahuquillo, A., and Capilla J. E. Stochastic Simulation of Transmissivity Fields Conditional to Both Transmissivity and Piezometric Data-I. Theory. *Journal of Hydrology*, 203, 162–174, 1997.

Goovaerts, P., 1997, *Geostatistics for Natural Resources Evaluation*, Oxford Univ. Press, New York, 483 p.

Gosselin, O., Aanonsen, S., Asvatsmark, A., Cominelli, A., Gonard, R., Kolasinski, M., Ferdinandi, F., Kovaic, L., and Neylon, K. (2003). *History Matching Using Time-Lapse Seismic (HUTS)* (SPE84464). SPE Annual Technical Conference and Exhibition, Denver, Colorado.

Govan, A., Primmer, T., Douglas, C., Moodie, N., Davies, M., and Nieuwland, F. (2005). *Reservoir management in a deepwater subsea field - The Schiehallion Experience* (SPE 96610). SPE Offshore Europe Conference, Aberdeen, UK.

Govan, A. *Developing the Atlantic Margin: the Schiehallion story*. Presented at SPE Young Professionals Forum, Aberdeen, 4 October 2006.

Grossmann, A., and Morlet, J. (1984). Decomposition of Hardy Functions into Square Integrable Wavelets of Constant Shape. *SIAM J. Math.. Anal.*, 15(4), 723–736.

Guyanguler, B. and Horne, R. *Uncertainty Assessment of Well placement Optimization.* Paper SPE 71625 presented at the SPE Annual Technical Conference and Exhibition, New Orleans, LA, 30 September to 3 October, 2001.

Hassani Pak, Ali A. (1998). *Geostatistics.* Tehran, Iran: Tehran university publications.

Hatchell, P., Kelly, S., Muerz, M., Jones, C., Engbers, P., Van Der Veeken, J., and Staples, R. (2002). *Comparing time-lapse seismic and reservoir model predictions in producing oil and gas fields*. EAGE Conference and Technical Exhibition, Florence, Italy.

Haugen, V., Natvik, L.-J., Evensen, G., Berg, A., Flornes, K., and Nævdal, G. *History Matching Using the Ensemble Kalman Filter on a North Sea Field Case*. Paper SPE 102430 presented at the SPE Annual Technical Conference and Exhibition, San Antonio, TX, 24–27 September 2006.

Holland, J. H. *Adaptation in Natural and Artificial Systems.* University of Michigan Press, Ann Arbor, 1975.

Hu, L. and Jenni, S. History Matching of Object-Based Stochastic Reservoir Models. *Soc. Petrol. Eng. J.*, 10(3), 312–323, September 2005.

Hu, L. Y. (2000a). Gradual deformation and iterative calibration of Gaussian-related stochastic models. *Math. Geol.*, 32, 87–108.

Hu, L. Y. (2000b). Gradual deformation of non-Gaussian stochastic simulations. In *Geostatistics*, 2000, Cape Town, Kleingeld, W. J., and Krige, O. G. (editors).

Hu, L. Y., and Le Ravalec-Dupin, M. (2004). An improved gradual deformation method for reconciling random and gradient searches in stochastic optimizations. *Math. Geol.*, 36, 703–719.

Hu, L. Y., Blanc, G., and Noetinger, B. (1999). *Gradual deformation and iterative calibration of sequential stochastic simulations*. 5th Ann. Conf. Int. Ass. Math. Geol., Trondheim, Norway, 493–498.

Huang, X., Meister, L., and Workman, R. (1997). *Reservoir Characterisation by Integration of Time-Lapse Seismic and Production Data* (SPE38695). SPE Annual Technical conference and Exhibition, San Antonio, Texas.

Huang, X., Meister, L., and Workman, R. (1998). *Improvement and Sensitivity of Reservoir Characterisation Derived from Time-Lapse Seismic Data* (SPE49146). SPE Annual Technical Conference and Exhibition, New Orleans, Louisiana.

Huang, X., Meister, L., and Workman, R. (1999). *Reconciling Time-Lapse Seismic Data and Production Data: Application to a Gas Field* (SPE56732). SPE Annual Technical Conference and Exhibition, Houston, Texas.

Jackson, D. D. The Use of a Priori Data to Resolve Non-Uniqueness in Linear Inversion. *Geophys. J. R. Astr. Soc.,* 57, 137–157, 1979.

Jacquard, P., and Jain, C. *Permeability Distribution from Field Pressure Data. Soc. Petrol. Eng. J.,* 5(4), 281–294, 1965.

Jahns, H. O. A Rapid Method for Obtaining a Two-Dimensional Reservoir Description from Well Pressure Response Data. *Soc. Petrol. Eng. J*., 6(12), 315–327, 1966.

Johnston, D., Shyeh, J., Eastwood, J., Khan, M., and Stanley, L. (1999). *Interpretation and modeling of time-lapse seismic data: Lena Field, Gulf of Mexico*. SEG International Exposition and Annual Meeting, Houston, Texas.

Kalman, R. A New Approach to Linear Filtering and Prediction Problems. *Trans. ASME, J. Basic Eng*., 82D, 35–45, 1960.

King, P. R., Muggeridge, A. H., and Price, W. G. (1993). Renormalization calculations of immiscible flow. *Transport in porous media*, Vol. 12, 237–260.

Knai, T. A. and Knipe, R. J. (1998). The impact of faults on fluid flow in the Heidrun Field. In: Jones, G., Fisher, Q. J. and Knipe, R. J. (editors) Faulting, Fault Sealing and Fluid Flow in Hydrocarbon Reservoirs. *Geological Society,* London, Special Publication, 147, 269–282.

Koster, K., Gabriels, P., Hartung, M., Verbeek, J., Deinum, G., and Staples, R. (2000). Time-lapse seismic surveys in the North Sea and their business impact. *The Leading Edge*, 19(03):286–293.

Kretz, V., Ravalec-Dupin, M. L. and Roggero, F. An integrated reservoir characterization study matching production data and 4D seismic. *SPE Reservoir Evaluation and Engineering*, 7(2), 116–122, 2004.

Kristiansen, P., Christie, P., Bouska, J., O'Donnovan, A., Westwater, P., and Thorogood, E. (2000). *Foinaven 4D: Processing and analysis of two designer 4Ds.* SEG International Exposition and Annual Meeting, Calgary, Canada.

Kromah, M. J., Liou, J., and MacDonald, D. G. *Step Change in Reservoir Simulation Breathes Life into a Mature Oil Field.* Paper SPE 94940 presented at the SPE Latin American and Caribbean Petroleum Engineering Conference, Rio de Janeiro, Brazil, 20–23 June, 2005.

Lamers, E. and Carmichael, S. (1999). *The Palaeocene Deepwater Sandstone Play West of Shetland.* 5th Conference Petroleum Geology of Northwest Europe, London, United Kingdom. The Geological Society.

Lancaster, S. and Whitcombe, D. (2000). *Fast-Track Coloured Inversion*. SEG International Exposition and Annual Meeting, Calgary, Canada.

Landa, J. L. and R. N. Horne. *A procedure to integrate well test data, reservoir performance history and 4-D seismic information into a reservoir description*, SPE 38653. SPE Annual Technical Conference and Exhibition, 1997.

Landrø, M. (2001). Discrimination between Pressure and Fluid Saturation Changes from Time-Lapse Seismic Data. *Geophysics*, 66(3):836–844.

Leach, H., Herbert, N., Los, A., and Smith, R. (1999). *The Schiehallion Development*. Conference Petroleum Geology of Northwest Europe, London, United Kingdom. The Geological Society.

Le Ravalec-Dupin, M. (2005). *Inverse stochastic modeling of flow in porous media Application to reservoir characterization*. Editions Technip.

Le Ravalec, M., Hu, L.-Y. (2007). Combining the Pilot Point and Gradual Deformation Methods for Calibrating Permeability Models to Dynamic Data. *Oil & Gas Science and Technology – Rev. IFP*, Vol. 62 (2007), No. 2, pp. 169–180.

Levenberg, K. (1944). A method for the solution of certain non-linear problems in least squares. *Quart. J Applied Math*., Vol. 2, 164–168.

Lia, O., More, H., Tjelmeland, H., Holden, L., and Egeland, T. (1997). Uncertainties in reservoir production forecasts. *American Association of Petroleum Geologists Bulletin*, 81, 775–801.

Liang, B., Alpak, F. O., Sepehrnoori, K., and Delshad, M. *A Singular Evolutive Interpolated Kalman Filter for Rapid Uncertainty Quantification.* Paper SPE 106170 presented at the 2007 SPE Reservoir Simulation Symposium, Houston, TX, 26–28 February, 2007.

Liang, B. (2007). *An Ensemble kalman filter model for automatic history matching*. PhD thesis. The University of Texas.

Liu, N., and Oliver, D. S. *Experimental Assessment of Gradual Deformation Method*. *Mathematical Geology*, 36(1), 65–77, 2004.

Litvak, M., Christie, M., Johnson, D., Colbert, J., and Sambridge, M. *Uncertainty Estimation in Prediction Predictions Constrained by Production History and Time-Lapse Seismic in a GOM Oil Field.* Paper SPE 93146 presented at the SPE Reservoir Simulation Symposium, Houston, TX, 31 January to 2 February, 2005.

Lorentzen, R. J., Berg, A. M., Nævdal, G., and Vefring, E. H. *A New Approach for Dynamic Optimization of Waterflooding Problems.* Paper SPE 99690 presented at the Intelligent Energy Conference and Exhibition, Amsterdam, The Netherlands, 11–13 April, 2006.

Lumley, D. and Behrens, R. (1998). Practical issues of 4D seismic reservoir monitoring: What an engineer needs to know. *SPE Reservoir Evaluation and Engineering*, pp. 528–538.

Lumley, D. (2004). Business and Technology Challenges for 4D Seismic Reservoir Monitoring. *The Leading Edge*, 23(11):1166–1168.

Lumley, D. E., Behrens, R. A., and Wang, Z. Assessing the technical risk of a 4D seismic project. *The Leading Edge*, 16(9), 1287–1292, 1997.

Lumley, D. E., Nur, A., Strandenes, S., Dvorkin, J., and Packwood, J. *Seismic monitoring of oil production: A feasibility study*. 1994 SEG Expanded Abstracts, 1994.

MacBeth, C. (2004). A Classification for the Pressure-Sensitivity Properties of a Sandstone Rock Frame. *Geophysics*, 69(2):497–510.

MacBeth, C. (2007). *An introduction to quantitave 4D seismic interpretation for dynamic reservoir description.* EAGE education day 2007.

MacBeth, C., and Stephen, K. (2008). Seismic scale saturation relations in turbiditer reservoirs undergoing waterflood. *European Association of Geoscientists & Engineers, Geophysical Prospecting*, 56, 693–714.

Macdonald, C. J., Tosdevin, M., and Tothill, M. D. (2004). *Report on the Schiehallion Full Field VIP Model FFM2003.*

Makhlouf, E. M., Chen, W. H, Wasserman, M. L., and Seinfeld, J. H. A General History Matching Algorithm for Three-Phase, Three-Dimensional Petroleum Reservoirs. *SPE Advanced Technology Series*, 1(2), 83–92, 1993.

Mantica, S., Cominelli, A., and Mantica, G. (2001). *Combining Global and Local Optimisation Techniques for Automatic History Matching Production and Seismic Data* (SPE66355). SPE Reservoir Simulation Symposium, Houston, Texas.

Manzocchi, T., Walsh, J. J., Nell, P., and Yielding, G. (1999). Fault transmissibility multipliers for flow simulation models. *Petroleum Geoscience*, 5, 53–63.

Marquardt, D. W. (1963). An algorithm for least squares estimation of non-linear parameters. *J. Soc. Indust. Appl. Math*., 11, p. 431.

Marsh, M. (2004). *4D in reservoir management - Successes and Challenges*. IOR Views e-newsletter, 8.

Marsh, M. (2004). *The use of 4D seismic in reservoir management.* EAGE/DLP course notes, February 2004.

de Marsily, G., Lavedan, G., Boucher, M., and Fasanino, G. Interpretation of Interference Tests in a Well Field Using Geostatistical Techniques to Fit the Permeability Distribution in a Reservoir Model. In *Geostatistics for Natural Resources Characterization, Part 2*, 831–849, Kluwer Academic Publishers, 1984.

Matheron, G. (1971). *The theory of regionalized variables and its applications.*

Mattax, C., and Dalton, R. (1990). *Reservoir Simulation. Society of Petroleum Engineering.* Richardson, Texas.

Mavko, G., Mukerji, T., and Dvorkin, J. (1998). *The Rock Physics Handbook. Tools for Seismic Analysis in Porous Media.* Cambridge University Press, Cambridge, UK.

Meadows, M. (2001). *Enhancement to Landrø's Method for Separating Time-Lapse Pressure and Saturation Changes*. SEG International Exposition and Annual Meeting, San Antonio, Texas.

Mezghani, M., Langlais, V., Lucet, N., and Fornel, A. (2004a). *Quantitative Use of 4D Seismic Data for Geological Modeling & Reservoir Characterization Through History Matching*. EAGE Conference and Technical Exhibition, Paris, France.

Mezghani, M., Fornel, A., Langlais, V., and Lucet, N. (2004b). *History matching and quantitative use of 4D seismic data for an improved reservoir characterization.* SPE 90420. SPE 2004 Annual Technical Conference and Exhibition.

Miranda, M. (2007). *Fault-induced bends on Schiehallion's North Channel.* Presented at DEVEX 15, 16 May 2007.

Nævdal, G., Mannseth, T., and Vefring, E. H. *Near-well reservoir monitoring through ensemble Kalman filter*. SPE 75235. SPE/DOE Improved Oil Recovery Symposium, 2002.

Nicotra, G., Godi, A., Cominelli, A., and Christie, M. *Production Data and Uncertainty Quantification: A Real Case Study*. Paper SPE 93280 presented at the SPE Reservoir Simulation Symposium, Houston, TX, 31 January to 2 February, 2005.

O'Donovan, A., Smith, S., and Kristiansen, P. (2000). *Foinaven 4D seismic - Dynamic reservoir parameters and reservoir management* (SPE 63294). SPE Annual Technical Conference and Exhibition, Dallas, Texas.

Oldenziel, T., van Ditzhuizen, R., and van Kruijsdijk, C. P. J. W. (2002). Geologic parameterization of reservoir model enhances history-match procedure. *The Leading Edge,* Vol. 21, No. 6, pp. 544–551.

O'Sullivan, A. E. (2004). *Modelling simulation error for improved reservoir prediction*. PhD thesis, Heriot-Watt University.

Ouenes, A., Brefort, B., Meunier, G., and Dupere, S. *A New Algorithm for Automatic History Matching: Application of Simulated Annealing Method (SAM) to Reservoir Inverse Modeling*. Paper SPE 26297, 1993.

Panda, M. N., Mosher, C., and Chopra, A. K. (2001). Reservoir modelling using scale-dependent data. *Soc. Petrol. Engr. Jour*. 6(2), 157–170.

Pannett, S., Slager, S., Stone, G., and Dekker, S. *Constraining a complex gas-water dynamic model using 4D seismic*. SPE 89793. SPE Annual Technical Conference and Exhibition, 2004.

Park, K. and Choe, J. *Use of Ensemble Kalman Filter with 3-Dimensional Reservoir Characterization*. Paper SPE 100178, presented at the SPE Europec/EAGE Annual Conference and Exhibition, Vienna, Austria, 12–15 June 2006.

Parker, J., Bertelli, L., and Dromgoole, P. (2003). 4D Seismic Technology. Special Issue, *Petroleum Geoscience*, 9(1), pp. 1–111.

Parr, R., Cowper, D., and Michener, B. (1999). *The Search for Mountains of Oil: Exploration Activity in the Atlantic Margin, West of Shetland (SPE56897).* SPE Offshore Europe Conference, Aberdeen, Scotland.

Pickup, G. E., Ringrose, P. S., and Sharif, A. (2000). Steady-state upscaling: From lamina-scale to full field model. *Soc. Petrol. Engr. Jour*. 5(2), 208–217.

Polikar, R. (2001). *The Engineer's Ultimate Guide to Wavelet Analysis*. The Wavelet Tutorials, Rowan University.
http://users.rowan.edu/~polikar/WAVELETS/WTtutorial.html

Portellaand, R. C. M., and Prais, F. *Use of Automatic History Matching and Geostatistical Simulation to Improve Production Forecast.* Paper SPE 53976 presented at the Latin American and Caribbean Petroleum Engineering Conference, Caracas, Venezuela, 21–23 April 1999.

Porter-Hirsche, J., and Hirsche, K. *Repeatability study of land data acquisition and processing for time lapse seismic*. SEG Expanded Abstracts, 1998.

Powell (1971). A hybrid method for non-linear equations. In *Numerical methods for non-linear algebraic equations*, P. Rabinowitz (editor), Gordon & Breach, p. 87.

RamaRao, B. S., LaVenue, A. M., de Marsily, G., and Marietta, M. G. (1995). Pilot point methodology for automated calibration of an ensemble of conditionally simulated transmissivity fields. Theory and computational experiments. *Water Resour. Res*., 31, 475–493.

Reinlie, S. T. *Analysis of Continuous Monitoring Data and Rapid, Stochastic Updating of Reservoir Models*. PhD dissertation, The University of Texas at Austin, May 2006.

Richardson, S., Herbert, N., and Leach, H. (1997). *How Well Connected is the Schiehallion Reservoir?* (SPE38560). SPE Offshore Europe Conference, Aberdeen, Scotland.

Rickett, J. and Lumley, D. E. Cross-equalization data processing for time-lapse seismic reservoir monitoring: A case study from Gulf of Mexico. *Geophysics*, 66(4), 1015–1025, 2001.

Robert, C. P. and Casella, G. (1999). *Monte Carlo Statistical Methods.* Springer-Verlag, New York, USA.

Rodrigues, J.R.P.: *"Calculating Derivatives for History Matching in Reservoir Simulators,"* paper SPE 93445 presented at the SPE Reservoir Simulation Symposium, Houston, TX, 31 January-2 February, 2005.

Roggero, F. and Hu, L. (1998). *Gradual Deformation of Continuous Models for History Matching* (SPE49004). SPE Annual Technical Conference and Exhibition, New Orleans, Louisiana.

Ross, C., Cunningham, G., and Weber, D. (1996). Inside the Cross Equalization Black Box. *The Leading Edge*, 15(11):1233–1240.

Rotondi, M., Nicotra, G., Godi, A., Contento F.M., Blunt M.J., and Christie, M.A.: *"Hydrocarbon Production Forecast and Uncertainty Quantification: A Field Application,"* paper SPE 102135 presented at the SPE Annual Technical Conference and Exhibition, San Antonio, TX, 24-27 September, 2006.

Sambridge, M. (1999a). Geophysical Inversion with a Neighbourhood Algorithm – Searching a Parameter Space. *Geophysical Journal International*, 138(2):479–494.

Sambridge, M. (1999b). Geophysical Inversion with a Neighbourhood Algorithm – Appraising the Ensemble. *Geophysical Journal International*, 138(2):727–746.

Sambridge, M. and Mosegaard, K. (2002). Montecarlo Methods in Geophysical Inverse Problems. *Reviews of Geophysics*, 40 (10.1029/2000RG000089).

Sarma, P., Durlofsky, L. J., and Aziz, K. *Efficient Closed-Loop Production Optimization under Uncertainty.* Paper SPE 94241 presented at the SPE/EAGE Annual Conference, Madrid, Spain, 13–16 June 2005.

Sarma, P., Chen, W. H., Durlofsky, L. J., and Aziz, K. *Production Optimization with Adjoint Models under Nonlinear Control-State Path Inequality Constraints.* Paper SPE 99959 presented at the Intelligent Energy Conference and Exhibition, Amsterdam, The Netherlands, 11–13 April, 2006.

Schlumberger, (2006) ECLIPSE reference manual.

Schlumberger, (2007) PETREL reference manual.

Sen, M., and Stoffa, P. L. (1995). *Global optimization methods in geophysical inversion*: Elsevier Science Publ. Co., Inc.

Sengupta, M., Mavko, G. and Mukerji, T. (2003). Quantifying subresolution saturation scales from time-lapse seismic data: a reservoir monitoring case study. *Geophysics* 68, 803–814.

Sivia, D. S. (1996). *Data Analysis: A Bayesian Tutorial,* Oxford University Press, Inc., New York.

Skjervheim, J.-A., Evensen, G., Aanonsen, S. I., Ruud, B. O., and Johansen, T. A. *Incorporating 4D seismic data in reservoir simulation models using ensemble Kalman filter.* SPE 95789, 2005.

Soldo, J. S. *Quantitative Integration of Time-Lapse Seismic Information Using Multiple Model History Matching and Engineering Data*. PhD thesis (2005). Heriot-Watt University.

Sønneland, L., Reymond, B., Thorsteinsen, H., Johansen, R., and Pedersen, L. (1996). *Reservoir Monitoring: Fluid Fronts Classification from Seismic and Well Log Data.* SEG International Exposition and Annual Meeting, Denver, Colorado.

Staples, R., Lamens, Y., and Beaumont-Smith (2004). *Monitoring injection in the Northern North Sea*. SPE/EAGE joint workshop, Copenhagen, Denmark.

Stephen, K. D., and MacBeth, C. (2006). *Reducing Reservoir Prediction Uncertainty Using Seismic History Matching (SPE 100295*). SPE Europec/EAGE Annual Conference and Exhibition held in Vienna, Austria, 12–15 June 2006.

Stephen, K. D., Soldo, J., MacBeth, C., and Christie, M. (2004a). *Practical dynamic updating of reservoir models using frequently acquired 4D seismic data.* Proceedings of the 66th EAGE Conference and Exhibition, Paris, France, 7–10 June, 2004.

Stephen, K. D., Soldo, J., MacBeth, C., and Christie, M. (2004b). *A multiple model approach to history matching and uncertainty analysis using time-lapse seismic*. Proceedings of the 9th European Conference on the Mathematics of Oil Recovery, Cannes, France, 20 August to 2 September, 2004.

Stephen, K. D., Soldo, J., MacBeth, C., and Christie, M. (2005). *Multiple Model Seismic and Production History Matching: A Case Study.* SPE94173. Proceedings of the 14th Europec Biennial Conference held in Madrid, Spain, 13–16 June 2005.

Stephen, K. D. Scale and process dependent model errors in seismic history matching. *Oil & Gas Science and Technology-Revue de l'IFP.* 62(2) Special Issue. pp. 123–136, 2007.

Subbey, S., Christie, M., and Sambridge, M. (2002). Uncertainty Reduction in Reservoir Modeling. In Chen, Z. and Ewing, R. (editors), *Fluid Flow and Transport in Porous Media: Mathematical and Numerical Treatment, Volume 295 of Contemporary Mathematics*, pp. 1–10. American Mathematical Society, Providence, Rhode Island.

Subbey, S., Christie, M., and Sambridge, M. *A Strategy for Rapid Quantification of Uncertainty in Reservoir Performance Prediction*. Paper SPE 79678 presented at the SPE Reservoir Simulation Symposium, Houston, TX, 3–5 February 2003.

Subbey, S., Christie, M., and Sambridge, M. Prediction under Uncertainty in Reservoir Modeling. *Journal of Petroleum Science and Engineering*, 44, 143–153, 2004.

Tarantola, A., and Valette, B. (1982). Inverse Problems Quest for Information. *Journal of Geophysics*, 50(2):159–170.

Traine A., Donatella A., and Marcelo, B. (2002). Seismic applications throughout the life of the reservoir. *Oilfield review 2002*, 40–65.

Tura, A., and Lumley, D. (1999). *Estimating Pressure and Saturation Changes from Time-Lapse AVO Data.* SEG International Exposition and Annual Meeting, Houston, Texas.

Vasco, D. W., Yoon, S., and Data-Gupta, A. Integrating Dynamic Data Into High- Resolution Reservoir Models Using Streamline-Based Analytic Sensitivity Coefficients. *Soc. Petrol. Eng. J.*, 389–399, December 1999.

Waggoner, J., Cominelli, A., and Seymour, R. (2002). *Improved Reservoir Modelling with Time-Lapse Seismic in a Gulf of Mexico Gas Condensate Reservoir* (SPE77514). SPE Annual Technical Conference and Exhibition, San Antonio, Texas.

Waite, M., and Rusdinadar, D. (1997). Seismic Monitoring of the Duri Steamflood: Application to Reservoir Management. *The Leading Edge*, 16(9):1275–1278.

Waite, M., Sigit, R., Rusdibiyo, A. H. P., and Satriana, D. (1997). *Application of Seismic Monitoring to Manage an Early-Stage Steamflood* (SPE37564). SPE International Thermal Operations and Heavy Oil Symposium, Bakersfield, California.

Walder, D. R., Howes, D. R., Mountford, C. F., and Parr, R. S. *Development Drilling Innovations for the Foinaven and Schiehallion fields, in the UK Atlantic Margin.* OTC 10990, Houston, 1999.

Walker, G., and Scott, L. (2007). *Assessing the accuracy of history matching predictions and the impact of time-lapse seismic data: A case study of the Harding reservoir*. Paper SPE 106019 presented at the SPEReservoir Simulation symposium, Houston, Texas, U.S.A., 26–28 February, 2007.

Walnut, F. D. (2003). *An Introduction to Wavelet Analysis.*

Wang, Z., Nur, A., 1988, Effect of temperature on wave velocities in sands and sandstones with heavy hydrocarbons, SPE Reservoir Eng., Vol.3, No.1, p158-164

Wen, X.-H., and Chen, W. H. *Real-time reservoir model updating using ensemble Kalman filter*. SPE 92991. SPE Reservoir Simulation Symposium, 2005.

Williams, G. J. J., Mansfield, M., MacDonald, D. G., and Bush, M. D. *Top-Down Reservoir Modelling*. Paper SPE 89974, presented at the SPE Annual Technical Conference and Exhibition, Houston, TX, 26–29 September, 2004.

Wu, Z., Reynolds, A. C., and Oliver, D. S. Conditioning Geostatistical Models to Two-Phase Production Data. *Soc. Petrol. Eng. J*., 3(2), 142–155, 1999.

Yeten, B., Durlofsky, L., and Aziz, K. (2002a). *Optimization of Well Type, Location and Trajectory*. Paper SPE 77565, presented at the SPE Annual Technical Conference and Exhibition, San Antonio, TX, 29 September to 2 October, 2002.

Yeten, B., Durlofsky, L. J., and Aziz, K. (2002b). *Optimization of Smart Well Control.* Paper SPE 79031, presented at the SPE International Thermal Operation and Heavy Oil Symposium and International Horizontal Well Technology Conference, Calgary, Alberta, Canada, 4–7 November, 2002.

Yielding, G., Overland, J. A., and Byberg, G. (1999a). *Characterisation of fault zones in the Gullfaks field for reservoir modelling*. In Fleet, A. J. and Boldy, S. A. R. (editors), Petroleum Geology of Northwest Europe: Proceedings of the 5th Conference. Geological Society, London, 1177–1185.

Yielding, G., Overland, J. A., and Byberg, G. (1999b). Characterisation of fault zones for reservoir modelling: An example from the Gullfaks Field, Northern North Sea. *American Association of Petroleum Geologists Bulletin*, 83–6, 925–951.

Yilmaz, O. (1987). *Seismic Data Processing*. SEG, Tulsa, U.S.A.

Zafari, M., and Reynolds, A. C. *Assessing the Uncertainty in Reservoir Description and Performance Predictions with the Ensemble Kalman Filter*. Paper SPE 95750, presented at the SPE 2005 SPE Annual Technical Conference and Exhibition, Dallas, TX, 9–12 October 2005.

Zhang, F., Skiervheim, J. A., Reynolds, A. C., and Oliver, D. S. *Automatic History Matching in a Bayesian Framework, Example Applications.* Paper SPE 84461, presented at the SPE Annual Technical Conference and Exhibition, Denver, CO, 5–8 October 2003.